DOCTORAL THESIS

Effects of top-of-rail friction modifiers on the friction, wear and cracks of railway rails

Saad Ahmed Khan

Operation and maintenance engineering

LULEÅ UNIVERSITY OF TECHNOLOGY

LULEÅ
UNIVERSITY
OF TECHNOLOGY

Effects of top-of-rail friction modifiers on the friction, wear and cracks of railway rails

Saad Ahmed Khan

Division of Operation, Maintenance and Acoustics
Department of Civil, Environmental and Natural Resources Engineering
Luleå University of Technology

Printed by Luleå University of Technology, Graphic Production 2019

ISSN 1402-1544
ISBN 978-91-7790-272-0 (print)
ISBN 978-91-7790-273-7 (pdf)

Luleå 2019

www.ltu.se

ACKNOWLEDGEMENTS

The research work presented in this thesis was carried out between March 2015 and February 2019 at the Division of Operation, Maintenance and Acoustics of Luleå University of Technology. I gratefully acknowledge Luleå Railway Research Center (JVTC) and the Swedish Transport Administration (Trafikverket) for financing the project.

I would like to express my gratitude to my supervisor, Professor Jan Lundberg, and my co-supervisors, Dr Christer Stenström and Associate Professor Matti Rantatalo. I am thankful for the confidence that they have placed in my capability to conduct this research work, and for all their support through sharing their ideas, proposing improvements, proofreading manuscripts, finding new ways, and always adopting a positive approach.

Many thanks are due to Ingemar Persson at AB DEsolver for assisting me by providing support for simulations and a large amount of useful information during my research.

Special thanks are extended to my ex-colleague and my project leader at Trafikverket, Matthias Asplund, for all his support during this project. I am also grateful to Per Gustafsson at LKAB, who helped us to decide the location of the TOR equipment installation and provided information in the initial phase of the project. I would also like to express my thanks to Emil Viberg from Infranord, who arranged for a security person to accompany me every time I went to the railway track for measurements, as well as Stephan Scheriau from Voestalpine Schienen GmbH in Austria for providing rail steel material that was used for making wear probes.

Furthermore, I would like to thank all my colleagues at the Division of Operation, Maintenance and Acoustics, especially my co-researcher Thomas Nordmark and laboratory technician Allan Holmgren. I would also like to thank all the PhD students and senior researchers at our division who helped me during the research work for my PhD. I am also grateful to all my friends in and outside the university who supported me during the work on this thesis, but who are too many to be mentioned by name.

My deep gratitude is owed to my parents, Asma and Zaheer Ahmed Khan, and to my wife, Hiba, and my son, Daniyal, for all the support and confirmation received from them; without them, my goal would never have been achieved.

Saad Ahmed Khan
February 2019
Luleå, Sweden

ABSTRACT

The railway is an economical and environmentally friendly mode of transport for long distances and heavy loads. The demands on the operators are increasing with increased competition in the market, and therefore they are currently demanding more track capacity. In the short term, the existing network is expected to deliver the increased capacity. In order to achieve increased capacity without introducing double track, either the axle load or the number of trains (i.e. the annual gross tonnage) needs to be increased, which will decrease the life of the rail and thus increase the maintenance cost. To increase the lifetime of the rails without compromising with regard to the axle load and speed, one must increase the strength of the rails, decrease the friction forces between the rails and wheels, or introduce a third body with anti-wear and anti-crack properties that can reduce the wear and rolling contact fatigue (RCF) without reducing the traction coefficient below the safety limit.

The friction forces depend on several variables, for example third bodies in the wheel-rail interface, the train dynamics, the wheel and rail profiles, etc. Third bodies in the wheel-rail interface are one of the important influencing factors. The additive third bodies with anti-wear properties and friction reduction capabilities reduces both the wear and the RCF. However, a friction coefficient in the wheel tread and the top of the rail below 0.3 can cause slippage and a long braking distance. To reduce the degree of utilised friction to a value close to 0.35 from dry conditions with a value of 0.55, and thereby reduce the wear, a product known as top-of-rail friction modifier (TOR-FM) was developed in North America and presented in 2003 at the heavy haul conference. The TOR-FM manufacturers claim that their products provide a fixed range of friction coefficients (μ) and Kalker's reduction factors in the wheel-rail interface. Kalker's reduction factor considers the tendency of creepage between the rail and wheel as a function of the friction forces at lower creepage levels. Field and laboratory tests in the USA, Canada and China have determined the benefits of using friction control products, which include the reduction of RCF, wear, corrugation, bogie hunting, noise, and fuel consumption without any side effects. In contrast, researchers at Luleå University of Technology (LTU) have found that such products in certain conditions give unacceptably low friction that can cause long braking distances and slippage. Initial measurements, before the starting of the present research, performed using a wayside TOR-FM system on the Iron Ore Line (IOL – "Malmbanan" in Swedish) could not show any benefits of implementing such systems.

Trafikverket is considering the implementation of the TOR-FM technology on the IOL. Directly implementing such technology can be inappropriate and expensive, because the reliability of a TOR-FM system has never been assessed for the conditions of the IOL. The IOL is the northernmost railway line in Sweden and is experiencing the problem of RCF, especially on its curves. This railway line is a single track and is mainly utilised by the ore freight trains operated by the Swedish mining company LKAB. The freight trains run by LKAB have an axle load of 30 tonnes, which is the heaviest in Europe. At present LKAB is planning to increase the axle load of their heavy haul trains to 32.5 tonnes, which will increase the RCF and wear issues.

The present research investigated the effects of TOR-FMs using computer-based simulations, laboratory tests and field tests. The results from all the tests and simulations were used to calculate the life cycle cost of wayside and on-board systems. The simulation results have shown that by reducing the friction, the RCF can be reduced. This reduction in the RCF is greater on narrow curves than on larger curves as the friction force decrease with an increase in the curve radius. Curves with a radius larger than 1,000 m are not prone to RCF. The damage index method used in the simulation has also shown that on circular curves with a radius smaller than 300 m, the so-called "magic wear" rate can be achieved. Magic wear means that the wear rate due to normal operation is equal to the crack generation rate. The field results obtained using a handheld tribometer have shown that by using a TOR-FM, both the wear and the friction coefficients can be reduced. The content of the TOR-FM can have a significant effect on the carry distance and, generally, non-drying FMs have a longer carry distance. Excessive use of TOR-FM may only cause unacceptably low friction and a high operational cost and result in an insignificant increase in the carry distance. In addition, it was also concluded that in the case of the wayside system during extreme winters, the equipment could have maintenance issues and thus a high operational cost. The on-board system is an economical alternative to the wayside system, as it has lower operation and maintenance costs. The results have also shown that snow and ice formation in the winter act as a lubricant. However, further investigations are needed to provide knowledge of the efficiency of such natural lubricants and their retention on the rail. The present research has taken the IOL as a case study, but the results will be applicable all over the world.

KEYWORDS: friction modifier, heavy haul, Iron Ore Line, Malmbanan, magic wear, railway, rolling contact fatigue (RCF), top-of-rail (TOR) lubrication, wear.

SAMMANFATTNING

Järnvägen är ett ekonomiskt och miljövänligt transportsätt för långa avstånd och tunga laster. Operatörernas krav ökar med ökad konkurrens på marknaden. Därför finns det för närvarande en efterfrågan på mer spårkapacitet. På kort sikt förväntas den befintliga järnvägen leverera den ökade kapaciteten. För att uppnå ökad kapacitet utan att införa dubbelspår måste axelbelastningen eller antalet tåg (årlig bruttoton) ökas, vilket minskar spårens livslängd och därmed ökar underhållskostnaderna. För att öka skenornas livslängd utan att behöva minska axelbelastningen och hastigheten måste man antingen öka slitstyrkan och spricktåligheten på skenorna eller minska friktionskrafterna mellan skenorna och hjulen eller införa så kallade "third bodies" med goda anti-sprick och slitageegenskaper.

Friktionskrafterna är beroende av flera variabler, till exempel "third bodies" i hjul-järnvägsgränssnitt, tågdynamik, hjulprofil etc. Bland alla faktorer är "third bodies" i hjul-järnvägsgränssnitt en av de viktiga faktorerna. Graden av nyttjad friktion påverkar kraftigt friktionskrafterna och därigenom slitage och rullande kontaktutmattning (RCF), vilket minskar livslängden på skenorna om friktionskoefficienten på toppen av skenorna är mindre än 0,3 kan emellertid bromssträckorna bli alltför långa på grund av glidning. För att styra graden av nyttjad friktion till nära 0,35 för att minskar slitage och friktionskrafterna i jämförelse med torra förhållanden, utvecklades en produkt som kallas top-of-rail friktionsmodifierare (TOR-FM) i Nordamerika och publicerades 2003 vid International Heavy Haul konferensen. TOR-FMs tillverkare hävdar att deras produkter ger konstant friktionskoefficient (μ) och Kalker's koefficient i hjul-järnvägsgränssnitt. Kalker's koefficient beaktar den grundläggande tendensen till krypning mellan skenan och hjulet som funktion av friktionskrafter vid lägre krypningsnivåer. Fält- och laboratorietester i USA, Kanada och Kina har kartlagt fördelarna med att använda friktionskontrollerande produkter som inkluderar minskning av RCF, slitage, korrugering, boggi hunting, buller och bränsleförbrukning. Däremot har forskare vid Luleå tekniska universitet funnit att sådana produkter under visa förhållanden ger oacceptabelt låg friktion och kan orsaka alltför långa bromssträckor genom slirning. Initiala mätningar utförda på Malmbanan innan projektet började, kunde inte några fördelar påvisas med att implementera sådana system.

Trafikverket överväger införa TOR-FM-tekniken på Malmbanan. Direkt implementering av TOR-FM-teknik kan dock vara olämpligt och dyrt, eftersom tillförlitligheten hos sådana system inte klarar de påfrestningar som uppstår vid Malmbanan. Malmbanan är den nordligaste järnvägen i Sverige och har problem med RCF i kurvor. Malmbanan är enkelspårig och används huvudsakligen för malmtransporter som drivs av det svenska gruvbolaget LKAB. Tågen från LKAB har en axelbelastning på 30 ton, vilket är den tyngsta i Europa. För närvarande planerar LKAB att öka axeltrycket på sina tunga tåg till 32,5 ton vilket ökar RCF, slitage ytterligare.

I föreliggande studie, undersöktes TOR-FM egenskaper genom datorbaserade simuleringar, laboratorietester och fälttester. Resultaten från samtliga tester har används för att beräkna livscykelkostnaden (LCC) för stationära och tågburna TOR-FM system. Simuleringsresultaten har visat att RCF kan reduceras genom att minska friktionen. Minskningen i RCF genom att minska friktionen har större betydelse för snäva kurvor an för större kurvor, eftersom friktionskrafterna minskar med ökande kurvradie. Kurvor större än 1000 m radie är inte benägna att uppvisa RCF. Skadeindex-

metoden vid simulering har också visat att "magic wear" kan uppnås på cirkulära kurvor som är mindre än 300 m i radie. Magic wear betyder att slitaget på grund av tågtrafiken är lika med sprickgenereringshastigheten. Fältresultaten i form av friktionsmätningar med hjälp av en handhållen tribometer har visat att friktionsminskning genom att använda TOR-FM, sammanfaller med minskat slitage. Innehållet i TOR-FM kan ha en signifikant effekt på den effektiva smörjsträckan (Spårsträckan som TOR-FM förmår att smörja). Överdriven smörjning kan innebära oacceptabelt låg friktion och höga kostnader, och endast en obetydlig ökning av den effektive smörjsträckan. Vidare har det konstaterats att utrustningen under vintertid har stora driftstörningar vilket orsakar stora underhållsproblem och höga driftkostnader. Tågburna system är därför ett ekonomiskt alternativ till stationära system, eftersom det har färre driftsproblem och underhållskostnader. Resultaten har också visat att snö och isbildning i vintertid fungerar som ett smörjmedel. Dock behövs mer forskning för att mäta effektivitet och varaktighet hos sådant naturligt smörjmedel. Den föreliggande studien har använt Malmbanan som en fallstudie. Resultaten kommer dock att kunna tillämpas över hela världen.

LIST OF APPENDED PAPERS

Paper 1

Khan, S. A., Persson, I., Lundberg, J. and Stenström, C. (2018) 'Prediction of the effects of friction control on top-of-rail cracks', Proceedings of the Institution of Mechanical Engineers, Part F: Journal of Rail and Rapid Transit, 232(2), pp. 484–494.

Paper 2

Khan, S. A., Persson, I., Lundberg, J. and Stenström, C. (2017) 'Prediction of top-of-rail friction control effects on rail RCF suppressed by wear', Wear, 380–381, pp. 106–114.

Paper 3

Khan, S. A., Lundberg, J. and Stenström, C. (2018) 'Carry distance of top-of-rail friction modifiers', Proceedings of the Institution of Mechanical Engineers, Part F: Journal of Rail and Rapid Transit, 232(10), pp. 2418–2430.

Related paper

Asplund, M., Khan, S. A. and Nordmark, T. (2017) 'Improved wheel-rail system of Sweden's Iron Ore Line', Proceedings of the 11th International Heavy Haul Conference, Cape Town.

DISTRIBUTION OF WORK

The content of this section has been shared and accepted by all the authors who have contributed to the papers. The contributions of each named author of the scientific papers included in this thesis can be divided into the following main activities:

1. formulating the fundamental ideas of the study (initial idea and model development),

2. data collection,

3. analysis of the data,

4. writing the paper and analysing the results,

5. revision of important intellectual content,

6. final approval for inclusion in the PhD thesis.

Contributions of the main authors and co-authors of the appended papers

	Paper 1	Paper 2	Paper 3
Saad Ahmed Khan	1 – 6	1 – 6	1 – 6
Jan Lundberg	1, 5, 6	1, 5, 6	1, 2, 5, 6
Christer Stenström	5, 6	5, 6	2, 5, 6
Matti Rantatalo			2
Ingemar Persson	1, 3	1, 3	

ABBREVIATIONS AND NOTATION

AOA	Angle of attack
DI	Damage index
EDX	Energy-dispersive X-ray
FI	Fatigue index
FM	Friction modifier
FM-A	Friction modifier from company A (water-based friction modifier)
FM-B	Friction modifier from company B (water-based friction modifier)
FM-C	Friction modifier from company C (oil-based friction modifier)
H_i	High rail at position i
HV	Vickers hardness
IOL	Swedish Iron Ore Line
JVTC	Järnvägstekniskt centrum (Luleå Railway Research Center)
k	Material shear strength
K	Archard's wear constant
kkr	Thousand Swedish kronor
kr	Swedish krona
L_i	Low rail at position i
L/V	Lateral/vertical
LCC	Life cycle cost
LKAB	Luossavaara-Kiirunavaara Aktiebolag, Swedish mining company.
MB	Malmbanan (Swedish name of the Iron Ore Line)
MBS	Multi-body simulation
MGT	Million gross tonnes
RCF	Rolling contact fatigue
RQ	Research question
T	Traction force
TOR-FM	Top-of-rail friction modifier
γ	Creepage

TABLE OF CONTENTS

PART 1

1 INTRODUCTION

1.1 Background

Flaws related to the wheel-rail interface are resulting in high maintenance costs and lower availability and reliability for both the infrastructure owner and the rolling stock owners in Sweden. This is a typical situation for infrastructure and rolling stock owners over the whole world. For example, the American Association of Railroads (AAR) estimates that the flaws occurring at the wheel-rail interface of trains as a result of ineffective lubrication cost the United States' railroads more than two billion dollars each year for the maintenance and replacement of rail and wheels (Spiryagin et al., 2013).

In order to increase efficiency, the rolling stock operators, especially in the case of heavy haul transportation, have expressed the desire to increase the axle load. An increased axle load will bring new challenges, as it will mean more wear and RCF inflicted on both the wheel and rail. One of the biggest problems at present hindering the load carrying capacity of the tracks is rolling contact fatigue (RCF). It is more severe on curves, where the traction forces are higher than those on tangent tracks, and it is an increasing problem for railways all over the world. Since the early 1900s, RCF in railways has been a subject of research all over the world (Grassie, 2005). Previously it had not been considered as a major problem, as the axle load and/or the speed then were comparably lower. Natural wear is not as catastrophic as RCF, but can change the wheel and rail profiles, which may increase the traction forces. It should be noted in this connection that wear and friction have no clear established relationship and that there is a possibility that different third bodies have different wear rates at the same friction coefficient. According to the Stribeck curve (see Section A.6 in the appendix), a fluid lubricant can have different wear rates at the same friction coefficient depending on the viscosity of the lubricant, the sliding speed and the applied load. However, in typical conditions on the railway, decreased friction often results in less wear and RCF. Therefore, to increase the loading capacity without increasing the RCF and natural wear, either the strength of the rails should be increased or somehow the tractive force between the rail and wheel should be decreased (Cannon and Pradier, 1996). A shakedown map (for details see Section A.3 in the appendix) was created which shows a relationship between RCF generation and friction; on decreasing the friction coefficient, the probability of RCF generation decreases. Other solutions which minimize the effect of RCF include achieving a so-called "magic wear" rate or implementing surface grinding, also known as artificial wear. The magic wear rate is the natural wear rate that is equal to the RCF generation rate. In general, the magic wear rate is not achieved and natural wear changes the rail profiles. Therefore, many infrastructure owners and managers use surface grinding, which is the process of removing a small surface layer of defects and retaining the rail profiles; however, surface grinding increases the wear rate of the rails and decreases their total lifespan (Ekberg and Kabo, 2005).

The research presented in this thesis focuses on the effect of top-of-rail friction modifier (TOR-FM), or simply friction modifier (FM), on the RCF and wear on rails. TOR-FM is a black- or grey-coloured thick liquid which looks similar to particles suspended in a solvent and has an appearance like conventional very soft grease. The manufacturers claim that by introducing TOR-FM as an added third body, the friction coefficient between the rail and wheel can be controlled and kept at a value

around 0.35. Figure 1 shows the desired friction coefficient range on the wheel tread and the top of the rail. The present research does not focus on lubrication of the gauge face and wheel flange, where a minimum level of friction is desired. By introducing FM in the wheel-rail interface, the friction forces can be reduced, which in turn decreases the wear and RCF. After studying the positive claims made by the TOR-FM suppliers and the positive results presented in some publications, the Swedish Transport Administration (Trafikverket) is considering the implementation of a TOR-FM system on the Swedish Iron Ore Line (IOL). The manufacturers have claimed that there is also a possibility that such a solution would make it possible to increase the axle load to meet the future demands of ore transportation, as TOR-FM decreases the friction forces in the wheel-rail interface. This method has been tested and evaluated by other infrastructure owners, but needs to be investigated in greater detail for Arctic conditions, since a full implementation involves a very large investment. Moreover, a previously conducted preliminary study could not find any positive reason for the implementation of wayside TOR-FM systems on the IOL (Asplund, Nordmark and Gustafsson, 2015; Lemma et al., 2014). Therefore, a detailed study was required to evaluate the benefits and disadvantages of such systems.

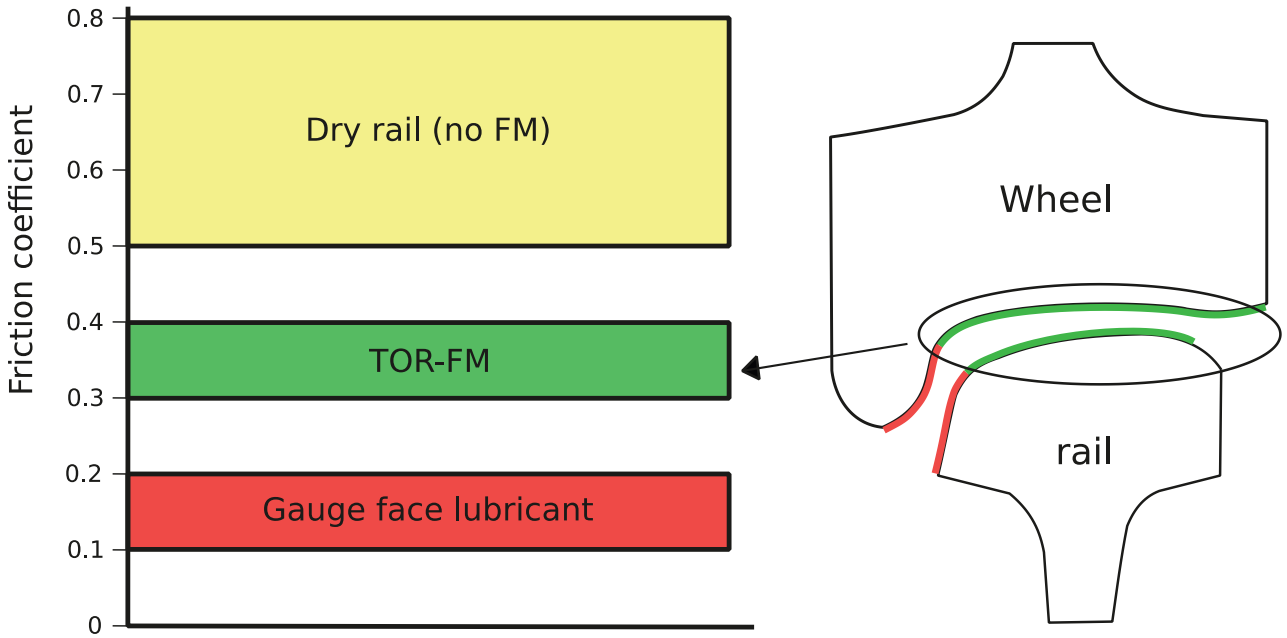

Figure 1. Desired friction coefficient range at different locations in the wheel-rail interface. Adapted from Stock et al. (2015).

1.2 Description of top-of-rail friction modifiers

A friction modifier used along with conventional lubricating oil consists of polar molecules that minimise the surface contacts during a sliding and rolling motion. As long as the frictional contact is moderate, these molecules provide a protective layer which minimises the wear of rubbing surfaces. If the contact pressure is high enough, then the molecules are sheared off, eliminating any potential benefits of the additives (Sunqing, Junxiu and Guoxu, 1999). In railway applications, a top-of-rail

friction modifier provides a protecting layer in the rail-wheel interface which minimizes the friction forces. This type of FM is a thick liquid which consists of soft particles suspended in a solvent and is applied between the top of the rail and the wheel tread as an additional third body. An FM reduces abrasive contact with asperities at the wheel-rail interface and, specifically, reduces the friction coefficient from high levels (0.5–0.8) under dry and FM-free conditions to an intermediate friction coefficient (0.3–0.4) (Hardwick, Lewis and Lewis, 2011).

In the present research, three different FMs were used, designated as FM-A, FM-B and FM-C. The benefits of all the FMs claimed by their manufacturers are similar, but their suppliers have not provided any declaration of ingredients. FM-A is a smoke-grey-coloured thick liquid similar to a latex paint and is designed to dry rapidly at the wheel-rail interface. The manufacturer claims that it contains no oil. FM-B is a black-coloured thick liquid that resembles black particles suspended in some solvent and appears like a conventional very soft grease that does not dry rapidly. By physical observation, it can be noted that FM-B contains some slow-drying solvent along with water, but the manufacturer states that FM-B is a water-based TOR-FM; it is classified as a water-based TOR-FM in the present research. FM-C is a smoke-grey-coloured thick liquid which looks like an oil paint. It is an oil-based FM, but is also designated as a TOR-FM in the present research as it is used for the same purpose as water-based FM.

Figure 2 (a) shows a wheel-rail interface where there is no FM and the third body consists mainly of brittle materials such as wear debris, oxides, sand, residue from trains, etc. On the application of an FM, the already present third body is mixed with the soft FM particles and carrier solvent, as shown in Figure 2 (b). The carrier solvent helps in distributing the FM particles. Figure 2 (c) shows a wheel-rail interface in a dry state where the FM particles stick to the rubbing surface and optimise the friction conditions through a shear displacement compensation mechanism in the third body layer. It is expected that stage c (Figure 2 (c)) in the case of FM-A will be reached very fast, as the manufacturing company claims this FM to be a fast-drying TOR-FM. Since FM-B is expected to be a slow-drying FM, it is expected that stage c (Figure 2 (c)) will be reached slowly or will never be reached with this FM, because the solvent will be partially evaporated or will not be evaporated at all. However, in the case of FM-C, it is expected that stage c will never be reached. The choice of solvent is critical, as the carry distance of the FM particles depends on the properties of the carrier solvent (Stock et al., 2016). The carrier solvent can further provide a reduction of friction through a mixed lubrication mechanism according to the Stribeck curve (Spikes, 1997).

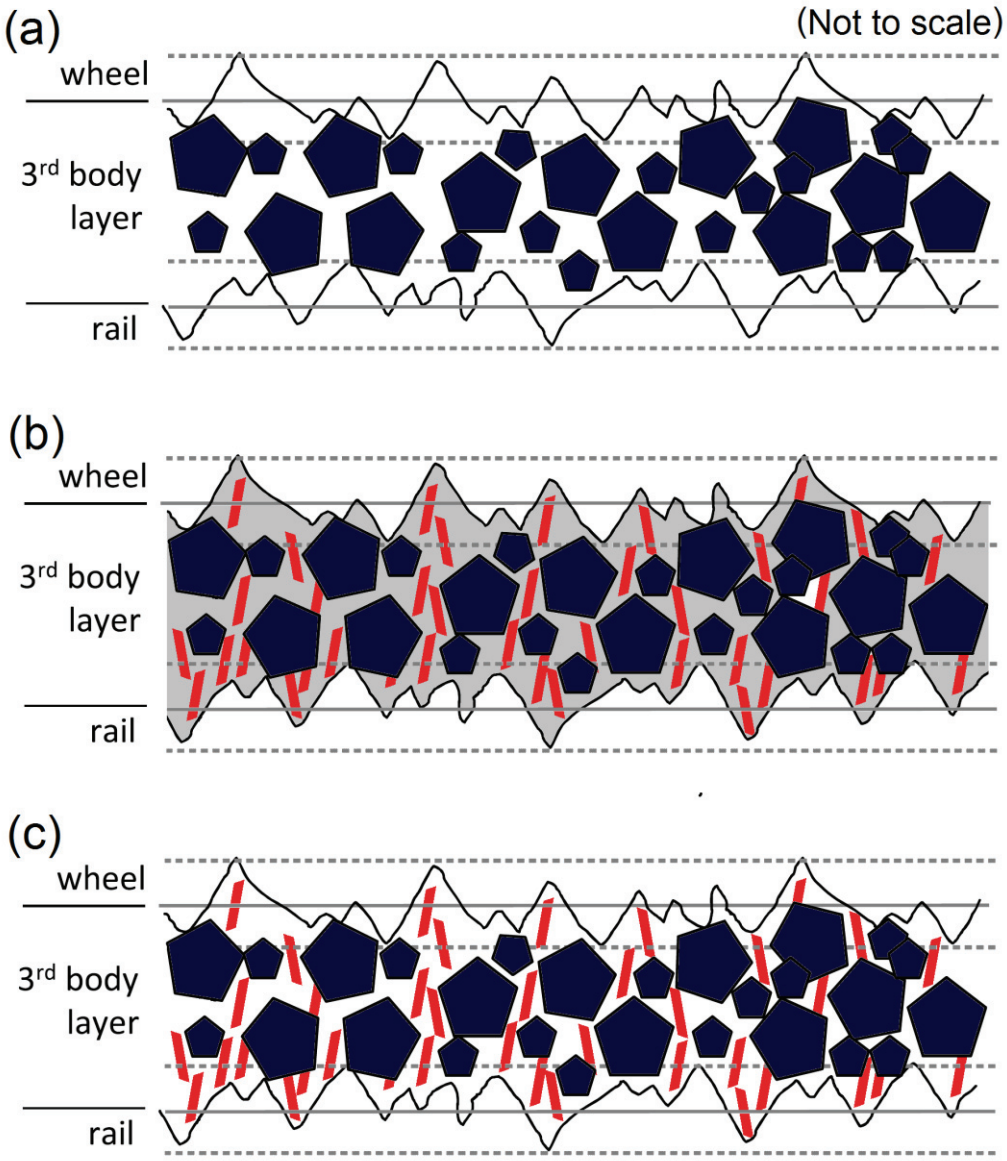

Figure 2. (a) Dry wheel-rail interface with a third body layer; a mixture of different third body materials, including wear debris, oxides, sand, etc. (b) FM particles with a carrier solvent at the wheel-rail interface providing a boundary or mixed lubrication conditions. (c) Dried FM particles adjust the shear properties of the third body layer, thereby adjusting to the desired friction level. Adapted from Stock et al. (2016).

Notes:-

- *In Sweden, all chemicals, including TOR-FMs, need to be approved by Trafikverket before they can be used on the railway track. All the TOR-FMs used in the present research have been approved by Trafikverket.*
- *Some authors use "lubricant" terminology for TOR-FMs irrespective of their base content. In contrast, some authors claim that only water-based FMs are TOR-FMs and all other types of TOR materials are TOR lubricants. From a tribological point of view, it is not incorrect to state that TOR-FM or FM is a lubricant. However colloquially, in the railway industry, the term "lubrication" is generally used for gauge face lubrication and "friction modifier" is used for TOR friction control substances. In the present research, the term TOR-FM or simply FM has been used for all fluid-based TOR-FMs irrespective of their base content.*

1.3 Malmbanan–The Iron Ore Line

The Iron Ore Line (IOL – Malmbanan in Swedish – shown in Figure 3) connects the ore mines in Kiruna and Malmberget to the seaports of Luleå in Sweden and Narvik in Norway. The IOL is a 398 km long railway line between Riksgränsen and Boden in Sweden. However, used colloquially, the term "IOL" often also includes the Ofoten Line from Riksgränsen at the Swedish-Norwegian border to Narvik in Norway and the northernmost part of Sweden's main railway line from Boden to Luleå. The total railway line from Narvik to Luleå is 473 km long. The railway line is a single-track electrified line mainly utilised by the ore freight trains operated by the Swedish mining company LKAB. The freight trains run by LKAB have an axle load of 30 tonnes, which is the heaviest in Europe. In addition, SJ operates passenger trains and CargoNet operates container freight trains on the IOL. The section connecting the mines to Narvik is designated as the northern loop and the section connecting the mines to Luleå is designated as the southern loop. The accumulated yearly tonnage on the northern loop is about 34 MGT and that on the southern loop is about 20 MGT (Asplund, Khan and Nordmark, 2017). The IOL has been in operation since 1903 (Viklund, 2012). The axle load was approximately 10 tonnes in 1903 (Viklund, 2012) and gradually increased to reach 30 tonnes at the end of 2000 (Nielsen and Stensson, 1999). A further increase in the axle load is expected in the future (Nordmark, 2016). The present research has taken the IOL as a case study and it is expected that the results will not differ significantly from the results of any studies performed in the future in other parts of the world with similar climate conditions.

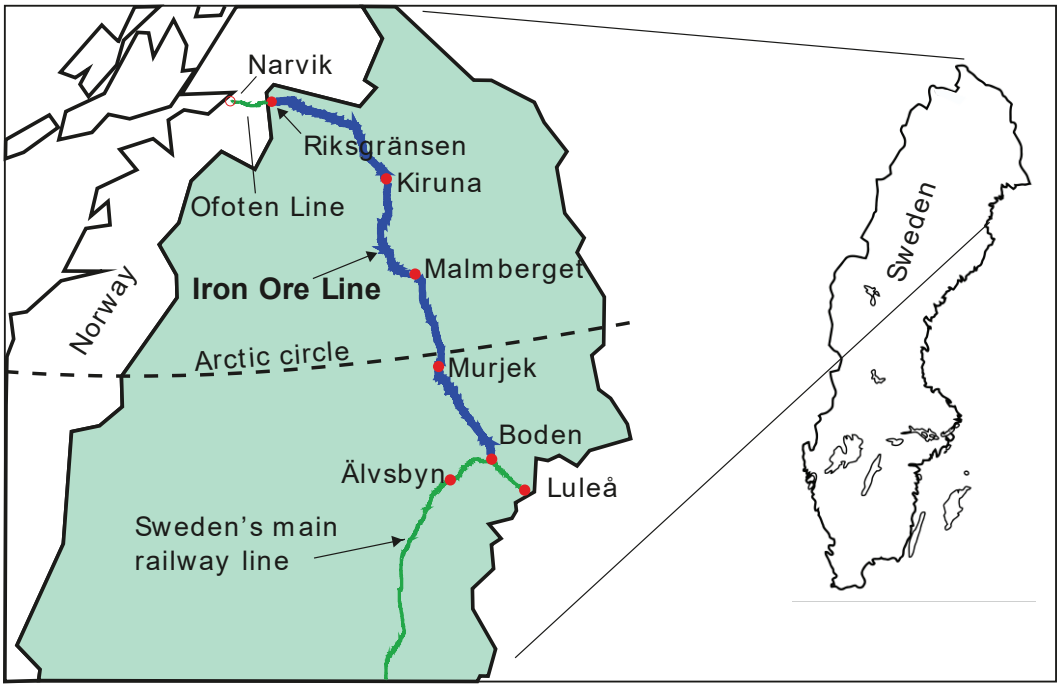

Figure 3. The Iron Ore Line, located in northern Sweden.

1.4 Problem statement

One of the main challenges for heavy haul train operators and infrastructure managers is to solve the increasing problems of wear and RCF. An additional challenge is to increase our knowledge of how to increase the lifetime of wheels and rails without compromising with regard to the high demands for traffic capacity. Trafikverket and LKAB desire to reap the benefits of a TOR-FM system in the form

of a reduction in the RCF and wear and a consequent increase in the life of the rails, but the technical and economic efficiency of such a system is not known, especially if installed in Nordic conditions.

At present, the freight trains operated by LKAB have an axle load of 30 tonnes, which LKAB is planning to increase to 32.5 tonnes, and the axle load is expected to increase even further in the future (Nordmark, 2016). The consequent increase in train tonnage will lead to a higher level of damage to the rail and wheels, resulting in higher maintenance costs for both Trafikverket and LKAB. All measures that can be taken to reduce these costs are a high priority. The expected increases in the axle load in the future make this issue even more important.

Wear, cracks and other defects in the wheel–rail interface are resulting in high maintenance costs and a lower service life for the wheel and rail. According to Trafikverket and LKAB, approximately 50% of the operational and maintenance costs of running a railway are generated in the wheel–rail interface. This is a typical situation for infrastructure and rolling stock owners over the whole world (Spiryagin et al., 2013). For this reason, it is of interest to study the influence of FM on the wheel–rail interface. According to Trafikverket and LKAB, most of the problems in the wheel–rail interface are due to contact fatigue, which is leading to an unacceptable increase in cracks. To avoid any formation of cracks above the safe limit, grinding of the rail is performed periodically; however, this is expensive, not only in terms of the maintenance cost, but also in terms of track access time and delays affecting timetables.

1.5 Aim and research questions

Aim

The aim of the research conducted for this thesis has been to investigate the effect of top-of-rail friction modifier on the wear, RCF and friction of rails and calculate the life cycle cost of a TOR-FM system.

Research questions (RQs)

RQ 1. What is the effect of friction control on the generation of RCF on rails according to the fatigue index and damage index methods?

RQ 2. What is the effect of TOR-FM on the wear, cracks and friction coefficient of rail in practice?

RQ 3. What is the life cycle cost of a TOR-FM system?

Table 1 Links the research questions to the published papers appended to this thesis.

Table 1. Linkage between the published research papers appended to the thesis and the research questions.

	Paper 1	**Paper 2**	**Paper 3**	**Thesis**
RQ 1	×	×		
RQ 2			×	×
RQ 3				×

2 STATE OF THE ART AND RESEARCH GAPS

2.1 State of the art

In this section, the results of a comprehensive literature review of TOR-FM are presented. The first tests of top-of-rail friction control were performed in the 1990s with the aim of overcoming the problem of RCF and wear (Eadie, 2014). However, gauge face lubrication had already been in existence since 1970 (Waara, 2006), but that is a topic which has not been focused on in the present research. The first research relating to TOR-FM was presented at a conference and published in 2003 (Eadie et al., 2003). Since then, a large amount of work has been carried out to explore the capability of different TOR-FMs to overcome problems like wear and RCF. In addition, researchers all around the world have also shown the positive effects of TOR-FM, which include the reduction of corrugation (Eadie et al., 2008; Eadie, Kalousek and Chiddick, 2002), the reduction of noise (Eadie, Santoro and Kalousek, 2005; Eadie and Santoro, 2006; Zoeteman, Dollevoet and Li, 2014). Some researchers have also explored friction management, which includes the performance of both gauge and top-of-rail lubrication to minimise the total wear and maximise the rail life (Lu et al., 2012). The present research focuses on the effect of TOR-FM on friction, wear and RCF.

In the following, a presentation of the state of the art is provided in three subsections, the first of which focuses on laboratory tests, the second on computer-based simulations, and the third on field tests. At the end of this chapter, the important conclusions of previous research are summarised to give an overall picture and draw conclusions concerning the research gaps.

2.1.1 Laboratory tests

In the case of TOR-FM, laboratory tests most often consist of pin-on-disc, twin-disc and full-scale rig tests. Details of each experiment are discussed below.

Matsumoto et al. (2004) used a 1:10 model test vehicle for investigating the effect of FM. The authors reported that controlling the friction between the wheel and rail was a direct and effective measure to improve the curving performance of bogies, because the curving performance of bogies depended to a great extent on the friction characteristics. The authors proposed that the "friction control" method not only controlled the friction coefficient, but also the friction characteristics, and stated that the friction characteristic was the damage caused at the interface of two surfaces. In conclusion, the authors stated that FM improved the curving performance in tight curves by reducing the friction and minimising the damage caused at the wheel-rail interface. The authors added that the creep characteristics of FM could be controlled by the amount of FM sprayed and the spraying interval.

Eadie et al. (2008) evaluated the effect of thin films of FM on the development of wear and RCF and compared the results obtained in a full-scale wheel-rail rig arrangement with the results of computer-based simulations. In the full-scale rig tests, the authors observed the best results when the FM was

applied after every 250 wheel passages. The wear and head check reduction for different application frequencies is shown in Figure 4. The y-axis represents the head check and wear rate and the x-axis represents the wheel passage intervals for the application of the FM; "dry" on the x-axis means that no FM has been applied. By comparing the result for the dry condition with that for the FM condition after 100,000 passages, a large difference in the wear can be noted. The authors claimed that the rail with FM applied at intervals of 250 and 50 wheel passages, i.e. with a higher application frequency, developed no cracks or head checks up to 100,000 wheel passages. Figure 5 shows the excellent condition of the rail surface when FM was applied at intervals of 250 wheel passages for a total of 100,000 passages along with the condition of new rail and rail without FM application for 100,000 passages.

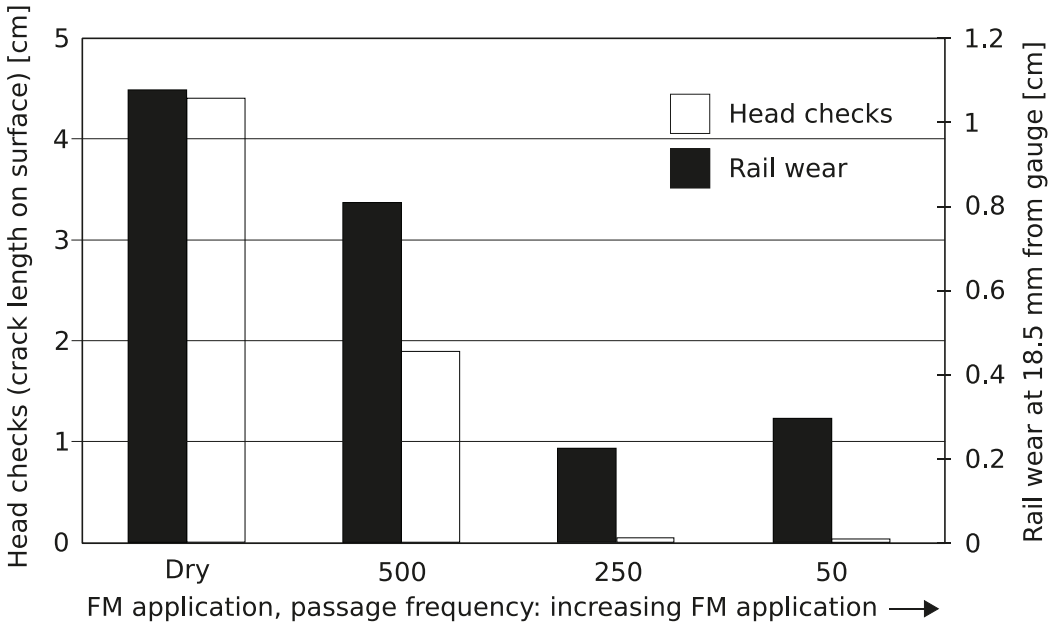

Figure 4. Effect of the FM application rate on wear and head check formation (Eadie et al., 2008).

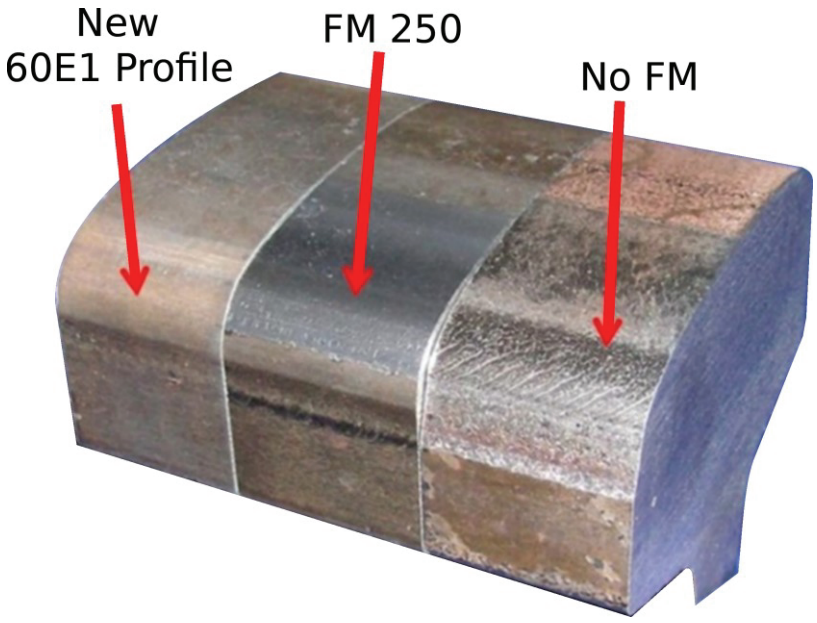

Figure 5. Rail samples (left to right): new 60E1 profile, rail with FM application at intervals of 250 passages and "dry" rail after 100,000 passages (Eadie et al., 2008).

Stock et al. (2011) examined the relative effects of FM on standard (R260) and premium (R350HT) rail using a test rig. Under dry conditions, the premium rail showed reduced wear and RCF generation compared to the standard rail. The authors claimed that the application of FM reduced the wear and RCF propensity for both the standard and the premium rail, with the best result achieved using a combination of R350HT and FM. The authors also claimed that the application of FM to pre-existing RCF cracks did not lead to an acceleration of the crack growth (e.g. by hydro-pressurization) under the experimental conditions used. The authors reviewed the field results for the effects of both premium rail and FM on the RCF, and the field results were found to be generally consistent with the test rig results. A summary of the results of the rig tests performed by the authors is shown in Figure 6. The y-axis represents the damage depth, which includes both the wear and the RCF. The x-axis represents the type of material, the third body condition, and the number of wheel passages ("k" on the x-axis represents 1,000).

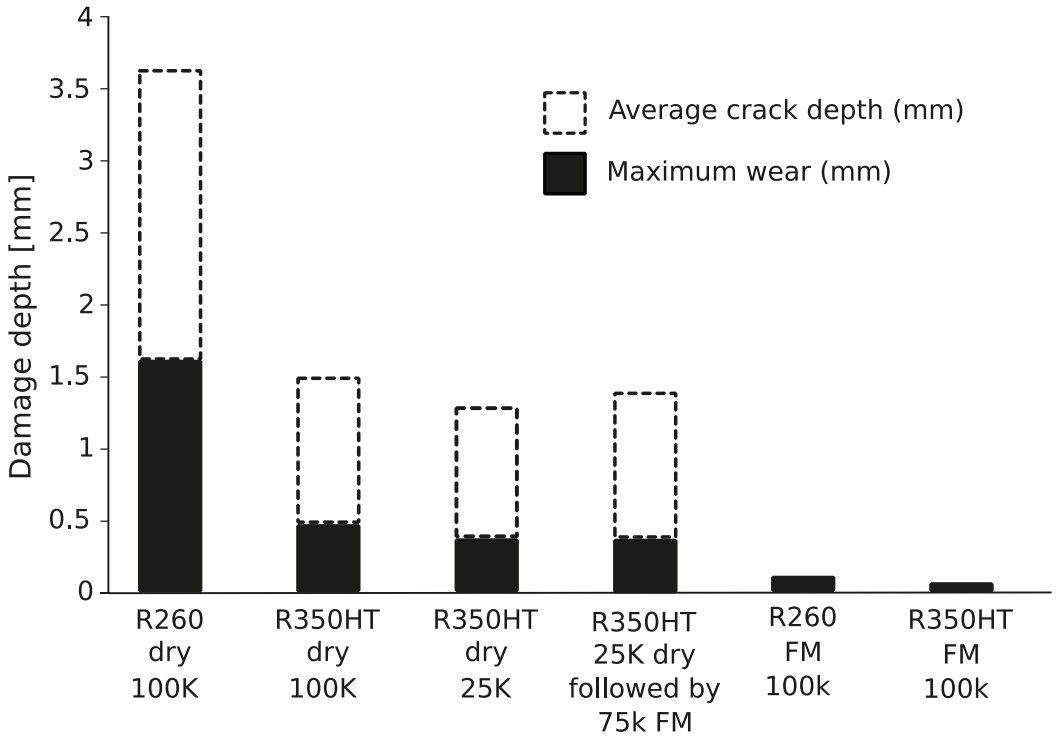

Figure 6. Combined damage of wear and RCF for selected rig tests; "k" on the x-axis represents 1,000 (Stock et al., 2011).

Zhu et al. (2013) investigated the friction in the wheel-rail interface using pin-on-disc testing. Factors such as humidity, temperature, and iron oxides or rust were studied and discussed. The materials used in the study were UIC60 900A rail and R7 wheel material. A contact pressure of 900 MPa and a sliding velocity of 0.01 m/s were used to perform all the tests. The authors concluded that friction is sensitive to humidity, and the friction coefficient decreases with an increasing relative humidity up to a saturation level, after which it becomes stable. However, in the case of heavy rust, friction becomes highly independent of the temperature and relative humidity.

Further, Abbasi et al. (2013) investigated the effects of FM on the characteristics of airborne particles generated in wheel and rail contacts by using a pin-on-disc machine. The contact pressure was 550 MPa. Three different particle measurement instruments were used to measure the airborne particle concentration, which is the number of particles per litre of air, in various particle-diameter size

intervals. The authors reported that the number of coarse particles released into the wheel–rail interface due to wear could be reduced by using water-based FM. However, they also reported that in the case of water-based TOR-FM, a high application rate was needed due to the vaporization of FM, especially in the case of a potentially high contact pressure such as that prevailing on railways.

Hardwick and Lewis (2014) reported that only water-based (dry film) FM minimised the generation of cracks and wear and suppressed the propagation of pre-generated cracks. They tested alternative TOR-FM materials on pre-existing RCF cracks. The experiments were performed using twin-disc testing equipment and the materials used were R8T wheel material and 260-grade rail. The lubricants assessed were water, water-based (dry film) TOR-FM, gauge face lubricant, synthetic oil-based TOR-FM, and grease-based TOR-FM. For all the measurements, the authors first performed 4,000 cycles in the dry condition, which allowed the establishment of damage prior to any product application. Subsequently, a further 21,000 cycles were performed with the alternative TOR-FM materials at an application rate of one drop per second to keep the contact flooded. The material loss per cycle with respect to the alternative FM materials is presented in Figure 7. In the case of the dry condition, the authors have shown the result for the first 4,000 cycles and that for the subsequent 21,000 cycles separately in the figure. Table 2 presents the crack parameters under the influence of the alternative TOR-FM materials. All the alternative FM materials, except for the water-based (dry film) TOR-FM, showed more damage than the dry (FM-free) condition even though there was a lower friction coefficient in the FM condition than in the dry condition; the gauge face lubricant is an exception with regard to wear. The authors also claimed that non-drying FM products (mainly oil-based FMs) would cause further deterioration to rails with pre-existing cracks.

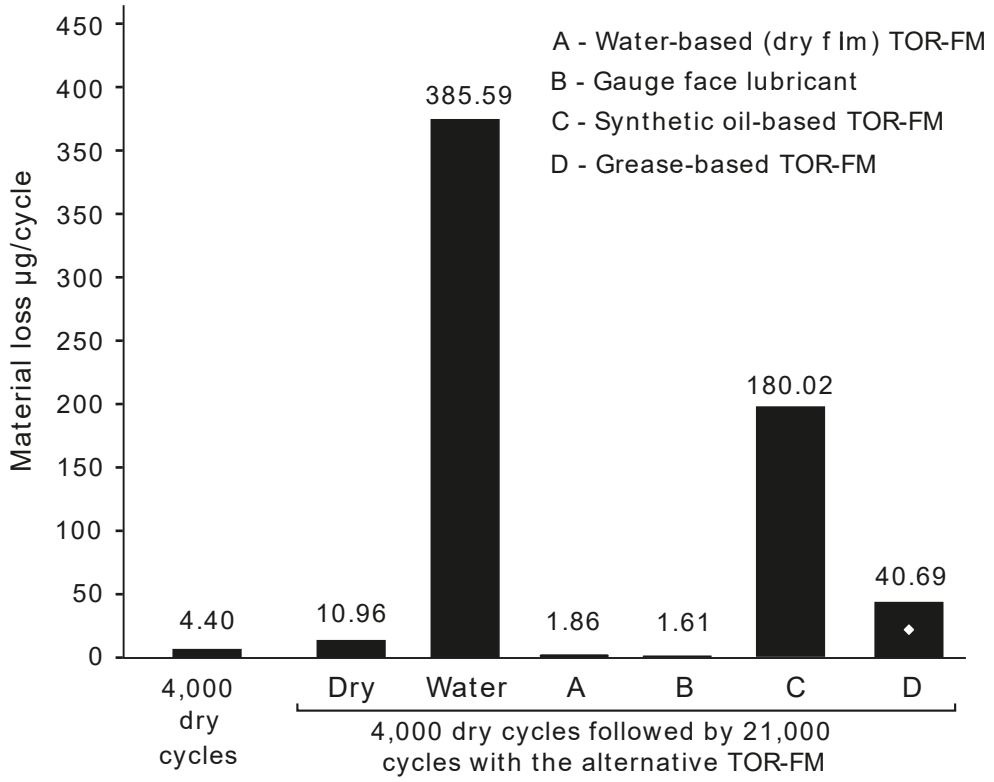

Figure 7. Material loss data for 260-grade rail material (Hardwick and Lewis, 2014).

Table 2. Crack parameters under different lubricating conditions (Hardwick and Lewis, 2014).

	Dry	Water	Water-based TOR-FM	Gauge face lubricant	Synthetic oil-based TOR-FM	Grease-based TOR-FM
Crack length [μm]	422−432	3316	150−214	1846−2430	2757	1586-1723
Crack depth [μm]	16.8	890	10−30	990	1319	375−555
Crack angle [°]	8	21.5	8	15−30	70-90	15 – 30
Average traction coefficient	0.37	0.22	0.1	0.07	0.07	0.06

Focusing on some recent research relating to TOR-FM, one finds that Galas et al. (2018) investigated the role of typical water-based FM constituents in terms of adhesion and film formation. The ball-on-disc apparatus was employed to achieve a rolling-sliding contact. The results showed that the lasting effect of these substances was controlled by the applied amount, whereas the average adhesion during the experiments was mainly affected by the substance composition. The performance of the substances was greatly affected by the evaporation of the base medium, but both "wet" and "dry" complex substances were able to reduce the wear rate, roughness and surface damage in comparison with dry conditions.

Seo et al. (2018) investigated the effects of an FM on wear, RCF and friction by using KS60 rail steel and RSW wheel steel in a twin-disc machine. The authors stated that the FM used was a hybrid FM with drying material characteristics. The tests were performed at 500 rpm at a contact pressure of 1,100 MPa. The discs were 60 mm in diameter and 6 mm in thickness. The authors also showed a relationship between the traction coefficient and slip ratio percentages ranging from 0 to 2%. It can be seen in Figure 8 that at a slip ratio of approximately 1%, saturated friction was achieved with a spraying interval of 0.5 seconds. The test under the FM condition was performed using three different spraying intervals: 0.2, 0.5 and 1.0 seconds. The amount of FM was not specified, but it was sprayed with the help of compressed air and the distance between the nozzle and disc was 30 mm. The progress of contact fatigue damage severely increased at a spraying of 0.2 seconds. The authors concluded that the wear under the dry condition was largest, while that under the water condition was minimum. However, the RCF generation was faster in both the water and the FM condition when compared to the dry condition. The authors explained that the FM induced a mixed condition that existed at the same time as the wet condition and the dry condition. According to the authors, the traction force due to the friction of the dry condition initiated cracks and the crack growth rate became faster due to the fluid entrapment mechanism under the wet condition. Fluid entrapment mechanisms in rails have been studied in greater detail by Fletcher, Hyde and Kapoor (2008) and Bogdański and Lewicki (2008).

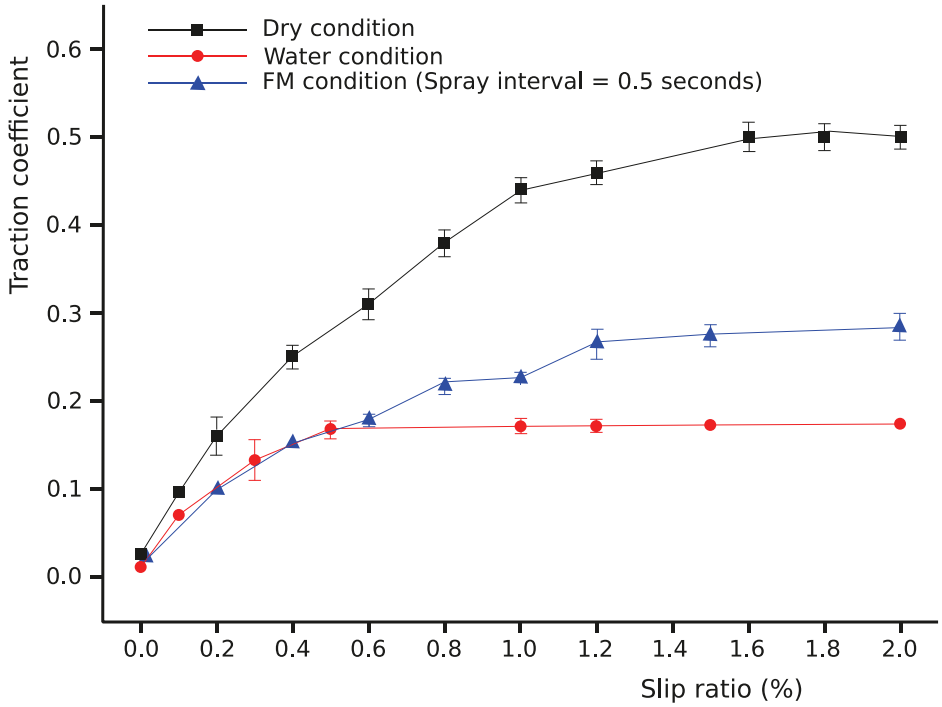

Figure 8. Comparison of traction coefficients in dry, water and FM conditions with a spraying interval of 0.5 seconds (Seo et al., 2018).

2.1.2 Computer-based simulations

Wear and RCF prediction for the wheel-rail interface using computer-based simulation, generally three-dimensional multi-body simulation (MBS), is emerging as an important topic in the field of railway research. Such prediction uses mathematical models and takes input from field and laboratory tests. Initially, models were developed to identify and improve the underlying operating conditions and/or investigate the potential root cause of the damage patterns (Ekberg et al., 2014; Pearce and Sherratt, 1991; Ekberg and Kabo, 2005; Burstow, 2004). Nia et al. (2015) and Dirks and Enblom (2011) predicted RCF and wear evolution on the wheels of different locomotives. Pombo et al. (2011) developed a wear prediction tool for steel railway wheels using three alternative wear functions. By using the properties of an FM, VanderMarel et al. (2013) investigated the energy savings to be gained from top-of-rail friction control by using models in a multibody software package. Two of the investigations relating to the effects of TOR-FM on wear and RCF are discussed below.

Spiryagin et al. (2013) simulated wear index using an MBS software package to interpret the relationship between wheel-rail wear and various friction conditions. For performing the simulations, first a relationship between friction coefficients and longitudinal creepage for the dry and applied-FM conditions was generated, as shown in Figure 9. The y-axis represents the friction coefficients and the x-axis represents the longitudinal creepage; the values of both are unitless and, therefore, the authors use "[-]" to denote the unit. Subsequently, the variations in the wear index with respect to the friction conditions at the wheel-rail interface were simulated. The simulated results are shown in Figure 10, where the y-axis represents the simulated wear index and the x-axis represents different wheels of a wagon. "B" stands for "bogie" and is followed by the bogie number in the wagon, "A" stands for "axle" and is followed by the axle number in the bogie, and "L" and "R" stand for the left and right wheels, respectively. The authors concluded that the leading axle had severe wear issues and by reducing the friction, a wear reduction of approximately 60% could be achieved.

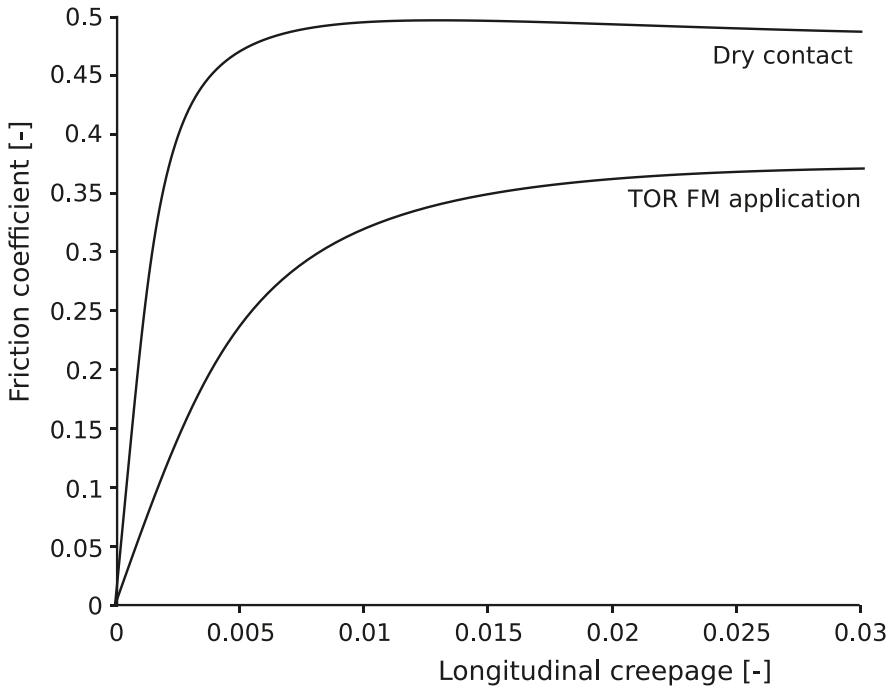

Figure 9. Relationship between friction coefficients and longitudinal creepage for the dry and applied-FM conditions (Spiryagin et al., 2013).

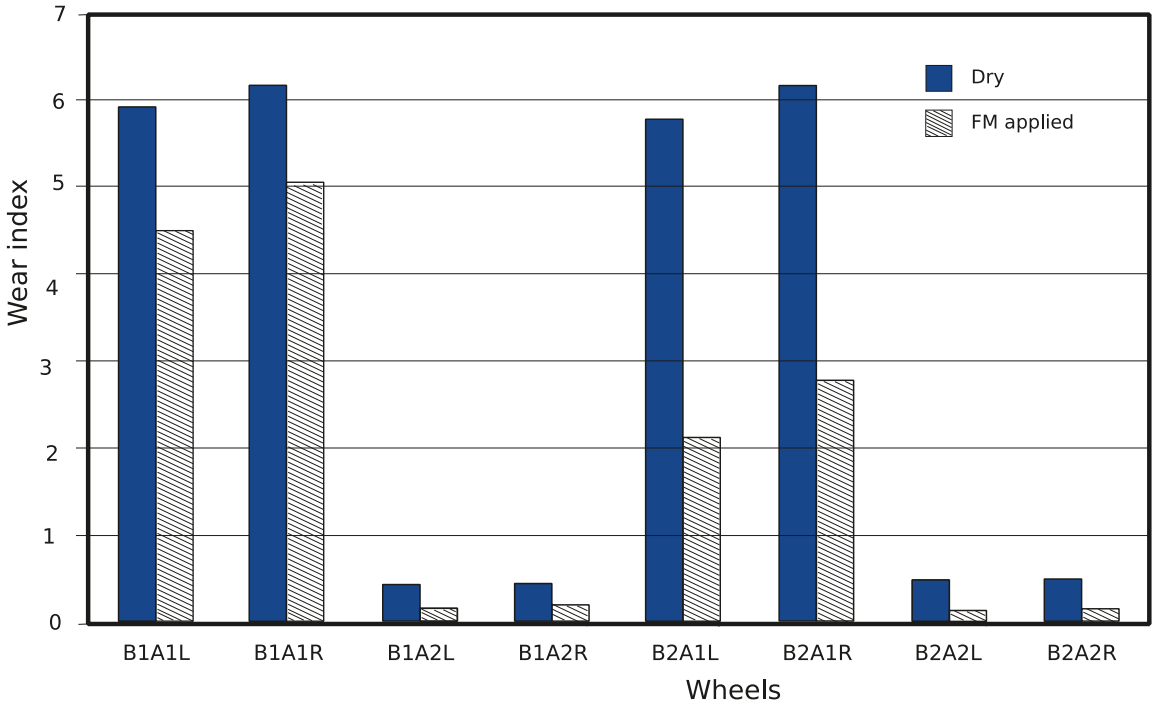

Figure 10. Simulated wear index comparison for the dry and applied-FM conditions (wheel description: B=bogie, A=axle, L=left, R=right) (Spiryagin et al., 2013).

Eadie et al. (2008) performed contact modelling along with a full-scale wheel-rail test rig evaluation as discussed in Section 2.1.1 above. The simulation results show a relation between the peak pressures (P_o), material shear strength (k) and traction coefficient on a shakedown diagram. In the dry (FM-free) condition, the normal pressures and tangential tractions were in the ratcheting zone, whereas in the applied-FM condition, the peak pressures and tractions shifted to the "safe" zone from the crack zone as shown in Figure 11.

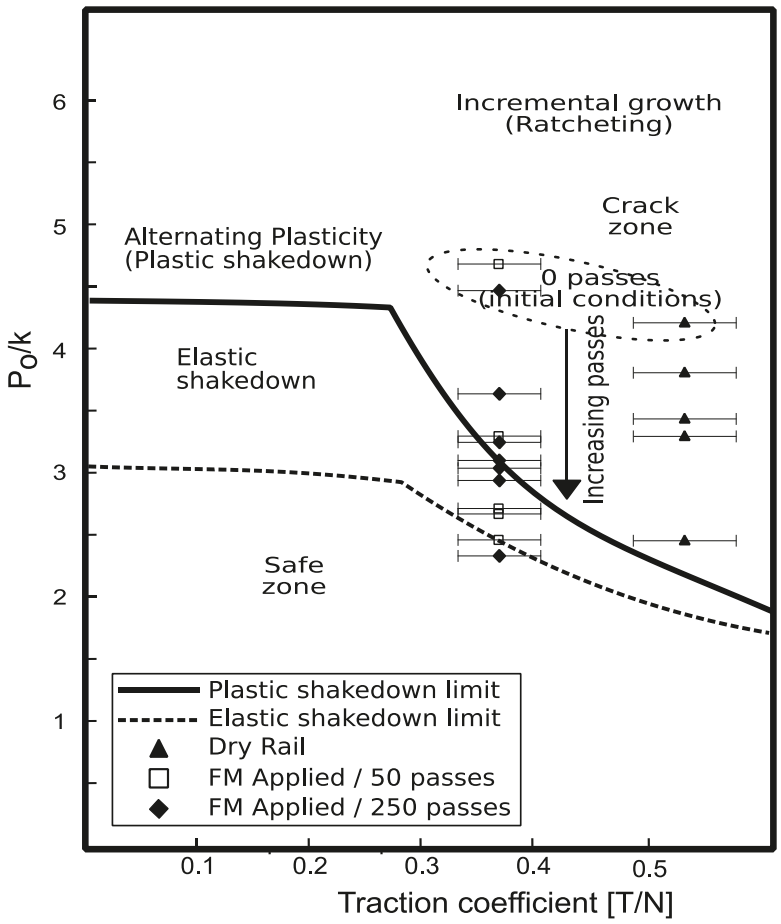

Figure 11. Shakedown diagram for the dry and FM conditions (Eadie, Elvidge, et al., 2008).

2.1.3 Field tests

The effects of TOR-FM on friction and wear have not only been tested in the laboratory, but also in field tests. Field tests relating to the effect of TOR-FM on RCF need to be explored since realistic parameters, for example third bodies, are not considered in laboratory measurements and computer-based simulations. Field tests are expensive and require a large amount of effort to perform measurements compared to laboratory tests and simulations. However, field measurements are more realistic since they have no scaling issues and in the field there are realistic third bodies and contact pressure; controlling all these factors in the case of laboratory tests and simulations is difficult. On the other hand, it can be difficult to vary parameters in the field.

The first field study using TOR-FM was published by Eadie et al. (2003). Two different application methods, an on-board and a wayside system, were used at Pueblo in the United States. The FM application rate was 0.5−1.5 L/mile (0.31−0.94 L/km) in the case of the on-board system and one litre per 1,000 axles in the case of the wayside system. The authors reported the head loss results normalised to tonnage as a function of the curvature when using the on-board system, as shown in Figure 12. The results obtained with no FM application concern the period from June 1997 to June 2001, while those for the FM application from the on-board system concern the period from June 2001 to June 2002. The data show that with the application of TOR-FM by the on-board system, the wear was reduced approximately by 67% (both the head and the gauge wear). The authors also measured the lateral forces for both the on-board and the wayside system and claimed a lateral force reduction of approximately 40%, as shown in Figure 13. The reduction of the lateral forces in the case

of the on-board method was greater than that in the case of the wayside TOR-FM method. In the case of the wayside system, two units were installed, one before and another after a curve with a 145 m radius (a 12 degree curve). A lateral force detector was installed approximately in the middle of the curve and approximately halfway between the two installed wayside units, i.e. at a distance of 1,036 and 1,189 m from unit one and two, respectively. Based on this, the authors claimed that the FM had a carry distance of at least 1,189 m since there was a reduction in the lateral forces when using TOR-FM.

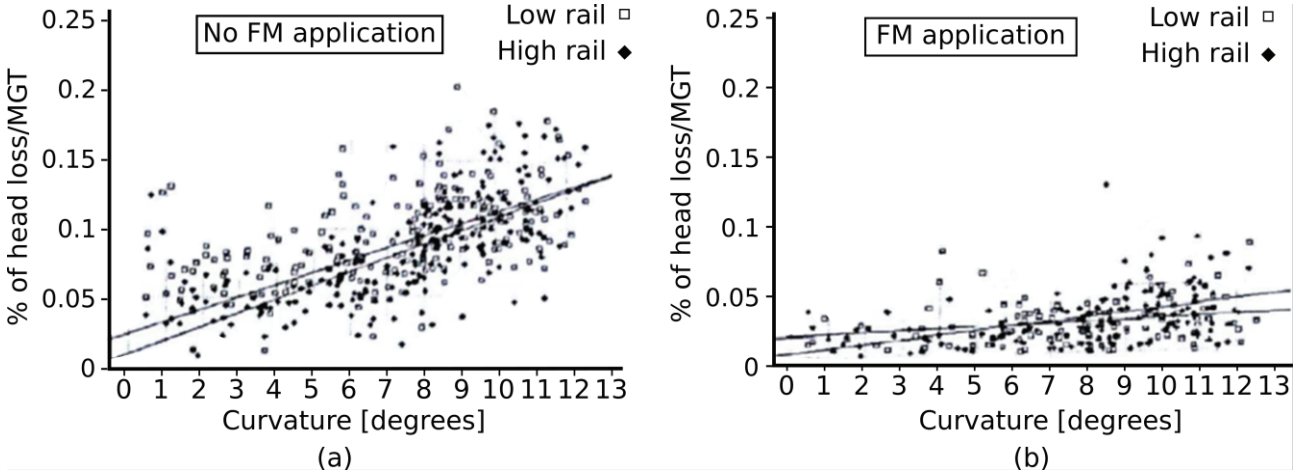

Figure 12. Head loss rate with respect to tonnage: (a) no FM application, (b) FM application by an on-board system (Eadie et al., 2003).

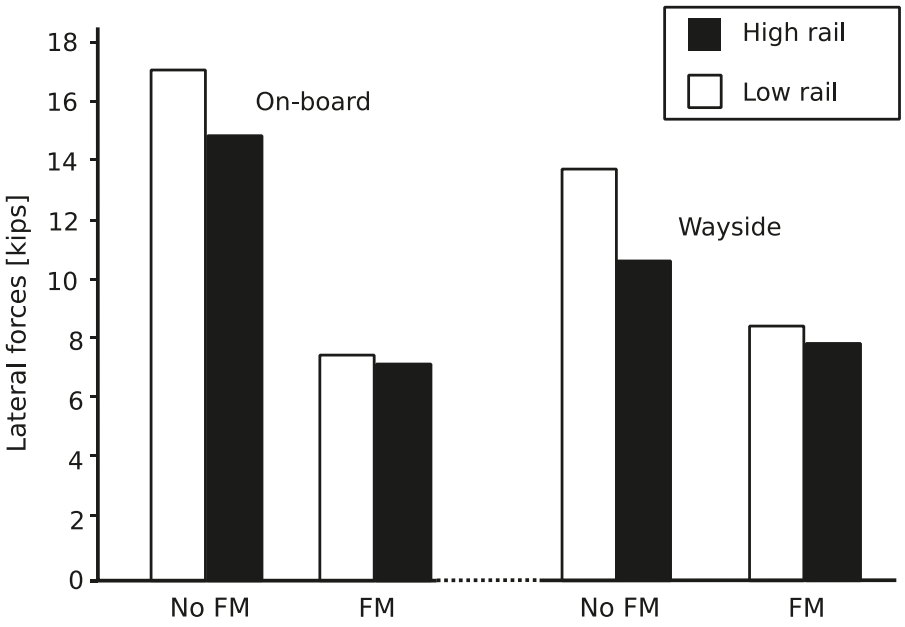

Figure 13. Comparison of the lateral force reduction achieved by the on-board and wayside application methods; 1 kips = 4.45 kN (Eadie et al., 2003).

Later, Eadie et al. (2006) published results from multiple wayside trials on heavy haul railways. The wayside TOR-FM system was extensively tested over widespread territories in North America with heavy haul railways. A consistent reduction in the lateral forces of 30% and rail wear reductions of up to 60% at three different test sites were reported. The typical coefficient of friction under North American freight transport conditions was measured with a hand-pushed tribometer from Salient Systems; the coefficient in the dry top-of-rail condition was found to be approximately 0.5, while that in the FM condition was found to be approximately 0.35. This reduction in the coefficient of friction

led to a significant reduction in the lateral forces, on average by 30%. Figure 14 summarizes the overall lateral force reduction at different sites on the low rail and high rail. The authors also defended the poor results obtained at site 4 (downgrade) (shown in Figure 14), explaining that they were due to the use of tread braking. Moreover, the authors suggested that the application of FM in the case of a downhill slope required a closer spacing of the TOR-FM units and/or an increase in the application rate for the FM. Since tread brakes remove FM from the wheel, a compensating increase in the FM was required. Another factor for the poor performance on curves running downhill could be the high wheel temperature caused by tread braking.

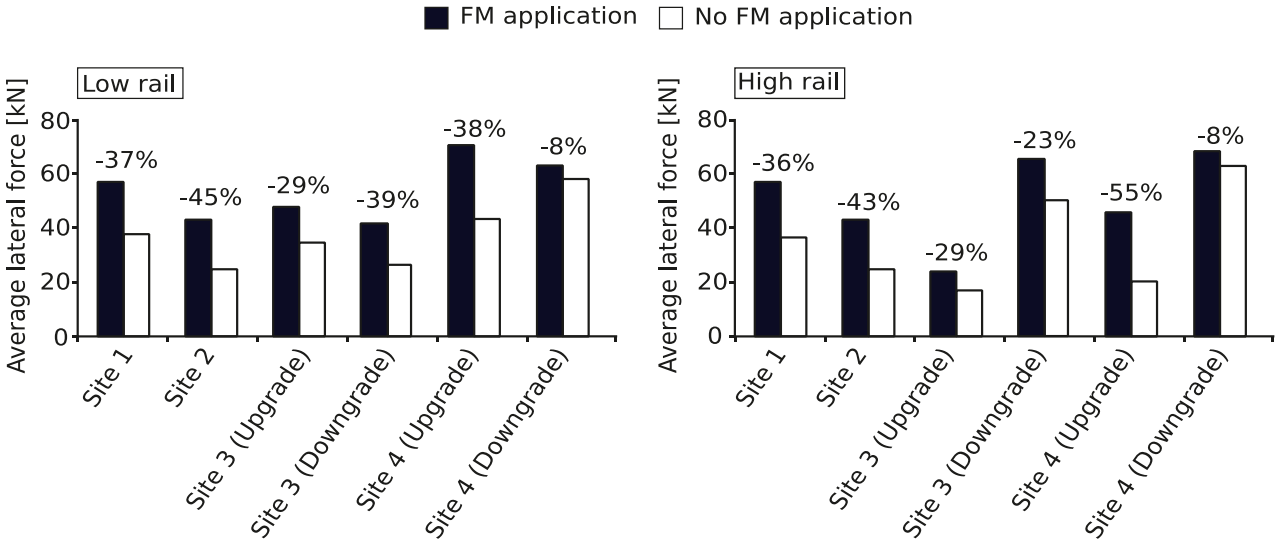

Figure 14. Lateral forces at different sites where the wayside system was installed, with and without FM; (a) low rail and (b) high rail (Eadie et al., 2006).

Oldknow et al. (2012) presented an analysis of the influence of materials that can be present in the so-called ''third-body layer'' at the wheel-rail interface on curving forces generated in heavy haul operating conditions. The authors explained that the third-body layer was the interfacial layer whose shear properties determined the bulk frictional characteristics that emerged in wheel-rail contact. The authors postulated that precipitation (rain) provided an effective form of lubrication at the wheel tread-rail head interface, reducing the curving forces and the corresponding wear. This postulate was explored by the authors through the analysis of lateral and vertical (L/V) force data collected under a wide range of environmental conditions in full-scale revenue-earning service. In the dry case, i.e. with no FM and water, it was found that there was an approximate friction coefficient of 0.5 with a wide scatter in the L/V forces. In the case of rainfall (without FM), an average friction coefficient of approximately 0.3 was found. In the case of the FM condition without rain, the authors discovered a narrow distribution of L/V values and an average friction coefficient of approximately 0.2. The impact of both precipitation and friction control was as follows: initially the friction coefficient was approximately 0.3 (corresponding to wet conditions), rising to a mode at approximately 0.4 (before friction control due to FM gains effectiveness) and then, with effective friction control due to FM in place, it dropped to a value slightly below 0.2.

All the results published until 2012 were mainly obtained through research conducted in North America. Zhou et al. (2013) published the results of a field test performed on a typical sharp curve of the heavy haul railway in China. For the application of FM, a wayside system was used. The TOR equipment was installed at a distance of 350 metres from the curve. The track radius was approximately 500 m and the rail was made of U75V steel (75 kg/m). The approximate load per train was 5,500

tonnes and the annual gross carrying weight was about 110−130 MGT, with an axle load from 21−23 tonnes. The average speed of the train was 60 km/h. The authors reported a wear of about 0.0125 mm/MGT and 0.010 mm/MGT on the high rail and low rail, respectively, when no FM was applied. When FM was applied, the results showed a wear of 0.0107 mm/MGT and 0.006 mm/MGT on the high rail and low rail, respectively. The decrease in the vertical wear of the high rail was about 14.4% and that of the low rail was about 40%.

Stock et al. (2016) explored the concept of TOR friction adjustment. The authors divided the TOR fluids into FMs and TOR lubricants. According to Stock et al. (2016), FMs are fast-drying materials that provide optimised friction conditions in the dry state through a shear displacement mechanism in the third body layer in the wheel-rail interface, over a wide range of application rates. TOR lubricants, on the other hand, are to be considered as non- or slow-drying products that provide a reduction of the friction coefficient through an application-rate-dependent mixed-mode lubrication mechanism. In "mix-mode lubrication", the non-evaporated carrier solvent of the FM contributes in decreasing the friction as a lubricant along with the FM particles. Stock et al. (2016) presented the results of a trial study conducted by Transportation Technology Inc. at a high tonnage loop with a length of 4,350 m to investigate different TOR materials under heavy haul conditions. Unfortunately, the trail study discussed by these authors could not be obtained by the author of this thesis. As described by the authors, the TOR materials were applied using a wayside TOR-FM system installed 880 m away from a lateral force measurement station. The results from the TOR material trials (see Figure 15) show a relationship between the lateral force reductions in percentage and the application rates of the different materials. The solid lines represent the results for the "water-based" products and the dashed lines represent those for the "oil-based" products. It can be seen from Figure 15 that the reduction in the lateral forces is highly dependent on the type of friction modifier used and the amount applied.

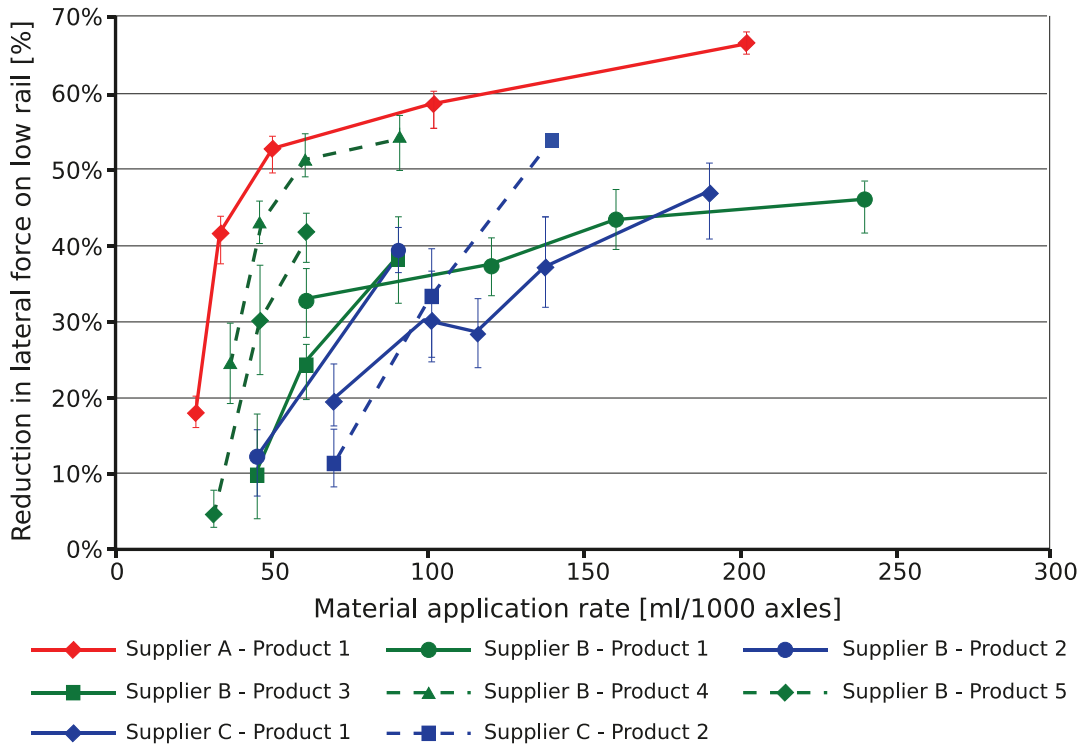

Figure 15. Lateral force on the low rail when different TOR-FM products from different suppliers were applied at different application rates using a wayside TOR-FM system located 800 m away from a lateral force measurement station (Stock et al., 2016).

Stock et al. (2016) also presented friction measurements obtained with a hand-pushed tribometer in research conducted by the Transportation Technology Center. According to Stock et al. (2016), the values obtained in this research only give a partial indication of the actual friction values since a hand-pushed tribometer only measures the friction between the tribometer wheel and the rail surface. According to the author of the present thesis, such a tribometer does not have a realistic contact pressure and the creepage is unknown. Figure 16 shows the relationship between the friction coefficient on the y-axis and the application rate of different types of TOR materials on the x-axis. The water-based TOR-FM shows a constant friction coefficient irrespective of the amount applied, while in the case of the oil-based and the hybrid TOR-FM, the friction coefficient decreases with an increase in the application rate. When comparing the products, the authors claimed that a fast-drying FM provided a number of proven benefits, for example wear reduction, RCF mitigation, fuel savings and corrugation suppression, without interfering with safe train operations. Non-drying TOR materials might provide similar benefits in areas that are directly related to a reduced friction coefficient, such as wheel-rail wear and fuel savings. With respect to carry-down characteristics, non-drying materials could provide improved benefits compared to drying materials. On the other hand, in areas like braking and traction, non-drying materials might entail some unintended side-effects or even risks.

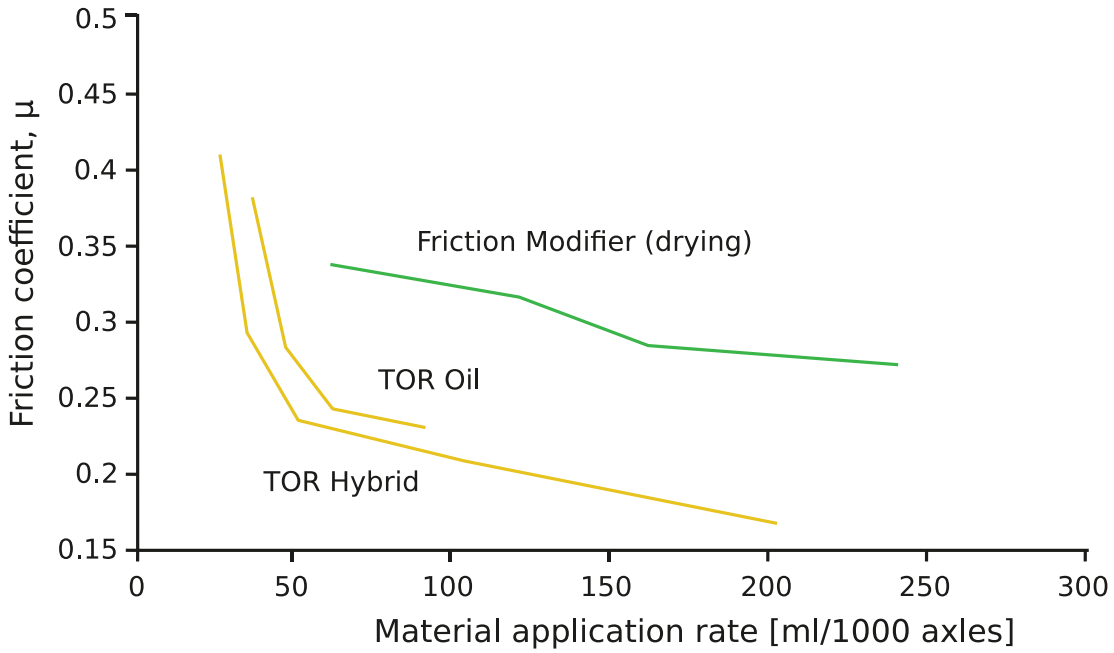

Figure 16. The friction coefficients obtained with different material application rates; it is assumed that 0.5 is the friction coefficient for dry conditions (Stock et al., 2016).

In one of the most recent field studies, Stock et al. (2017) investigated the wheel wear and defects of unit coal trains running over the same track. One of the fleet was equipped with an on-board TOR-FM system and was compared with another train that lacked such a system. The authors claimed that through the application of TOR-FM, the total wheel replacements for both the TOR-FM-equipped train and the non-equipped train were reduced. The TOR-FM-equipped train showed a reduction of 60.2% for wheel replacements in comparison with the train that was not equipped with TOR-FM. The authors also claimed that the calculated wheel wear rates based on flange height measurements were reduced by 54% for the train with TOR-FM equipment. Another claim was that the application of TOR-FM also helped the non-equipped train to reduce the wear by 23%. The authors suggested that the reported improvements in the wheel performance for the train that was not equipped with

the TOR-FM system were due to the benefits of retention of TOR-FM applied to the same track which both utility trains operated on.

Based on all the above tests, one can establish that it has been claimed that TOR-FM controls the friction coefficient between the rails and wheels and keeps it to a value near 0.3, as well as achieving a wear reduction of up to 65%. Contrasting with these claims are the results published by Lundberg et al. (2014) for friction coefficients obtained between the rails of IOL and the wheels on a 360 tonne and 10,800 kW IORE locomotive. The friction was measured using the locomotive's inbuilt traction-force measurement system. The locomotive used consisted of a pair of connected locomotives, which hauled 68 fully loaded wagons (120 tonnes/wagon). The measurements were performed with and without water-based FM on the IOL between Kiruna in Sweden and Narvik in Norway. The friction coefficient tests were repeated at the same time and place using a conventional hand-pushed tribometer and the results were compared with the results from the train. The authors concluded that the real friction coefficient was highly dependent on the amount of applied FM. The application of a large amount of FM could result in unacceptably low friction coefficients, on average 0.13 to 0.16. Even a thin layer of FM had a low friction coefficient, on average 0.23. An additional claim was that the hand-pushed tribometer generally measured excessively high friction coefficients compared with the real values and was not capable of indicating accurate tendencies.

Lemma et al. (2014) and Asplund et al. (2015) also studied TOR-FM systems on the IOL. To control the friction of the wheel-rail interface, wayside equipment was used at two locations. By using a hand-pushed tribometer, a friction coefficient was measured which was the same as that for a dry condition, even though a wayside TOR-FM system was present and functioning. The authors claimed that the friction measured with a tribometer had a high precision, but its accuracy compared to the real friction between the wheel and rail was unknown. They did not find any significant difference between the situation before and the situation after the application of TOR-FM on the IOL. Based on their investigation, the authors concluded that they had not, as yet, been able to find a reason for implementing TOR-FM lubrication on the IOL. The authors also stated that the reason for the poor performance of TOR-FM could be the good quality of the wheels and rail in Sweden. They suggested that more research was needed to determine when TOR-FM would give advantages and reduce the life cycle cost for the wheel-rail system.

Table 3 summarises all the important conclusions and/or claims made by authors who have conducted research relating to TOR-FM systems.

Table 3. Summary of the state of the art.

Laboratory tests	
Conclusions	***Reference***
• The curving performance is improved in tight curves by using TOR-FM. • When FM is applied, the creep characteristics can be controlled by the amount of spraying. • Friction control methods not only control the friction coefficient, but also minimise the damage caused at the wheel-rail interface.	Matsumoto et al. (2004)

• TOR-FM gives best results when applied at intervals of 250 revolutions. With this application rate, the wheel developed no cracks or head checks up to 100,000 wheel passages.	Eadie et al. (2008)
• The application of FM reduces the wear and the RCF tendency for both standard and premium rail, with the best result being achieved with a combination of R350 HT and FM. • The application of FM to pre-existing RCF cracks did not lead to an acceleration of the crack growth (e.g. by hydro-pressurization).	Stock et al. (2011)
• Friction is sensitive to humidity and the friction coefficient decreases with an increasing relative humidity up to a saturation level, after which it becomes stable. • In the case of heavy rust, the friction becomes highly independent of the temperature and relative humidity.	Zhu et al. (2013)
• The number of coarse particles released into the wheel-rail interface due to wear can be reduced by using water-based TOR-FM. • Water-based TOR-FM should only be used after considering the high replacement rate needed due to vaporization.	Abbasi et al. (2013)
• FM not only minimises the generation of cracks and wear, but also suppresses the propagation of pre-generated cracks.	Hardwick and Lewis (2014)
• The lasting effect of TOR-FM is controlled by the applied amount, whereas the average adhesion during the experiment is mainly affected by the substance composition. • The performance of substances is greatly affected by evaporation of the base medium.	Galas et al. (2018)
• With an increase in the FM spray rate, the progress of pre-existing RCF increases. • Contact fatigue damage under the FM condition occurred faster than that under the water condition. • Cracks were initiated by the traction force due to the friction of the dry condition, and the crack growth rate became faster due to the fluid entrapment mechanism under the wet condition.	Seo et al. (2018)
Computer-based simulations	
• A wear reduction of approximately 60% was reported in the case of the leading axle of the bogie.	Spiryagin et al. (2013)
• When using the shakedown method, with a reduction in the friction coefficient, the peak pressure and traction forces move from the ratcheting zone (i.e. crack zone) to the non-ratcheting zone (i.e. crack-free zone).	Eadie et al. (2008)
Field tests	
• A lateral force reduction of 30−50% and a reduction in wear of 60−75% were reported.	Eadie et al. (2003)

• The carry distance obtained by using a wayside TOR-FM system was 1,036−1,189 m.	
• A reduction in the lateral forces of up to 30% and reductions of up to 60% in the rail wear rate were observed at three different test sites. • The typical coefficient of friction measured with a hand-pushed tribometer in the dry top-of-rail condition was approximately 0.5, and with the TOR-FM applied, the corresponding coefficient was approximately 0.35. • In the case of a downhill slope (downgrade), more TOR-FM application is needed due to tread braking.	Eadie et al. (2006)
• In the dry case, i.e. with no TOR-FM and water, a friction coefficient of approximately 0.5 was obtained with a wide scatter in the L/V forces. • In the case of rain without TOR-FM, an average friction coefficient of approximately 0.3 was obtained. • In the case of FM in dry conditions (without rain), a narrow distribution of the L/V force values and an average friction coefficient of approximately 0.2 were obtained. • In the case of both water and FM, initially the friction coefficient was approximately 0.3 (corresponding to wet conditions), rising to a mode at approximately 0.4 (before friction control due to FM gains effectiveness) and then, with effective friction control due to FM in place, it dropped to a value slightly below 0.2.	Oldknow et al. (2012)
• When TOR-FM was used, the vertical wear of the high rail decreased by 14.4% and that of the low rail decreased by 40%.	Zhou et al. (2013)
• The application of a large amount of FM can result in unacceptably low friction coefficients, on average 0.13−0.16. • Even a thin layer of FM results in a low friction coefficient, on average 0.23. • Hand-pushed tribometers generally measure excessively high friction coefficients compared with the real values and are not capable of indicating accurate tendencies.	Lundberg et al. (2014)
• By using a hand-pushed tribometer, the friction coefficient was measured to be more or less the same as that in the dry condition, even if the TOR-FM equipment was in operation in the area of track being investigated. • The hand-pushed tribometer has high precision, but its accuracy compared to the real friction between the wheel and rail is unknown. • No reason was found for implementing TOR-FM lubrication using a wayside system on the IOL.	Asplund et al. (2015) & Lemma et al. (2014)
• The adhesion level, especially in the case of TOR-oils, is influenced by the amount applied. • All types of TOR material might provide similar benefits in areas that are directly related to a reduced friction coefficient, such as wheel-rail wear and fuel savings. • The non- and the slow-drying FM can have better carry-down characteristics compared to the fast-drying FM, but may cause long braking distances and undesirably low traction.	Stock et al. (2016)

• The total wheel replacements of a TOR-FM-equipped train were reduced by 60.2%. • The TOR-FM-equipped train also reduced the wheel replacements of the non-TOR-FM-equipped train by 23%, due to the benefits of retention of TOR-FM applied to the same track.	Stock et al. (2017)

2.2 Research gaps

While conducting the above survey of the state of the art, it was observed that most of the studies around the world which had shown positive results for FM had either been based on laboratory tests or performed in collaboration with a North American company. In contrast, independent researches (Lemma et al., 2014; Asplund et al., 2015; Lundberg et al., 2014; Seo et al., 2018) have produced contradicting results. Asplund et al. (2015) stated the following: *"Based on this investigation, the conclusion to be communicated to the infrastructure manager is that we have not, as yet, been able to find a reason for implementing TOR-FM lubrication on the IOL."* According to Asplund et al. (2015), one reason why there is not a big difference between the situation before and the situation after the application of TOR-FM on the IOL could be the good quality of Swedish wheels and the high standard of rail maintenance being practised in Sweden compared to other railways in the world. This good maintenance of the wheel-rail system results in good steering and ride comfort on the track, with only small dynamic forces being transferred from the train to the track (Asplund, Nordmark and Gustafsson, 2015). The reasons why the independent research does not show any positive results represent a scientific gap of knowledge that needs to be filled. A deeper investigation of this research area is required to ascertain why and how the field results obtained on the IOL are not in agreement with those obtained in other parts of the world.
Moreover, there are a number of additional research gaps that need to be investigated with respect to TOR-FM systems, as described below.

- Depending on the train dynamics and loading condition, the friction requirements for avoiding cracks can differ. It is important to investigate the value of the friction coefficient required to avoid cracks in different loading conditions.
- On the one hand, TOR-FM can reduce the fatigue stresses, but on the other hand, the TOR-FM trapped in cracks can eventually widen the cracks when trains are passing. Studying the state of the art, one finds that Seo et al. (2018) argued that the crack growth rate of pre-generated cracks became faster due to the fluid entrapment mechanism, even in the case of FM with drying material characteristics. However, Hardwick and Lewis (2014) argued that water-based (fast-drying) FM not only minimised the generation of cracks and wear, but also suppressed the propagation of pre-generated cracks. Hardwick and Lewis (2014) also claimed that oil-based FMs catalysed the RCF propagation if cracks were already present. Therefore, further knowledge is required to enable us to evaluate the type of FM to use and the appropriate amount to apply, in order to avoid crack propagation problems and to determine whether FM trapped in cracks is an issue.
- Natural third bodies and moisture play an important role in controlling wear, friction and cracks. Laboratory tests never consider realistic third bodies. Depending on the weather and location, the characteristics of realistic third bodies can change. Oldknow et al. (2012) performed field tests including the effect of moisture, but a deep investigation is needed to study the effects of realistic third bodies.

- Depending on their content, different FMs can have different carry distances and friction properties (Stock et al., 2016). In order to calculate the number of units of TOR-FM equipment required on a particular length of track, information about the exact carry distance is very important. This carry distance information will also affect the life cycle cost calculations.
- It is a well-known fact that wear and friction have no direct relationship. The anti-wear properties of the different FMs can be different and independent of the friction coefficient provided by them. Therefore, the relationship between friction and wear with the application of different friction modifiers needs investigation.
- The life cycle cost of the different TOR-FM systems needs to be calculated. One needs to investigate when and how TOR-FM systems are financially feasible, and one needs to determine the requirements for the use of TOR-FM and the best practice for its application.

The present research has filled knowledge gaps as follows.

- Investigated the effect of different friction coefficients and loads on the RCF by using a fatigue and damage index method in an MBS software package.
- Using a wayside TOR-FM system, investigated the effect of a water-based friction modifier on the RCF, friction and roughness for a period of two years.
- Investigated the wear and friction characteristics of two different water-based FMs and one oil-based FM both in field and laboratory conditions by using a realistic contact pressure and sliding speed.
- Investigated the effect of realistic third bodies by comparing measurements performed using a handheld tribometer in the laboratory and the field.
- Investigated the carry distance of two different water-based FMs on both the rail and wheel. The carry distance measurements explained why Lemma et al. (2014) and Asplund, Nordmark and Gustafsson (2015) could not, through their initial measurements, see any benefits to be derived from using a combination of water-based FM and a wayside system.
- Calculated the life cycle cost when using a water-based FM with a wayside or an on-board system.

3 RESEARCH METHODS

This chapter describes the different methods used for achieving the objectives of the present research and discusses why certain methods or tools were used. The research methods included computer-based simulations and laboratory and field experiments, performed to investigate the different TOR-FMs. Table 4 summarises all the measurements and calculations performed in the present research. The table also lists the FMs used for the different experiments and specifies the journal papers in which the results have been published.

Table 4. Details of all the investigations performed in the research for this thesis.

Research methods		**FM used**	**Investigations**		
Computer-based simulations		_	Fatigue index ⋆ Damage index ⋆⋆		Life cycle cost calculations
Laboratory tests		FM-A, FM-B, FM-C	Friction & wear	EDX analysis⋆⋆⋆	
Field tests	**Phase 1**	FM-A, FM-B	Friction & wear Roughness Profile Crack follow-up	Carry distance measurement⋆⋆⋆	
	Phase 2	FM-A, FM-B		Carry distance measurement⋆⋆⋆	
	Phase 3	FM-A, FM-B, FM-C	Friction & wear		

⋆ Published in Paper 1, ⋆⋆ Published in Paper 2, ⋆⋆⋆ Published in Paper 3

Table 5 summarises the details of all the industrial participants who helped with their expert advice during the research work for this thesis.

Table 5. Details of industrial participants who helped with their expert advice during the research for this thesis.

Position	**Organisation**	**Field of expertise**
Service and warehouse manager	Supplier of the wayside system	Lubrication technology and costing
Head of Sales & Consultant	Supplier of the on-board system	Technology and development
Track specialist	Trafikverket	Specialist in maintenance management
Track technician	Trafikverket	Specialist in track and turnouts
Railway maintenance engineer	LKAB	Rolling stock expert

3.1 Computer-based simulations

The simulation software used in the present research was a multi-body simulation (MBS) package from GENSYS. It contains mass-spring-damper physical models and geometrical equations for representing different parts of the track and the train. The package used in the present research was updated with models of the IOL track and the Fanoo wagon used by LKAB freight trains; for details see Section B in the appendix. All the models had already been validated by Bogojevic et al. (2011), Persson (2015) and Hossein Nia (2017). To generate outputs, the MBS models used wheel-rail contact mechanics based on the Hertz theory, in combination with the simplified theory by Kalker called FASTSIM (Kalker, 1982). The outputs from the MBS, such as the creep forces, the creepage and the size of the contact area, etc., were used in the prediction methods; an illustration of the forces generated at the wheel-rail contact is provided in Figure 17. The first RCF prediction method used in the present research was based on the shakedown method; for details of the method, see Section A.4 in the appendix. Another method used was a combined RCF and wear prediction method, which involved a trade-off between wear and RCF; for details see Section A.5 in the appendix. Both the methods predicted only the risk of RCF in the form of an index.

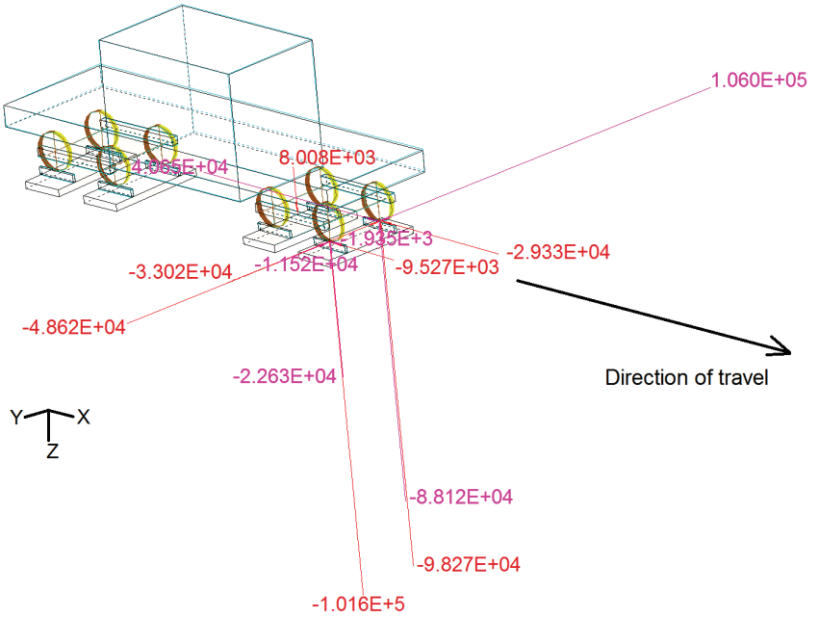

Figure 17. Dynamic model of a wagon and a track section, showing the forces [N] generated during a negotiation of a 200 m curve. The length of the bars represents the magnitude of the generated forces.

The final index, i.e. the output from the simulations, depended on the contact pressure, creep force and creepage, etc., which are sensitive to numerous factors, including the wheel and rail profiles, bogie suspension, track stiffness, and the stiffness and damping between the ground, ballast bed and rails. Because the present work focused on the effects of friction control on the wear and RCF, all the parameters apart from the friction values were kept constant for all the simulations. To determine the effect of FM theoretically, updating the friction coefficient and a reduction factor to Kalker's coefficient is sufficient. The influence of third body particles such as dust from the environment and different additives in the FM, e.g. anti-wear additives, is ignored. Since LKAB is planning to increase the axle load of their trains, the simulations were also performed using high axial loads.

3.1.1 Curves details

The curve radius in the simulations varied from 200 to 3,000 m and the cant (super-elevation) values ranged from 15 to 0 cm, which represent the narrowest and the largest curve, respectively. The cant values used in the simulations were the intermediate cant values for heavy haul and passenger railway traffic; for the exact cant values, see Table 6. The speed of the train was fixed at 60 km/h, which is the speed of the fully loaded freight trains run by LKAB. As informed by Trafikverket, in the case of the IOL, the track sections having a radius of 1,500 m or above are considered as tangent track. However, in the simulations, curves with a radius of up to 3,000 m were considered, in order to acquire a broader view.

Table 6. Cant values used in the simulations for the respective curve radii.

Curve radius [m]	Cant [m]
200	0.15
300	0.15
400	0.10
500	0.10
1,000	0.05
2,000	0.00
3,000	0.00

As shown in Figure 18, all the curves used in the simulations had a total track length of 700 m. It is not possible to combine a tangent track and a circular curve with cant directly; therefore, a transition curve is added to give a smooth transition between the tangent track and the circular curve. These transition curves can be parabolic or linear. In the present simulations, only linear transition curves were used, as in practice the advantages of parabolic curves are very small (Andersson, Berg and Stichel, 2014).

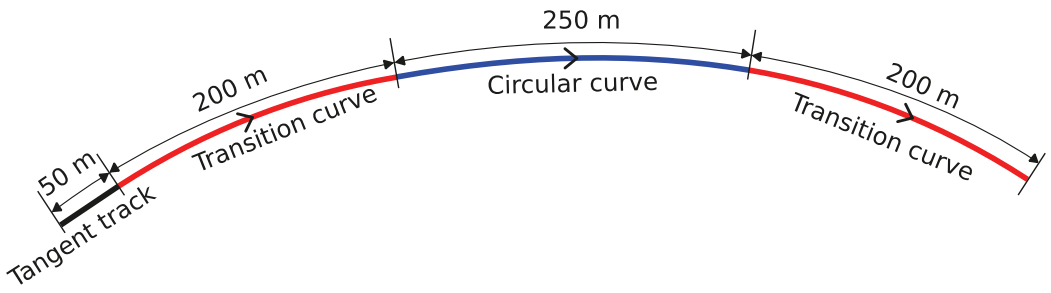

Figure 18. Length of the various zones of the curve used in simulations.

3.1.2 Friction values

Practically, in dry conditions, the rail surfaces always have some deposits from the environment and trains (e.g. moisture, dust, industrial precipitation, wear debris, and fallen leaves) (Dollevoet, 2010). These deposits (third bodies) generally act as a lubricant, change the shear forces between the rail and wheel, and hence reduce or increase the friction coefficient and the degree of utilised friction, i.e. the degree of slip in the rolling contact. To compensate for these changes (generally a reduction) in the creepage due to third bodies in the simulation software, a correction factor is required. In the present study, a correction factor was applied with the help of Kalker's reduction factor. The MBS software

gives the speed-difference between the two surfaces constituted by the wheel and the rail without considering any effect of a lubricant. In order to take the effect of a lubricant into consideration, the creepage between the wheel and rail is reduced. Therefore, the actual speed-difference between the rubbing surfaces is not sent to FASTSIM for calculating the creep force. Instead, a reduced amount of creepage is given as input to FASTSIM as a creep relaxation. In the case of FM-free rail conditions with the presence of surface deposits (natural lubricants), a friction coefficient of 0.5 and a Kalker's reduction correction factor of 60% are considered. In the case where an FM has been applied, Kalker's reduction correction is even lower. For the lowest friction coefficient used here, 0.2, a Kalker's reduction correction of 15% is considered (Suda et al., 2005). Kalker's reduction factor for the intermediate friction coefficients of 0.4 and 0.3 are unknown. However, these values can be interpolated using the highest and lowest values. In the present research, intermediate Kalker's reduction factor values of 45% and 30% were assumed for friction coefficients of 0.4 and 0.3, respectively. These interpolated values covered the gap between the maximum and minimum values, and therefore a proper trend could be studied. Details of all the friction coefficients and Kalker's reduction factors used in the simulations are shown in Figure 19. It should be noted that a change in the applied load could cause both the friction coefficients and Kalker's reduction factors to vary. The simulations of the present research used coefficients derived using laboratory tests (Suda et al., 2005) under a single load and used those coefficients to cover a range of loads. To cover the variation in the coefficients due to a change in the loads, a range of coefficients was used which covered the lowest and highest practical values. In all the cases, on reaching full slip, the traction coefficient became constant. As a simplification, for each friction value, a fixed Kalker's reduction factor was chosen (as shown by the dots in Figure 19) which was independent of the creepage and traction forces.

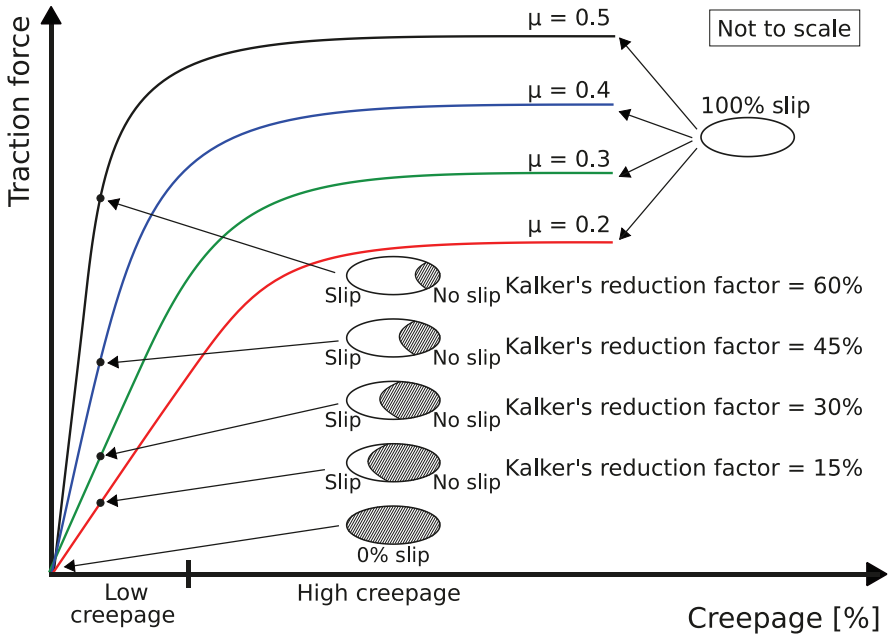

Figure 19. Traction force-creepage diagram, showing the trend with different levels of friction control (combinations of friction coefficient and Kalker's reduction factor) with respect to the traction force.

Note:- The simulation results discussed in the present thesis are for the leading axle of the first bogie of the wagon. The leading axle often experiences higher forces than the trailing axle, and therefore the leading axle is more prone to damage (Oldknow, Eadie and Stock, 2012).

3.1.3 Wheel-rail interface

The wheel and rail compose the connection between the rolling stock and the infrastructure, and the wheel and rail profiles are very important to regulate both the wear and RCF (Dollevoet, 2010). Any adjustment between the wheel and rail profiles affects the contact area, which in turn affects the creep forces. On the main track of the IOL, there are four main rail profiles, namely the 60E1, MB1, MB4 and MB5; MB stands for Malmbanan (i.e. IOL) profile (Asplund, Khan and Nordmark, 2017). The 60E1 is the base profile for a new rail and all the MB profiles are specialised profiles for the IOL. The rails are transformed into these MB profiles using a grinding process depending on the location and requirement. On a narrow curve, the MB1 profile is used for the high rail and the 60E1 for the low rail. The MB4 rail profile is the standard profile for tangent tracks on the IOL. The wheel profile used for the wagons of the freight trains run by LKAB is the WP4 and that of the locomotive is the recently developed WPL5V2 profile (Asplund, Khan and Nordmark, 2017). Since the present research focuses on the heavy haul trains run by LKAB, therefore, wheel profiles from LKAB freight trains were selected for the simulations. The wheels of the freight train from LKAB and rail of the IOL are generally well maintained and in relatively good shape.

The profiles remain new for a short period compared to the entire lifetime of the rail and wheel, and therefore worn profiles are more realistic. The simulations in the present research used worn profiles, as shown in Figure 20, as an input. The rail profiles were measured by the author of the present thesis and the wheel profiles were measured by Thomas Nordmark (a PhD student at LTU) using a laser-based device, the Calipiri 40 from NEXTSENSE GmbH. As can be observed in Figure 20, both the high and low rail profiles have an inclination of 1/30, a standard inclination in Sweden. These wheel and rail profiles are special profiles, with generally two or more contact points between the rail and wheel. These contact points depend on the facets generated by the grinding of the rail and wheel. The standard steel grade used for the IOL is 350 LHT rail steel.

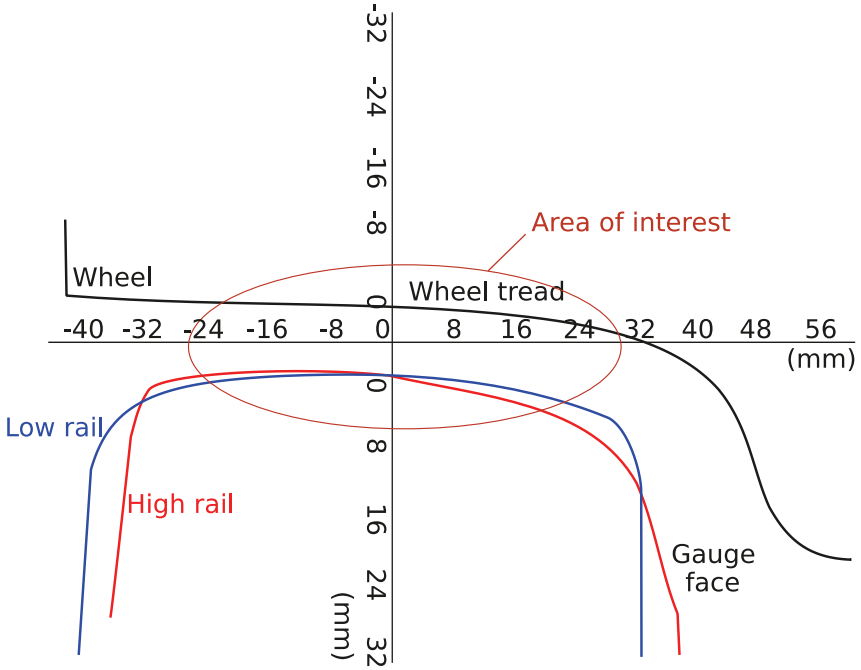

Figure 20. Worn profiles of wheels and rail (both high and low) used in the simulations.

3.2 Laboratory experiments

This section discusses energy dispersive X-ray (EDX) analysis and the laboratory test applied for the wear and friction measurements using the FricWear 2017 tribometer; for details see Section C in the appendix. The EDX analysis was performed as part of the carry distance experiments.

3.2.1 EDX analysis

EDX analysis was used for the analysis of the third body samples collected on cotton swabs in the carry distance experiments. The fundamental principle of this analysis is that each element has a unique atomic structure which gives a unique set of peaks on its electromagnetic emission spectrum (Goldstein et al., 2003). It should be noted that the height of a peak may not be proportional to the element's weight % (wt%). For each sample, an EDX analysis for element detection was performed at five different locations on the cotton swab. Figure 21 shows the image of a sample from FM-A subjected to EDX and the output from the EDX analyser showing the peaks for different elements of this TOR-FM.

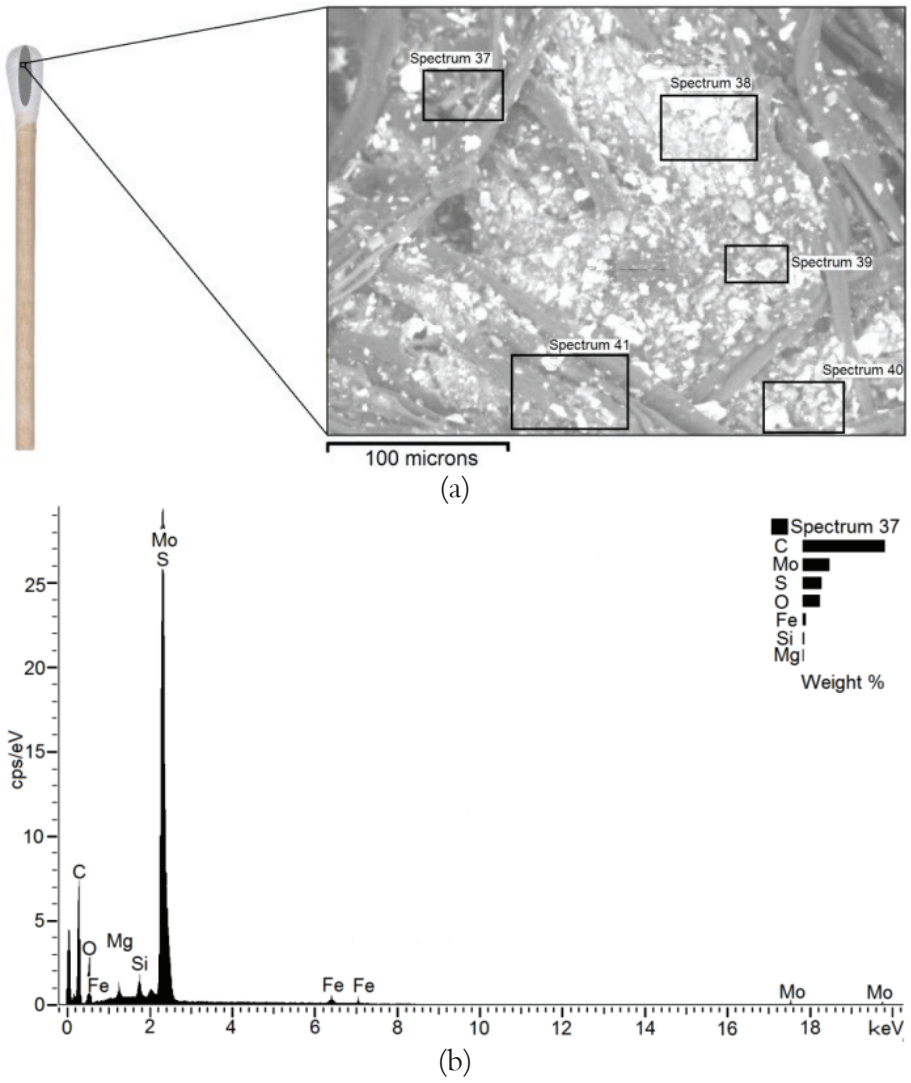

Figure 21. Example of an EDX result for FM-A: (a) image of a sample subjected to EDX analysis showing the five locations focused on and (b) output of the analyser for one of the five locations focused on.

The samples from the top of the rail at the distributing bars and a reference sample, which was taken from the top of rail located approximately 35 km away, were compared. Depending on the FM in question, some extra elements were found in the samples taken at the distributing bars for the FM. These elements were designated as the key indicator elements. The distance from the point of application to the location on the rail where these elements were detected was considered as the carry distance of the FM.

3.2.2 Friction and wear measurements

This section explains the methods used in the comparison of TOR-FMs using the FricWear 2017. For details of the FricWear 2017, see Section C in the appendix. In the present research, the friction and wear measurements were performed in the laboratory and in phase 1 and 3 of the field measurements. This section only discusses the friction measurements carried out in the laboratory and in phase 3, in which the FM was applied manually on the top of the rail. In the laboratory measurements, a piece of rail removed from the IOL due to RCF was used. The material of the rail was 350 HT steel, which has a surface hardness of 468 HV (1,520 N/mm^2). In all the experiments, a spherical probe with a diameter of 5 mm and a dead weight of 2.3 kg was used, given a maximum pressure of approximately 2,100 MPa.

Initially, the friction measurements in the laboratory were performed using a steel ball-bearing ball by making TOR-FM films of four different thicknesses, as shown in Figure 22. The purpose of these friction measurements was to decide the amount of FM for the wear experiments, since the number of wear probes was limited. Figure 22 (a) shows an example of an excessive amount of TOR-FM; to form this layer, approximately 3 ml of FM was applied on a section of 30 cm, spread with the help of a silicon spatula. An example of a moderate amount of FM is shown in Figure 22 (b); the excess FM was cleaned off with a piece of paper so that some amount of FM could be seen on the top of the rail, but the exact amount of FM is not known. For forming an FM film designated as "a very small amount", shown in Figure 22 (c), the surface was cleaned properly and was gently patted with the piece of paper used for cleaning off the excess FM. Figure 22 (d) shows a surface which was properly cleaned using an ethanol-alcohol-based cleaner, followed by air-drying, and thus was free from any third body.

Since different amounts of FM do not show any variation in the friction coefficient in the initial friction measurements, an amount of FM corresponding to the amount per metre used in the phase 2 measurements (for details of the phases, see Table 4) was used in both the laboratory tests and the field tests of phase 3 in order to create consistency. In phase 2, 15 ml of FM was applied on a 7.4 m section of the rail, see Section 3.3.2. Therefore, in the laboratory measurements, 1 ml of the FM was applied on a length of 50 cm, since this was expected to form a film thickness of approximately 50 μm, i.e. the same film thickness as in phase 2. While applying the FM it was realised that if one had applied a lesser amount than 1 ml, it would have been challenging to form a homogenous layer, especially in field conditions, where the limited time available due to the pressure of traffic puts extra mental pressure on the operator.

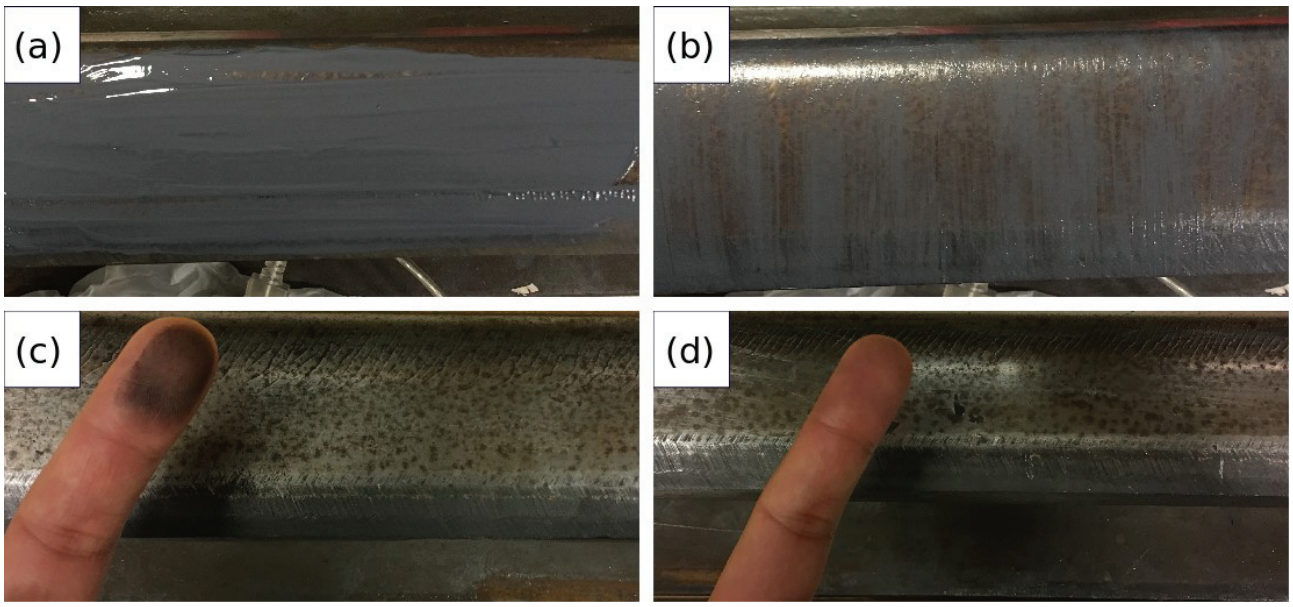

Figure 22. Examples of the different TOR-FM film thicknesses used in the present research: (a) an excessive amount of FM, (b) a moderate amount of FM, (c) a very small amount of FM and (d) a cleaned surface.

Before performing the actual wear measurements, a sliding test was performed in which the probes were slid for different distances. This test was performed to calculate the change in the contact pressure in relation to the sliding distance. On sliding the probe, the tip wears and the contact area increases, and therefore the pressure decreases. As shown in Figure 23, the probes were dragged over a distance ranging from 6 cm to 14 cm. The wear scar was measured and the actual contact pressure was calculated after every step. It was concluded from the sliding measurements that in order to have an average pressure of 860 MPa, which is an average pressure in the wheel-rail contact of a 30 tonne IOL wagon, the probes should not be dragged more than 12 cm.

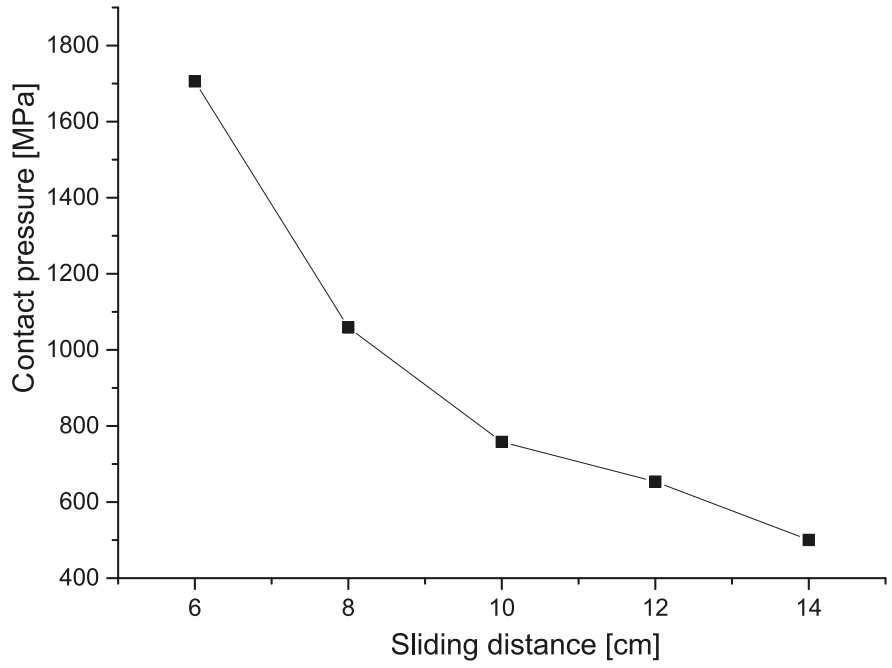

Figure 23. Reduction of the maximum contact pressure with different sliding distances.

After deciding the sliding distance, the next step was to decide the sliding speed. The present research focuses on the top of the rail in contact with the wheels of the freight trains operated by LKAB, which run at a speed of 60 km/h (16.7 m/s). The contact between the top of the rail and the wheel tread often has partial slippage. The overall area in the slip region does not have the same sliding velocity everywhere; therefore, to perform the wear experiment, an approximate average sliding velocity in the contact area was calculated. Figure 24 provides a schematic diagram showing the different radii and deformation heights of the wheel. Equation 9 shows the formula for calculating the approximate sliding velocity at different locations in the contact.

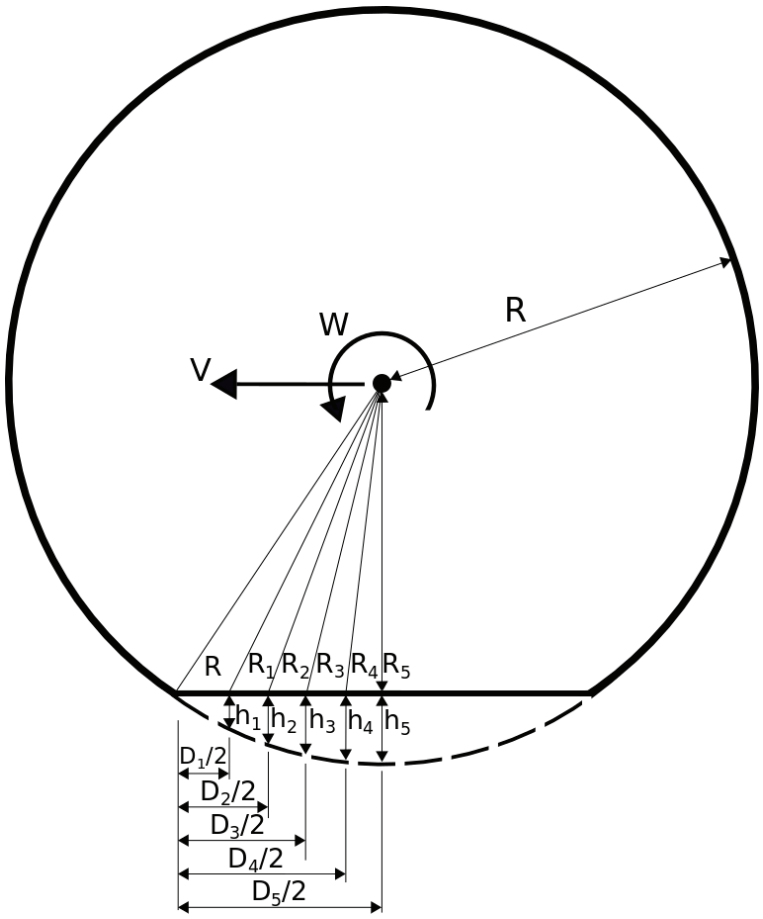

Figure 24. Schematic diagram showing the different radii and deformation heights of the wheel.

The calculation of the sliding velocity was performed by the author as part of the present research as follows:

V is the actual velocity of a wheel due to slip;

V' is the maximum theoretical velocity of a wheel without slip;

the maximum sliding speed is

$$\Delta V = V' - V = w(R - R_5) \quad (1)$$

$$= w(R - (R - h_5)) \quad (2)$$

$$= \mathrm{wh_5} \tag{3}$$

Assuming that the sliding velocity in the contact band is directly proportional to the deformation height (h_i), then the sliding velocity with different deformed radii (R_i) can be represented as

$$\Delta \mathrm{V} = \mathrm{wh_i} \tag{4}$$

Using Pythagoras' theorem,

$$\frac{\mathrm{D_i}}{2} = \sqrt{\mathrm{h_i}(2\mathrm{R} - \mathrm{h_i})} \tag{5}$$

On solving the above equation for h,

$$\mathrm{h_i} = \mathrm{R} \pm \sqrt{\mathrm{R}^2 - \frac{\mathrm{D_i}^2}{4}} \tag{6}$$

Since is it known that h cannot be greater than R,

$$\mathrm{h_i} = \mathrm{R} - \sqrt{\mathrm{R}^2 - \frac{\mathrm{D_i^2}}{4}} \tag{7}$$

Putting the value of h in equation 4,

$$\Delta \mathrm{V} = \mathrm{w}\left(\mathrm{R} - \sqrt{\mathrm{R}^2 - \frac{\mathrm{D_i^2}}{4}}\right) \tag{8}$$

$$\Delta \mathrm{V_i} = \mathrm{V} - \frac{\mathrm{V}}{\mathrm{R}} \sqrt{\mathrm{R}^2 - \frac{\mathrm{D_i^2}}{4}} \tag{9}$$

Taking the velocity as 60 km/h (16.67 m/s) and the diameter as 1.2 m, which are the standard train speed and the standard locomotive wheel diameter, respectively, the sliding velocity at different locations in the wheel–rail contact was calculated as shown in Figure 25. The sliding velocity at location R3, which is 0.5 mm/s, is assumed as the average velocity of the sliding in the contact area.

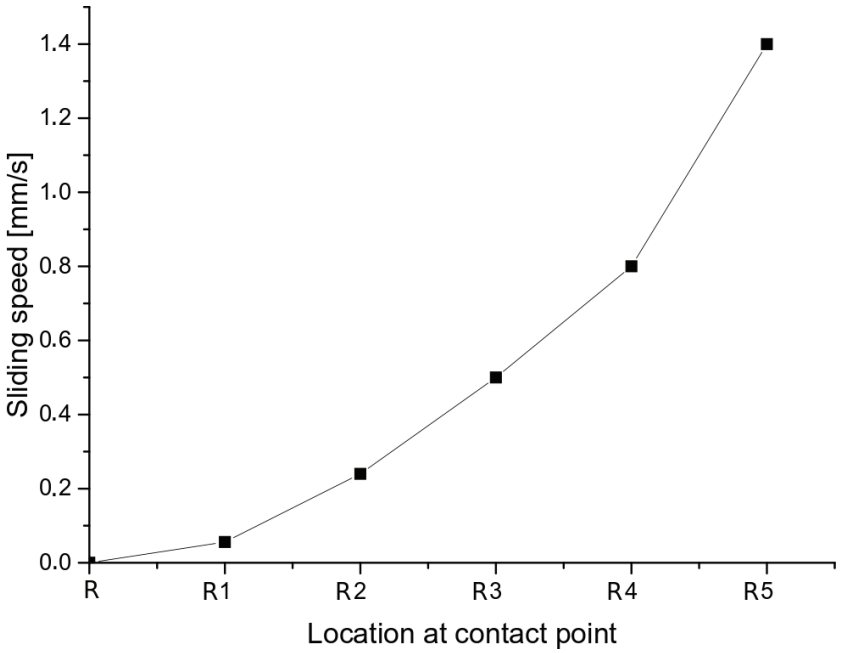

Figure 25. Sliding velocities at different locations in the wheel-rail contact.

In order to compare the wear and friction results obtained in the laboratory and the field measurements, the same parameters were used in the field and in the laboratory measurements. The field tests performed to compare the FMs are designated as phase 3 field experiments. All the parameters of the measurements performed in the laboratory and phase 3 are summarised in Table 7.

Table 7. Summary of all the parameters used in friction and wear measurements in the laboratory and phase 3.

Parameters	**Value**
Area of the rail on which TOR-FM was applied	20,000 mm^2 (400 × 50 mm)
Load applied (vertical force)	22.63 N
Spherical diameter of the sliding probe	5 mm
Sliding speed	0.5 mm/s
Sliding distance	12 cm
Hardness of the wear probe	426 HV ≈ 1,350 N/mm^2
Hardness of the rail	468 HV ≈ 1,520 N/mm^2
Maximum Hertzian pressure	2,100 MPa

3.3 Field experiments

In the present research, the field experiments were performed in three phases. In phase 1, wayside equipment was used and the measurements were carried out periodically to follow the degradation of the rails. In phase 2 and 3, the FM was applied manually. Phase 2 focused on the carry distance measurements and phase 3 measured the friction and wear using the FricWear 2017 tribometer.

3.3.1 Phase 1 measurements

In phase 1, wayside equipment (shown in Figure 26 (a)) was installed before a curve with a 395 m radius at Gullträsk in Sweden for the distribution of the TOR-FM. The installed equipment is powered by a 12 V battery, which is recharged by an attached solar panel and wind turbine since no electricity is available at this place. A wheel-detecting sensor (shown in Figure 26 (d)) is attached to the rail and sends a signal to the equipment for every wheel passage. The equipment is set to discharge a specific amount of FM on the rail when it detects a wheel. The FM is pumped from the tank to the distributing bars through hoses. The FM is carried forward on the rail when a wheel passes over the pool of FM created by the distributing bars installed on a side of both the high and low rail. As recommended by the suppliers of the FMs, the distributing bars of the respective manufacturers were used. Figure 26 (b) shows the distributing bars from the FM-A manufacturer and Figure 26 (c) shows the distributing bars from the FM-B manufacturer. The same main unit was used for both the TOR-FMs since it has the capability to function with both types of distributing bars and FMs. In the present research, the pump was set at the maximum level of 1 litre per 1,000 axles, which is approximately four times the amount recommended by the suppliers. This excessive amount of FM was used so that the real carry distance and other claimed benefits would not be underestimated. Initially, the tank was filled with FM-A for approximately ten months, after which the tank was cleaned and filled with FM-B. To avoid any mixing of the two FMs, sample collections for carry distance of FM-B were performed two months after changing the FM.

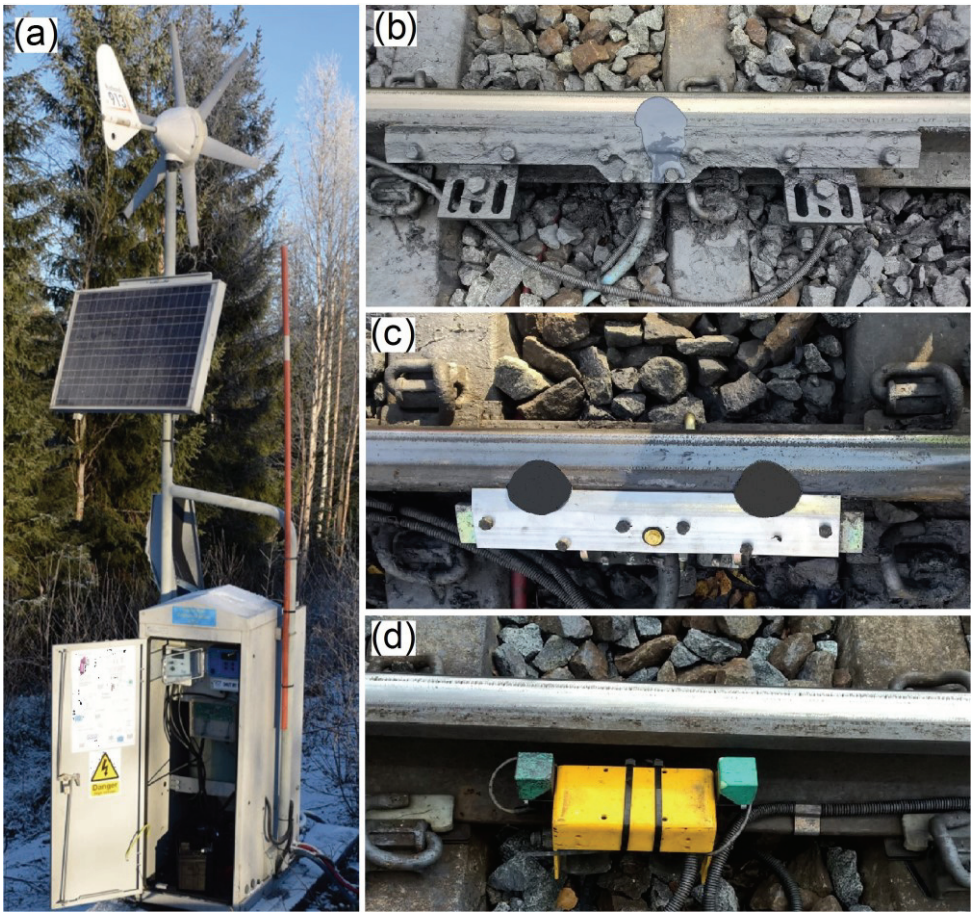

Figure 26. The wayside TOR-FM equipment installed at Gullträsk in Sweden: (a) main unit, (b) distributing bars used for FM-A, (c) distributing bars used for FM-B, and (d) wheel detecting sensor.

The aim of this phase of the field tests was to measure the reduction in the RCF and wear obtained by using TOR-FM in field conditions. The degradation on two similar curves was compared, one of which was equipped with the wayside TOR-FM system, while the other lacked such a system. The curve having the TOR-FM system was designated as the TOR curve and the other curve was designated as the reference curve. Figure 27 shows a schematic diagram illustrating the location of both the TOR curve and the reference curve. Details of all the experiments performed, with the measurement dates and the status of the wayside equipment, are shown in Table 8.

Table 8. Details of all the measurements performed in phase 1.

Location	Measurements \ Date →	01-09-2015	30-10-2015	14-12-2015	01-03-2016	03-05-2016		24-05-2016	30-09-2016	04-11-2016	12-05-2017	
	Status of the equipment →	NW	W	NW	NW	W		W	W	W	W	
TOR curve (Gulltråsk)	Friction	✓	×	✓	×	✓	Grinding (12 May to 18 May 2016)	×	×	✓	×	Grinding (2 July to 8 July 2017)
	Carry distance	✓	✓	×	×	✓		×	×	✓	×	
	Roughness	✓	✓	✓	✓	✓		✓	✓	×	✓	
	Profile	✓	✓	✓	×	✓		✓	✓	×	✓	
	Cracks	✓	✓	✓	✓	✓		×	×	×	×	
	Temperature	×	✓	✓	✓	✓		✓	✓	✓	✓	
Reference curve (Murjek)	Friction	✓	×	✓	×	Not performed due to a shortage of time		×	×	This slot was dedicated at Gulltråsk for FricWear 2017	×	
	Carry distance	✓	✓	×	×			×	×		×	
	Roughness	✓	✓	✓	✓			✓	✓		×	
	Profile	✓	✓	✓	×			✓	✓		✓	
	Cracks	✓	✓	✓	✓			✓	✓		✓	
	Temperature	×	×	×	×			×	×		×	

1. ✓:- measurement performed
2. ×:- measurement not performed
3. NW:- the TOR-FM wayside equipment was not working
4. W:- the TOR-FM wayside equipment was working

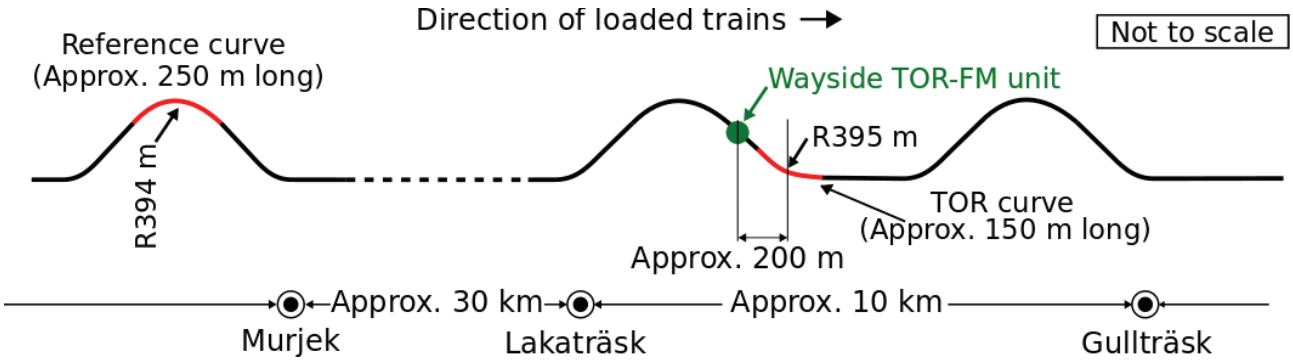

Figure 27. Schematic diagram showing both the TOR curve and the reference curve on the IOL.

In phase 1, all the measurements presented in Table 8 were performed at three different locations in each curve, and the locations were selected in such a way that the measurements were performed on both circular and transition sections of the curve. As shown in Figure 28, a total of six measurement points were selected for following the degradation on each curve. Since the equipment was installed only at one location, the effect of the carry distance of the TOR-FM on the rail degradation could also be measured. As shown in Figure 28, the high rail is represented by "H" and the low rail by "L". "H" and "L" are followed by a number representing the measurement point in question.

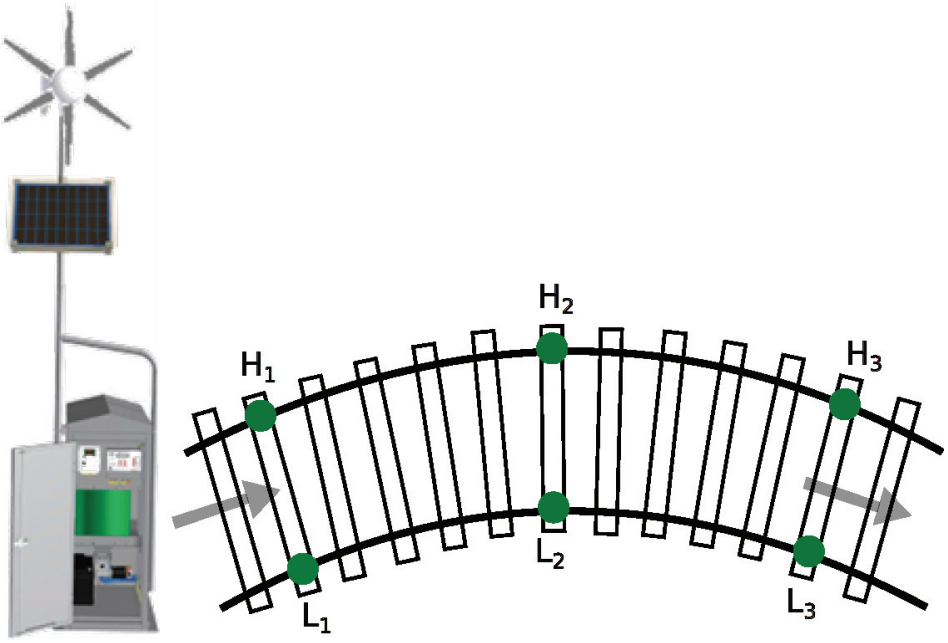

Figure 28. Measurement locations on both the curves.

The phase 1 experiment started on 18th August 2015 and the FM used in the first year of phase 1 was FM-A. However, since it was realised that the carry distance of FM-A was very poor, this FM was changed to FM-B on 13th September 2016. Along with the FM, the distributing bars were also changed to bars recommended by the company concerned. The field tests were stopped on 2nd October 2017.

The carry distance of the two FMs tested in phase 1, especially that of FM-A, was very short in comparison with the carry distance claimed by the manufacturer. Supplier A offered an explanation which can possibly be supported by research performed by Stock et al. (2016) and which asserts that a water-based FM is carried forward with the help of the wheels and is partially transferred to the rail as long as the FM is wet. However, as soon as the carrier solvent evaporates, i.e. becomes dry, the FM

particles will adhere to the wheel and limit further inter-surface material transfer between the rail and wheel. However, this may not be true in the case of FM-B, whose solvent is expected to contain an additive together with water.

Below, a description of all the measurements performed in phase 1 is provided.

3.3.1.1 Friction measurements

Friction measurements were performed using the FricWear 2017 device; for a description of the equipment, see Section C in the appendix. The first two measurements were performed using the first version of the FricWear device on 01/09/2015 and 14/12/2015. The third set of measurements were performed on 03/05/2016 using the second version of the FricWear device. The last set of friction measurements of phase 1 were performed 04/11/2016 using the latest version of the FricWear device, called the FricWear 2017, as shown in Figure 29.

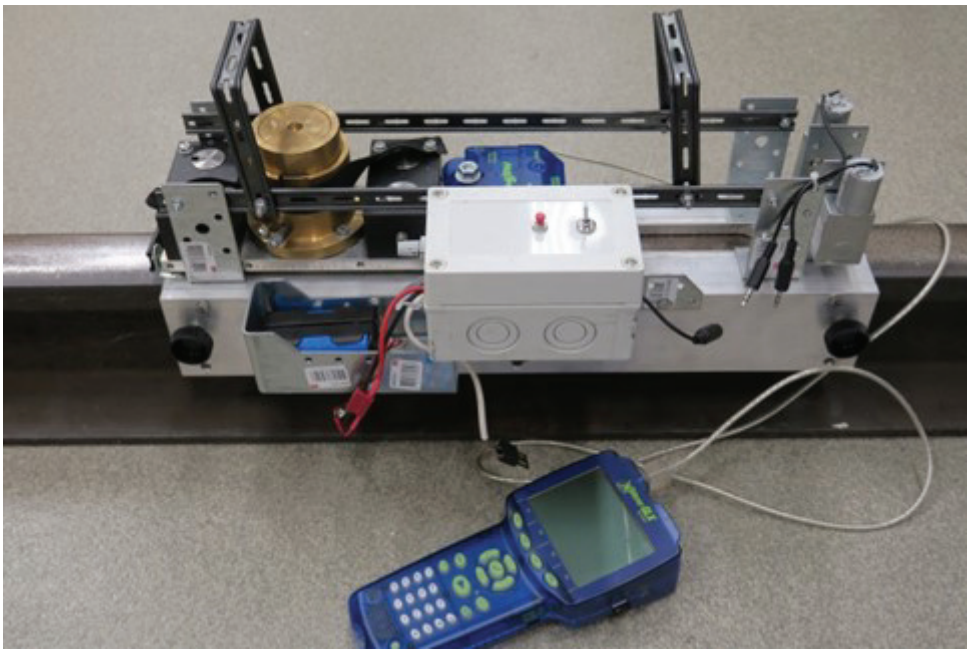

Figure 29. The FricWear 2017.

3.3.1.2 Carry distance measurements

The carry distance experiments were performed in both phase 1 and 2. The procedure adopted involved the samples being collected on a cotton swab from the top of the rail and wheel, up to 3 km from the location of the application at particular intervals. The samples were analysed in the EDX equipment to determine the distance to which the key indicator elements were present. In phase 1, the samples were collected at the locations where the stationary TOR-FM equipment was installed. In phase 2, the samples were collected from both the rail and the wheel on a track section where the TOR-FM had been applied manually. Cotton swabs dipped in a mixture of alcohol and ester were used to collect surface deposits (third bodies) from both the wheel and rail, at various distances from the point of application. The samples were collected using a plastic slot measuring 4×60 mm^2, and the swab was rubbed inside the entire slot to collect the maximum possible amount of the third bodies available within the slot. Afterwards, the third bodies on the swabs were analysed using an EDX

analyser, which provides elemental identification and quantitative compositional information. A summary of all the experiments is shown in Table 9.

Table 9. Summary of all the experiments, including the application method at both locations and the respective positions on both the rail and wheel where the samples were collected.

Phase	Location	Application method	Measured object	Position of the sample collection
1	Gullträsk	Wayside equipment	Rail	Running surface
2	Kiruna	Manual application	Rail	Running surface
			Wheel	Running surface
			Wheel	Contact band

3.3.1.3 Roughness measurements

Roughness measurements were performed using a portable surface roughness tester, namely a Surftest SJ-210 from MITUTOYO, as shown in Figure 30. This device has an accuracy of ±0.005 μm. The roughness was always measured on the contact band visible on the top of the rail, as only that region comes into contact with the wheel.

Figure 30. Surface roughness tester, Surftest SJ-210 from MITUTOYO (photo credit: Thomas Nordmark).

3.3.1.4 Profile measurements

The rail profiles were measured using a Calipiri 40 from NextSense GmbH, as shown in Figure 31. This is a laser-based non-contact profile measurement device, with an accuracy of less than ±80 μm and a repeatability of less than ±35 μm.

Figure 31. A photo showing rail profile measurement using a Calipiri 40 (photo credit: Thomas Nordmark).

3.3.1.5 Crack measurements

The cracks were detected through visual inspection. In the initial phase, dye penetrants were also used, but such penetrants were not efficient in sub-zero temperatures or during rainfall. In order to measure the depth of the cracks, a handheld instrument was used which functions based on the potential difference method, as shown in Figure 32. This instrument is first calibrated with the help of known artificial cracks. After calibration, the instrument's probe is placed on the crack and an estimated crack depth is given based on the potential drop between probes. Since the device only provides information on the length of the crack and does not give any data on the angle of the crack, the depth of the crack from the surface is not known.

Figure 32. Crack depth measuring instrument along with its calibration block of 350 HT steel.

3.3.1.6 Temperature measurements

To measure the temperature, a battery-powered data logger that keeps track of the temperature and humidity was installed on a railway pole near the wayside equipment at Gullträsk. In the present research, only the temperature was monitored and the measurement range of the device is from −40 to +70°C. The temperature data were collected between October 2015 and August 2017. On March 2016, the data collection points increased from one data point in six hours to one data point per hour, to obtain better results. The device measures the temperature and is then connected to the USB port of a computer to display the stored data.

3.3.2 Phase 2 measurements

The experiments of phase 2 were performed at the LKAB station in Kiruna in Sweden. The purpose of these tests was to measure the carry distance of two different TOR-FMs. The tests were performed using an IORE locomotive, which has an axle load of 30 tonnes and is currently operational on the IOL. In the second phase, 15 ml of FM was applied manually with a brush on 7.4 m of rail. The length of rail on which the FM was applied was double the circumference of the locomotive wheel so that the wheel would have a theoretical chance multiplied by two to pick up the FM. The amount of FM applied was four times the amount recommended by the suppliers, as in the case of the stationary equipment used in phase 1 of the study. As shown in Figure 33, FM-A was applied to the left rail and FM-B to the right rail.

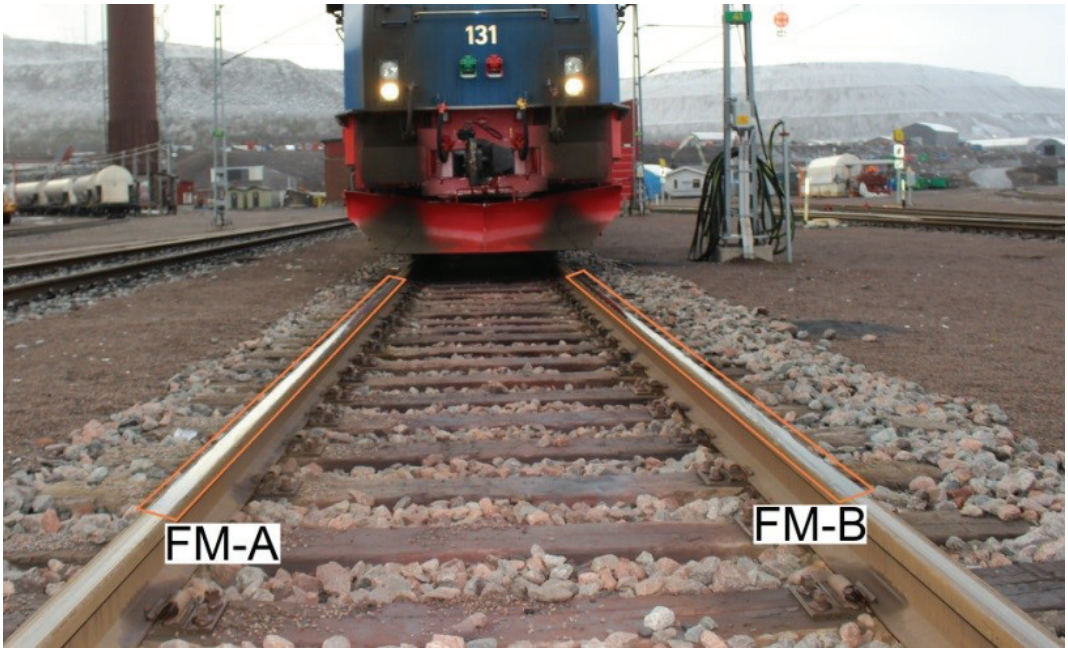

Figure 33. Phase 2: IORE locomotive standing before a section of rail on which FM was applied manually; FM-A was applied to the left rail and FM-B to the right rail.

In the case of the wheels, which were included in phase 2, the samples were collected following two different approaches, for detail see Table 9. In the first approach, the samples were collected from the complete running surface of the wheel, while in the second approach, the samples were collected only from the middle of the contact band, as shown in Figure 34. The reason for applying the second approach was that there is a small contact area at the wheel-rail interface which experiences all the traction forces, and FM is required in this particular area. However, due to the pressure at the wheel-

rail interface, the FM can easily be pressed out to the edges of the contact area (see Figure 34) or some grooves and stay there for a long distance without coming into the wheel-rail contact.

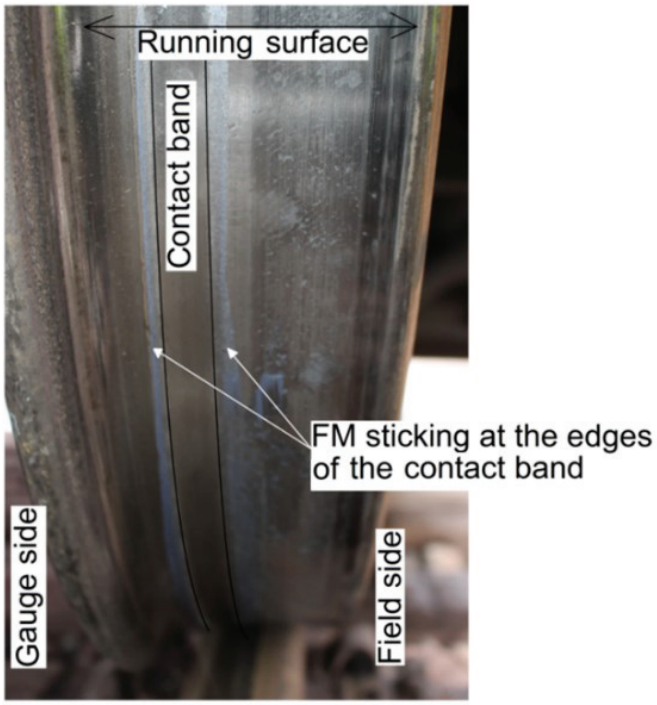

Figure 34. Photo showing the various zones of the wheel, along with the FM sticking on the edges of the contact band.

3.3.3 Phase 3 measurements

The experiments in phase 3 were performed at Luleå Railway Station in Sweden. This is not a part of the IOL, but freight trains operated by LKAB pass this location to reach Luleå harbour. The properties of the track here are the same as those on the IOL. The main purpose of these tests was to measure the friction and wear using a handheld FricWear 2017. Details of the phase 3 experiments are discussed in Section 3.2.2, "Friction and wear measurements".

3.4 Life cycle cost calculation

According to "Application guide - life cycle cost calculation" (*IEC 60300-3-3*, 2017), which is used by Trafikverket for calculations of the life cycle cost (LCC), the life cycle of an asset can be subdivided into the following six phases:

- concept and definition,
- design and development,
- manufacturing,
- installation,
- operation and maintenance,
- disposal.

As per the guidance for the maintenance strategy of Trafikverket, three phases are used for LCC analysis (Nissen, 2009); the LCC is also called the owner/customer perspective life cycle (Ben-Daya, Kumar

and Murthy, 2016). For the asset owner, the cost connected with the development and manufacturing stages is the acquisition cost, since these stages are carried out by the vendor. The phases used in the present research were as follows:

- acquisition and installation,
- operation and maintenance,
- disposal (phase-out).

The following formulas are used for the calculation of the LCC:

the LCC of the rail = rail replacement cost + grinding cost + disposal cost;

the LCC of the FM application equipment = acquisition and installation cost + operation and maintenance cost (FM + man + parts) + disposal cost.

For the calculation of the LCC in the present research, investments that occur at different time periods have been considered and, therefore, the discounting rate technique has been used to compare costs in the present value. Inflation has not been considered as the LCC has been used in the present research for comparing the reduction in cost by using a product. A real (inflation-free) economic discount rate of 3.5% has been used in the present research, since this is the standard discount rate used by Trafikverket (Nordlöf, 2014). The standard formulas used for calculating the principal amount in the present value are the following:

in the case of a single investment,

$$P = \frac{A}{(1+r)^n} \tag{10}$$

in the case of recurring investments,

$$P = \sum_{i=0}^{n} \frac{A_i}{(1+r)^n} \tag{11}$$

where:
A is the future value of the investment or loan,
P is the present value of the principal investment amount,
r is the discount rate,
n is the number of years during which the money is invested or borrowed.

The IOL experiences a variety of natural and operational conditions which can affect the exact cost of operation and actions such as maintenance actions. Consequently, it is not practical to accommodate all the inputs and, in some cases, values were used which were qualified guesses made by experts in the field in question; for details of the experts engaged in the present research, see Table 5. Each expert professional had significant experience in his or her field and thus could give a realistic average cost for different activities.

In the present research, the focus has been directed on the curves of the IOL since curves are subjected to more traction forces and thus more damage. Both the Swedish and the Norwegian parts of the IOL

consist of a large number of curves. However, the present research focuses only on the southern loop of the IOL, as stationary equipment was installed on the southern loop.

In the computer-based simulations of the present research, curves with a radius smaller than 500 m were classified as sharp curves. Curves with a radius between 500 and 1,000 m were classified as moderate and curves with a radius larger than 1,000 m were classified as large curves. However, the classification of Trafikverket used in the LCC calculations of the present research is slightly different and is shown in Table 10. The table also shows the "curve type" classification used by Trafikverket. In the simulations of the present research, curves with a radius larger than 1,000 m were classified as large curves, but according to Trafikverket, curves with a radius larger than 850 m are classified as large. Therefore, in the LCC calculations of the present research, the curves from type A to type D were included, as they are more prone to RCF and need the application of FM.

Table 10. Sharp and moderate curve details in the southern loop of the IOL.

Type of curves	Radius [m]	Classification in LCC calculations	Number of curves
A	< 550	Sharp curve	60
B	550 – 650	Moderate curve	97
C	650 – 750		
D	750 – 850		
E	> 850	Large curve/Tangent track	–
T	Tangent		–

The IOL has mixed traffic, but the contribution of the freight trains run by LKAB to the total tonnage is the largest. Each freight train operated by LKAB has 68 wagons and each wagon has an axle load of approximately 30 tonnes (which LKAB is planning to increase to 32.5 tonnes), which adds up to approximately 8,600 tonnes including the locomotive. The average daily frequency, the axle load in the loaded condition, and the average number of wagons of the different trains running in both directions on the southern loop of the IOL are provided in Table 11. This table presents average values based on data retrieved from the JVTC Research Station at Sävast in Sweden. For details of the equipment at the research station, see Nordmark et al. (2014). On average 27 trains in both directions pass the curve each day. For the calculation of the LCC, it was assumed that 14 trains passed the curve in one direction and one set of on-board equipment was sufficient per train irrespective of the number of wagons.

Table 11. Average daily frequency, axle load in the loaded condition, and average number of wagons of the different trains running in both directions on the southern loop of the IOL

Type of trains	Frequency per day	Axle load when loaded [tonnes]	Average number of wagons
Freight trains run by LKAB	4–6	29–31.5	68
Other freight trains	8–10	21–25	30
Passenger trains	12–16	19–20	2

On the IOL, periodic grinding is used as a maintenance process to remove RCF and retain the profile of the rail. As informed by Trafikverket, on average the grinding process is performed after 15 MGT have passed over the rails; generally this happens once per year on the southern loop, which has an accumulated annual tonnage of 20 MGT. The average grinding cost is 50 kr/m. According to Trafikverket, the cost of replacing rail is 4,000 kr/m and the average lifetime of the rail in different curve sections is given in Table 12.

Table 12. Average lifespan of the rail in different curves.

Curve radius [m]	**Lifespan [MGT]**
Less than 550	300
550 to 1,000	600
Above 1,000	900

Based on the computer-based simulations, field tests, laboratory tests, and the advice of experts belonging to our industrial partners (presented in Table 5), the following inputs were used for calculating the LCC.

- The LCC was calculated for a period of 15 years, which is equivalent to the life of the rail on curves with a radius smaller than 550 m.
- The length of the curve = 450 m (assumption based on the average curve length on the IOL).
- The cost of a TOR-FM per litre = 160 kr (a 19 L bucket of water-based FM costs 3,000 kr).
- The RCF reduction by using TOR-FM = 50% (assumption based on expert advice, see Section 5.3.4 for details).
- Grinding is performed once per year when no FM is applied and the frequency changes to once every two years when FM is applied.
- The wear reduction using TOR-FM = 40% (normalised average wear reduction when using FM-A and FM-B measured by the FricWear 2017, see Table 28).
- The disposal cost = 10% of the purchase cost. For rail replacements, the disposal cost is 0 kr (according to Trafikverket).
- The man-hour cost for an authorised railway worker = 750 kr (according to Trafikverket).
- The lifespan of the wayside equipment = 15 years (assumption based on expert advice).
- The lifespan of the on-board system = 15 years (assumption based on expert advice).
- An accumulated load of 20 MGT is equivalent to one year since the annual total load on the southern loop is 20 MGT.
- The total number of trains passing in one direction in a day = 14 (assumption based on the traffic on the southern loop of the IOL).
- The transportation cost per visit for repairs = 1,300 kr (amount paid by LTU per visit for repairs).
- The number of axles passing in one direction = 1,500 (assumption based on the traffic on the southern loop of the IOL).
- The installation cost of the system = two days salary for an authorised railway worker (according to the manufacturer).
- The TOR-FM consumption in the case of wayside equipment (all curve radii) = 300 ml/1,000 axles (manufacturer specification).
- The TOR-FM consumption in the case of an on-board system (all curve radii) = 30 ml/km/rail (manufacturer specification).
- The carry distance of the FM when wayside equipment is used = 450 m (measured in the carry distance experiments).

Assumptions:

- The tamping cost and other maintenance costs are not considered.
- The reduction in damage other than wear and RCF, for example corrugation, hunting, etc., is not considered.
- The reduction in damage on the wheel by using a TOR-FM system is not considered.
- The wear reduction is the average wear reduction for FM-A and FM-B, as only these FMs were tested in phase 1 and 2.
- The typical life of a TOR-FM application system (both a wayside and an on-board system) can vary from 10-15 years, depending on the manufacturer and use. For ease of calculation, the life of both the wayside and the on-board system is assumed to be 15 years.
- Since the wear reduction used is the average wear reduction for FM-A and FM-B (water-based FMs), the FM consumption recommended for water-based FMs was used. The quantity of FM required could not be determined in the present research, therefore, the manufacturers' recommendations were used.
- On average three units of wayside equipment can be fixed per day, considering the travel time and the waiting time due to railway traffic, and each unit requires service four times per year (assumption based on experience).
- On average five units of on-board equipment can be fixed per day and each unit requires service twice per year (assumption based on experience).

Note:- The on-board system was not used in the field tests of the present research. However, the LCC was calculated for both the wayside and the on-board system. For details of the on-board system, see Section D in the appendix.

4 SUMMARY OF THE APPENDED PAPERS

This section summarises the published papers. Paper 1 and 2 deal with the computer-based simulations. Both these papers have the same inputs, but the methods used for the simulations are different. The simulations treated in the first paper used the fatigue index (FI) method, while those treated in the second paper used the damage index (DI) method. Paper 3 was based on the field tests in which the carry distances of two different FMs were measured.

4.1 Paper 1

Title: Prediction of the effects of friction control on top-of-rail cracks.

Purpose: The purpose of this study was to simulate the generation of cracks in different friction conditions and with different axle loads using rail and vehicle models from the IOL and the fatigue index (FI) method.

Abstract: RCF is a major problem affecting railway tracks, especially in curves, since it leads to a higher maintenance cost. By optimizing the top-of-rail friction, the wear and cracks on the top of the rail can eventually be reduced without causing too long a braking distance. There are several research articles available on crack prediction, but most of the research has focused either on the rail without friction modifier or on the wheels with and without friction control. In the study presented in this paper, in order to predict the formation of surface-initiated RCF, a range of friction coefficients with different Kalker's reduction factors has been assumed. Kalker's reduction factor takes care of the basic tendency of creepage as a function of the traction forces at lower creepage. The assumed range covers possible friction values from those for non-lubricated rail to those for a minimum measured friction control on the top of the rail using friction modifier. A fatigue index (FI) method based on the shakedown theory was used to predict the generation of surface-initiated RCF. Simulations were performed using multi-body simulation, for which inputs were taken from the IOL in the north of Sweden. The effect of friction control was studied for different curve radii, ranging from 200 m to 3,000 m, and for different axle loads from 30 tonnes to 40 tonnes at a constant train speed of 60 km/h. One example of a result is that a maximum friction coefficient (μ) of 0.2 with a Kalker's reduction factor of 15% is needed in the case of trains with a heavy axle load to avoid crack formation.

4.2 Paper 2

Title: Prediction of top-of-rail friction control effects on rail RCF suppressed by wear.

Purpose: The purpose of this study was to simulate the generation of cracks in different friction conditions and with different axle loads using rail and vehicle models from the IOL and the damage index (DI) method, which considers the effect of wear.

Abstract: RCF and wear, two major deterioration processes, limit the lifetime of rails. These deterioration processes are even more severe on the curves of tracks used by heavy haul trains. Because wear is a material removing process, it can suppress the formation of RCF (also known as surface-

initiated cracks). On railways, cracks are associated with a higher risk of instigating a catastrophic failure than wear; hence, it is comparatively better to have wear than to have cracks. By controlling the top-of-rail friction, both of these deteriorating processes can be reduced to enhance the lifetime of the rails. In order to achieve these possible advantages, the infrastructure manager of the Swedish railway network is planning to implement top-of-rail friction control technology on the IOL in northern Sweden, where RCF is a major problem on curves. The study presented in this paper used a DI method in a multi-body simulation software package to predict the probability of RCF formation with the suppressing effects of wear for different friction control values. The effect of friction control is simulated for curve radii ranging from 200 to 3,000 m and axle loads ranging from 30 to 40 tonnes at a constant train speed of 60 km/h. The findings show that on very sharp circular curves, i.e. curves with a radius < 300 m, RCF can be eliminated without friction control due to the high wear rate. On moderate curves, i.e. curves with a radius from 500 to 1,000 m, a friction coefficient (μ) of 0.3 or lower, with a Kalker's coefficient of 30% or lower is required to avoid RCF.

4.3 Paper 3

Title: Carry distance of top-of-rail friction modifiers.

Purpose: The purpose of this study was to investigate the carry distance of friction modifiers on both the rail and wheel.

Abstract: Rail problems such as corrugation, RCF, noise and wear have been increasing with an increase in the railway traffic. Top-of-rail friction modifiers (TOR-FMs) are claimed by their manufacturers in the railway industry to provide a well-established tool for overcoming the above-mentioned problems. There are various methods for applying friction modifiers at the wheel-rail interface, among which stationary wayside systems are recommended by TOR-FM manufacturers when a distance of a few kilometres is to be covered. TOR-FM manufacturers also claim that by using wayside equipment, TOR-FM can be spread over a minimum distance of 3 km, over which it maintains a friction coefficient of $\mu = 0.35 \pm 0.05$. To determine the carry distance of TOR-FM, some researchers have used tribometers to measure the friction coefficients. However, moisture and deposits from the environment and trains can alter the top-of-rail friction and give a misleading indication of the presence of a friction modifier. Therefore, the friction coefficient itself is not a clear indicator of the presence of TOR-FMs. In the study presented in this paper, cotton swabs dipped in a mixture of alcohol and ester were used to collect surface deposits (the third body) from both the wheel and rail, at various distances from the point of application. Subsequently, the third body collected on the cotton swab was analysed using energy-dispersive X-ray analysis. The results have shown that the maximum carry distance of TOR-FMs on the top of the rail is 70 m when using a TOR-FM from one manufacturer and 450 m when using a TOR–FM from another manufacturer. The corresponding carry distances on the contact band of the wheel are limited to 100 m and 340 m, respectively. Friction modifier was detected on the edges of the contact band over a distance up to 3 km, but this did not minimise the damage or friction at the wheel-rail interface.

5 RESULTS AND DISCUSSION

In this chapter, the results are discussed based on the RQs, with the different subsections explaining how the respective RQs have been answered.

5.1 Results and discussion relating to RQ 1

RQ 1. What is the effect of friction control on the generation of RCF on rails according to the fatigue index and damage index methods?

In this section, results relating to RQ 1 are presented and discussed. This question was answered in Paper 1 and 2. Two different methods were used in an MBS software package to answer this question. The first was the fatigue index (FI) method, which is based on the shakedown theory. The second was the damage index (DI) method, which is a combination of shakedown and energy dissipation theory. For details of the FI and DI methods, see Section A.4 and A.5 in the appendix, respectively. According to the author of the present thesis, the DI method is considered more realistic than the FI method as the former also considers the effect of wear on the generation of RCF. Both methods provide information on the risk of generating cracks in the form of an index. In the case of the FI method, the track irregularities were used, while in the case of the DI method, the track irregularities were removed to obtain noise-free results.

The FI and DI results for the different friction control levels are shown as a function of the distance in the curve in Figure 35. The results are arranged in such a way that the FI and DI results for both the high and the low rail can be compared. In both the methods, the index is highly sensitive to the friction coefficient. Since it is known that sharper curves have high traction forces, the results from the sharpest curve used in the simulation were used for the comparison of the effect of friction reduction.

In the case of the FI method, by reducing the friction coefficient from 0.5 to 0.3, the index values are reduced by more than 50%. On reducing the friction coefficient to 0.2, the index becomes negative, i.e. the probability of crack generation becomes zero. In the case of the DI results, in the circular part of the curve, it is seen that the wear dominates the RCF generation; i.e. in this case, it has crossed the magic wear rate. At the magic wear rate, the wear is equal to the RCF generation rate. When comparing the results generated using the DI and the FI method, it can be seen that the wear starts to dominate the RCF in the transition zone. However, in the transition zone, the index reaches the RCF (positive) zone. By reducing the friction coefficient from 0.5 to 0.3, the index in the transition zone is just on the border of the safe zone. On reducing the friction coefficient to 0.2, the index becomes negative, i.e. the probability of crack generation becomes zero.

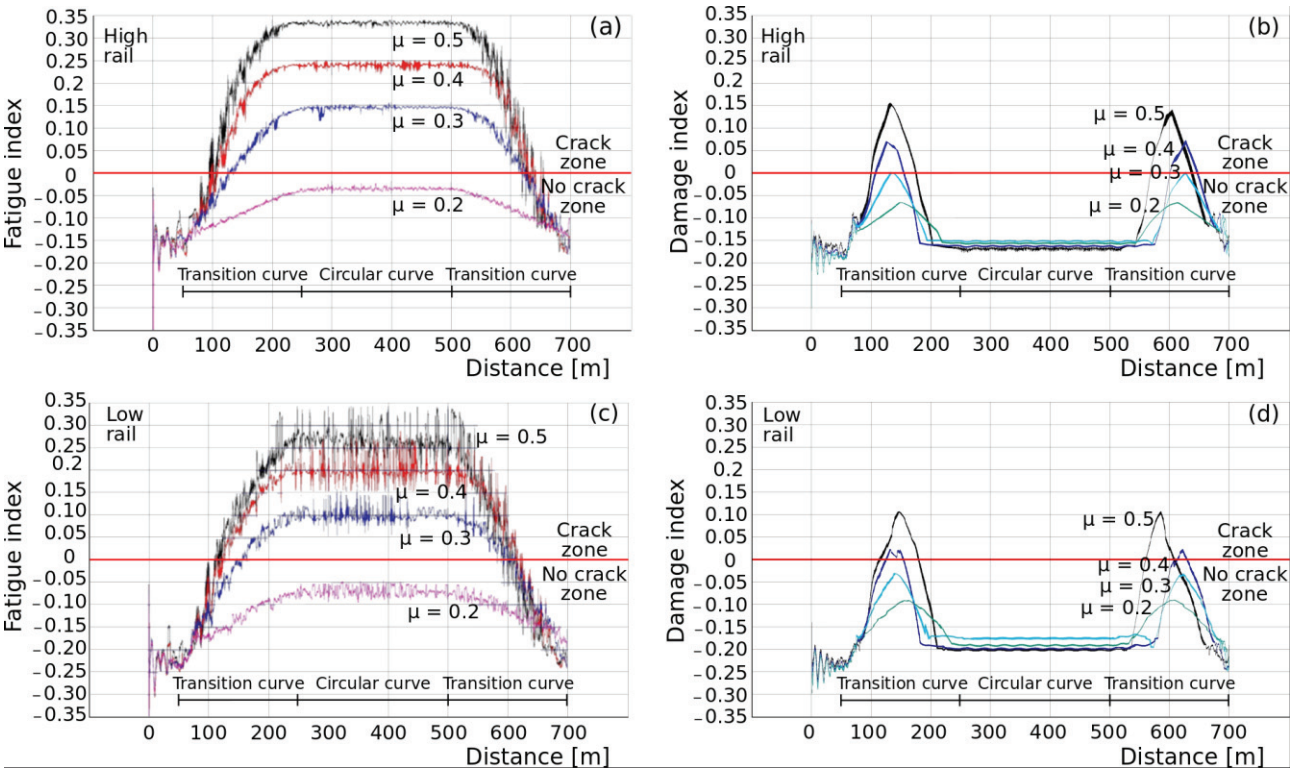

Figure 35. FI and DI results for a curve with a 200 m radius at different friction values with respect to the distance: (a) FI results for the high rail, (b) DI results for the high rail, (c) FI results for the low rail, and (d) DI results for the low rail.

It is not convenient here to present the index values for the complete 700 m-long simulated track section for the different friction values and with respect to the different curve radii. Therefore, the 95th percentile of the index values was used to represent the whole 700 m-long simulated track section. The maximum index value depends on the length of the simulation, and the longer a simulation is, the bigger is the risk that the wheel will pass a larger track irregularity. Therefore, the 95th percentile value was chosen instead of the maximum value, because the former is a stable value and independent of the length of the simulation. The 95th percentile means that 95% of the time, the index values are at or below the 95th percentile value. Conversely, 5% of the index values may exceed this value, but those 5% are ignored. To sum up, first the 95th percentile value of the complete circular or tangential curve was calculated as a representative value. Then the representative index values of either an entire circular curve or an entire transition curve were plotted on the y-axis with respect to the different curve radii on the x-axis.

Figure 36 represents the FI values for the different curve radii and friction control values. In this figure, the y-axis represents the 95th percentile of the FI values for the complete curve, and the x-axis represents the curve radii. It can be observed in the figure that by increasing the curve radius, the FI values decrease. This is because, when the curve radius is increased and the other parameters are kept constant, the traction forces decrease. Another aspect that can be observed is that with an increasing curve radius, the difference in the FI values between the different friction control values decreases. The reason for this is that, with larger curve radii, the traction forces are generally lower and, hence, the reduction in the FI due to friction control is not significant. The difference in the FI values is small for curve radii ≥ 1,000 m. For curve radii of 1,000 m and higher, the FI value almost stabilises and all

the values (for the high rail at μ=0.5) are within the safe zone. Therefore, from an RCF point of view, friction control does not play any major role for curves with a radius larger than 1,000 m.

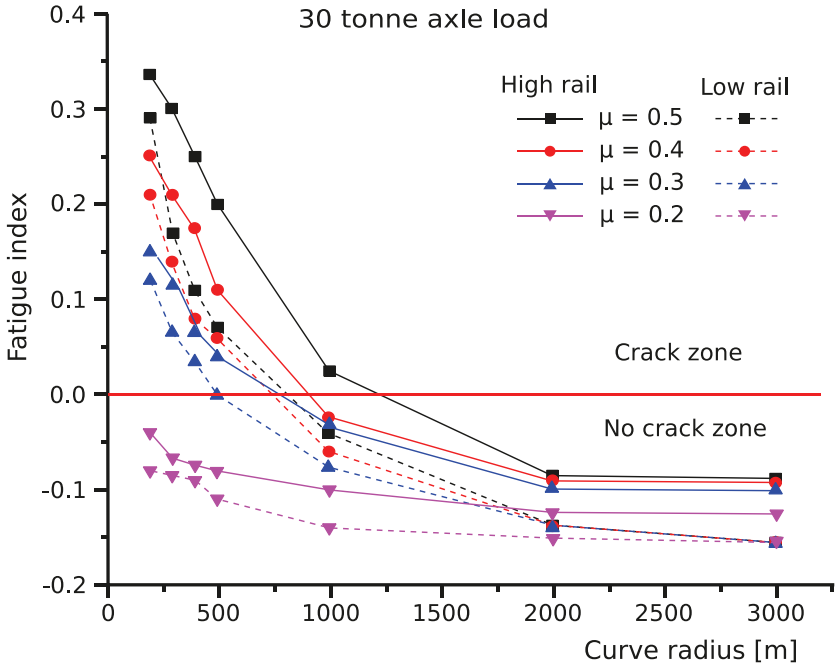

Figure 36. FI values (95th percentile) for all the curves with a radius from 200 m to 3,000 m at various friction control levels, both for the high and the low rail.

In the case of the DI results, there is a significant difference in the DI values between the circular and the transition curve. Therefore, the DI graphs showing the results for the different curve radii are shown separately for the circular and the transition curve in Figure 37.

As the wear rate in the circular section of the sharp curves is high, the probability of RCF is eliminated. In the case of the transition curve of curves with a radius of 200 m, the DI values are higher than those in the case of the circular curve. Due to the larger radius of the transition curve as compared to the circular curve of the same track section, the wear rate is not sufficient to eliminate the RCF on the complete transition curve. Therefore, in the case of a very sharp curve, there will be RCF only on the transition curve, as in the circular sharp curve (R < 300 m), the wear rate will be high enough to eliminate the RCF. Moreover, the trend of more RCF occurring on transition curves has been observed by the IOL track specialist at Trafikverket on some sharp curves in the field. The wear rate gradually decreases with an increase in the curve radius. When the curve radius reaches 400 m, the wear rate is already insufficient to suppress the formation of RCF. With an increasing curve radius, the creep forces decrease, which decreases the energy dissipation and, hence, both the wear and the probability of RCF. However, for curves with radii from 300 to 1,000 m, the creep force (and hence the wear) is insufficient to suppress RCF formation.

From the DI figures, it can be concluded that the curves with a radius smaller than 1,000 m are more prone to RCF when there is no friction control. It can be observed in Figure 37 that in the case of curves with radii smaller than 1,000 m, when the friction is controlled and kept at μ = 0.4 with a corresponding Kalker's reduction factor of 45%, the probability of RCF is decreased, but this level of friction control is inadequate to eliminate RCF formation. At a friction control value of μ = 0.3 or lower with a Kalker's reduction factor of 30% or lower, the DI values are in the RCF-free zone for

both the high and the low rails for all the curve radii. Based on Figure 37, it can be concluded that a friction coefficient value of 0.3 or lower with a Kalker's reduction factor of 30% or lower is required to avoid RCF on curves with a radius smaller than 1,000 m.

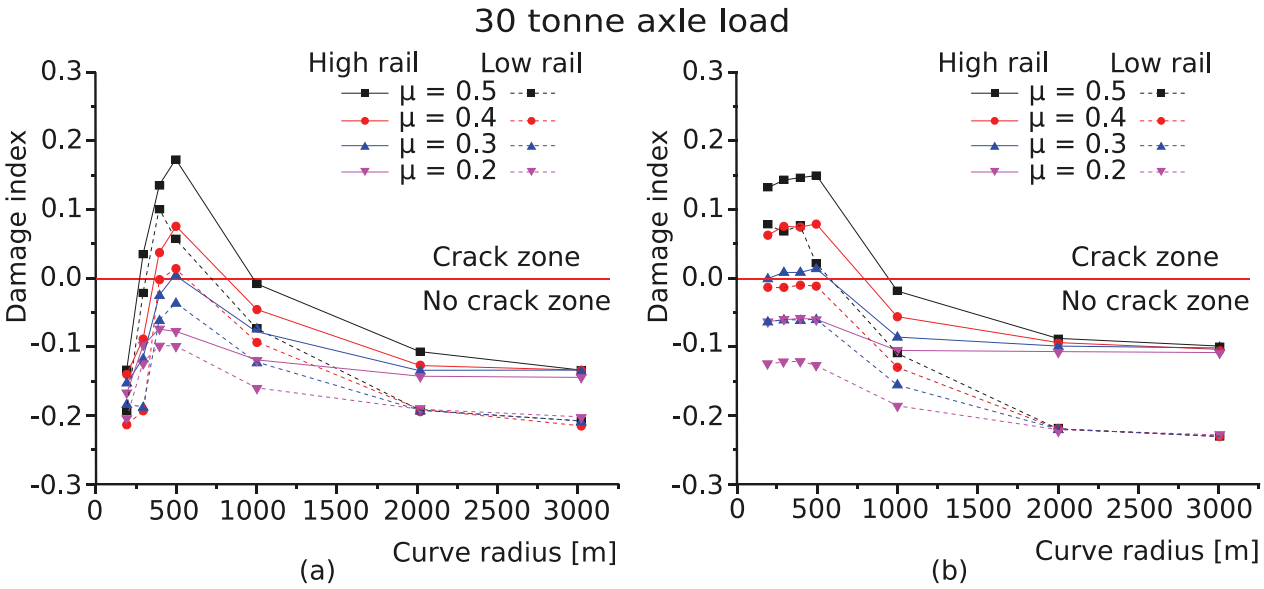

Figure 37. DI values (95th percentile) for all the curves from 200 m to 3,000 m at various friction control levels, both for the high and the low rail: (a) circular curves and (b) transition curves.

Notes:-

- *The FI and DI results for the higher axle load were published in the appended papers and are not discussed in this thesis since the results for axle loads of 32.5 − 40 tonnes are similar to those for a 30 tonne axle load. On increasing the load from 30 to 40 tonnes, there was an insignificant change in the FI and DI values because when increasing the axle load, the contact area between the rail and wheel also increases. The indexes are proportional to the contact pressure and not to the load.*
- *According to Trafikverket, curves larger than 1,500 m on the IOL are considered as equivalent to tangent track. In the case of tangent track, the forces on both the rails (both left and right) are the same. However, the results from the MBS are different for the right and the left rail in the case of the larger curves. This is because the high and low rail profiles used in the simulations were different. For the high rail, the profile used was the MB1 and for the low rail, the profile used was the 60E1.*

5.2 Results and discussion relating to RQ 2

RQ 2. What is the effect of TOR-FM on the wear, cracks and friction coefficient of rail in practice?

In this section, results relating to RQ 2 are presented and discussed. This section is divided into three parts. The first part discusses the results relating to the wayside side equipment, i.e. for the phase 1 experiments. The second part discusses the results for the carry distance experiments, which were published in Paper 3. The third section discusses the wear and friction properties of different TOR-FMs, which were investigated in phase 3 and the laboratory experiments.

5.2.1 Results relating to the wayside equipment

In this subsection, the results of the phase 1 measurements, which concerned the wayside equipment, are presented and discussed. Figure 38 shows the working status of the equipment during the period

when FM-A was investigated. The equipment worked for 72 days out of a total of 389 days, which means an availability of 0.185. Since it was observed that the carry distance of FM-A was very short, it was decided to switch to FM-B. The working status of the wayside equipment during the period when FM-B was installed is shown in Figure 39. During the first year of the field tests, many maintenance issues of the wayside equipment on the IOL were explored. In spite of the frequent inspections and maintenance actions, the wayside equipment worked for 163 days out of a total of 384 days when FM-B was installed, which means an availability of 0.425. During the project, it was also concluded that the wayside equipment should be shut down during the winter, as the temperature could go down to −40°C and the snow depth could be more than a metre. In such conditions, the survival of the battery would become impossible and the FM would freeze as well.

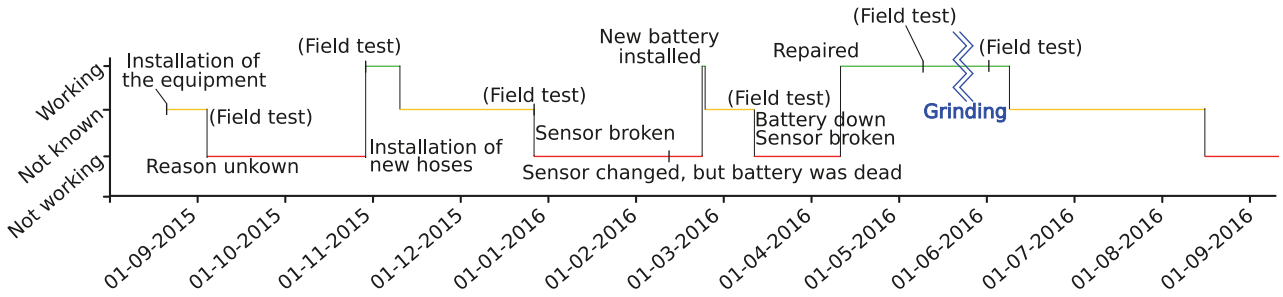

Figure 38. Working status of the wayside equipment from 18th August 2015 to 12th September 2016, when FM-A was investigated.

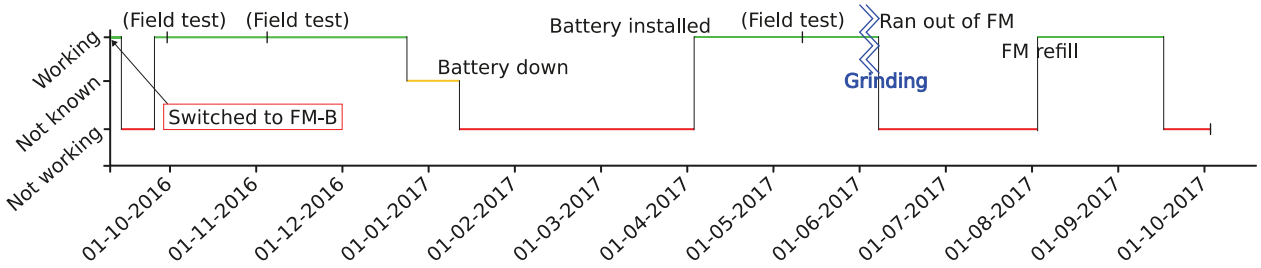

Figure 39. Working status of the wayside equipment from 13th September 2016 to 12th October 2017, when FM-B was investigated.

Figure 40 shows some of the breakdowns of the wayside equipment and the following are some of the reasons for the breakdown of the wayside equipment:

- breakage of the sensor due to infrastructure maintenance operations;
- the sensor sometimes being moved too close to or too far from the rail due to vibrations from trains;
- the gap between the rail and the distributing bars increasing due to vibrations from trains or maybe due to the maintenance vehicle with rubber tyres;
- winter issues such as:
    - the battery dying in the winter due to extreme cold or due to a lack of wind and sun;
    - the viscosity of the FM increasing with decreasing temperature, with FM-A freezing at −16°C and FM-B at −12°C.

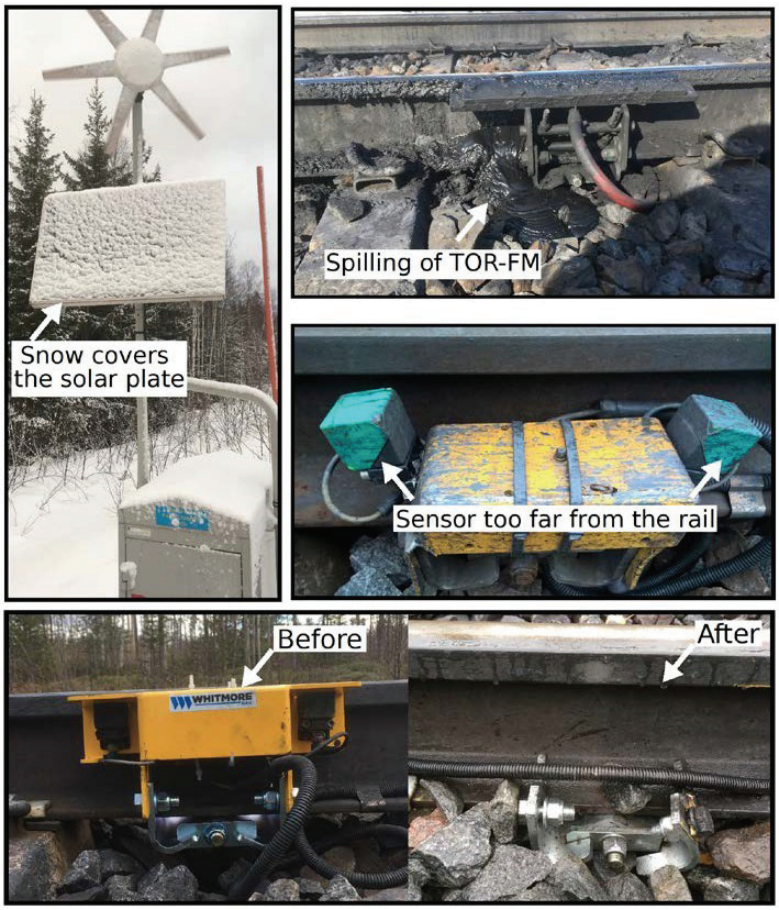

Figure 40. Different breakdowns of the wayside equipment experienced on the IOL during the investigations.

5.2.1.1 Friction measurement results

In the initial stage of the project, during most of the field visits, the equipment was out of order. In spite of that, the friction measurements were performed and the trend of friction on the rail in different weather conditions could be studied.

Table 13 shows the friction results from a field visit on 1st September 2015, when the weather was dry and sunny, with a temperature of around 6°C in the morning and 13°C in the afternoon, and the equipment was not working. A lower friction coefficient was expected at Gullträsk due to the presence of morning frost.

Table 13. Friction results from the field visit on 1st September 2015.

	High rail	**μ**	**Low rail**	**μ**
Gullträsk	H_1	0.48	L_1	0.52
	H_2	0.41	L_2	0.39
	H_3	0.46	L_3	0.40
Murjek	H_1	0.51	L_1	0.66
	H_2	–	L_2	–
	H_3	0.48	L_3	0.63

Note:- For an explanation of the symbols H_i and L_i, see the paragraph before Figure 28 in Section 3.3.1.

Table 14 shows the results from the field visit on 14th December, when the equipment was not working. The weather was clear, but there was no sun and the temperature was between −23°C and −27°C without snow. At both locations, the friction was approximately 0.3, and it is expected that at these low temperatures, a thin layer of ice is formed on the rail and when something slides over it, the ice layer melts and causes a reduction in the friction (Lyu, Bergseth and Olofsson, 2016). The difference in friction between the high and the low rail could be due to the grinding marks on the high rail, since the lateral forces (not shown here) have also shown a high fluctuation for H_1 and H_2 at Gullträsk.

Table 14. Friction results from the field visit on 14th December 2015.

	High rail	**μ**	**Low rail**	**μ**
	H_1	0.41	L_1	0.27
Gullträsk	H_2	0.37	L_2	0.31
	H_3	0.28	L_3	0.25
	H_1	0.31	L_1	0.32
Murjek	H_2	–	L_2	–
	H_3	–	L_3	–

Note:- For an explanation of the symbols H_i and L_i, see the paragraph before Figure 28 in Section 3.3.1.

On 3rd May 2016, the whole day was dedicated to friction measurement at Gullträsk. In this field test, the equipment was working and was filled with FM-A. The weather was dry and sunny and the temperature was approximately 10°C. All the measurements were performed on the low rail in the curve, as it was expected that the high rail would cause inconsistency in the results due to the presence of grinding marks up to the middle of the top of the rail. The measurements that were performed 6 m from the equipment were considered as TOR-FM experiments. Since it was known that the carry distance of FM-A is limited to 70 m, a location at a distance of 500 m was considered as an FM-free area. In addition, the friction was also measured at a maximum contact pressure of 2,100 MPa by manually applying an excessive amount of friction modifier. The results are shown in Figure 41, where the friction coefficients at three different speeds are shown on the y-axis with respect to five different contact pressures shown on the x-axis. In the case of the FM-free condition, the average friction is approximately 0.55. With the presence of FM, i.e. 6 m from the distributing bar, the average friction is approximately 0.3. However, on applying an excessive amount of friction modifier, the friction drops to approximately 0.15. It can also be seen that the friction coefficient in most cases is independent of the maximum contact pressure within the range 1,550−2,100 MPa, while a slight variation is shown in the friction with a change in speed.

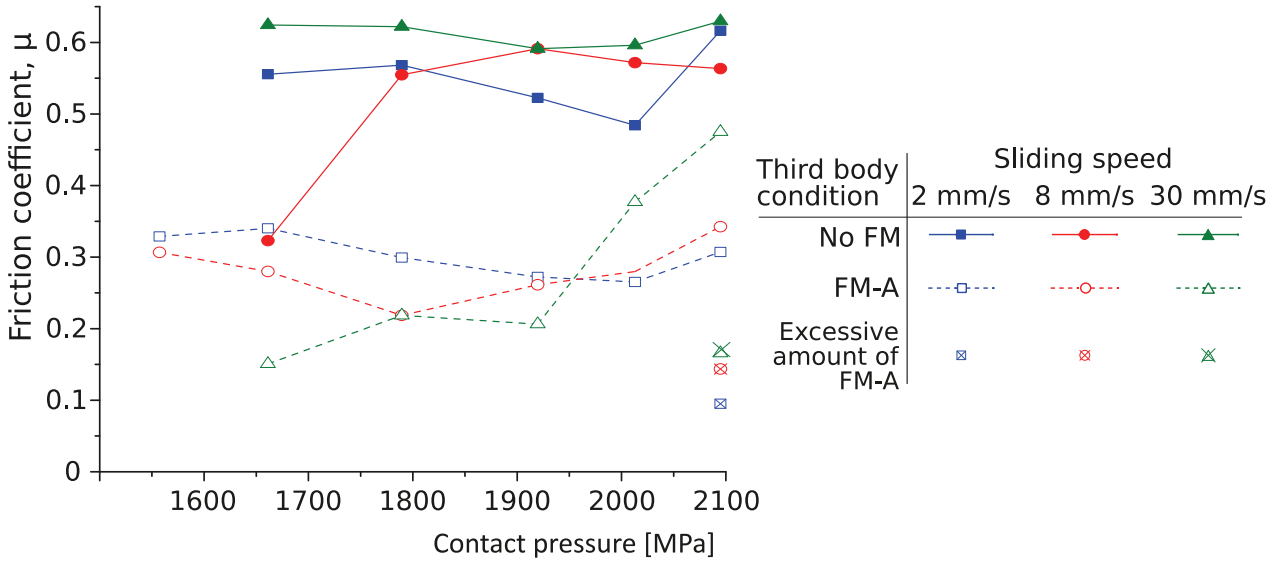

Figure 41. Friction values at different speeds with the presence of FM.

On the field visit on 4th November 2016, the equipment was working and was filled with FM-B. This field test was mainly dedicated to friction measurements and carry distance measurements at Gullträsk. The weather was snowy and highly humid and the temperature was approximately 1°C during the measurements. The friction was measured using both a ball-bearing ball and wear probes made of 350 LHT steel. Unfortunately, the wear could not be measured as the probe tip had been destroyed through mishandling. It can be seen in Table 15 that the friction coefficients at the equipment and 5 km away from the equipment are nearly the same, although no trace of the FM was observed 5 km away from the equipment. The results show that snow can cause an unacceptably low friction coefficient, as low as approximately 0.2, irrespective of the speed of sliding. However, the ball-bearing ball test showed a wide variation in the friction, which can be due to the surface roughness of the rail at the particular location where the measurement was performed.

Table 15. Friction results from the field visit on 4th November 2016.

Rubbing surface	**μ at a sliding speed of 1 mm/s**		**μ at a sliding speed of 5 mm/s**	
	6 m from the TOR equipment	5 km from the TOR equipment	6 m from the TOR equipment	5 km from the TOR equipment
Ball-bearing ball	0.12	0.19	Not available	0.28
Wear probe (350 LHT steel)	0.19	0.21	0.19	0.16

Table 16 summarises all the results of the friction measurements performed in phase 1. The table shows the average values in different weather conditions and with different third bodies. It can be seen that snow, extreme winter conditions and morning frost also decrease the friction coefficient and act as a lubricant or FM. The experiment in the snow condition also confirms that the FMs are not capable of increasing the friction coefficient in the case of snow and that an excessive amount of FM can even cause unacceptably low friction. However, it is expected that lubrication due to snow, rain or ice formation will remain only for a few wheel passages and may not be valid for a complete train. To know the degree of retention of such natural lubrication in practice, more research is needed.

Table 16. Summary of the friction tests in the phase 1 experiments.

Date of the field test	Temperature	Rain/snow/ sunny/morning frost	FM condition	Average friction Coefficient, μ
01-09-2015	Approx. 6°C	Morning frost/dew	No FM	0.44
	Approx. 13°C	Sunny/dry	No FM	0.57
14-12-2015	–23 to –27°C	Dry/no sun	No FM	0.32
03-05-2016	Approx. 10°C	Sunny/dry	FM-A	0.31
			No FM	0.55
			Excessive amount of FM-A	0.14
04-11-2016	Approx. 1°C	Snow	FM-B	0.17
			No FM	0.21

5.2.1.2 Roughness results

The results show that there is no particular trend in the change in roughness. In addition, no difference was found between the surface where TOR-FM had been applied and the surface where no TOR-FM had been applied. In most cases, at the location without spalling on the contact band, the average roughness (R_a) was between 0.10 and 0.17 μm. Figure 42 shows an example of the measurements performed on the running band on the top of the rail. The roughness diagram also shows the bearing area curve (BAC), also known as the Abbott-Firestone curve. The BAC has an S-shape appearance for many surfaces. The horizontal axis of the BAC represents the bearing area lengths as a percentage of the total assessment length of the profile and the vertical axis represents the heights of the profile (Gadelmawla et al., 2002).

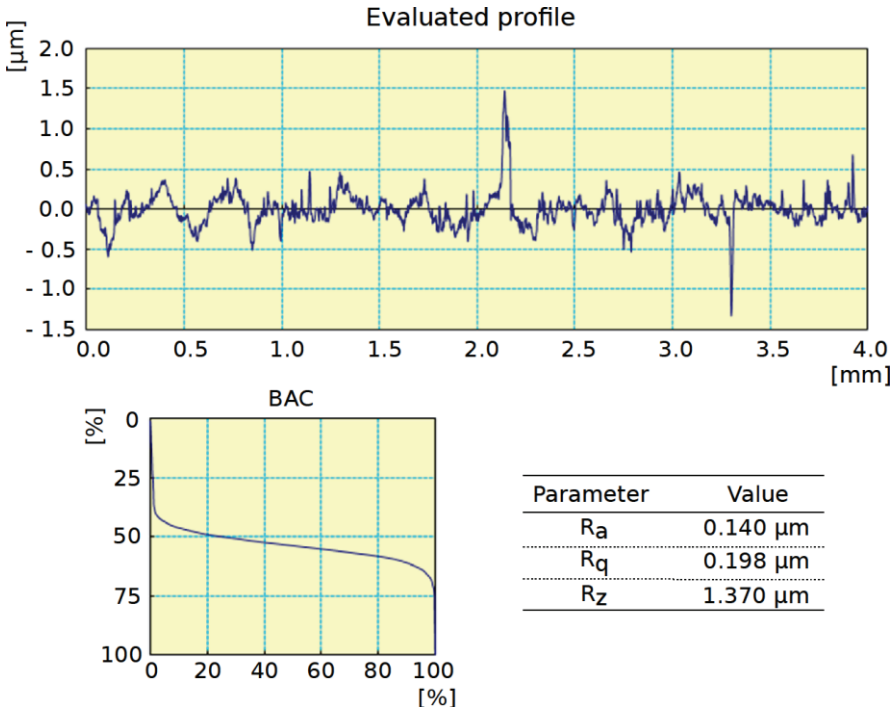

Figure 42. An example of the roughness results obtained on 24th May 2015.

5.2.1.3 Profile measurements

As stated earlier, the southern part of the IOL has annual grinding to remove RCF and retain the rail profiles. Therefore, the changes in the profiles between the consecutive grinding instances were compared. In the first year of phase 1, the availability of the installed equipment was poor and the carry distance of FM-A was limited to 70 m; therefore, the change in the profiles was not evaluated. The results of the profile measurements from 24th May 2016 to 12th May 2017 (a period of 353 days), i.e. during the second year of phase 1, are shown in Table 17.

According to the working status chart (Figure 39), the wayside equipment worked for 140 days, which means an availability of 39.7%. During most of this period, the tank was filled with FM-B. A slight reduction in wear is noticed at the gauge face of the transition zone, i.e. for H_1 and H_3. However, since the difference in wear is near the margin of accuracy of the equipment and the availability of the equipment was low, it is not sensible to draw any concrete conclusions from these one-year measurements. Due to the annual grinding practice, there was only a one-year window available for a follow-up of the damage on the rail. However, the results show that a period of one year was not sufficient to see any significant saving with the available equipment. The results show that the reference curve exhibits slightly lower wear than the curve where TOR-FM was applied; a possible reason for this may be the higher work-hardening of the reference rails, especially of the high rail, which was older. Unfortunately, it was not possible to obtain the exact age difference between the rails at these locations.

Table 17. Change in profiles (Wear) on reference and TOR curve.

Measurement location	**Wear on both the reference and the TOR curve**				**Wear reduction when TOR-FM is applied**	
	Gullträsk (TOR)		**Murjek (reference)**			
	Top of rail [mm]	Gauge face [mm]	Top of rail [mm]	Gauge face [mm]	Top of rail [mm]	Gauge face [mm]
L_1	0.17		0.06		−0.11	
H_1	0.14	0.77	0.05	0.84	−0.09	0.07
L_2	0.1		0.05		−0.05	
H_2	0.34	1.22	0.3	1.0	−0.04	−0.22
L_3	0.27		0.17		−0.1	
H_3	0.04	0.38	0.11	0.55	0.07	0.17

5.2.1.4 Crack follow-up

The crack follow-up shows that cracks were observed only before the first grinding. The cracks were seen in the middle and at the end of the low rail of the TOR curve at Gullträsk, i.e. at L_2 and L_3. The maximum length of the cracks was measured to be 2.4 mm, while the angle of the cracks is unknown. The cracks were already present when the field tests were started and the history of the cracks is

unknown. After the grinding, all the cracks were removed. No cracks were observed for the next one-year period, at the end of which the field tests were stopped as the project was approaching its end. The details of the crack follow-up are shown in Table 18. The results show that cracks were not generated when TOR-FM was used, since no crack was seen after the grinding when FM-B was used. However, the availability of the TOR-FM equipment was low and no cracks were observed on the reference curve in the period of two years. Therefore, there is a possibility that some other factor (for example the weather or surface hardness) limited the generation of cracks.

Table 18. Crack follow-up during the complete field test at Gullträsk

Crack follow-up at Gullträsk					
Date	**L_2**				**L_3**
	Crack 1	**Crack 2**	**Crack 3**	**Crack 4**	**Crack 1**
01-09-2015	0.2	0.7	1.3	No crack was found	No crack was found
30-10-2015	0.1	0.2	0.6	No crack was found	No crack was found
14-12-2015	0.3	1.2	1.8	No crack was found	No crack was found
01-03-2016	0.2	1.2	1.9	No crack was found	No crack was found
03-05-2016	0.7	1.4	2.4	0.7	0.3
Grinding					
24-05-2016	No cracks were observed				
30-09-2016	No cracks were observed				
04-11-2016	The focus was only on the wear, friction and carry distance				
12-05-2017	No cracks were observed				

5.2.1.5 Temperature measurements

Figure 43 shows the temperature measurements at Gullträsk from October 2015 to August 2017. The number of data collection points was increased after a certain point in time, which explains the denser part of the graph at the end. It should be noted that the graph also shows high temperatures during the summer due to sunlight shining directly on the measuring equipment. Since the main interest was the low temperature during the winter, these higher temperatures could be ignored. Figure 43 shows that from December to March (i.e. during the winter season), the average temperature was below –15°C. In the north of Sweden in the winter there is a very deep layer of snow, which covers the solar panel. Furthermore, the sun is available for a short period and at some locations is not available at all. The wind turbine generates an amount of electricity that is limited and insufficient to run the equipment. In the winter, not only does the survival of the battery become difficult, but also the TOR-FM freezes

or becomes too viscous to move. It is also expected that TOR-FM is not needed in the winter season as the snow and the ice layer act as a lubricant. However, this condition may be valid only for a few axle passages, after which the snow and the ice layer may be removed. Considering all the conditions prevailing, it is recommended that the equipment should be shut down during the winter.

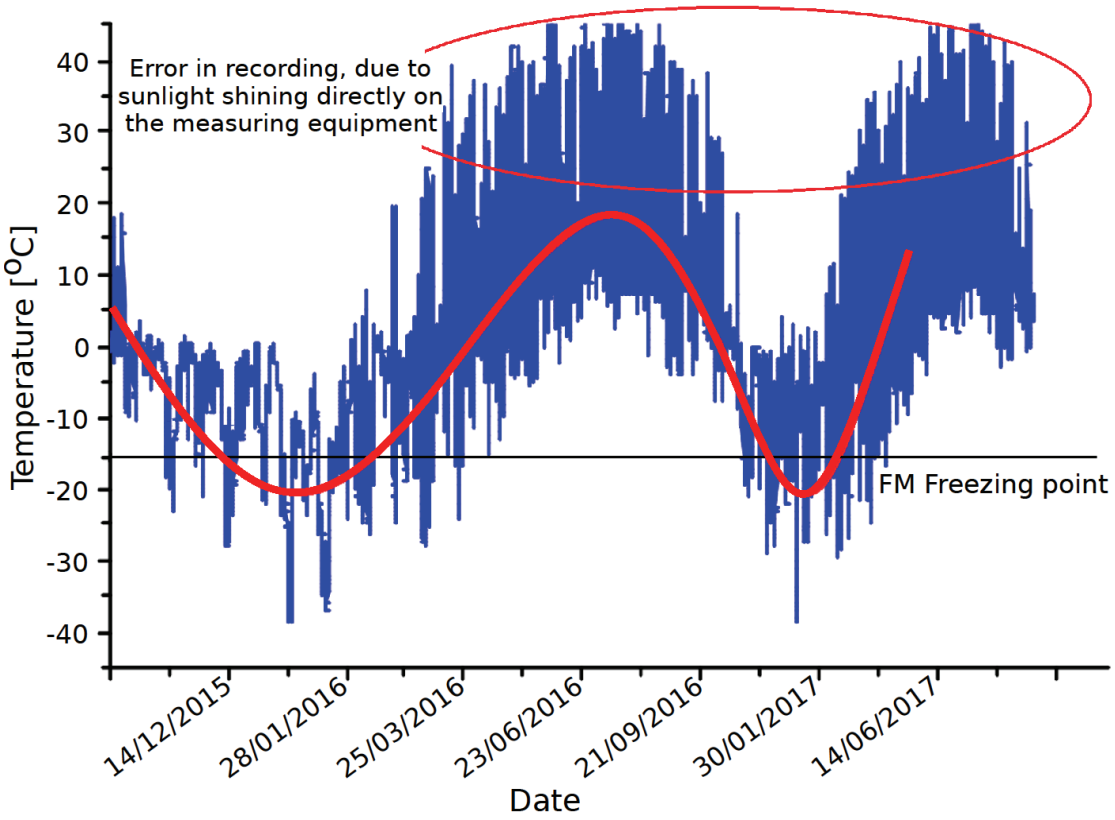

Figure 43. Temperature follow-up at Gullträsk, from 30/10/2015 to 02/10/2017.

5.2.2 Carry distance experiments

This and the following subsections present the results of the EDX analysis and the carry distance experiments. Before the carry distance experiments commenced, EDX analysis was used to calibrate the wt% of the elements present in FM-A and FM-B samples. Subsequently, the carry distances of these two TOR-FMs were measured in both phase 1 and 2.

The element weight percentages (wt%) detected with EDX analysis for FM-A, FM-B and the reference sample (free from FM) are presented in Table 19. The FM samples were collected from the pools of FM at the distributing bars, while the reference sample was collected 35 km away from the installed wayside equipment. As indicated in Table 19 with "ticks", two elements not found in the reference sample were observed in FM-A: magnesium (Mg) and molybdenum (Mo). With regard to FM-B, in addition to Mg and Mo, barium (Ba) was also observed to be an element present in FM-B, but not in the reference sample. These elements were denoted as key indicator elements in the present research since one can conclude from their presence that FM is present. Other elements that could represent the ingredients of the FMs were either present in the reference sample or present in FM-A and FM-B in negligible quantities, and hence were ignored.

Table 19. Element wt% of both the FMs and the reference, i.e. the FM-free sample. The elements indicating the presence of FMs are ticked. Each result is an average of five measurement points with a standard deviation.

Elements	Element (wt%)			Key indicator elements	
	FM-A	**FM-B**	**Reference (FM free)**	**FM-A**	**FM-B**
C	35.8 ± 16.5	30.1 ± 12.3	30.9 ± 7.4		
O	17.9 ± 4.6	29.1 ± 9.1	30.8 ± 7.2		
Mg	3.6 ± 1.4	7.2 ± 3.4	0.1 ± 0.1	✓	✓
Si	6.4 ± 3.1	7.7 ± 3.9	3.1 ± 1.9		
S	12.1 ± 7.6	8.2 ± 5.5	1.9 ± 0.9		
Fe	0.8 ± 0.1	0.6 ± 0.1	36.9 ± 11.8		
Zn	1.3 ± 0.3	0.0 ± 0.0	0.0 ± 0.0		
Mo	16.1 ± 12.8	15.3 ± 10.7	0.0 ± 0.0	✓	✓
Ba	0.14 ± 0.03	8.7 ± 3.7	0.0 ± 0.0		✓
W	1.0 ± 0.2	0.0 ± 0.0	0.0 ± 0.0		

5.2.2.1 Phase 1: Carry distance results for the wayside equipment

The carry distance results for the wayside station were obtained at an application rate of one litre per 1,000 axles, which is approximately four times the recommendation of the manufacturer. FM-A, which is claimed to have no oil content, shows a poor carry distance of 70 m. This carry distance is extremely short when compared with the claim of the manufacturer that the carry distance is more than 3 km. In the case of FM-B, which is believed to contain a non-drying additive, this TOR-FM shows a carry distance of up to 450 m, i.e. approximately six times longer than that of FM-A, but still notably less than the 5 km claimed by the manufacturer. Table 20 summarises the carry distances measured for each element.

Table 20. Carry distance corresponding to each key indicator element – phase 1 results.

Elements	Carry distance [m]	
	FM-A	**FM-B**
Mg	60	360
Mo	70	450
Ba	–	325

5.2.2.2 Phase 2: Carry distance on a wheel and rail with a limited amount of FM applied manually

This subsection is divided into three parts. The first part discusses the carry distance on the top of the rail, the second discusses the carry distance on the whole width of the running surfaces of the wheels, and the third discusses the carry distance on the wheel-rail contact band.

Samples collected from the top of the rails: As shown in Table 21, FM-A is carried forward over a distance up to 65 m and FM-B is carried forward over a distance up to 320 m. It is observed that FM-A dried faster than FM-B and could not be transferred to the rail over a longer distance than 65 m. However, FM-B dries slowly and is transferred a longer distance.

Table 21. Carry distance corresponding to each key indicator element – phase 2 results for the top of the rail.

Elements	Carry distance [m]	
	FM-A	**FM-B**
Mg	50	160
Mo	65	320
Ba	–	290

Samples collected from the complete running surfaces of the wheels: As shown in Table 22, for both the FMs, a carry distance of more than 3 km was observed on the complete running surface of the wheel. It should be noted that this result does not mean that the FMs came into the wheel-rail contact band, since the FMs mainly stuck to the edges of the contact band or in some cavity in the wheel. Therefore, samples from the middle of the contact band were collected and are discussed in the following.

Table 22. Carry distance corresponding to each key indicator element – phase 2 results for the complete running surface of the wheel.

Elements	Carry distance [m]	
	FM-A	**FM-B**
Mg	>3,000	>3,000
Mo	>3,000	>3,000
Ba	–	>3,000

Samples collected from the wheel-rail contact band: As discussed earlier, when a wheel passes over a pool of FM, as in the case of the stationary equipment, due to pressure and splashing, the FM reaches and sticks to the non-contact running surface of the wheel and stays there for a long distance. However, the actual need of the FM is on the contact band. Therefore, in this section, samples were collected from the middle of the contact band and the results proved to be contrary to those for the complete running surface. Table 23 shows that on the wheel-rail contact band, FM-A was detected

over a distance up to 100 m, while the key indicator elements for FM-B were detected over a distance up to 340 m.

Table 23. Carry distance corresponding to each key indicator – phase 2 results for the contact band of the wheel.

Elements	Carry distance [m]	
	FM-A	**FM-B**
Mg	0	105
Mo	100	340
Ba	–	155

An overview of all the experiments is presented in Table 24, which summarises all the carry distance results for both FMs.

Table 24. Summary of carry distances for FM-A and FM-B.

Source	Position of sample collection	Carry distance [m]	
		FM-A	**FM-B**
Manufacturer's claim		3.2–6.4 km	5 km
When supplied continuously by the stationary equipment	Top of rail	70	450
When applied once manually	Top of rail	65	320
	Wheel's running surface	>3,000	>3,000
	Wheel's contact band	100	340

5.2.3 Comparison of different TOR-FMs in the field and the laboratory

This subsection discusses the results relating to friction and wear measurements carried out in the laboratory and the phase 3 field experiments. In order to determine the effect of the quantity of FM on the friction, different layers of FM were formed in the laboratory to execute the friction measurements. The measurements were performed at room temperature and humidity. Since the manufacturing of the wear probes is expensive, these experiments were performed as a pre-study to the wear experiments. Figure 44 consists of diagrams showing the different lateral forces recorded using a force sensor from Pasco. As shown in Figure 44, the cleaned surface has a wide fluctuation band of lateral forces, but on the application of FM, the fluctuation band becomes narrow. In the case of FM-

C, which is an oil-based FM, the fluctuation always has a narrow band irrespective of the amount of FM.

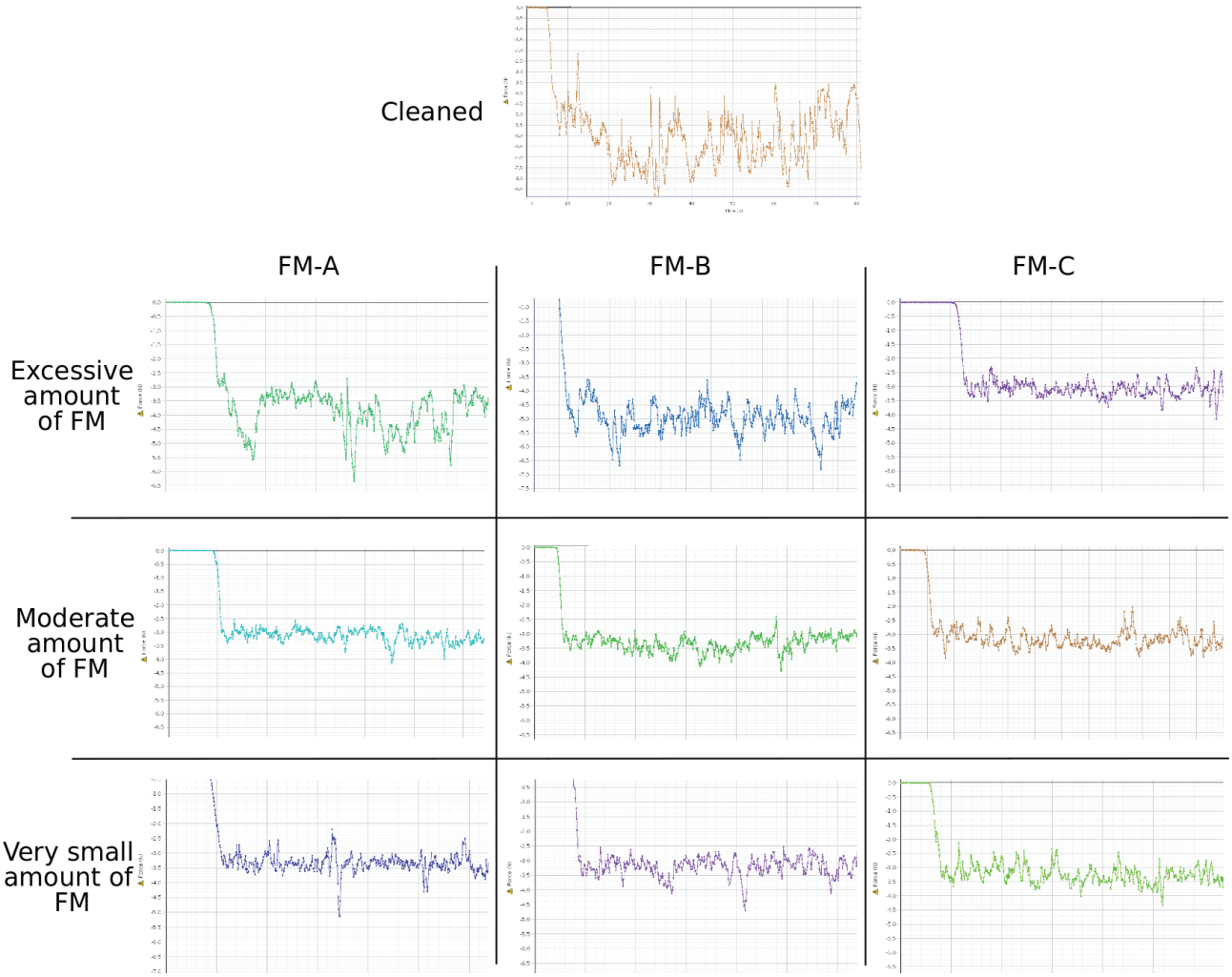

Figure 44. Lateral forces with different film thicknesses and measured in the laboratory.

Table 25 shows the friction coefficient when different amounts of three different FMs have been applied. The cleaned surface in room conditions without any third body shows a friction coefficient of 0.28 and the coefficient can fall to a value lower than 0.20 even after a very small amount of FM has been applied. When studying the results, it can be observed that even a small amount of FM decreases the friction coefficient, and increasing the amount of FM does not decrease the friction coefficient further. However, in the case of a real railway wheel, the amount of FM applied can influence the friction due to the large scale of the real wheel scenario.

Table 25. Friction coefficient with different film thicknesses.

Third body condition	Amount of FM	Measurement number	Lateral force	Vertical force	Friction
Cleaned		1	6.42	22.63	0.28
		2	6.22	22.63	0.27
		3	6.31	22.63	0.28
FM-A	Excessive amount	4	3.13	22.63	0.14
		5	3.01	22.63	0.13
		6	2.83	22.63	0.12
	Moderate amount	7	3.28	22.63	0.14
		8	3.29	22.63	0.15
		9	3.27	22.63	0.14
	Very small amount	10	3.17	22.63	0.14
		11	3.35	22.63	0.15
		12	3.18	22.63	0.14
FM-B	Excessive amount	13	3.25	22.63	0.14
		14	3.52	22.63	0.16
		15	3.45	22.63	0.15
	Moderate amount	16	3.32	22.63	0.15
		17	3.41	22.63	0.15
		18	3.45	22.63	0.15
	Very small amount	19	4.44	22.63	0.20
		20	3.54	22.63	0.16
		21	3.98	22.63	0.18
FM-C	Excessive amount	22	3.28	22.63	0.14
		23	3.37	22.63	0.15
		24	3.10	22.63	0.14
	Moderate amount	25	3.24	22.63	0.14
		26	3.17	22.63	0.14
		27	3.09	22.63	0.14
	Very small amount	28	3.10	22.63	0.14
		29	3.15	22.63	0.14
		30	3.37	22.63	0.15

Figure 45 and Table 26 show the wear versus the friction coefficients in the laboratory conditions. The wear constant "K" was calculated using Archard's wear method and is directly proportional to the wear. Archard's wear method is discussed in detail in Section A.2 in the appendix. FM-A and FM-C show good repeatability and give an average friction coefficient of 0.1 and an average wear constant of 3×10^{-5}. FM-B and the FM-free condition show good repeatability with regard to friction, but poor repeatability in terms of the wear constant. The wear constants of two of the measurement points in the case of the FM-free condition are close to those of the FM condition, but one of the measurement points exhibits a significant difference. This poor repeatability in terms of the wear constant could be due to a difference in roughness at the location of measurement. When studying the average wear reduction for each FM compared to that for the dry condition in Table 26, one can observe that FM-C shows a reduction of approximately 74%, FM-A shows a reduction of

approximately 67% and FM-B shows a reduction of approximately 45%, which is the smallest reduction.

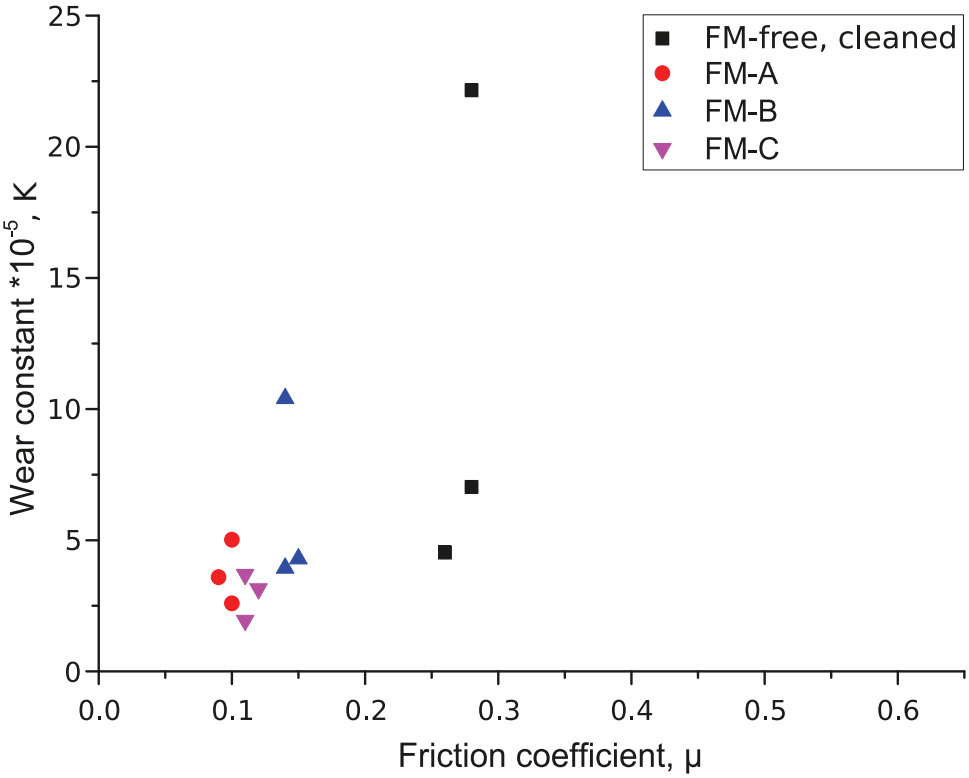

Figure 45. Graph showing the relation between the wear constant and the friction coefficient of different third bodies in the laboratory conditions.

Table 26. Summary of the wear and friction results for different third bodies in the laboratory conditions.

Third body condition	Probe number	Measured friction value	Avg. diameter [μm]	Wear volume $\times 10^{-5}$ [mm^3]	Wear constant $\times 10^{-5}$ (K)	Avg. wear constant $\times 10^{-5}$ (K)	% reduction in wear
FM free, cleaned	1	0.28	291.25	14.14	7	11.2	0.00
	2	0.26	261.00	9.12	4.5		
	3	0.28	388.00	44.57	22.2		
FM-A	4	0.09	246.25	7.22	3.6	3.7	67
	5	0.10	227.00	5.21	2.6		
	6	0.10	267.75	10.10	5		
FM-B	7	0.14	252.00	7.92	3.9	6.2	45
	8	0.15	257.50	8.64	4.3		
	9	0.14	321.25	20.93	10.4		
FM-C	10	0.11	248.00	7.43	3.7	2.9	74
	11	0.12	238.25	6.33	3.2		
	12	0.11	211.25	3.91	1.9		

Figure 46 and Table 27 show the wear versus the friction coefficient based on results obtained in tests performed in the field with real third bodies. The measurements were carried out on the track at Luleå Railway Station, which is used by heavy haul trains operated by LKAB. As can be observed in Figure 46, when FM has been applied, the friction coefficient shows good repeatability when compared to the friction coefficients measured for the FM-free condition. However, the wear constant shows poor repeatability in all the cases except for FM-C and FM-free, cleaned condition. This poor repeatability could be due to the inhomogeneous nature of the third bodies and the difference in roughness at different spots. FM-C shows the maximum reduction of wear in relation to the FM-free and untouched condition, but the average wear constants and friction coefficient for all the FMs are slightly higher than the wear constants obtained in the laboratory measurements. Differences in the wear constants are to be expected due to the presence of real third bodies on the top of the rail. These third bodies can consist of moisture, dirt, water, snow, lubricant deposits, brake pad deposits, cargo deposits, pollution, etc. The most interesting results are those for the FM-free and untouched surface and the FM-free and cleaned surface. In both these cases, no FM was applied, and a comparison of the results reveals that by removing the third bodies, a wear reduction of 72% can be observed, which is higher than the wear reduction of FM-A and FM-B. Dirks (2015) reported that in the field the wear was approximately four times lower than in the laboratory measurements due to the presence of third bodies which act as a lubricant. However, the present results have shown that in the field the wear of a surface with the presence of third bodies is approximately four times higher than that of a cleaned surface with no third bodies. This shows that the wear and friction are highly dependent on the third bodies. The values can vary greatly, and in this case there is an eightfold difference between the results obtained by Dirks (2015) and those obtained in the present research.

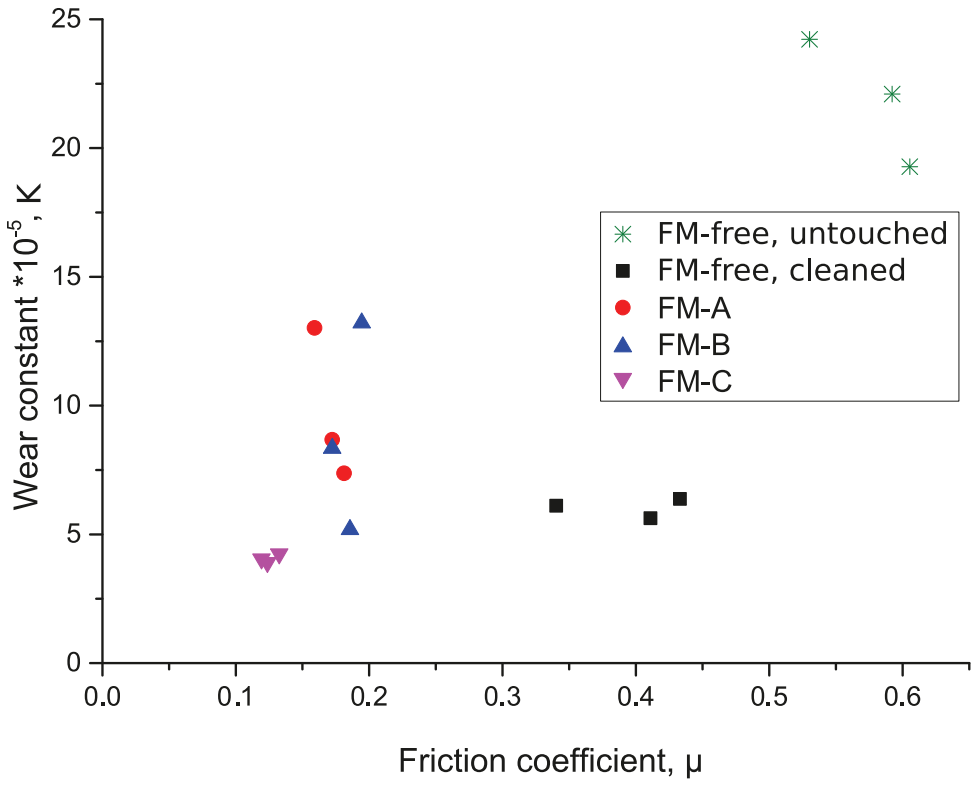

Figure 46. Graph showing the relation between the wear constant and the friction coefficient of different third bodies in the field conditions.

Table 27. Summary of the wear and friction results for different third bodies in the field conditions.

Third body condition	Probe number	Measured friction value	Avg. diameter [μm]	Wear volume $\times 10^{-5}$ [mm^3]	Wear constant $\times 10^{-5}$ (K)	Avg. wear constant $\times 10^{-5}$ (K)	% reduction in wear
FM free, untouched	1	0.53	396.75	48.73	24.2	21.9	0.00
	2	0.59	387.75	44.45	22.1		
	3	0.61	374.75	38.78	19.3		
FM free, cleaned	4	0.43	284.25	12.83	6.4	6.0	72
	5	0.34	281.25	12.29	6.1		
	6	0.41	275.50	11.32	5.6		
FM-A	7	0.17	307.00	17.45	8.7	9.7	56
	8	0.16	339.75	26.19	13		
	9	0.18	294.75	14.83	7.4		
FM-B	10	0.17	304.00	16.78	8.3	8.9	59
	11	0.19	270.00	10.44	5.2		
	12	0.19	341.00	26.58	13.2		
FM-C	13	0.12	253.75	8.14	4.1	4.1	81
	14	0.12	251.50	7.86	3.9		
	15	0.13	256.75	8.54	4.2		

The wear measurements have shown that a significant reduction in wear was achieved by using TOR-FM, but the measured friction coefficients were lower than the standard friction coefficient for safe operation (Lundberg et al., 2014). The reason for the low friction could be an excessive use of TOR-FM. In the laboratory experiments, the amount of FM did not significantly affect the friction coefficient. However, in the field, different amounts of FM behaved differently, probably due to the presence of natural third bodies on the rail, and maybe due to the larger scale of the wheel-rail contact interface area in the field experiments.

The results of the FricWear 2017 measurements were compared with the friction values measured using a fully loaded heavy haul train on the IOL (Lundberg et al., 2014). Lundberg et al. (2014) measured the friction coefficient in the FM-free and water-based FM conditions directly from torque and slip measurements performed with the locomotive's inbuilt traction-force measurement system. Comparing the friction results for the water-based FMs (FM-A and FM-B) of the present research with the friction results of the study conducted by Lundberg et al. (2014), it was observed that the FricWear 2017 measured higher friction values compared to the friction values measured by the locomotive, i.e. the real friction values. The values of the friction coefficient measured by the FricWear 2017 are higher by a factor of 1.9 and 1.3 in the FM-free and untouched condition and the FM-free and cleaned condition, respectively. In the case of the water-based FMs (FM-A and FM-B), the FricWear 2017 gave higher friction values by a factor of 1.4. Such a difference in the friction values is

to be expected due to the scaling factor. Because of the scaling factor, roughness plays an important role since the size of the ball-bearing ball and wear probe used in the FricWear 2017 is very small when compared to the actual wheel of a train. However, more research is needed to determine the exact reason for the difference in results.

No similar study has been performed to measure the actual wear on the rails using FM in similar conditions. It is known that wear and friction have no established relationship, but in many cases it has been observed that with an increase in the friction, the wear increases. Therefore, the measured wear values were normalised assuming a linear relationship between wear and friction, and the normalised values were used for the LCC calculations. When calculating the LCC, using wear reduction values obtained at unacceptably low friction values as the real values would be incorrect. Therefore, the wear reduction was normalised to the wear at a friction coefficient of 0.3. According to the manufacturers of the FMs, the friction coefficient should always be about 0.3, unless the amount of FM applied is too large or too small. The normalisation is carried out by simply making a linear relationship between the friction coefficient and the wear constant by taking the average values of the field tests. The normalised wear constant values of the respective FMs are the values obtained at a friction coefficient of 0.3, as shown in Figure 47. The exact values of the wear constant and the reduction in wear at the normalised value are shown in Table 28. It can be seen that the normalised wear constants of the different FMs do not show as big a variation as the measured wear constants. Normalisation is a conservative approach implemented to avoid wrong estimation of the LCC.

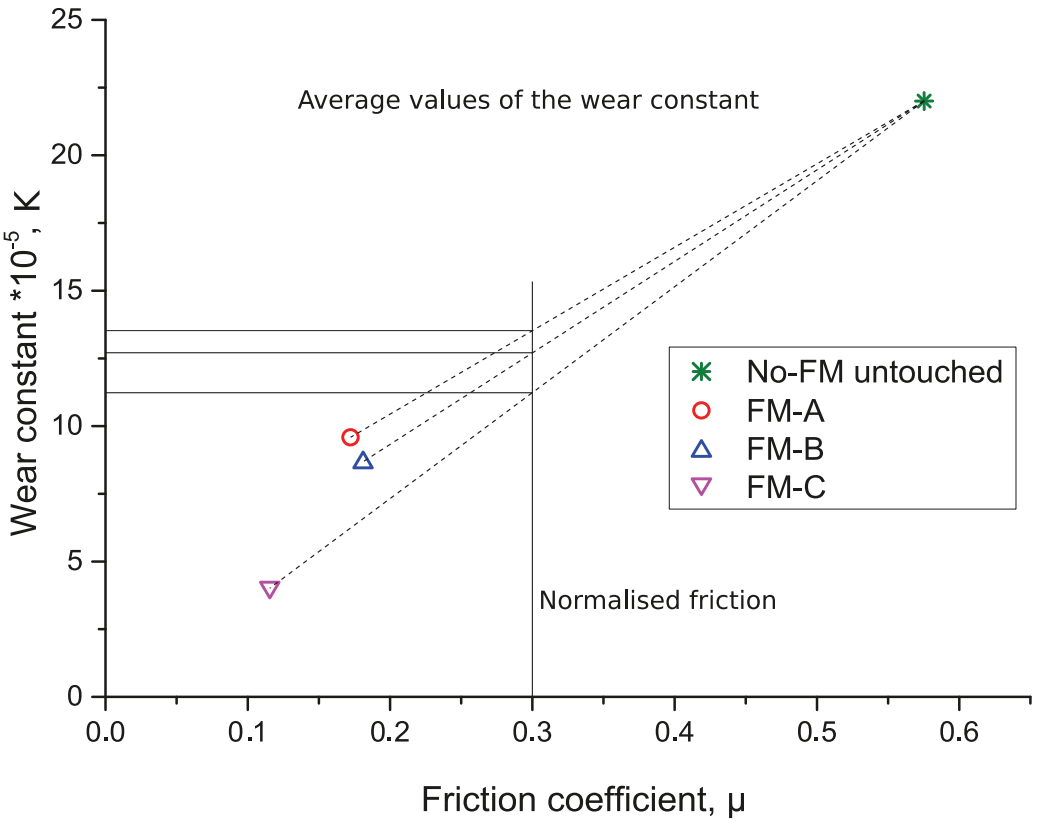

Figure 47. Normalisation of the average friction values of different friction modifiers.

Table 28. Normalisation of the average friction values of different friction modifiers.

Third body condition	Avg. wear constant [$\times 10^{-5}$ (K)]	Avg. wear constant at μ=0.3 [$\times 10^{-5}$ (K)]	Normalised wear reduction at μ=0.3	Increased life of rail at normalised wear rate
No FM, untouched	21.9	–	–	–
FM-A	9.7	13.5	38%	61%
FM-B	8.9	12.7	42%	72%
FM-C	4.1	11.2	49%	96%

As shown in Table 28, the normalised wear reduction for FM-A and FM-B is 38% and 42%, respectively. For the LCC calculations, the average value for FM-A and FM-B was used, i.e. 40%, as only these FMs were used in the field tests conducted for the present research. FM-A and FM-B are designated as water-based FMs by their manufacturers and the recommended consumption specified by the manufacturers is 30 ml/km/rail. FM-C is designated as an oil-based FM and the recommended consumption specified by its manufacturer is approximately 5 kg per 10,000 km, which is much lower than the consumption recommended by the manufacturers of the water-based FMs.

The increase in the lifetime of a rail is calculated as follows. Let us assume, for example, that the life of a rail is 15 years without FM; on applying FM, the wear is reduced by 40%, which means that if the rail is wearing at a rate of 1 mm/year without FM, then the wear will be reduced to 0.6 mm/year by applying FM. Therefore, instead of lasting 15 years at a wear rate of 1 mm per year, the rail will last 25 years at a wear rate of 0.6 mm per year (15 ÷ 0.6 = 25), which represents a 66.67% increase in the life of the rail.

5.3 Results and discussion relating to RQ 3

RQ 3. What is the life cycle cost of a TOR-FM system?

In the following subsections, the results relating to RQ 3 are presented and discussed, i.e. the results for the LCC calculations. The input for the LCC calculations was taken from the experiments performed in the present research. All the costs were calculated for 300 MGT, which is equivalent to a lifetime of 15 years.

5.3.1 LCC of the rail without considering TOR-FM systems

The LCC of rail after 15 years was calculated as follows:

$$\text{LCC of rail} = \text{rail replacement cost} + \left(\sum_{i=1}^{14} \frac{\text{grinding cost}}{(1+r)^i}\right) + \text{disposal cost}$$

Acquisition cost and installation cost = cost of acquisition and installation (per metre) × length
= 4,000 × 450 = 1,800,000 kr

Grinding cost (maintenance) = grinding cost per metre × length of the curve
= 50 × 450 = 22,500 kr

Disposal cost of the rail = 0 kr (Trafikverket gives the rail to the contractor to be scrapped.)

Table 29 and Table 30 show the LCC of the rail without considering TOR-FM effect for curves less than 550 and curves between 550 and 850 respectively.

Table 29. LCC of rail without considering the TOR-FM effect for curves with a radius smaller than 550 m.

Year	Phase	Cost	Formula used	Cost in present value
0	Acquisition	1,800,000	–	1,800,000
1–14	Maintenance (Grinding)	22,500	$\sum_{i=1}^{14} \frac{22{,}500}{(1+0.035)^i}$	245,712
15	Disposal	0		0
Total present value				2,045,712

Table 30. LCC of rail without considering the TOR-FM effect for curves with a radius from 550 to 850 m.

Year	Phase	Cost	Formula used	Cost in present value
0	Acquisition	900,000	–	900,000★
1–15	Maintenance (Grinding)	22,500	$\sum_{i=1}^{15} \frac{22{,}500}{(1+0.035)^i}$	259,142
Total present value				**1,159,142**

★*In the case of curves with a radius between 550 and 850 m, the life of the rail is double the life of the rail in curves with a radius smaller than 550 m, and therefore the acquisition cost was divided by 2 and the disposal cost was not considered.*

LCC for curves with a radius smaller than 550 m (60 curves)
= 2,045,712 × 60 = 122,742,720 kr

LCC for curves with a radius between 550 and 850 m (97 curves)
= 1,159,142 × 97 = 112,436,774 kr

5.3.2 LCC of the wayside equipment

Acquisition cost

Acquisition cost	= 250,000 kr
Installation cost	= 12,000 kr
Total acquisition and installation cost	= 262,000 kr

Operation cost

Consumption of FM per day per curve passages per day	= Applied FM amount per axle × number of axle		
	= (300/1,000) × 1,500		
	= 450 ml	= 0.45 L	
FM consumption per year per curve	= 0.45 × 365	= 164.25 L	
FM cost per year	= 164.25 × 160	= 26,280 kr	≈ 26,000 kr

Material cost

Table 31 shows the replacement frequency recommended by the manufacturer and the cost of each part.

Table 31. Life expectancy and cost of different parts of the wayside system, provided by the manufacturer.

Parts	Replacement frequency	Part cost
Battery	2 years	2,600
Control box	5 years	42,000
Fasteners	5 years	1,500
Blade and pump hose	2 years	21,700
Wheel sensors (×2)	3 years	6,200

Man cost

One day cost per man = 750 × 8 = 6,000
Transportation cost = 1,300 kr

Total man cost per unit of equipment per year

$$= \frac{(\text{man cost per day} + \text{transportation cost}) \times \text{number of visits per year}}{\text{Number of units of equipment repaired in a day}}$$

$$= \frac{(6{,}000 + 1{,}300) \times 4}{3} = 9{,}733.33 \approx 9{,}700 \text{ kr}$$

Disposal (phase-out) = 25,000 kr

Table 32 shows the LCC of a unit of wayside equipment for 15 years when FM is applied on a single curve.

Table 32. LCC of a unit of wayside equipment.

Year	Phase		Unit cost / Cost per year	Formula used	Cost in present value
0	Acquisition		262,000		262,000
0–14	Operation and maintenance	FM cost	26,000	$\sum_{i=0}^{14} \frac{26{,}000}{(1+0.035)^{i}}$	309,934
0–14		Man cost	9,700	$\sum_{i=0}^{14} \frac{9{,}700}{(1+0.035)^{i}}$	115,629
Every 2nd year		Battery	2,600	$\sum_{i=1}^{7} \frac{2{,}600}{(1+0.035)^{2i}}$	13,953
Every 2nd year		Blade and pump hose	22,000	$\sum_{i=1}^{7} \frac{22{,}000}{(1+0.035)^{3i}}$	118,060
Every 3rd year		Wheel sensors	6,200	$\sum_{i=1}^{4} \frac{6{,}200}{(1+0.035)^{3i}}$	19,288
Every 5th year		Control box	42,000	$\sum_{i=1}^{2} \frac{42{,}000}{(1+0.035)^{5i}}$	65,137
Every 5th year		Fasteners	1,500	$\sum_{i=1}^{2} \frac{1{,}500}{(1+0.035)^{5i}}$	2,326
15th year	Disposal		25,000	$\frac{25{,}000}{(1+0.035)^{15}}$	14,922
Total present value					**921,249**

Total cost of wayside equipment for 60 curves = 921,249 × 60 = 55,274,940 kr

Total cost of wayside equipment for 97 curves = 921,249 × 97 = 89,361,153 kr

5.3.3 LCC of the on-board equipment

Acquisition cost

Acquisition cost = 65,000 kr
Installation cost = 12,000 kr
Total acquisition and installation cost = 77,000 kr

Operation cost

TOR-FM consumption per train per curve per year = consumption per km × length of curve
= 30 × 2 × 0.45 × 365 = 9,855 ml ≈ 10 L
Total cost of FM per year for 60 curves = 10 × 160 × 60 = 96,000 kr
Total cost of FM per year for 157 curves = 10 × 160 × 157 = 251,200 kr ≈ 251,000 kr

Material cost

Table 33 shows the replacement frequency recommended by the manufacturer and the cost of each part.

Table 33. Life expectancy and cost of different parts of the on-board system, provided by the manufacturer.

Parts	Replacement frequency	Part cost [kr]
Nozzle tip (×2)	6 months	600
Complete nozzle set	2 years	2,400
Elastomers	8 years	15,000

Man cost

One-day cost per man = 750 × 8 = 6,000 kr

Total cost per year per unit of equipment

$$= \frac{\text{man cost per day} \times \text{service required per day}}{\text{number of units of equipment that can be fixed in a day}} = \frac{6{,}000 \times 2}{5} = 2{,}400$$

Disposal (phase-out) = 6,500 kr

Table 34 shows the LCC of an on-board system for 15 years when FM is applied on curves with a radius smaller than 550 m (60 curves) and all curves with a radius smaller than 850 m (157 curves) using a single unit of equipment.

Table 34. LCC of an on-board system when FM is applied on 60 and 157 curves.

Year	Phase		Unit cost / Cost per year	Formula used	Cost in present value (60 curves)	Cost in present value (157 curves)
0	Acquisition		77,000	–	77,000	77,000
0–14	Operation and maintance	FM cost (60 curves)	96,000	$\sum_{i=0}^{14} \frac{96{,}000}{(1+0.035)^i}$	1,144,370	–
0–14		FM cost (157 curves)	251,000	$\sum_{i=0}^{14} \frac{251{,}000}{(1+0.035)^i}$	–	2,992,051
0–14		Man cost	2,400	$\sum_{i=0}^{14} \frac{2{,}400}{(1+0.035)^i}$	28,609	28,609
0–14		Nozzle tips	1,200	$\sum_{i=0}^{14} \frac{1{,}200}{(1+0.035)^i}$	14,305	14,305
Every 2nd year		Complete nozzle set	2,400	$\sum_{i=1}^{7} \frac{2{,}400}{(1+0.035)^{2i}}$	12,879	12,879
Every 8th year		Elastomers	15,000	$\frac{15{,}000}{(1+0.035)^8}$	11,391	11,391
15th year	Disposal		6,500	$\frac{6{,}500}{(1+0.035)^{15}}$	3,880	3,880
Total present value per on-board system when FM is applied on 60 curves					**1,292,434**	–
Total present value per on-board system when FM is applied on 60 curves					–	**3,140,115**

LCC for 14 trains with FM applied on 60 curves = 1,292,434 × 14 = 18,094,076 kr

LCC for 14 trains with FM applied on 157 curves = 3,140,115 × 14 = 43,961,610 kr

Note:- In the case of the on-board system, a single system for each train could be used on all the curves; therefore, the operation cost in the LCC is calculated separately for curves with a radius smaller than 550 m and curves with a radius between 550 and 850 m.

5.3.4 LCC of rails when considering the TOR-FM effect

The average wear reduction at the normalised friction coefficient (0.3), as measured by the FricWear 2017 for FM-A and FM-B, was 40%. The results of the MBS (using the DI method) showed that with a friction value of 0.3, the probability of crack generation will reach near or below zero. Only the DI method was used for calculating the LCC as it more realistic than the FI method in that it considers the effect of wear as well. However, in practice, the forces in the real wheel-rail interface can be higher than the simulated values due to irregularities and other deformations, and, in addition, grinding is needed to restore the rail profile shape due to wear. Therefore, in the present research, it was assumed that the frequency of grinding is reduced to half by using TOR-FM.

For calculating the LCC of the rails considering the TOR-FM effect, the acquisition and installation cost of the rail will remain the same. However, the life of the rails will increase as the wear is reduced by 40% and the life will increase by approximately 66%. Therefore, the life of the rails will increase to 500 MGT and 1,000 MGT in the case of curves with a radius smaller than or equal to 550 m and curves with a radius smaller than or equal to 850 m, respectively. The grinding is assumed to take place once every two years instead of once per year.

Acquisition cost and installation cost

For curves with a radius smaller than 550 m = (4,000 × 450 × 60) × (300/500)
= 64,800,000 kr

For curves with a radius between 550 and 850 m = (4,000 × 450 × 97 × 0.5) × (600/1,000)
= 52,380,000 kr

Maintenance cost

The grinding frequency will decrease to once every two years and, therefore, the total number of grinding occasions will be seven and the cost of grinding will be the same as in the case of no FM application.

Disposal cost of the rail = 0 kr

Table 35 and Table 36 present the LCC considering the TOR-FM effect for a curve with a radius smaller than 550 m and a curve with a radius from 550 to 850 m, respectively.

Table 35. LCC considering the TOR-FM effect for a curve with a radius smaller than 550 m.

Year	Phase	Cost	Formula used	Cost in present value
0	–	1,080,000	–	1,080,000
0–14	Grinding (Maintenance)	22,500	$\sum_{i=1}^{7} \frac{22{,}500}{(1+0.035)^{2i}}$	120,743
Total present value				**1,200,743**

Table 36. LCC considering the TOR FM effect for a curve with a radius from 550 to 850 m.

Year	Phase	Cost	Formula used	Cost in present value
0	–	540,000	–	540,000
0–14	Grinding (Maintenance)	22,500	$\sum_{i=1}^{7} \frac{22{,}500}{(1+0.035)^{2i}}$	120,743
Total present value				**660,743**

LCC for 60 curves with a radius smaller than 550 m = 1,200,743 × 60 = 72,044,580 kr

LCC for 97 curves with a radius from 550 to 850 m = 660,743 × 97 = 64,092,071 kr

5.3.5 Reduction in the grinding and rail replacement cost when FM is applied

Table 37 and Table 38 compare the LCC when FM is applied and the LCC when FM is not applied, and present the reduction in the rail replacement cost and the grinding cost in percentage. The results show that the wayside equipment does not provide any economic benefits. It may have some economic benefits for extremely narrow curves, e.g. curves with a radius smaller than or equal to 300 m, but more research is needed to ascertain that. The on-board system has shown a positive reduction in the grinding and the rail replacement cost when FM is applied and hence is an economical method of FM application. The moderate curves with a radius between 550 and 850 m have a lower LCC per curve. However, the amount of FM used for moderate curves is the same as that used for sharp curves. Since the FM cost (an operational cost) is a significant part of the LCC, it results in lower savings when considering a large number of moderate curves.

Table 37. Calculation of the savings to be gained by using a wayside TOR-FM system.

Curve radius (number of curves)	Grinding and rail replacement cost when no FM is applied [kkr]	When FM is applied using a wayside system			Reduction in cost when FM is applied [%]
		Grinding and rail replacement cost [kkr]	Cost of the TOR-FM system [kkr]	Total LCC [kkr]	
Curves < 550 m (60 curves)	122,743	72,045	55,275	127,320	−4
Curves between 550 & 850 m (97 curves)	112,437	64,092	89,361	153,453	−36
Curves < 850 m (157 curves)	235,180	136,137	144,636	280,773	−19

Table 38. Calculation of the savings to be gained by using an on-board TOR-FM system.

Curve radius (number of curves)	Grinding and rail replacement cost when no FM is applied [kkr]	When FM is applied using an on-board system			Reduction in cost when FM is applied [%]
		Grinding and rail replacement cost [kkr]	Cost of the TOR-FM system [kkr]	Total LCC [kkr]	
Curves < 550 m (60 curves)	122,743	72,045	18,094	90,139	27
Curves between 550 & 850 m (97 curves)	–	–	–	–	–
Curves < 850 m (157 curves)	235,180	136,137	43,926	180,063	23

6 CONCLUSIONS

The conclusions are presented according to the respective research questions.

6.1 Conclusions relating to RQ 1

RQ 1. What is the effect of friction control on the generation of RCF on rails according to the fatigue index and damage index methods?

Conclusions:

In this subsection, the conclusions relating to RQ 1 are presented.

- According to the FI method, without considering the effect of wear, on the top of the rails of the curves with a radius smaller than 1,000 m, a friction coefficient of 0.20 or lower with a Kalker's reduction of 15% or lower is required to avoid RCF.
- According to the DI method, considering the effect of wear, on the top of the rails of the curves with a radius smaller than 1,000 m, a friction coefficient of $\mu = 0.3$ or lower with a Kalker's coefficient of 30% or lower is required to avoid RCF.
- According to both the FI and the DI method, the top of the rails of the curves with a radius of 1,000 m or higher does not experience RCF, and friction control has therefore no major role from an RCF point of view.
- According to the DI method, for curves with radii smaller than 300 m, there will be no RCF (30 tonnes axle load is an exception) in the circular part of the curve, even without friction control, as the wear dominates the RCF. However, on the transition curve, i.e. the part of the whole curve at the beginning and the end of the curve, the wear rate is insufficient to avoid RCF and this part of the curve will experience RCF if the friction is above 0.3.
- The FI and DI values are not sensitive to the axle load. The FI and DI values depend on the pressure and, when the axle load is increased, the contact area increases; therefore, any increase in the contact pressure is insignificant. This implies that the curve radius and friction have much more impact on the crack generation than the axle load.

6.2 Conclusions relating to RQ 2

RQ 2. What is the effect of TOR-FM on the wear, cracks and friction coefficient of rail in practice?

Conclusions:

This research question was investigated in three different phases.

6.2.1 Phase 1 field measurements

- Due to the low availability of the wayside equipment and the frequent grinding of the rails, no conclusion could be drawn from the profile, roughness and crack measurements.
- The present wayside equipment does not seem to be feasible as it can entail a high maintenance cost, especially in the winter.

- TOR-FM may freeze or become highly viscous and stiff in the winter, which in the region concerned is a season calculated to last approximately 3.5 months.
- The presence of moisture can cause totally misleading results. Even a small amount of moisture can reduce the friction coefficient.
- With snow on the rails, at 1°C, even though TOR-FM was not present, the friction coefficient was lower than 0.30. This low friction was due to the presence of snow, which melts when coming between the rubbing surfaces and acts as a lubricant.
- At −23°C or below, without snow on the rails, even though TOR-FM was not present, the friction coefficient was approximately 0.30. A possible explanation for this may be that, at extremely low temperatures (in the present case −23°C or below), through condensation, an ice layer forms on the rail surfaces due to a drop in the saturation vapour pressure in the air. The ice layer melts during sliding and acts as a lubricant, but may dry up after a few wheel passages.

6.2.2 The carry distance experiments of phase 1 and 2

- When an FM is supplied continuously at the rate of one litre per 1,000 axle passages using wayside equipment, maximum carry distances of 70 m for FM-A and 450 m for FM-B were observed on the top of the rail. For both the FMs, the carry distance was much shorter than that claimed by the manufacturers, which is 3 to 6 km for FM-A and 5 km for FM-B.
- The FM can stay for a distance longer than 3 km on the non-contact running surface of the wheel after being pressed out to the edges of the wheel-rail contact band. Once the FM has been pressed out from the contact band, the FM does not re-enter the contact band and is hence of no use.

6.2.3 Phase 3 and laboratory friction and wear experiments

In these experiments, three different FMs were tested using the FricWear 2017.

- The laboratory measurements showed that a cleaned rail surface had an average friction coefficient of 0.27. However, after applying FM, the friction coefficient was reduced to 0.11 for FM-A, 0.14 for FM-B and 0.10 for FM-C. The wear reduction in relation to the cleaned surface was 67%, 45% and 74% for FM-A, FM-B and FM-C, respectively.
- The field measurements showed that a surface without FM had an average friction coefficient of 0.58. However, after applying FM, the friction coefficient was reduced to 0.17 for FM-A, 0.18 for FM-B and 0.12 for FM-C. The wear reduction in relation to the FM-free and untouched surface (with real third bodies on it) was 56%, 59% and 81% for FM-A, FM-B and FM-C, respectively.
- Real third bodies in the FM-free condition on the top of the rail of the IOL increase both the friction and wear, which is contrary to the general belief that natural third bodies act as a lubricant.

6.3 Conclusions relating to RQ 3

RQ 3. What is the life cycle cost of a TOR-FM system?

Conclusions:

- The wayside equipment is economically unfeasible for the IOL as it has a negative reduction in the maintenance (grinding and rail replacement) cost when the cost of FM application is added. The negative reduction is −4% when FM is applied on curves with a radius smaller than 550 m and −19% when FM is applied on all curves with a radius smaller than 850 m.
- The on-board system has a significantly lower operation and maintenance cost than the wayside equipment. The reduction in the maintenance (grinding and rail replacement) cost when the cost

of FM application is added is 27% when FM is applied on curves with a radius smaller than 550 m and 23% when FM is applied on all curves with a radius smaller than 850 m.

- TOR-FM is associated with a major cost in the LCC. Its cost represents approximately 28% of the total cost in the case of the wayside system and approximately 90% of the total cost in the case of the on-board system. Optimising the use of the FM can further reduce the total cost of using an FM application system.

Note:- The above conclusions are based on the application of the water-based TOR-FMs and only wear and RCF have been covered in the present research. Issues other than wear and RCF such as corrugation, noise and energy consumption have not been considered in the present research. Moreover, the reduction of wear and RCF on wheels could be an extra benefit, but this has not been covered either in the present research.

7 SCOPE OF FUTURE RESEARCH

The research presented in this thesis has explored several reasons for the breakdown of the wayside system for FM application. If these shortcomings are remedied, the reliability of the equipment can be significantly increased. However, breakdowns due to maintenance vehicles will still be an issue on the IOL. Another option could be to install an on-board system on a locomotive and perform and analyse similar measurements on the wheel. On-board systems are cheaper and give faster results as the wheel experiences traction forces all the time when the train is in operation. It should also be noted that due to the limited material transfer properties of the fast-drying FM, there is a possibility that in the case of long trains such as the freight trains operated by LKAB, more than one on-board system may be required to cover all the wheels of the trains.

Another question that needs attention is the possibility of crack propagation caused by FM trapped in cracks. On the one hand, FMs can reduce the fatigue stresses, but on the other hand, the FM trapped in cracks can eventually widen the cracks when trains are passing. When studying the state of the art in this field, one finds that Hardwick and Lewis (2014) have argued that water-based friction modifier (with drying characteristics) not only minimises the generation of cracks and wear, but also suppresses the propagation of pre-generated cracks, while non-drying (oil-based) FM can catalyse the propagation of pre-generated cracks. However, Seo et al. (2018) have argued that the crack growth rate of pre-generated cracks becomes faster due to the fluid entrapment mechanism, even in the case of the FM with drying characteristics. Therefore, a deeper insight into this issue is required to enable us to evaluate the correct TOR-FM to use and the appropriate amount to apply to avoid the generation of cracks and minimise the propagation of cracks once they are generated. The computer-based simulations performed at LTU (Khan et al., 2017; Khan et al., 2018), have shown that a reduction of the amount of FM can reduce the RCF, but the behaviour of the different FMs in the field from an RCF point of view needs to be investigated.

It was observed in the LCC calculations that TOR-FM is associated with a major cost, and therefore an optimisation of the use of TOR-FM is required. In order to optimise the use of FM, a characterisation of TOR-FM is required to determine the best practice for on-board FM systems in different conditions. FM is needed in different quantities at different locations; for example, the traction forces on curves are higher and, therefore, curves require a larger amount of FM. Besides a characterisation of FM, there is a need to develop a digital system that will continuously measure the traction forces in the wheel-rail interface and give feedback to the on-board system. This will assist in minimising the consumption of TOR-FM, for example during moist weather. Another important topic that needs to be explored is total friction management, which includes the use of both TOR-FM and gauge face lubrication. When a train is negotiating a curve, the major forces are on the top of the low rail and the gauge corner of the high rail. Therefore, a proper combination of TOR-FM application and gauge face greasing will reduce the consumption of lubricant and FM and maximise the benefits of friction control. There are also possibilities that uses of TOR-FM on both low and high rail eliminate the use of gauge face lubrication.

APPENDIX

A. BASIC THEORIES USED IN THE THESIS

A.1 Hertz contact theory

The Hertz contact theory was used in calculating the maximum contact pressure in simulations and wear and friction measurements using the FricWear 2017.

The Hertz contact theory is applicable to a broad range of engineering contact problems due to its computational efficiency. The contact point is influenced by the contact pressure and has a shape that can be expressed as a Hertz contact area (Hertz, 1882). For ease of calculation, the wheel and rail can be equated to two spheres in contact with each other, as shown in Figure 48. The maximum contact pressure (P_{max}) and the contact size (a) in the sphere-sphere contact are expressed by equation 12 and 13, respectively.

Equation 12 to 17 have been taken from Hamrock and Dowson (1981) and the following assumptions were made by the author to determine the solutions of Hertz contact problems.

- The strains are small and within the elastic limit.
- The surfaces are continuous and non-conforming (implying that the area of contact is much smaller than the characteristic dimensions of the contacting bodies).
- Each body can be considered an elastic half-space.
- The surfaces are frictionless.

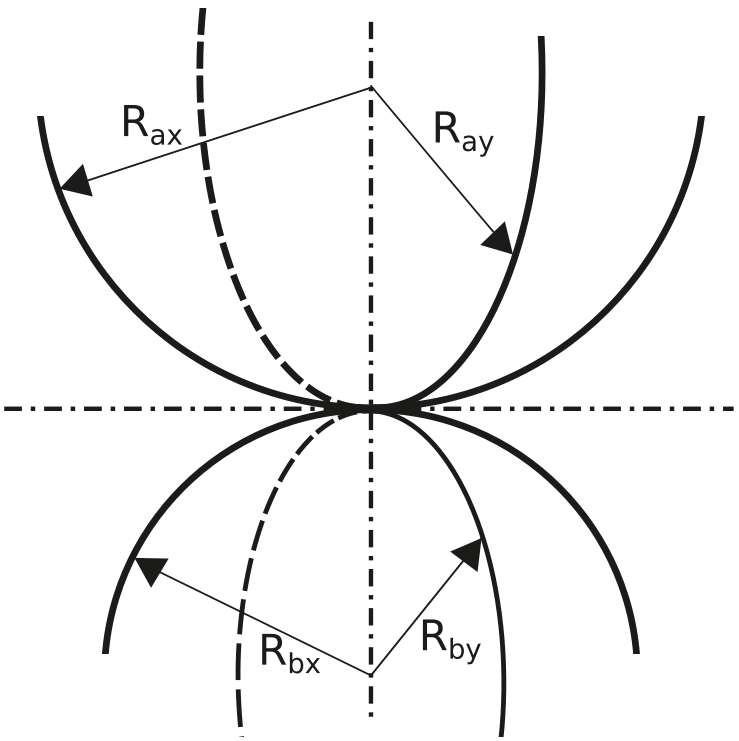

Figure 48. Two spheres in contact, spherical Hertz contact (Hamrock and Dowson, 1981).

The maximum pressure can be calculated as follows:

$$p_{max} = \frac{3F}{2\pi a^2} \tag{12}$$

and a is calculated as follows

$$a = \sqrt[3]{\frac{6k^2 \varepsilon F R}{\pi E'}} \tag{13}$$

where:
F [N] is the vertical load,
E [N/mm^2] is Young's modulus,
R [mm] is the equivalent radius, and
ν is Poisson´s ratio.

The value of ε and k are dependent on the ratio between R_x and R_y, and for the case used in the present research, $\varepsilon = 1.57$ and $k = 1$.

R is calculated as follows:

$$\frac{1}{R} = \frac{1}{R_x} + \frac{1}{R_y} \tag{14}$$

$$\frac{1}{R_x} = \frac{1}{R_{ax}} + \frac{1}{R_{bx}} \tag{15}$$

$$\frac{1}{R_y} = \frac{1}{R_{ay}} + \frac{1}{R_{by}} \tag{16}$$

E' is calculated as follows:

$$\frac{1}{E'} = \frac{1-\nu_a^2}{E_a} + \frac{1-\nu_b^2}{E_b} \tag{17}$$

A.2 Archard's wear

Archard's wear equation was used in calculating the wear constant in the case of wear measurement using the FricWear 2017.

Archard's wear method has already been used successfully for predicting wear on wheels (Jendel, 2002; Nia, Casanueva and Stichel, 2015; Dirks, 2015) and rail (Orvnäs, 2005). All the studies referred to above took input from laboratory experiments. Dirks (2015) showed that the wear coefficient (Archard's equation) for full-scale field tests was about four times lower than that for pin-on-disc tests. However, this correction factor is highly dependent on the third bodies present and the moisture condition.

Archard's wear law is a simple method for describing sliding wear and is based on the theory of asperity contact. According to Archard's wear method (Archard, 1953), the wear volume V_{wear} [m^3] can be calculated with equation 18:

$$V_{wear} = \frac{KWL}{H} \tag{18}$$

where:
V [m^3] is the total volume of wear debris produced,
K [unitless] is a wear constant,
W [N] is the total normal load,
L [m] is the sliding distance,
H [N/m^2] is the hardness of the softest contacting surfaces.

One important feature of Archard's wear method is that there will be no wear in the adhesion zone of the contact since the sliding distance is zero (zero slip velocity). The wear coefficient "K" can be determined by laboratory measurements and expressed in a wear map depending on the sliding velocity and contact pressure. An example of a wear map for dry (FM-free) conditions is shown in Figure 49. It can be concluded from the example in this figure that the sliding velocity and contact pressure have a substantial impact on the wear coefficient.

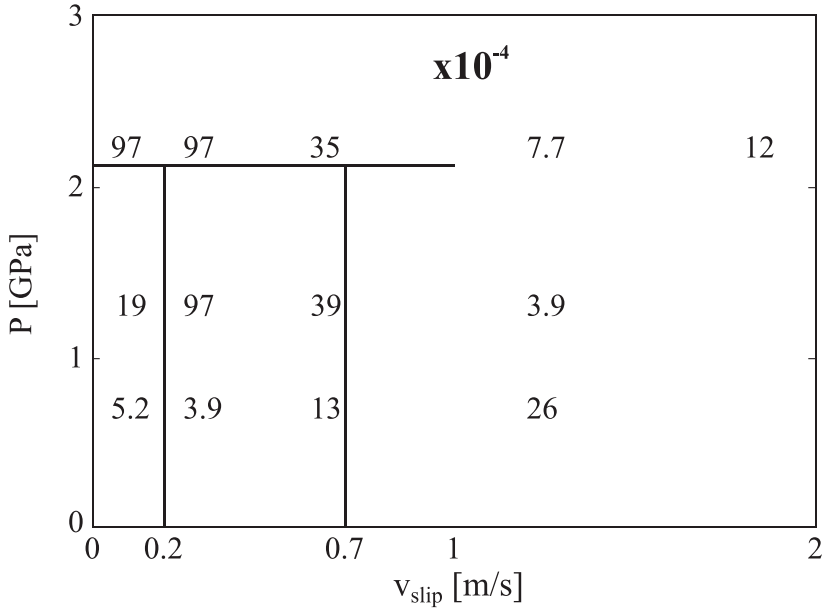

Figure 49. Wear map with wear coefficients for the non-lubricated condition, derived from pin-on-disc testing (Zhu, Sundh and Olofsson, 2013). The numbers inside the wear map show the wear coefficients for different regions of contact pressure and slip velocity,

A.3 Rolling contact fatigue (RCF) and the shakedown diagram

This section presents RCF and the shakedown diagram, which were used in the FI and the DI method.

Rail and wheel cracks are formed due to rolling contact fatigue and can be divided into head checks, squats and taches ovales (Cannon et al., 2003). Taches ovales are commonly considered to be defects that develop inside the railhead due to longitudinal cavities caused by the presence of hydrogen.

However, due to improved steel production techniques, taches ovales rarely occur in the base rail material, but still sometimes occur at welds (Dirks, 2015). The initiation of head checks and squats on the surface is caused by a combination of high normal and tangential stresses in the wheel-rail interface. Squats only occur in the rail, whereas head checks can occur in both the rail and the wheels (Dirks, 2015). Squats are caused by local irregularities in the track surface that lead to high dynamic contact stresses. The initiated cracks grow inside the rail at a shallow angle to the rail surface until a depth of a few millimetres. This often leads to "spalling" of the material from the surface of the rail. Some cracks, however, can turn down into the rail, which can cause the rail to break, which can lead to catastrophic accidents (Dollevoet, 2010).

Around 40 years ago, RCF was not considered as a major problem within the European rail community. The UIC rail defect catalogue, which was published in 1979, makes no specific reference to RCF (Cannon and Pradier, 1996). However, today the RCF initiated on or near the surface of the rails is considered as one of the major problems in railways (Cannon and Pradier, 1996). The influence of strain hardening on the cumulative plastic deformation under repeated rolling and sliding was proposed and tested by Bower and Johnson (1989). They came up with an often-used method (the shakedown map, see Figure 50) of the cyclic stress-strain behaviour of the deforming material.

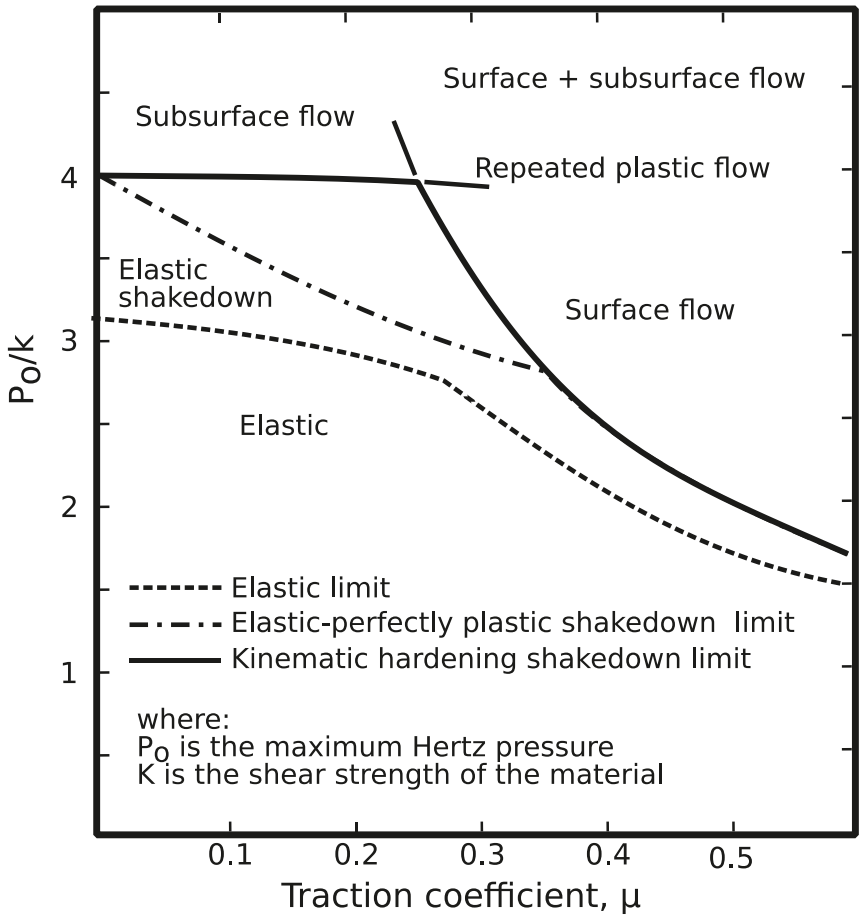

Figure 50. Shakedown map for line contact for a perfectly plastic and kinematically hardening material. Adapted from Johnson (1989).

It should be noted that shakedown maps are derived under the presumption of full slip. The MBS of the present research used the shakedown map according to Johnson (1989) and the shape of the Kalker curve was not changed, but the amount of creepage was reduced. Furthermore, the shakedown map

does not predict a fatigue life, but only indicates that a surface flaw will occur, in which case RCF is likely to occur (Ekberg, Kabo and Andersson, 2002). From Figure 50, one can observe that to keep the material outside the range of repeated plastic flow, i.e. safe from RCF, the values on the y-axis, for P_o/k, should be reduced or the value on the x-axis, for the traction coefficient, should be reduced. P_o corresponds to the peak pressure in the Hertz pressure distribution and k represents the material's shear yield strength. A conclusion of Ekberg, Kabo and Andersson (2002) was that if the applied load exceeds the elastic limit, then some plastic deformation takes place under the first passage of the load. However, incremental plastic deformation will not necessarily take place due to the formation of protective residual stresses through the plastic deformation and strain hardening of the material. Repeated plastic flow will only take place if the load exceeds the shakedown limit, but the effects mentioned above tend to cause the deforming material to 'shake down' to an elastic state. This effect was further explained and divided into four different categories by Johnson (1989) as shown in Figure 51.

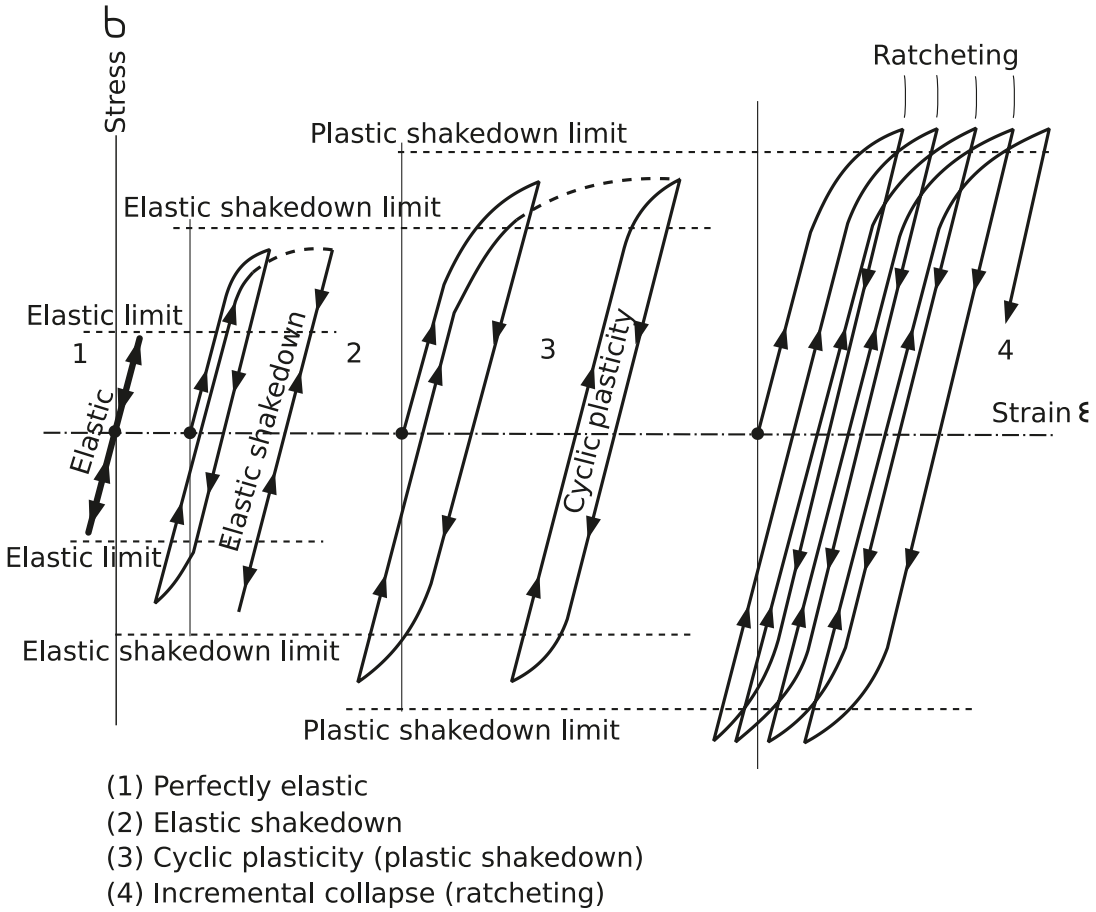

Figure 51. Material response to cyclic loading (Johnson, 1989).

Below is a brief explanation (Johnson, 1989) of all the limits shown in Figure 51.

Elastic: When the maximum value of the cyclic load does not exceed the yield stress of the material, the behaviour will be perfectly elastic throughout.

Elastic shakedown: This phenomenon occurs when the maximum value of the load exceeds the elastic limit, but due to the changes brought about by plastic flow, the steady cyclic state does not exceed the elastic shakedown limit.

Plastic shakedown (cyclic plasticity): This phenomenon occurs when the maximum value of the cyclic load exceeds the elastic shakedown limit and the steady cyclic state consists of a closed plastic stress–strain loop with no net accumulation of unidirectional plastic strain.

Ratcheting (incremental collapse): This phenomenon occurs when the maximum value of the cyclic load exceeds the plastic shakedown limit and the steady state consists of an open cycle of plastic strain, such that an increment of unidirectional plastic strain is accumulated with each cycle of stress.

A.4 Fatigue index (FI) method

The FI method was used in the prediction of the effects of friction control on top-of-rail cracks

To predict the generation of surface-initiated cracks caused by RCF, the fatigue index (FI) method (Ekberg, Kabo and Andersson, 2002) was used. Ekberg, Kabo and Andersson (2002) suggested three fatigue indexes, FI_{surf}, FI_{sub} and FI_{def}, and the MBS of the present research only used the first index, FI_{surf}, which predicts the surface-initiated RCF and is based on the shakedown map. According to the FI method, the occurrence of RCF depends upon the contact pressure, the creep forces in the contact area and the material yield stress in shear. If the external stresses of the working point (WP) exceed the threshold value, which is known as the shakedown limit, surface cracking will occur due to accumulated plastic strain, see Figure 52.

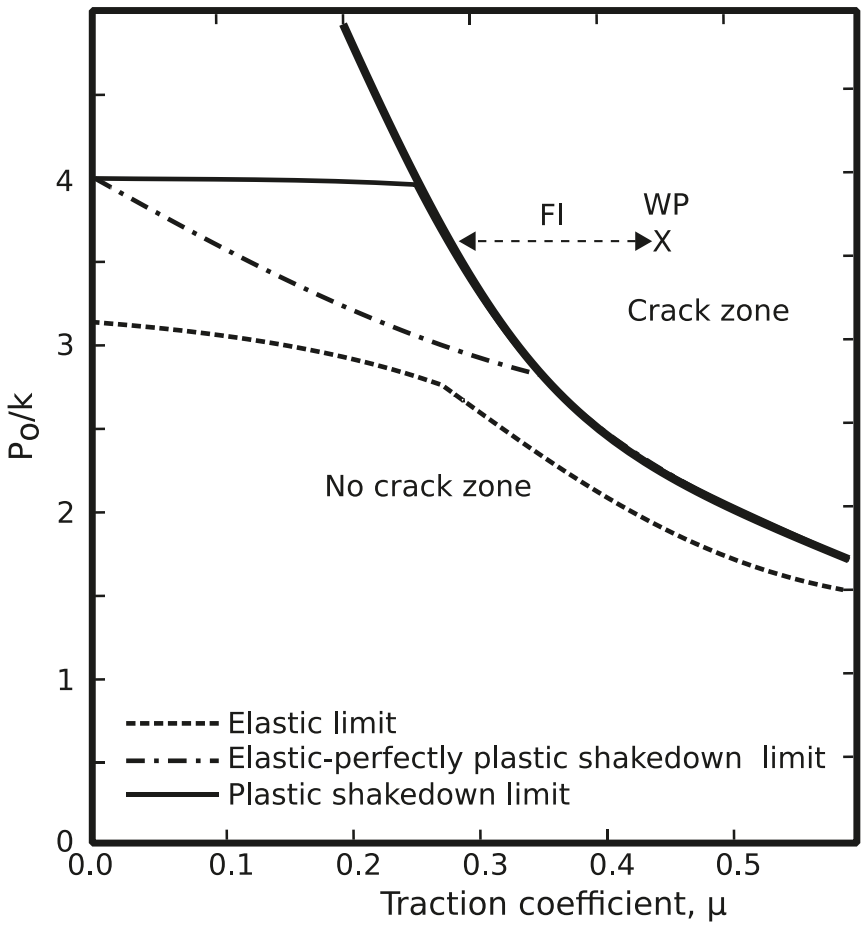

Figure 52. Shakedown map. Surface fatigue is predicted if the working point (WP) (defined by the material yield stress in shear, contact geometry and applied load) is outside the thick line. Adapted from Dirks and Enblom (2011).

The location of the threshold value in the shakedown diagram is a function of the maximum Hertzian contact pressure (P_o in [N/m^2]) divided by the shear strength of the material (k in [N/m^2]) on the y-axis, and the utilised friction coefficient (μ) on the x-axis. The shear strength (k) depends on the material of the rail and the contact pressure mainly depends on the contact area and applied load. The utilised friction coefficient (μ) depends on the creepage and the third body (e.g. dust, water or FM) between the rail and wheel. The friction coefficient is defined as the quotient between the creep forces tangential to the contact surface (F_t [N]) and the normal to the contact point (F_n [N]):

$$\mu = \frac{F_t}{F_n} = \frac{\sqrt{F_{nx}^2 + F_{ny}^2}}{F_n} \qquad (19) \quad \text{(Ekberg, Kabo and Andersson, 2002)}$$

where F_{nx} and F_{ny} are the longitudinal and the lateral creep force tangential to the contact surface in [N], respectively.

A surface fatigue index (FI) is defined as follows:

$$FI = \mu - \frac{k}{p_o} \qquad (20) \quad \text{(Ekberg, Kabo and Andersson, 2002)}$$

The value of the FI indicates the extent to which the shakedown limit has been exceeded. This shakedown limit is the threshold value for the crack generation. Damage is assumed to occur for FI > 0 (Figure 52). The FI value does not give any information about the propagation of cracks or the number of cracks.

The limitation of the FI prediction method is that the applied shakedown diagram is derived under full-slip conditions. The contact between the top of the rail and the running surface of the wheel while the train is negotiating a curve are often in full slip; however, the contact between the top of the rail and the wheel's running surface on tangent track is often in partial slip. In the case of partial slip, the maximum principal shear stress is higher than that in the case of full slip (Dirks, 2015), but in the case of lower friction, the difference in shear strength between full and partial slip is small (Dirks, 2015). Dirks (2015) also argued that the FI method does not consider the creepage and wear, although they can be an important variable in determining the fatigue life.

A.5 Damage index (DI) method

The DI method was used in the prediction of top-of-rail friction control effects on rail RCF suppressed by wear.

RCF and wear are two different processes and have no established relationship. To obtain a realistic output from the MBS, a combination of wear and RCF is required as excessive wear can minimize or, in some cases, eliminate RCF. Burstow (2003) combined the shakedown method and the energy dissipation method to create a combined index method, as shown in Figure 53. The shakedown limit, which is also sometimes known as the dynamic shakedown curve, represents the limit for generating

RCF without considering the effect of wear. Energy dissipation, which is a product of creep force and creepage, is used to calculate the factored wear rate. A combined damage index is a combination of the shakedown limit and the factored wear rate.

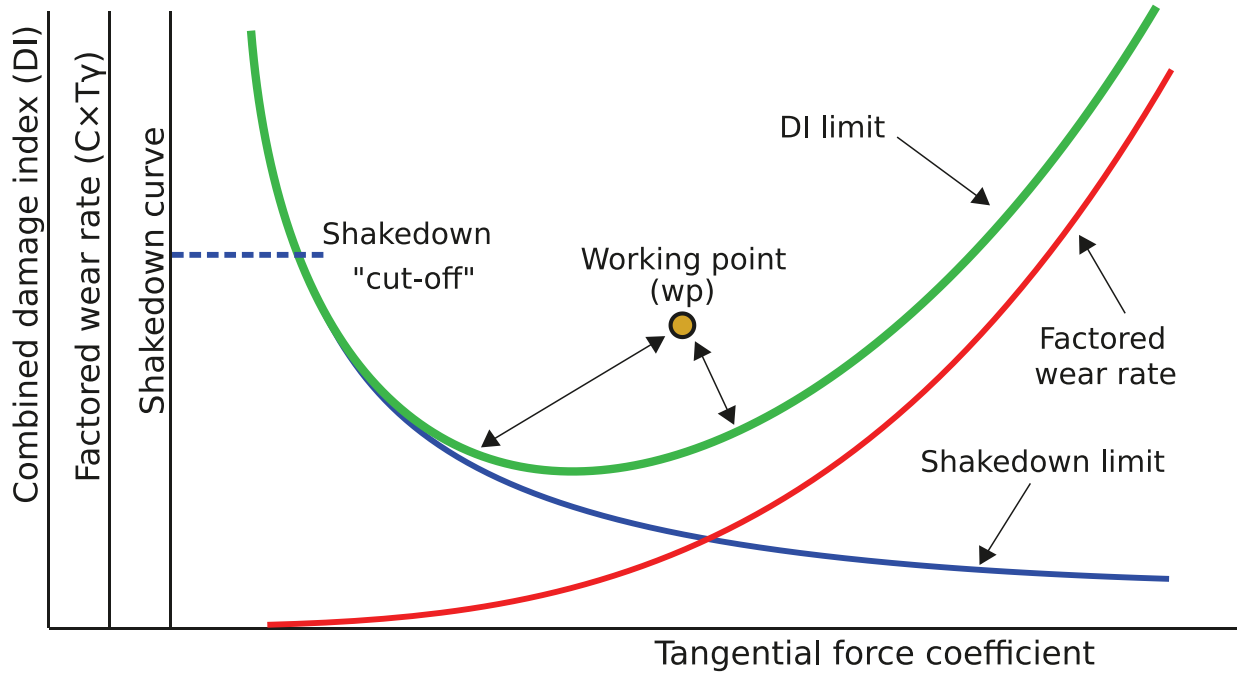

Figure 53. Combined damage index limit based on the shakedown limit and the factored wear rate. Adapted from Burstow (2003).

As explained by Burstow (2003), when the working point (WP) lies above the combined damage index limit, as shown in Figure 53, RCF will exist, and the displacement of the WP from the border of the combined damage index limit defines the value of the damage, which has been called the damage index (DI) in the present research. The DI value can be calculated using the formula given in equation 21. A positive value of the DI indicates the generation of a crack. If the WP lies below the combined DI limit, then the DI values are negative and there is no RCF. In the case of no RCF, a low value for the energy dissipation indicates that the pressure is not sufficient to generate any crack; however, a high value for the energy generation indicates that wear has dominated the formation of RCF.

$$DI = FI - C\,(T\gamma) \qquad (21)$$ (Burstow, 2003)

where FI represents the fatigue index value (Ekberg, Kabo and Andersson, 2002), which is based on the shakedown theory (Bower and Johnson, 1991), and $C\,(T\gamma)$ represents the factored wear rate based on the energy dissipation. The fatigue index method is explained in Section A.4 in the appendix.

The energy dissipation approach was introduced by Pearce and Sherratt (1991) and relates the material loss to the energy in the contact using the $T\gamma$ wear number, where T is the tractive force (normal force × traction coefficient) and γ is the creepage in the contact. The process is semi-empirical and can be relied on when establishing wear coefficients using sliding (pin-on-disc) or rolling-sliding (twin-disc) wear experiments. Laboratory experiments and dynamic simulations have yielded a relationship between wear rates and energy dissipation which depends on the properties of the material. Energy dissipation is the sum of the individual products of local traction forces (T) and local creepage (γ), which can be calculated as shown in equation 22:

$$T\gamma = T_x\gamma_x + T_y\gamma_y \qquad (22)$$ (Pearce and Sherratt, 1991)

As the wear rate is a function of the energy dissipation, the factor C, included in equation 21, is required so that wear and RCF can be combined. In the present research, this constant was calculated using the DI graph developed by Evans, Lee and Hon (2008), see Figure 54. The material used by these authors was 350-grade steel, which has similar properties to the steel used in the rails of the IOL. In the simulations carried out in the present research, the value of C until $T\gamma$ reaches 135 is considered as zero. In this zone, the wear is mild to medium, which is not sufficient to suppress the probability of RCF generation, and therefore it can be ignored. According to the Evans diagram (Figure 54), after $T\gamma$ = 135, the wear starts reducing the RCF generation and the line has a constant slope. By using Figure 54, the value of C can be calculated at the shakedown cut-off value by keeping DI = 0 at $T\gamma$ = 400 in equation 21.

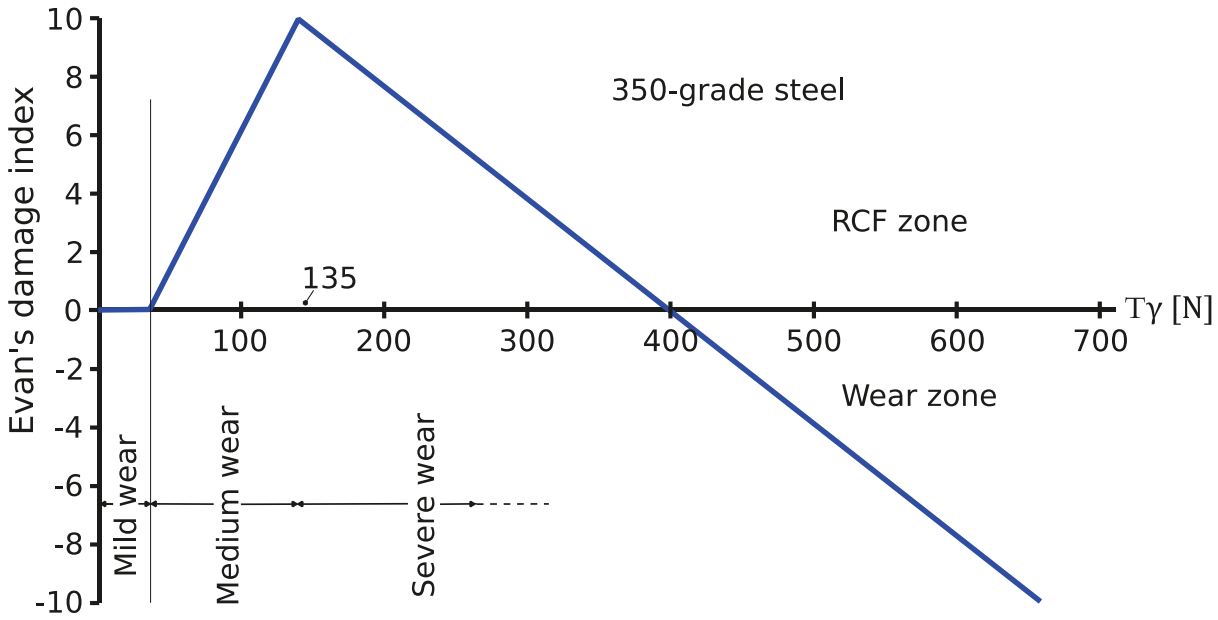

Figure 54. Relationship of the Evans DI to energy dissipation (Tγ) for 350-grade rail steel. Adapted from Evans, Lee and Hon (2008).

A limitation of the DI method is that it does not take spin creepage into account, which can be up to 6–7% (Alarcón et al., 2015) of the total creepage. It should also be considered that the DI method has an empirical nature and needs calibration for each material and third body interface (Dirks, 2015). In the opinion of the author of the present thesis, such indices are generated by performing a laboratory test or a dynamic simulation, both of which lack a realistic environment and realistic third body interfaces. Moreover, laboratory tests have a problem of scale.

Note:- In the present research, the energy dissipation, i.e. the effect of wear in the DI method, was not considered until it reached the value of Tγ = 135, as shown in Figure 54, i.e. when the Evans damage index started decreasing. Before this value of energy dissipation, the wear is negligible. In Figure 53, it is shown as the shakedown "cut-off".

A.6 Stribeck curve

The forms of lubrication used in different applications can be divided into two categories: solid lubrication and fluid (liquid or gaseous) lubrication (Bhushan, 2013). A water-based FM (fast-drying) will fall into the category of solid lubrication after drying, while oil-based (non-drying) FM and water-based FM before completely drying will come under the category of fluid lubrication. A summary of the lubrication regimes observed in fluid lubrication without an external pumping agency is provided by the Stribeck curve (Stribeck, 1902), as shown in Figure 55. The Stribeck curve is a relationship between the coefficient of friction and the relative sliding velocity multiplied by the viscosity per normal pressure. The Stribeck curve can also be classified based on the film parameter (λ) value as shown in Figure 55. The relationship between λ and the film thickness (h) is shown in equation 23:

$$\lambda = \frac{h}{\left(f_1^2 + f_2^2\right)^{1/2}} \qquad (23) \quad \text{(Hamrock and Dowson, 1981)}$$

where:
f_1 is the root mean square surface finish of surface 1,
f_2 is the root mean square surface finish of surface 2.

The regimes of the Stribeck curve (Stribeck, 1902) are explained below and further details can be found in books in the field of tribology (Bhushan, 2013; Torbacke, Rudolphi and Kassfeldt, 2014; Hamrock and Dowson, 1981).

Hydrodynamic lubrication: Hydrodynamic or full-film lubrication is the condition where the load carrying surfaces are completely separated by a film of lubricant. This is a stable regime of lubrication and metal-to-metal contact does not occur during the steady state operation of the bearing.

Elastohydrodynamic lubrication: Elastohydrodynamic lubrication is the condition where a lubricant has been introduced between surfaces that are in rolling contact, such as in ball and rolling element bearings. In this lubrication regime, the load is sufficiently high for the surfaces to deform elastically during the hydrodynamic action, but metal-to-metal contact does not occur during the steady state operation of the bearing.

Mixed lubrication: Mixed lubrication is the condition where some asperity contact may occur. Generally, the tallest asperities of the bounding surfaces will protrude through the film and occasionally come into contact.

Boundary lubrication: Boundary lubrication is the condition where the fluid films are negligible and there is a considerable asperity contact. The physical and chemical properties of thin surface films are of significant importance, while the properties of the bulk fluid lubricant are insignificant.

Note:- In practice, wear always occurred in the tests where TOR-FM was applied on the wheel-rail interface or in the wear tests using the tribometer, which means that the regime was mixed or boundary lubrication. However, on some occasions (e.g. when an excessive amount of FM was applied) an elastohydrodynamic regime or may be hydrodynamic regime might have been achieved.

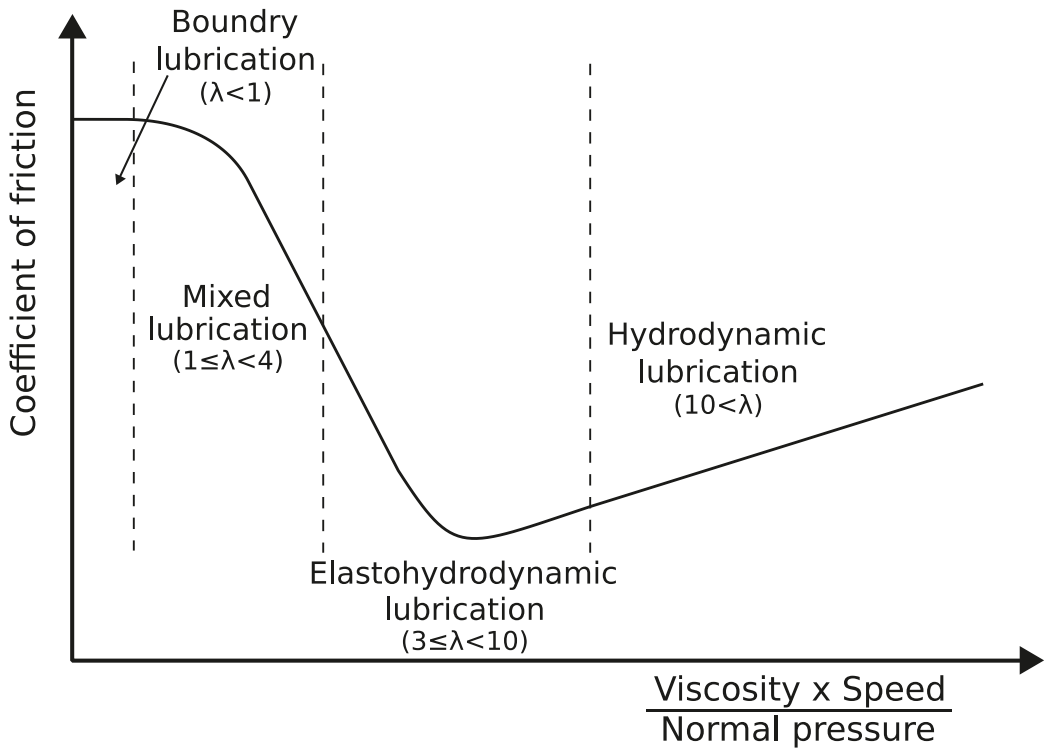

Figure 55. Schematic representation of the Stribeck curve, showing the different lubrication regimes (h is the film thickness and λ is the film parameter, see equation 23). Adapted from Hamrock and Dowson (1981).

B. VEHICLE AND TRACK MODELS USED IN THE SIMULATIONS

The models used in the simulations performed with the MBS software were not developed by the author of the present thesis. Some basic background information on these models is presented and discussed below.

The present iron ore wagons used on the IOL are the so-called Fanoo wagons, which run on Amsted Rail's Motion Control® bogie, which is a three-piece M-976 bogie with load-sensitive frictional damping. The Fanoo wagons contain two units, one of which is called the master unit and the other is called the slave unit. The controller of the braking system is attached to the master wagon as shown in Figure 56.

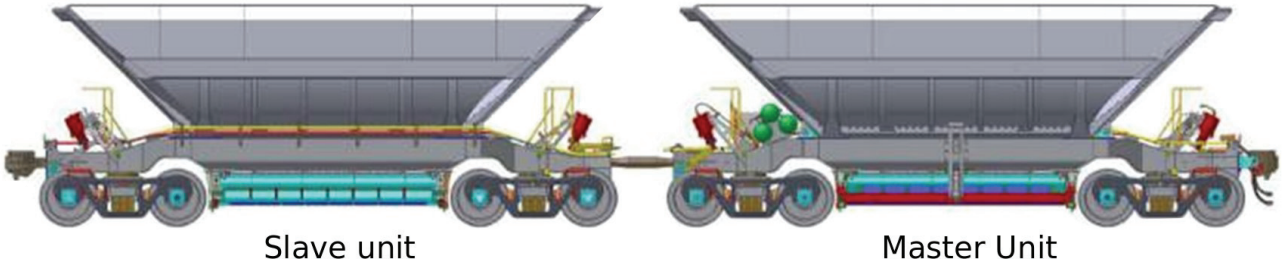

Figure 56. A two-unit Fanoo iron ore wagon (Nia, 2014).

The model for the Fanoo wagon used in the present research has four axles mounted on two individual three-piece bogies. These bogies have a primary suspension between each axle and side frame and a secondary suspension between the side frames and the bolster beam. The primary suspension is relatively soft, which promotes good radial self-steering capabilities on curves; this gives a small angle of attack and thus creates smaller traction forces. Such an arrangement maintains a good running performance on curves, but limits the highest possible speed on tangent tracks because of hunting oscillation (Nia, Jonsson and Stichel, 2014).

The main parts of the Motion Control® bogie from Amsted Rail are discussed below following the numbering of parts in Figure 57. These three-piece bogies have become very popular because they are cheap and have a simple design.

1. Side frame – This is connected to the bolster (2) with the coil spring assembly (5) and to the wheelset (7) with the adapter (6).
2. Bolster – The central plate on the bolster connects the bogie to the car body.
3. Side bearer – This carries some of the load from the car body and increases the stability of the vehicle due to increased damping in the longitudinal direction.
4. Friction wedge – This is a wedge between the bolster and the side frame which, through friction, provides damping.
5. Coil spring assembly – This is the main suspension of the bogie.
6. Adapter – This connects the wheelset (via a bearing) with the side frame and provides an elastic coupling in the lateral and longitudinal directions.
7. Wheelset.

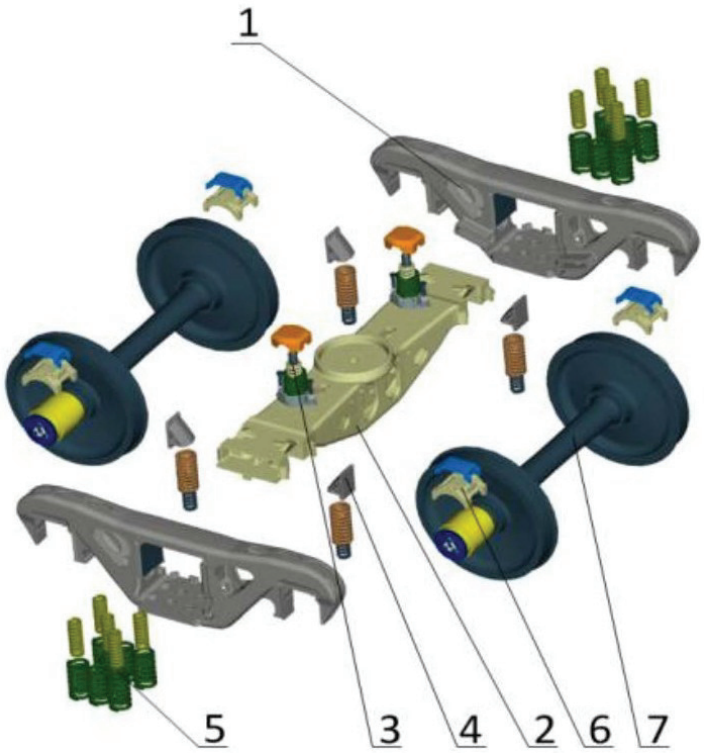

Figure 57. The main parts of the three-piece bogie used in the iron ore wagon. See the paragraph before this figure for a description of the numbered parts (Bogojevic, Jönnson and Stichel, 2011).

Many authors have used MBS to analyse the dynamic behaviour of wagons with three-piece bogies (Pombo et al., 2011; Dirks and Enblom, 2011). The author of the present thesis used the MBS software GENSYS (2018), which has an already developed and validated model of the Fanoo wagon. Bogojevic, Jönnson and Stichel (2011) used similar models provided by the GENSYS (2018) software, compared the curving performance to calculated lateral contact forces for the mentioned three-bogie system, and validated the models by comparing the simulation results with on-track data. Some important parts of the bogie model explained by Berghuvud and Stensson (1998), which were also used in the present research, are discussed below.

The primary suspension is a rubber pad called Adapter Plus, which is located between the axle box and the side-frame and is modelled as an elastic stiffness and damping in parallel as shown in Figure 58.

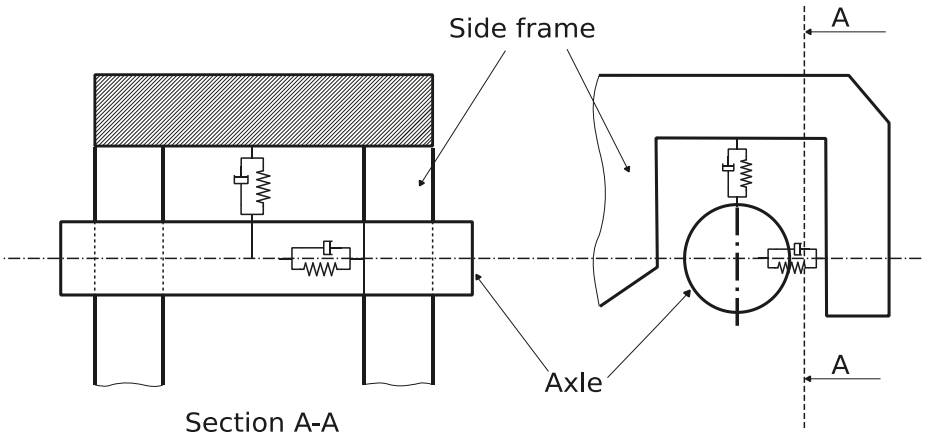

Figure 58. Primary suspension modelled as elastic damping and stiffness in parallel in three dimensions (Berghuvud and Stensson, 1998).

The wedges are modelled as massless bodies, and the position of the wedge is calculated by solving the local equilibrium equations. Normal contact forces acting on the surfaces of the wedge are used to calculate the friction forces in the friction block. The coupling in the contact surface between the bolster and the wedge is modelled as a one-dimensional friction block, and the friction surface between the wedge and the side frame is modelled as a two-dimensional friction block in the lateral and the vertical direction, as shown in Figure 59.

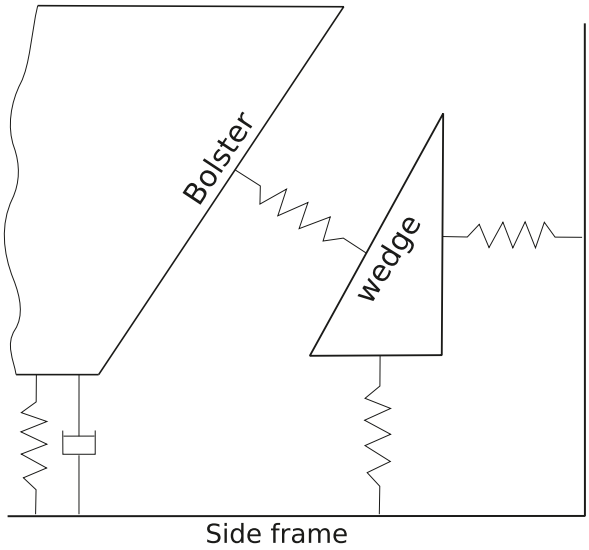

Figure 59. Couplings in the secondary suspension of a three-piece bogie (Berghuvud and Stensson, 1998).

The friction coefficient between the wedges and the bolster is estimated to be around 0.15 (a hardened cast iron wedge in contact with cast steel), while the friction coefficient between the wedges and the side frame is estimated to be around 0.38 (hardened cast iron in contact with a hardened steel plate). However, the friction level varies from morning to night and is dependent on the weather conditions, the roughness of the surfaces, etc. A very low friction level saturates the friction force and decreases the warping stiffness significantly, while a very high friction level increases the risk of a stick condition between the wedge and the side frame, leading to very high peak vertical wheel-rail forces. All the friction contacts in the suspension system, such as the couplings between the side frame and wedge, the wedge and bolster, and the side bearers and centre plate, are modelled with Saint-Venant elements (Sun and Cole, 2008).

The car body basket and the bogie bolster are connected via the centre plate and the side bearers. The side bearers are placed at both ends of the bolster and carry 10% of the vertical load when the wagon is loaded. The main coupling elements are the vertical nonlinear elastic stiffness and a longitudinal friction element. The connection between the car body and the centre plate is set via five connection points at the centre, front, back, left side, and right side of the plate, which bears the remaining 90% of the load. The couplings are defined as two-dimensional friction elements in the x-y plane. Figure 60 shows the car body and bolster connections.

Some of the other model assumptions can be summarized as follows.

- The car body, bolster, side frames, wheelset, and wheels are modelled as rigid bodies.
- The side bearers always have contact with the car body.

- Clearances between elements are implemented in the model, for example clearances between the bolster–side frame and the axle–side frame, etc.

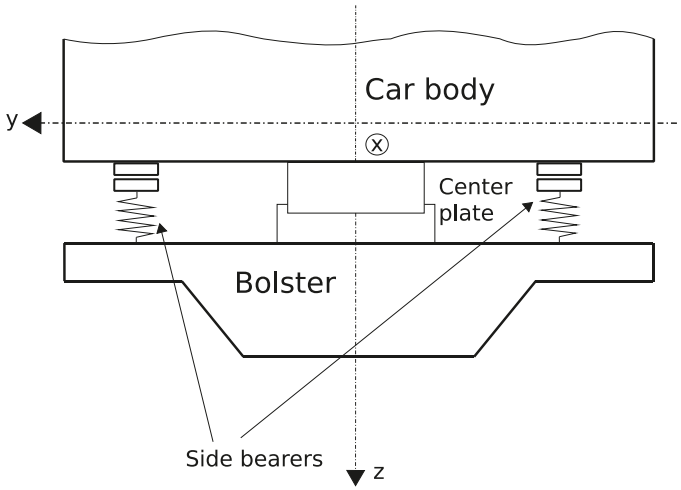

Figure 60. Connection between the car body and the bolster (Nia, 2014).

In the present research, the vehicle speed was set at 60 km/h for all the simulated track sections. Figure 61 summarizes the entire vehicle model for the vertical direction. For further details on the vehicle and track model, see Nia, Jönsson and Stichel (2014) and Bogojevic, Jönnson and Stichel (2011).

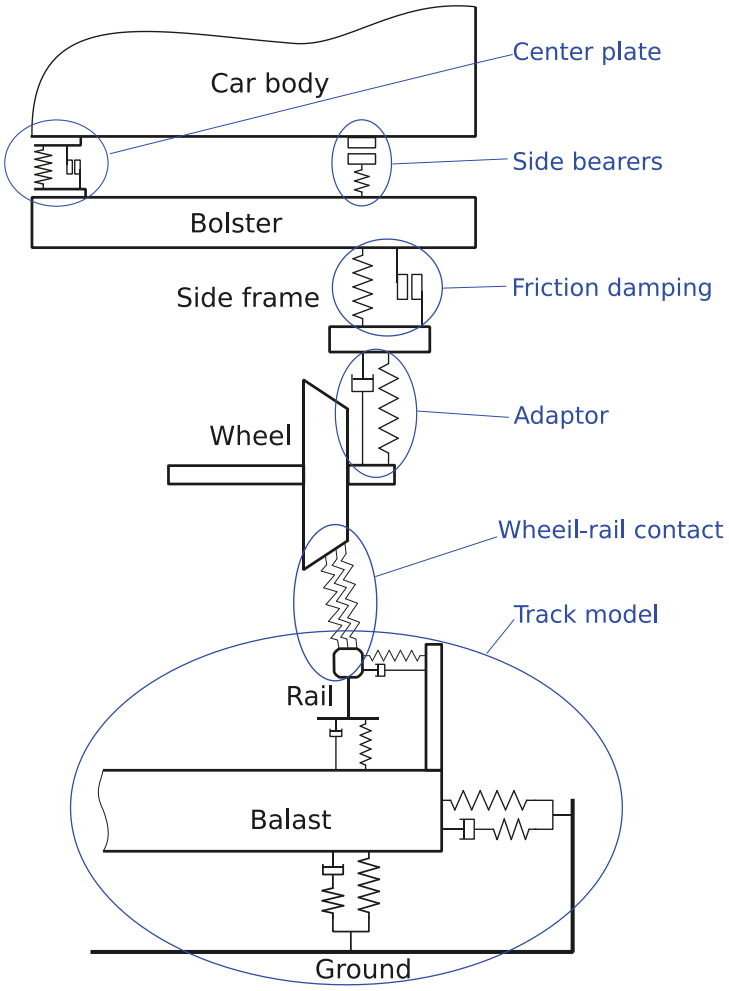

Figure 61. Connection between masses in the vertical direction (Berghuvud and Stensson, 1998).

C. FricWear 2017 TRIBOMETER

The device is used in the present research for measuring friction and wear.

The contact mechanism in the wheel-rail system is well defined (Zhu, 2011; Andersson, Berg and Stichel, 2014) in the form of mathematical equations. These equations are also used by computer-based simulations for which coefficients and constants, for example the friction coefficient, Kalker's coefficient and Archard's wear constant, are derived from classical laboratory tests such as the pin-on-disc and the twin-disc test (Eadie et al., 2008; Abbasi et al., 2013; Challen, Oxley and Hockenhull, 1986). Such laboratory tests lack the important influence of the third body (moisture, dirt, water, snow, lubricant deposits, brake pad deposits, cargo deposits, and pollution, etc.). Moreover, laboratory tests sometimes lack the correct contact pressure and are associated with a scale factor. For the performance of field measurements, a hand-pushed tribometer has been used by many researchers (Harrison, McCanney and Cotter, 2002; Nia, Jonsson and Stichel, 2014; Lemma et al., 2014). It progressively increases the braking torque of the measuring wheel until slip occurs between the measuring wheel and the rail surface. However, the value of the slip between the tribometer wheel and the rail is unknown. In addition, this device is associated with a scale factor and lacks a realistic contact pressure, which can influence the measurement of the friction coefficient.

In practice, it is difficult to control all the parameters in laboratory conditions and, therefore, there is a need to perform measurements in real environments, i.e. in the field. It is this need which motivated the development of the FricWear 2017 tribometer, a device invented and designed at Luleå University of Technology in Sweden by Jan Lundberg (Swedish patent no: SE 540 066 C2). This instrument can easily be carried out into the field and used to measure the wear and the friction coefficient, taking realistic third bodies into account, for example moisture, dirt, water, snow, lubricant deposits, brake pad deposits, cargo deposits, and pollution.

The FricWear 2017 tribometer was designed for measuring friction coefficients and wear constants both in real-life conditions in the field and in the laboratory. It was designed especially for measuring friction coefficients and wear properties in railway applications, but can also be used in many other areas of application to measure wear and friction. In field measurements, the important influence of the third body (moisture, dirt, oxides, water, snow, lubricant deposits, brake pad deposits, cargo deposits, and pollution, etc.) is taken into consideration. The instrument has the ability to match the weight of a fully loaded ore train when measuring wear and friction on railway tracks in operation. However, a disadvantage is that scaling is still a possible source of error.

The FricWear 2017 was developed in many phases. The first prototype of the device (see Figure 62) consisted of brass blocks (acting as a dead weight) resting on three steel balls which were pulled by hand through a weight measurement device (substitute for a force sensor). The dead weight and ball diameter were used in such a way that a maximum pressure of approximately 2,100 MPa could be reached, which represents a realistic pressure in the wheel-rail interface of a fully loaded heavy haul train. The initial friction measurements during field visit 1 and 2 were carried out using this initial version of the FricWear tribometer. The basic principle is to measure the horizontal forces when

pulling a weight at the desired contact pressure. The friction coefficient (μ) can be calculated simply by dividing the horizontal forces by the known vertical force. All the versions of the FricWear tribometer use the same principle, but the third version of the device, the FricWear 2017, is more user-friendly than the previous versions.

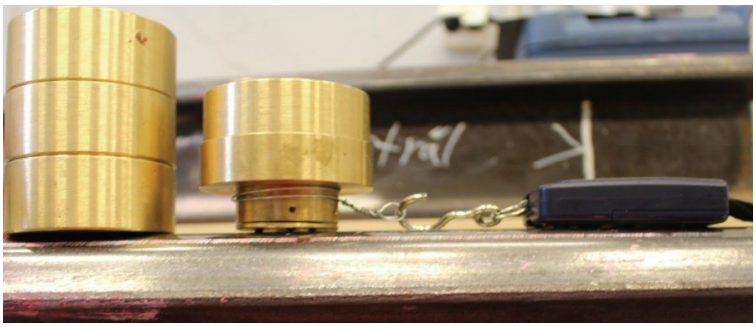

Figure 62. First version of the FricWear tribometer.

After two field visits, a housing was made in which the dead weight could be inserted, and this housing could be mounted on the rail. Figure 63 shows a picture of the second version. In this version, the dead weight rested on a single ball, which meant that a smaller weight was required to achieve the maximum pressure of 2,100 MPa. In this version, an external motor was used for pulling the dead weight resting on the ball or pin.

Figure 63. Second version of the FricWear tribometer.

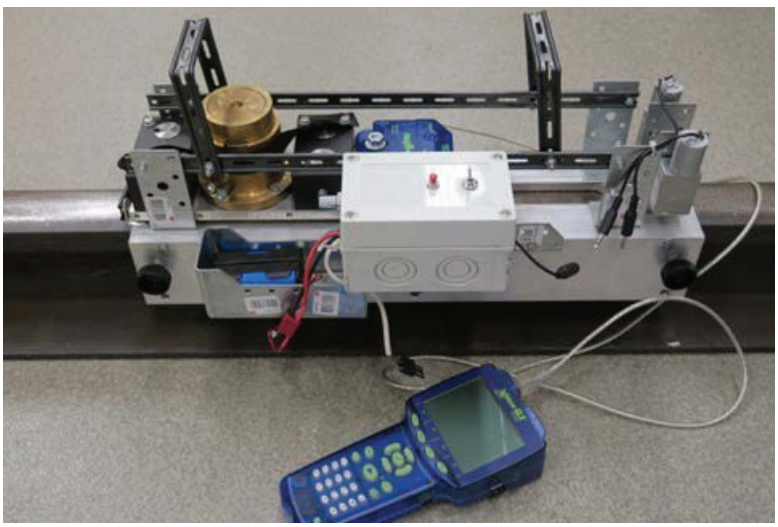

Figure 64. The FricWear 2017 (the third and final version of the tribometer).

Figure 64 shows the third and final version of the tribometer, which is known as the FricWear 2017. The vertical force is known from the weight of the piston and can vary from 9 N to 22.6 N, while the horizontal force can be measured using an oscilloscope. The vertical load can be varied to represent trains with different axle loads, for example a passenger train (with or without passengers), a freight train or a fully loaded ore train. The technical specifications of the equipment are given in Table 39.

Table 39. Specifications of the FricWear 2017 tribometer.

Overall weight	5.6 kg
Maximum height	15 cm
Maximum length	31 cm
Maximum width	20 cm
Operating temperature	−50 to +50°C
Speed	0.25 – 5 mm/s
Contact pressure ***(Ball with a diameter of 5 mm and without wear)***	1,500 – 2,100 MPa

In order to calculate the wear, a wear piston or probe (shown in Figure 65) together with the desired amount of dead weight is dragged for a desired length, and during this process, a scar will form on the tip of the wear probe. The diameter of this scar can be measured using an optical microscope and thus the wear volume can be calculated, see Figure 66. After calculating the wear volume, the wear constant (K) can easily be calculated using Archard's equation. It should be noted that the cylinder should not be dragged over a long distance, since an increase in the wear increases the contact area, which dramatically decreases the contact pressure, see Figure 23.

The active radius of the wear piston is accurately manufactured to give a spherical radius of 2.5 mm within a tolerance of ±0.01 mm. The wear piston can also be replaced by an ordinary ball-bearing ball with a spherical diameter of 5 and 11 mm, in order to achieve a suitable spectrum of contact pressure. The maximum Hertz pressure (P_{max}) using the supplied weight and ball diameter (d) combinations can be calculated using equation 24:

$$P_{max} = \left(\frac{6FE^2}{\pi^3(1-\nu^2)d^2}\right)^{\frac{1}{3}} [N/m^2] \qquad (24)$$ (Hamrock and Dowson, 1981)

where:
F = mg, E = 2.1 × 1011 N/m^2 (for steel), and ν = 0.3.

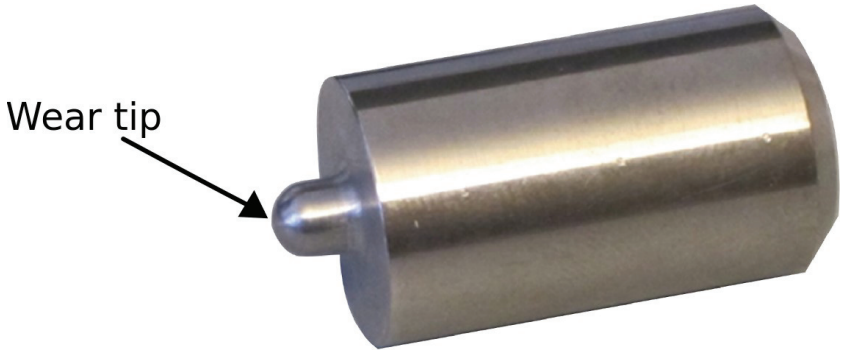

Figure 65. Wear piston for measuring wear in the FricWear 2017.

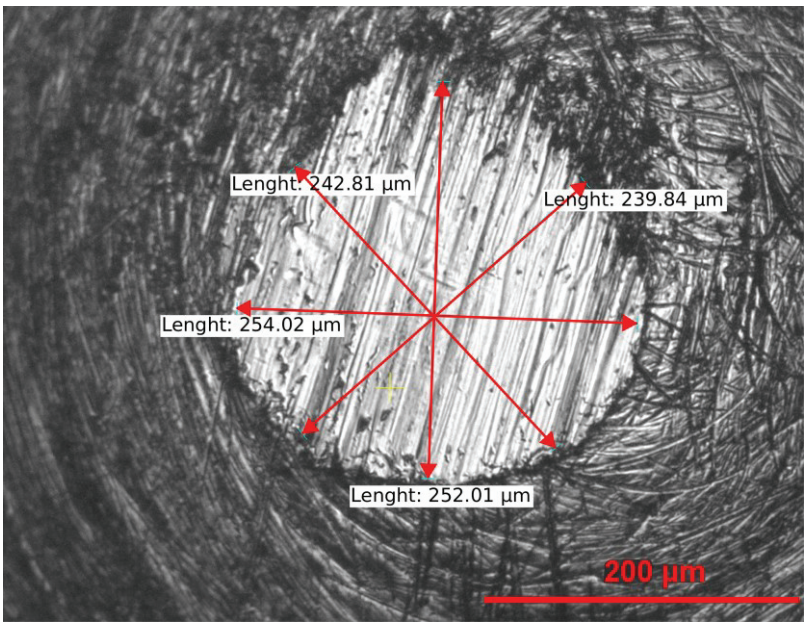

Figure 66. Wear scar at the tip of the piston under an optical microscope.

Note:- The surface roughness of the probes and steel ball used with the FricWear 2017 is different from (generally smoother than) the surface roughness of the rail, which can slightly affect the friction and wear measurements.

Advantages of the instrument

- The third body is taken into consideration.
- The instrument is portable.
- The contact pressure and shear speed are variable.
- The instrument can measure both the friction coefficient and the wear constants for many possible material combinations.
- The instrument can deliver appropriate inputs for simulation tools.
- The instrument is easy to understand from a pedagogical point of view.

Disadvantages of the instrument

- The instrument is only suitable for measurements over short distances (not continuous measurements).
- A refurbishment of the wear pistons has to be performed before each wear measurement occasion.
- The scaling effects are only considered through adjusting the contact pressure.
- An optical microscope is needed for the wear constant measurements.

D. ON-BOARD SYSTEM

Brief description of on-board TOR-FM system, as its LCC was calculated.

At present, there are two types of on-board lubrication systems, namely the solid stick and the fluid-based on-board TOR-FM system. The present research considers only the fluid-based system, which sprays a small amount of FM on the top of the rail.

The spray system (shown in Figure 67 (a)) is generally mounted on the locomotive, which while travelling sprays a specific amount of FM on the railhead or the running surface of the wheel. The FM is sprayed for a predefined period by means of compressed air (at 6−8 bar). If no compressed air is available in the vehicle, a compressor unit will also have to be installed. The nozzles (see Figure 67 (b)) are installed in such a way that crosswinds will not interrupt the application of the FM. The FM reservoir can be placed inside or outside the locomotive, and an example of a reservoir installed inside a locomotive is shown in Figure 67 (c). The spray command is carried out by one or more solenoid valves in the system. The manufacturer of FM-C (an oil-based TOR-FM) claims that 5 kg (equivalent to 5 litres) of FM-C are sufficient for 10,000 km. The supplier of the water-based FMs claims that the application of 22 to 38 ml/km/rail is required for these FMs. The present research has mainly investigated the water-based FMs and has focused on the curves where the traction forces are higher and require proper lubrication. Therefore, in the LCC calculations for the on-board system, a consumption of 30 ml/km/rail was used for calculating the operation cost of the on-board system, as recommended by the manufacturers of the water-based FMs.

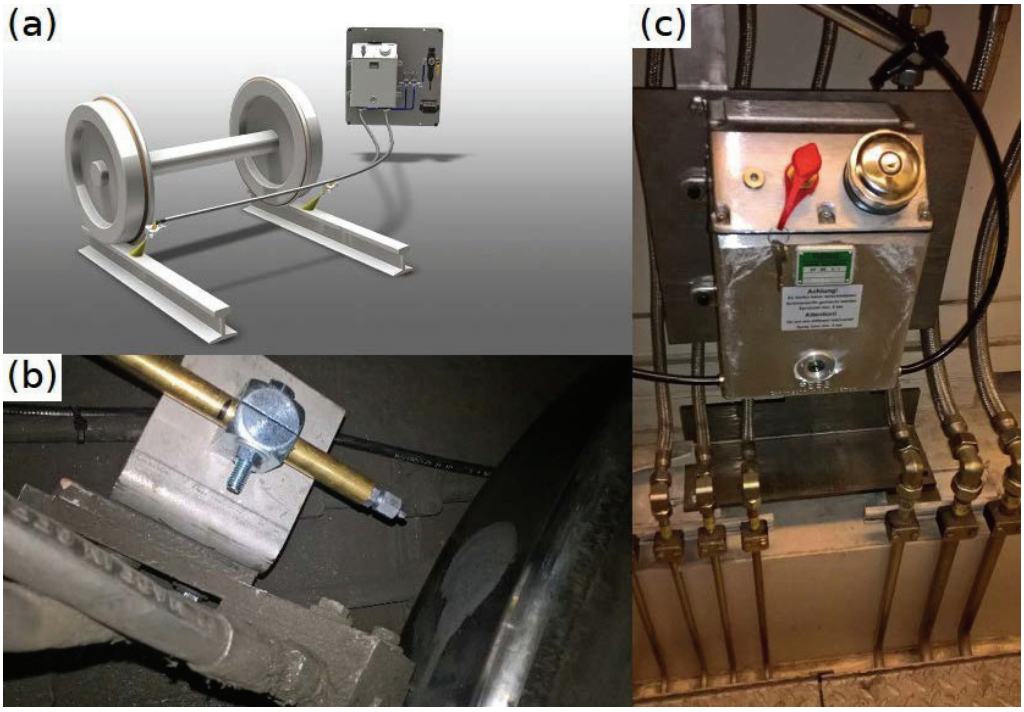

Figure 67. On-board TOR-FM system: (a) schematic diagram of the spray system, (b) nozzle spraying FM on the wheel tread (foto credit: Ivo Heinimann, LKAB) and (c) FM reservoir with distributing pipes (foto credit: Ivo Heinimann, LKAB).

.

The on-board system is also capable of using GPS technology and, hence, can automatically spray the required amount of FM at the desired locations. All the signals available from the spraying system and the compressor unit are registered in the control unit and can be used for monitoring and control. A thin film is formed directly on the place where the FM is needed.

The acquisition and maintenance cost of the on-board system is much lower than that of the wayside system. In general, an on-board system is four times cheaper than a wayside system. In the case of an on-board system, preventive maintenance is recommended by the manufacturer every 30,000 km and replacement of all the wear parts and elastomer parts every eight years. The replacement frequency is based on the information from the supplier. Since all the maintenance and refilling of the FM for an on-board system can be carried out at a depot, no transportation cost is required for these actions.

REFERENCES

Abbasi, S. *et al.* (2013) 'Pin-on-disc study of the effects of railway friction modifiers on airborne wear particles from wheel-rail contacts', *Tribology International*, 60, pp. 136–139. doi: 10.1016/j.triboint.2012.11.013.

Alarcón, G. I. *et al.* (2015) 'The influence of rail lubrication on energy dissipation in the wheel/rail contact: a comparison of simulation results with field measurements', *Wear*, 330–331, pp. 533–539. doi: 10.1016/j.wear.2015.01.008.

Andersson, E., Berg, M. and Stichel, S. (2014) *Rail vehicle dynamics*. Stockholm: KTH.

Archard, F. (1953) 'Contact and rubbing of flat surfaces', *Journal of Applied Physics*, 24(8), pp. 981–998. doi: 10.1063/1.1721448.

Asplund, M., Khan, S. A. and Nordmark, T. (2017) 'Improved wheel-rail system of Sweden' s Iron Ore Line', in *Proceedings of International Heavy Haul Association Conference (IHHA 2017)*. Cape Town.

Asplund, M., Nordmark, T. and Gustafsson, P. (2015) 'Comparison of TOR lubricating systems on the iron ore line', in *Proceedings of International Heavy Haul Association Conference (IHHA 2015)*. Perth.

Berghuvud, A. and Stensson, A. (1998) 'Dynamic behaviour of ore wagons in curves at Malmbanan', *Vehicle System Dynamics*, 30(3–4), pp. 271–284. doi: 10.1080/00423119808969452.

Bhushan, B. (2013) *Principles and applications of tribology*. John Wiley.

Bogdanski, S. and Lewicki, P. (2008) '3D model of liquid entrapment mechanism for rolling contact fatigue cracks in rails', *Wear*, 265(9–10), pp. 1356–1362. doi: 10.1016/j.wear.2008.03.014.

Bogojevic, N., Jönnson, P. and Stichel, S. (2011) 'Iron ore transportation wagon with three-piece bogies – simulation model and validation', *Heavy Machinery*, pp. 39–44.

Bower, A. F. and Johnson, K. L. (1991) 'Plastic flow and shakedown of the rail surface in repeated wheel-rail contact', *Wear*, 144(1–2), pp. 1–18. doi: 10.1016/0043-1648(91)90003-D.

Bower, A. and Johnson, K. (1989) 'The influence of strain hardening on cumulative plastic deformation in rolling and sliding line contact', *Journal of the Mechanics and Physics of Solids*, 37(4), pp. 471–493. doi: 10.1016/0022-5096(89)90025-2.

Burstow, M. C. (2003) *Whole life rail model application and development: development of a rolling contact fatigue damage parameter. A report produced for Railway Safety & Standards Board*. Derby.

Burstow, M. C. (2004) *Whole life model application and development for RSSB: continued development of an RCF damage parameter. A report produced for Railway Safety & Standards Board*. Derby.

Cannon, D. F. *et al.* (2003) 'Rail defects: an overview', *Fatigue and Fracture of Engineering Materials and Structures*, 26(10), pp. 865–886. doi: 10.1046/j.1460-2695.2003.00693.x.

Cannon, D. F. and Pradier, H. (1996) 'Rail rolling contact fatigue research by the European Rail

Research Institute', *Wear*, 191(1–2), pp. 1–13. doi: 10.1016/0043-1648(95)06650-0.

Challen, J. M., Oxley, P. L. B. and Hockenhull, B. S. (1986) 'Prediction of Archard's wear coefficient for metallic sliding friction assuming a low cycle fatigue wear mechanism', *Wear*, 111(3), pp. 275–288. doi: 10.1016/0043-1648(86)90188-2.

Dirks, B. (2015) *Simulation and measurement of wheel on rail fatigue and wear. Doctoral Thesis*. Stockholm: KTH.

Dirks, B. and Enblom, R. (2011) 'Prediction model for wheel profile wear and rolling contact fatigue', *Wear*, 271(1–2), pp. 210–217. doi: 10.1016/j.wear.2010.10.028.

Dollevoet, R. P. B. J. (2010) *Design of an anti head check profile based on stress relief. Doctoral thesis*. Enschede: University of Twente. doi: 10.3990/1.9789036530736.

Eadie, D. T. *et al.* (2003) 'Top of rail friction control: lateral force and rail wear reduction in a freight application', in *Proceedings of International Heavy Haul Association Conference (IHHA 2003)*. New Delhi, pp. 7–35.

Eadie, D. T. *et al.* (2006) 'Implementation of wayside top of rail friction control on North American heavy haul freight railways', in *Proceedings of the Seventh World Congress on Railway Research*. Montreal, pp. 2–11.

Eadie, D. T., Santoro, M., *et al.* (2008) 'Field studies of the effect of friction modifiers on short pitch corrugation generation in curves', *Wear*, 265(9–10), pp. 1212–1221. doi: 10.1016/j.wear.2008.02.028.

Eadie, D. T., Elvidge, D., *et al.* (2008) 'The effects of top of rail friction modifier on wear and rolling contact fatigue: full-scale rail-wheel test rig evaluation, analysis and modelling', *Wear*, 265(9–10), pp. 1222–1230. doi: 10.1016/j.wear.2008.02.029.

Eadie, D. T. (2014) *New materials for top of rail friction control in heavy haul operation: directions, risks and opportunities, PPT, Heavy Haul Seminar, WRI 2014.*

Eadie, D. T., Kalousek, J. and Chiddick, K. C. (2002) 'The role of high positive friction (HPF) modifier in the control of short pitch corrugations and related phenomena', *Wear*, 253(1–2), pp. 185–192. doi: 10.1016/S0043-1648(02)00098-4.

Eadie, D. T. and Santoro, M. (2006) 'Top-of-rail friction control for curve noise mitigation and corrugation rate reduction', *Journal of Sound and Vibration*, 293(3–5), pp. 747–757. doi: 10.1016/j.jsv.2005.12.007.

Eadie, D. T., Santoro, M. and Kalousek, J. (2005) 'Railway noise and the effect of top of rail liquid friction modifiers: changes in sound and vibration spectral distributions in curves', *Wear*, 258(7–8), pp. 1148–1155. doi: 10.1016/j.wear.2004.03.061.

Ekberg, A. *et al.* (2014) 'Identifying the root causes of damage on the wheels of heavy haul locomotives and its mitigation', *Proceedings of the Institution of Mechanical Engineers, Part F: Journal of Rail and Rapid Transit*, 228(6), pp. 663–672. doi: 10.1177/0954409714526165.

Ekberg, A. and Kabo, E. (2005) 'Fatigue of railway wheels and rails under rolling contact and thermal loading-an overview', *Wear*, 258(7–8), pp. 1288–1300. doi: 10.1016/j.wear.2004.03.039.

Ekberg, A., Kabo, E. and Andersson, H. (2002) 'An engineering model for prediction of rolling contact fatigue of railway wheels', *Fatigue Fracture of Engineering Materials Structures*, 25(10), pp. 899–909. doi: 10.1046/j.1460-2695.2002.00535.x.

Evans, J. R., Lee, T. K. Y. and Hon, C. C. (2008) 'Optimising the wheel/rail interface on a modern urban rail system', *Vehicle System Dynamics*, 46, pp. 119–127. doi: 10.1080/00423110701882355.

Fletcher, D. I., Hyde, P. and Kapoor, A. (2008) 'Modelling and full-scale trials to investigate fluid pressurisation of rolling contact fatigue cracks', *Wear*, 265(9–10), pp. 1317–1324. doi: 10.1016/j.wear.2008.02.025.

Gadelmawla, E. S. *et al.* (2002) 'Roughness parameters', *Journal of Materials Processing Technology*, 123(1), pp. 133–145. doi: 10.1016/S0924-0136(02)00060-2.

Galas, R. *et al.* (2018) 'The role of constituents contained in water-based friction modifiers for top-of-rail application', *Tribology International*, pp. 87–97. doi: 10.1016/j.triboint.2017.08.019.

GENSYS (2018). Available at: http://www.gensys.se (Accessed: 1 August 2018).

Goldstein, J. I. *et al.* (2003) *Scanning electron microscopy and X-ray microanalysis*. Springer. doi: 10.1007/978-1-4615-0215-9.

Grassie, S. L. (2005) 'Rolling contact fatigue on the British railway system: treatment', *Wear*, 258(7–8), pp. 1310–1318. doi: 10.1016/j.wear.2004.03.065.

Hamrock, B. J. and Dowson, D. (1981) *Ball bearing lubrication: elastohydrodynamics of elliptical contacts*. John Wiley.

Hardwick, C. and Lewis, R. (2014) 'The effect of alternative top of rail friction materials on pre-existing rolling contact fatigue cracks', in *in Second International Conference on Railway Technology: Research Development and Maintenance*. Stirlingshire, Scotland, pp. 1–17.

Hardwick, C., Lewis, S. and Lewis, L. (2011) 'The effect of friction modifiers on wheel/rail isolation at low axle load', *Wear*, 271(1–2), pp. 71–77. doi: 10.1016/j.wear.2010.10.036.

Harrison, H., McCanney, T. and Cotter, J. (2002) 'Recent developments in coefficient of friction measurements at the rail/wheel interface', *Wear*, 253(1–2), pp. 114–123. doi: 10.1016/S0043-1648(02)00090-X.

Hertz, H. (1882) '"Über die Berührung fester elastische körper und über die Härte"', in *Verhandlungen des Vereins zur Beförderung des Gewerbefleisses*. Leipzig.

IEC 60300-3-3 (2017) *Dependability management – Part 3-3: Application guide – life cycle costing; IEC 60300-3-3. Geneva: International Electrotechnical Commission.*

Jendel, T. (2002) 'Prediction of wheel profile wear-comparisons with field measurements', *Wear*, 253(1–2), pp. 89–99. doi: 10.1016/S0043-1648(02)00087-X.

Johnson, K. L. (1989) 'The strength of surface in rolling contact', *Journal of Mechanical Engineering Science*, 203(3), pp. 151–163.

Kalker, J. J. (1982) 'A fast algorithm for the simplified theory of rolling-contact', *Vehicle System*

Dynamics, 11(1), pp. 1–13. doi: 10.1080/00423118208968684.

Khan, S. A. *et al.* (2017) 'Prediction of top-of-rail friction control effects on rail RCF suppressed by wear', *Wear*, 380–381, pp. 106–114. doi: 10.1016/j.wear.2017.03.010.

Khan, S. A. *et al.* (2018) 'Prediction of the effects of friction control on top-of-rail cracks', *Proceedings of the Institution of Mechanical Engineers, Part F: Journal of Rail and Rapid Transit*, 232(2), pp. 484–494. doi: 10.1177/0954409716674984.

Lemma, Y. *et al.* (2014) 'Top-of-rail friction measurements of the Swedish Iron Ore Line', in *in 3rd International Workshop and Congress on eMaintenance*. Luleå.

Lu, X. *et al.* (2012) 'Friction management on a Chinese heavy haul coal line', *Proceedings of the Institution of Mechanical Engineers, Part F: Journal of Rail and Rapid Transit*, 226(6), pp. 630–640. doi: 10.1177/0954409712447170.

Lundberg, J. *et al.* (2014) 'Measurements of friction coefficients between rails lubricated with a friction modifier and the wheels of an IORE locomotive during real working conditions', *Wear*, 324–325, pp. 109–117. doi: 10.1016/j.wear.2014.12.002.

Lyu, Y., Bergseth, E. and Olofsson, U. (2016) 'The effect of subzero temperature and snow on the tribology of wheel-rail contact', *Civil-Comp Proceedings*, pp. 1–13.

Matsumoto, K. *et al.* (2004) 'A method to apply friction modifier in railway system', *JSME International Journal*, 47(2), pp. 482–487. doi: 10.1299/jsmec.47.482.

Nia, S. H. (2014) *An investigation of the iron-ore wheel damages using vehicle dynamics simulation. Licentiate Thesis*. Stockholm: KTH.

Nia, S. H. (2017) *On heavy-haul wheel damages using vehicle dynamics simulation. Doctoral thesis*. Stokholm: KTH.

Nia, S. H., Casanueva, C. and Stichel, S. (2015) 'Prediction of RCF and wear evolution of iron-ore locomotive wheels', *Wear*, 338–339, pp. 62–72. doi: 10.1016/j.wear.2015.05.015.

Nia, S. H., Jonsson, P. A. and Stichel, S. (2014) 'Wheel damage on the Swedish Iron Ore Line investigated via multibody simulation', *Proceedings of the Institution of Mechanical Engineers, Part F: Journal of Rail and Rapid Transit*, 228(6), pp. 652–662. doi: 10.1177/0954409714523264.

Nielsen, J. C. O. and Stensson, A. (1999) 'Enhancing freight railways for 30 tonne axle loads', *Proceedings of the Institution of Mechanical Engineers, Part F: Journal of Rail and Rapid Transit*, 213(4), pp. 255–263. doi: 10.1243/0954409991531191.

Nissen, A. (2009) 'LCC-analysis for switches and crossings: A case study from the Swedish railway network', *International Journal of COMADEM*, 12(2), pp. 10–19.

Nordlöf, P. (2014) *Summary of the Swedish debate on discount rate*.

Nordmark, T. *et al.* (2014) *The wheel profile measurement system at Sunderbyn, Sweden: final report*. Luleå.

Nordmark, T. (2016) *Vagnsrapport - provtåg 32,5 tons axellast*. Kiruna.

Oldknow, K., Eadie, D. T. and Stock, R. (2012) 'The influence of precipitation and friction control agents on forces at the wheel/rail interface in heavy haul railways', *Proceedings of the Institution of Mechanical Engineers, Part F: Journal of Rail and Rapid Transit*, 227(1), pp. 86–93. doi: 10.1177/0954409712452240.

Orvnäs, A. (2005) *Simulation of rail wear on the Swedish light rail line Tvärbanan. Master thesis*. Stockholm: KTH.

Pearce, T. G. and Sherratt, N. D. (1991) 'Prediction of wheel profile wear', *Wear*, 144(1–2), pp. 343–351. doi: 10.1016/0043-1648(91)90025-P.

Persson, I. (2015) 'GENSYS ib railway vehicler modeling', in Iwnicki, S. (ed.) *The Manchester benchmarks for rail vehicle simulation*. Volume 31. Taylor & Francis, pp. 91–100.

Pombo, J. *et al.* (2011) 'Development of a wear prediction tool for steel railway wheels using three alternative wear functions', *Wear*, 271(1–2), pp. 238–245. doi: 10.1016/j.wear.2010.10.072.

Seo, J. W. *et al.* (2018) 'Effect of friction modifier on rolling contact fatigue and wear of wheel and rail materials', *Tribology Transactions*, 61(1), pp. 19–30. doi: 10.1080/10402004.2016.1271487.

Spikes, H. A. (1997) 'Mixed lubrication - an overview', *Lubrication Science*, 9(3), pp. 221–253. doi: 10.1002/ls.3010090302.

Spiryagin, M. *et al.* (2013) 'Research methodology for evaluation of top-of-rail friction management in Australian heavy haul networks', *Proceedings of the Institution of Mechanical Engineers, Part F: Journal of Rail and Rapid Transit*, 228(6), pp. 631–641. doi: 10.1177/0954409714539943.

Stock, R. *et al.* (2011) 'Influencing rolling contact fatigue through top of rail friction modifier application - a full scale wheel-rail test rig study', *Wear*, 271(1–2), pp. 134–142. doi: 10.1016/j.wear.2010.10.006.

Stock, R. *et al.* (2015) 'Top of rail friction control for heavy haul: status and opportunities', in *AusRAIL PLUS*. Melbourne: AusRAIL PLUS 2015, pp. 24–26.

Stock, R. *et al.* (2016) 'Material concepts for top of rail friction management – classification, characterization and application', *Wear*, 366–367, pp. 225–232. doi: 10.1016/j.wear.2016.05.028.

Stock, R. *et al.* (2017) 'Wheel and rail life extension with on-board top of rail friction control', in *International Heavy Haul Association Conference (IHHA 2017)*. Cape Town, pp. 2–6.

Stribeck, R. (1902) 'Die wesentlichen Eigenschaften der Gleit- und Rollenlager, Zeitschrift des Vereins Deutscher Ingenieure 36', *Zeitschrift des Vereins Deutscher Ingenieure*, pp. 1341–1348, 1432–1438, and 1463–1470.

Suda, Y. *et al.* (2005) 'Development of onboard friction control', *Wear*, 258(7–8), pp. 1109–1114. doi: 10.1016/j.wear.2004.03.059.

Sun, Y. Q. and Cole, C. (2008) 'Vertical dynamic behavior of three-piece bogie suspensions with two types of friction wedge', *Multibody System Dynamics*, 19(4), pp. 365–382. doi: 10.1007/s11044-007-9085-z.

Sunqing, Q., Junxiu, D. and Guoxu, C. (1999) 'A review of ultrafine particles as antiwear additives

and friction modifiers in lubricating oils', *Lubrication Science*, 11(3), pp. 217–226.

Torbacke, M., Rudolphi, Å. K. and Kassfeldt, E. (2014) *Lubricants: introduction to properties and performance*. Wiley.

VanderMarel, J. *et al.* (2013) 'A predictive model of energy savings from top of rail friction control', *Wear*, 314(1–2), pp. 155–161. doi: 10.1016/j.wear.2013.11.037.

Viklund, R. (2012) *Riksgränsbanans elektrifiering Stat och företag i samverkan: 1910-1917. Doctoral thesis*. Luleå: LTU.

Waara, P. (2006) *Lubricants Influence on Wear in Sharp Rail Curves. Doctoral thesis*. Luleå: LTU. doi: 10.1108/00368790110393910.

Zhou, Y., T.Wang and S.Wang (2013) 'Field studies of the effect of top of rail friction modifier on wheel/rail interaction of heavy-haul railway', in *Proceedings of International Heavy Haul Association Conference (IHHA 2013)*. New Delhi, pp. 329–334.

Zhu, Y. (2011) *Adhesion in the wheel-rail contact. Doctoral thesis*. Stockholm: KTH.

Zhu, Y., Olofsson, U. and Chen, H. (2013) 'Friction between wheel and rail: a pin-on-disc study of environmental conditions and iron oxides', *Tribology Letters*, 52(2), pp. 327–339. doi: 10.1007/s11249-013-0220-0.

Zoeteman, A., Dollevoet, R. and Li, Z. (2014) 'Dutch research results on wheel/rail interface management: 2001-2013 and beyond', *Proceedings of the Institution of Mechanical Engineers, Part F: Journal of Rail and Rapid Transit*, 228(6), pp. 642–651. doi: 10.1177/0954409714524379.

PART 2

Paper 1: Prediction of the effects of friction control on top-of-rail cracks

Khan, S. A., Persson, I., Lundberg, J. and Stenström, C. (2018) 'Prediction of the effects of friction control on top-of-rail cracks', Proceedings of the Institution of Mechanical Engineers, Part F: Journal of Rail and Rapid Transit, 232(2), pp. 484–494.

Original Article

Institution of MECHANICAL ENGINEERS

Journal of RAIL AND RAPID TRANSIT

Proc IMechE Part F:
J Rail and Rapid Transit
2018, Vol. 232(2) 484–494

DOI: 10.1177/0954409716674984
journals.sagepub.com/home/pif

SAGE

Prediction of the effects of friction control on top-of-rail cracks

Saad Ahmed Khan[1], Ingemar Persson[2], Jan Lundberg[1] and Christer Stenström[1]

Abstract

Rolling contact fatigue is a major problem connected with railway tracks, especially in curves, since it leads to higher maintenance costs. By optimising the top-of-rail friction, the wear and cracks on the top of the rail can eventually be reduced without causing very long braking distances. There are several research articles available on crack prediction, but most of the research is focused either on rail without a friction modifier or on wheels with and without friction control. In the present study, in order to predict the formation of surface-initiated rolling contact fatigue, a range of friction coefficients with different Kalker's reduction factors has been assumed. Kalker's reduction factor takes care of the basic tendency of creepage as a function of the traction forces at lower creepage. The assumed range covers possible friction values from those for non-lubricated rail to those for rail with a minimum measured friction control on the top of the rail using a friction modifier. A fatigue index model based on the shakedown theory was used to predict the generation of surface-initiated rolling contact fatigue. Simulations were performed using multi-body simulation, for which inputs were taken from the Iron Ore line in the north of Sweden. The effect of friction control was studied for different curve radii, ranging from 200 m to 3000 m, and for different axle loads from 30 to 40 tonnes at a constant train speed of 60 km/h. One example of a result is that a maximum friction coefficient (μ) of 0.2 with a Kalker's reduction factor of 15% is needed in the case of trains with a heavy axle load to avoid crack formation.

Keywords

Rolling contact fatigue, fatigue index, friction modifier, friction control, rail

Date received: 2 June 2016; accepted: 25 September 2016

Introduction

For longer distances and heavy loads, the railway system is still the most economical means of transportation. Because of increasing competition, railway operators are continuously working to improve the overall operational efficiency.[1,2] In order to achieve higher operational efficiency, the axle load needs to be increased. An increased axle load increases the traction forces between the rail and wheel, which in turn increase the wear and the rolling contact fatigue (RCF) and, consequently, increases the maintenance cost of the infrastructure. As reported by Trafikverket (the infrastructure manager in Sweden), the lifetime of the rail is limited, especially in the case of heavy haul lines, mainly due to RCF on the top of the rail, which basically causes surface-initiated cracks. The traction forces are even more severe in small-radius (sharp) curves, which make such curves more prone to damage. Ignorance of cracks due to RCF at their initial stage can lead to a catastrophic accident, as cracks propagate fast once they have been generated. Wear is also considered as a damaging effect, but generally it is not as catastrophic as cracks and sometimes artificial wear (grinding) is carried out to remove surface cracks. However, grinding is expensive in terms of both resources and track access time, and there is therefore always a need to increase the time interval for grinding. To increase the lifetime of the rails without compromising on the axle load and speed, one must either increase the strength of the rails or decrease the traction forces between the rails and wheels.

Unlike road vehicles (e.g. cars and buses), trains do not have steering mechanisms. Practically, a train is steered partially with the help of the rolling radius difference between the high and low wheel of the same axle, and partially with the help of the wheel flange. Ideally, the rolling radius difference between

[1]Division of Operation and Maintenance, Luleå University of Technology, Sweden
[2]AB DEsolver, Östersund, Sweden

Corresponding author:
Saad Ahmed Khan, Division of Operation and Maintenance, Luleå University of Technology, Luleå SE-97187, Sweden.
Email: saad.ahmed.khan@ltu.se

the high and low wheels should be enough to negotiate the curve, but practically this is not the case, as a result of which the outer wheel flange hits the rail to negotiate the curve. When the flange hits the rail, this results in a wheel contact consisting of two point contacts (valid for the special wheel and rail profiles of heavy haul trains); one point is located between the wheel tread and the top of the rail and the other point between the wheel flange and rail gauge.[3] In some special cases, the wheel and rail can have more than two contact points due to facets created by grinding, but those cases are not covered in this study. The motion between the wheel tread and the top of the rail is a rolling motion (not an ideal rolling), which makes the train run, whereas the motion between the wheel flange and rail gauge (especially in the case of heavy haul trains) is generally a pure sliding motion, which helps in steering and keeps the axle in a confined position to avoid derailment. The flange sliding behaviour is dependent on the rail–wheel profile and for some profiles it may not consist of a pure sliding motion. The degree of flange sliding depends on the rail–wheel profile, the curvature of the track and the stiffness of the primary suspension.

The shakedown diagram was developed by Bower and Johnsson[4] who used it in a study on the modelling of near-surface plastic deformation caused by repeated wheel–rail contact and reported that, by reducing the utilised friction coefficient between the rail and wheel and thus minimising the traction forces, the probability of RCF formation could be controlled. The friction between the wheel flange and rail gauge should be as low as possible (which is not focused in this paper), if the wheel–rail profiles are designed to have a pure sliding motion. However, excessively reduced friction between the rail head and wheel tread can cause slippage and/or too long a braking distance. Therefore, the utilised friction between the wheel tread and the top of the rail (rail running surface) needs to be controlled and kept within a particular range of friction coefficients. This friction coefficient range provides the minimum possible traction forces without wheel slippage or a long braking distance. The top-of-rail friction modifier, whose use was first reported in 2003 by Eadie et al.,[5] has emerged as a possible solution to traction force control. Top-of-rail friction modifier (TOR-FM) is a product which, according to the claims of the manufacturers, controls the friction coefficient and keeps it in a certain range between the rail head and wheel tread. TOR-FM has been tested and even implemented at several North American heavy haul railway sites.[6] It has also been studied in combination with gauge face lubrication (which is also known as friction management) in China[7] and Australia.[8] In addition, many laboratory tests have been performed using a twin-disc test rig[9] and a full-scale rail–wheel test rig,[10] and a reduction in both wear and cracks has been reported.

Sweden's Iron Ore Line (IOL), situated in the north of the country, is mainly used for transporting iron ore from the mines in Kiruna and Malmberget to the seaports of Luleå in Sweden and Narvik in Norway. Till date, no TOR friction control has been implemented on this line and cracks are a major problem on the line, especially in curves. Before starting a field test, the performance of simulations is recommended, as they are cheaper and faster than field tests.[3] Simulation models with correct inputs can predict the effect of friction control on wheel–rail damage and can be used to understand the effect of friction on rail damage. Another advantage of such prediction models is their ability to analyse the life cycle cost of using a friction controller in the wheel–rail interface. Ekberg et al.[11] developed a fatigue index (FI) model based on the shakedown diagram to predict the generation of surface-initiated RCF on railway wheels. This model has been verified and validated by researchers in the past few years.[12]

The present study is part of a project called the Top of the Rail (TOR) Project, which is supported by the railway infrastructure manager in Sweden, Trafikverket. The project includes both field tests and computer-based simulations. The results from this study will be compared with the results from future field tests performed for validation purposes. After successful validation, it will be possible to use the results of simulations to calculate the economic efficiency of the TOR system.

Methods

In the present study, simulations were performed using measurement data (obtained using track inspection trains and a handheld laser device) from in-service wheels and rail on the IOL. The reason for using profiles of in-service (used) wheels and rail was that they generally generate different contact forces (ranging from higher to lower) due to asperities and surface deformation.[13] For performing simulations, a range of friction coefficients with different Kalker's reduction factors was used. Kalker's reduction factor takes care of the basic tendency of creepage as a function of the traction force at lower creepage.[14] The assumed friction control values (including both the friction coefficient and the Kalker's reduction factor), along with the measured rail–wheel profiles and track irregularities, were input into a multi-body simulation (MBS) from the GENSYS[15] software. In 2015, the wheel and rail profiles were measured using a Calipiri 40 device from Nextsense, and the track irregularities (the longitudinal level, line, cant and gauge irregularities) were measured by a special track recording train (IMV100). The MBS performed the wheel–rail contact mechanics modelling, which is based on Hertzian theory in combination with Kalker's simplified theory of rolling contact (the FASTSIM algorithm).[16]

Friction values

Traditionally, the friction coefficient between surfaces is measured using a pin-on-disc, twin-disc[17] or full-scale test rig[13] in laboratories. However, in small laboratory tests, one encounters a scaling factor problem and the problem of achieving realistic surface roughness and ambient conditions, e.g. snow, humidity, deposits from brakes, dust from ore and the environment, etc. Big-rig tests overcome the scale factor, but real field conditions and surface roughness are still not feasible. To achieve realistic environmental conditions, a handheld tribometer can be used, but with such a tribometer there is a lower contact pressure between the contact surfaces than there is in real wheel–rail contact. This lower contact pressure leads to unrealistic estimations of the friction between the rail and wheel.[18] One of the most reliable ways to obtain realistic values for the friction between the rail and wheel is to use a friction measurement device installed on board a locomotive,[18] although this method is impractical owing to its high cost. The on-board device measures the friction under natural environmental conditions, uncontrolled by humans. The values measured using the on-board friction measurement device and the values calculated from laboratory tests contradict each other, which could be due to differing ambient conditions. In the case of the on-board device, the ambient conditions (e.g. the surface roughness, temperature, humidity, third body, etc.) are considered, but they can vary dramatically. Therefore, a range of intermediate friction coefficient values was used for the simulations in the present study (see Figure 1). The future solution regarding friction measurement could be an improved handheld device for use in the field. The cost of the equipment should be low and the contact pressure should be the same as that of the wheel–rail contact.

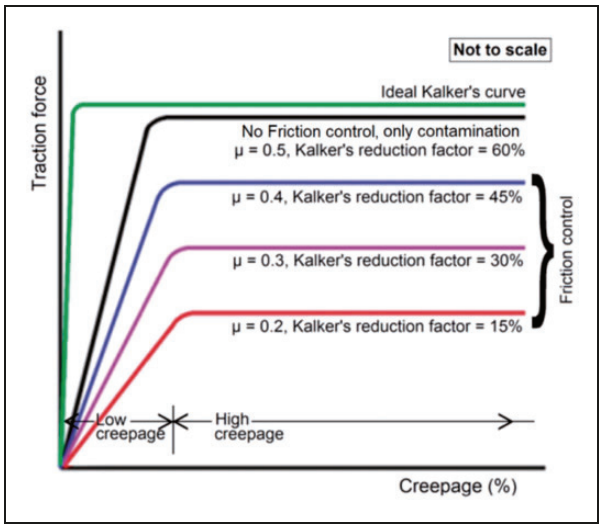

Figure 1. Traction force–creepage diagram, showing the trend with different levels of friction control (combinations of friction coefficient and Kalker's reduction factor) with respect to the traction force. The horizontal line indicates full slip and the slanting line indicates partial slip. Adapted from VanderMarel et al.[14]

Another important factor that needs to be considered is that the friction between the rail and wheel rarely involves full slip and often involves partial slip. Measurements made by Johnson[19] showed that Kalker's theory applies to ideal wheels and rails. According to this theory, which focuses on the ideal condition, the partial slip condition (the topmost slanting line in Figure 1) occurs when there are very small creepage values. If the surfaces are contaminated, the friction coefficient is reduced and a reduction factor has to be introduced; i.e. contamination acts as a lubricant/friction modifier. On the introduction of a reduction factor, partial slip (the second slanting line from the top in Figure 1) occurs when there are comparatively larger creepage values. A friction coefficient of 0.5 and a reduction factor of 60% in the ideal Kalker's curve were used in the present study to predict the non-lubricated (dry) condition.[3] The friction modifier decreases not only the friction coefficient but also the slope of the partial friction approximately four times (a reduction factor of 15% of ideal Kalker's curve).[14] In other words, at any given value of creepage, the friction modifier gives much lower traction forces. The Kalker's reduction factor used for each individual friction coefficient is shown in Figure 1.

For the Kalker's reduction factors of 60% for $\mu = 0.5$ and 15% for $\mu = 0.2$, reduction factors were derived from the results of VanderMarel et al.[14] and they represent the highest and the lowest limit. The reduction factors for $\mu = 0.4$ and $\mu = 0.3$ are assumed values selected between the highest and the lowest values. Using these combinations of a friction coefficient and a reduction factor, the simulations performed imitated the presence of the friction modifier on the top of the rail.

Friction modifiers are generally water-based lubricants, which can be applied directly on the top of the rail, forming a micron-scale friction modifier film after drying.[17] It is claimed by the manufacturers that these films control the friction coefficient and keep it in a particular range, depending on the amount of friction modifier applied and the chemical composition of the modifier. For the present simulations, a fixed value of Kalker's reduction factor was chosen for each individual friction coefficient and for the complete railway curve. The values used in the present study are based on laboratory tests, and no relation was specified between the amount of lubrication and/or base solvent used on the real tracks and the friction control values used in the simulation.

In practical cases, on reaching the full-slip condition at higher creepage levels, the traction force is not constant with respect to the creepage. In dry conditions (i.e. no lubrication and/or contamination), when the creepage is increased, the traction force decreases

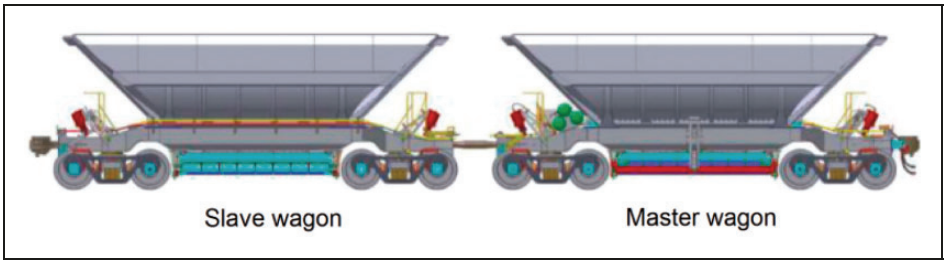

Figure 2. Two-unit iron ore wagon (Fanoo wagon).[21]

slightly, i.e. the saturated friction has a negative slope,[20] which generally leads to stick-slip between the rail and wheel. It is claimed by the manufacturers that, when the friction modifier is used, the traction force never decreases with increasing creepage, i.e. the friction modifier leads to a positive slope at a higher creepage level. For ease of calculation, the zero slope shown in Figure 1 was used for the saturated condition in all cases.

Wagon model and loads

The multi-body dynamic model of the iron ore wagon, together with the track system, was built using the GENSYS software.[15] The present iron ore wagons (also known as Fanoo wagons) have four axles with two individual three-piece bogies (Figure 2). The bogies have primary suspension between the axle and side frames and secondary suspension between the side frames and the bolster beam. The primary suspension, which is connected between the axle and side frame, is relatively soft to give the wheel sets good radial self-steering capabilities, so that the wagon can easily negotiate sharp curves. However, this soft suspension system, which is intended to enhance the steering capabilities of the bogie, limits the maximum running speed of the train due to hunting oscillation.[3] Hunting oscillations are unwanted sinusoidal movements of the axle due to a difference in the rolling radius between the high and low wheel of the same axle. These oscillations cause equilibrium problems after reaching a particular train speed.

Iron ore wagons are connected in pairs: one of the units is called the master wagon and the other is called the slave wagon. The controller of the braking system is attached to the master wagon. The total weight of each wagon for the simulations was taken from a realistic range of 120–160 tonnes (a 30 to 40 tonne axle load) with an increment of 10 tonnes (a 2.5 tonne axle load). At present, an axle load up to 30 tonnes is used and 32.5 tonnes is under testing for Swedish heavy haul trains, but work is in progress to increase the axle load further. The weight distribution of the individual parts, which were considered as rigid bodies, is given in Table 1. For further details of the wagon design, see Nia,[21] where a similar model was used.

Table 1. Weight distribution of the different parts of the wagon.

Parts	Number of units	Weight (kg)
Car body	1	12536
Bolster beam	2	1050
Side frame	4	400
Axle	4	1341

Table 2. Cant (superelevation) used in the field for the respective curve radii and used in the simulation.

Curve radius (m)	Cant (m)
200	0.15
300	0.15
400	0.1
500	0.1
1000	0.05
2000	0
3000	0

Curve data

For the simulations, the curve radius varied from 200 m to 3000 m and the speed of the train for all the curves was fixed to 60 km/h. This range of radii covers the possible curve radii present in the north of Sweden. The actual cant values designated to the respective curve radii by Trafikverket and used in the simulations are given in Table 2.

All the simulations were performed for a track length of 700 m, as shown in Figure 3. The circular curve was 250 m in length and a transition curve of 200 m was added before and after the circular curve. Before the first transition curve, a 50 m long tangent track was also included to give a smooth start with lower traction forces. The direction of the bend in all the simulations was towards the right. Therefore, the left rail is denoted as the high rail and the right rail as the low rail.

Wheel and rail profiles

To obtain realistic results, in-service profiles from the IOL were chosen for the simulations. The exact profile inputs are shown in Figure 4. The WP4 wheel profile is the base profile and is used for both the high and the low wheels on the axle, whereas the rail has the 60E1 base profile. The base profile of the rails is valid only for new profiles, because, after the first grinding, the profile of the high rail is changed to the MB1, while the low rail retains the 60E1 profile. The profiles used in the simulation were measured approximately 6 months after grinding was executed. Both the high and the low rails have an inclination of 1/30, which is also reflected in Figure 4. The properties of the 350LHT rail material were used, as that same material is used on the IOL. For further details of the steel, see Voestalpine.[22]

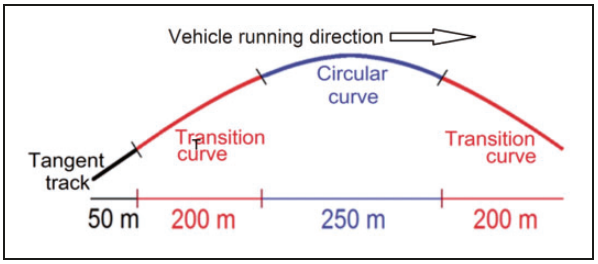

Figure 3. Schematic diagram showing the different zones of the 700 m curve (with a 50 m long tangent track) used in the simulation.

RCF prediction model

The possible forces were generated using multi-body dynamic simulations of the rail–wheel interaction. The output from the dynamic simulations, which consists of the contact forces, creepage, contact position, the size of the contact area, etc., were put into the RCF prediction model.

To predict the generation of surface-initiated cracks (caused by RCF), the FI method,[11] which is based on the shakedown theory,[4] was used. According to the FI model the occurrence of RCF depends on the contact pressure, the creep forces in the contact area and the material yield stress in shear. If the external stresses of the working point (WP) exceed the threshold value, which is known as the shakedown limit, surface cracking will occur due to accumulated plastic strain (see Figure 5).

The location of the threshold value (shakedown limit) in the shakedown diagram is a function of the maximum Hertzian contact pressure (P_o in N/m^2) divided by the shear strength of the material (k in N/m^2) in the y-axis, and the utilised friction coefficient (μ) in the x-axis. The shear strength (k) depends on the material of the rail, and the contact pressure mainly depends on the contact area and applied load. The utilised friction coefficient (μ) depends on the creepage and the third body (e.g. dust, water or friction modifier) between the rail and wheel. The friction coefficient is defined as the quotient of the creep forces tangential to the contact surface (F_t in N) and the

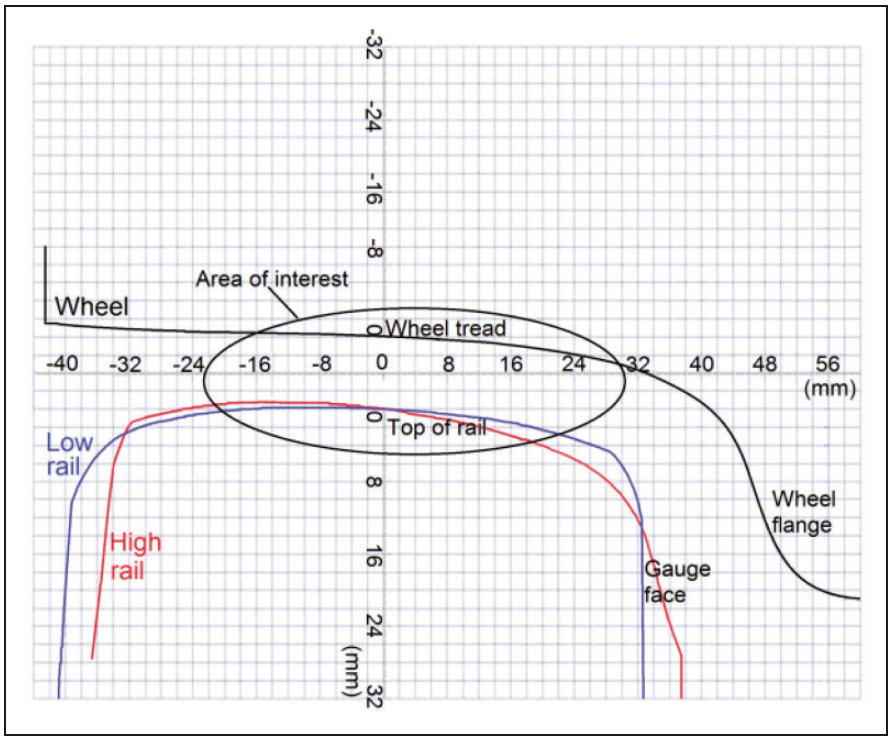

Figure 4. Worn profiles of wheels and rail (both high and low) used in the simulations.

normal to the contact point (F_n in N)

$$\mu = \frac{F_t}{F_n} = \frac{\sqrt{F_{nx}^2 + F_{ny}^2}}{F_n} \quad (1)$$

where F_{nx} and F_{ny} are the longitudinal and lateral creep force tangential to the contact surface in N, respectively.

A surface fatigue index (FI), which is a measure of the probability of RCF initiation, is defined as follows[11]

$$FI = \mu - \frac{k}{p_o} \quad (2)$$

The value of the FI indicates the extent to which the shakedown limit has been exceeded. This shakedown limit is the threshold value for crack generation. The FI is basically the transformation of the threshold curve of the shakedown diagram into a horizontal line. Damage is assumed to occur for $FI > 0$ (Figure 5). The FI method gives only the probability of crack generation, which is presented in the form of an index chart, and does not give any information about the propagation of cracks or the number of cracks.

The limitation of the FI prediction model is that the applied shakedown diagram is derived under full-slip conditions. The contact with the gauge corner of a rail is often in full slip, but the contact on the top of the rail is often in partial slip. In the case of partial slip, the maximum principal shear stress is higher than that of full slip,[23] but in the case of lower friction the difference in shear strength between full and partial slip is small.[23] Moreover, the FI method does not take the creepage into account, although creepage can be an important variable in determining the fatigue life, nor does the FI method take the possible influence of wear into account, which can also be seen as a limitation.

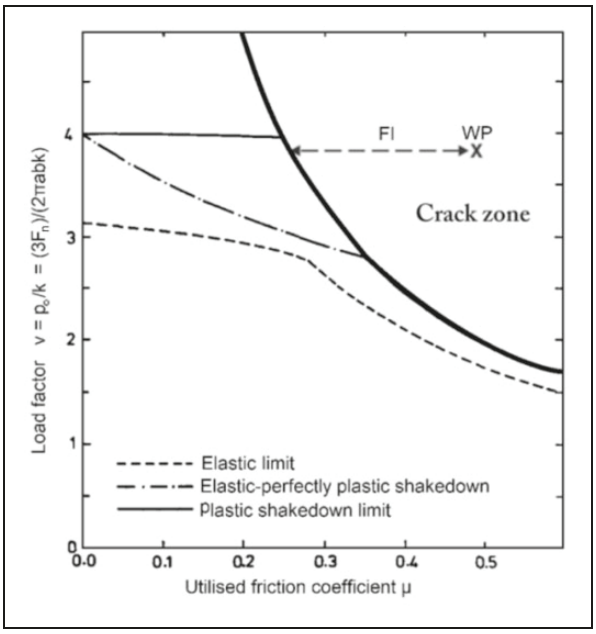

Figure 5. Shakedown map. Surface fatigue is predicted if the working point (WP) (defined by the material yield stress in shear, contact geometry and applied loading) is outside the thick line. Adapted from Dirk et al.[12]

Results and discussion

The results shown below are from the leading axle of the first bogie of the wagon. The leading axle often experiences higher forces than the trailing axle and, therefore, the leading axle is more prone to damage.[24] This makes the leading axle more eligible for the selection for simulations.

Fatigue index chart for the sharpest curve

The FI chart for the different friction control levels is shown as a function of the position in the curve in Figure 6(a) and (b) for high and low rails, respectively. These figures represent the effect of friction control on the probability of crack generation in the complete curve, including the transition curve, and show how the index changes from the tangent track to the curve track.

The initial 50 m of the track, starting at 0 m, represent the tangent track. In this zone, the FI values are at the minimum level since the traction forces are small because of the tangent track. After that the transition curve starts, the traction forces between the rail and wheel start to increase and, with this increase in the traction forces, the FI values also increase. The FI values stabilise on reaching the circular curve (at 250 m) and remain stable in the whole circular curve (250–500 m). In the circular curve, if no external force is applied, the motion is also known as quasi-static motion. Due to the quasi-static behaviour in the circular curve, the traction forces remain contant, but small disturbances are noted due to track irregularities. At the end of the circular curve (after 500 m), the FI values again go down to the initial FI values generated on the tangent track. One can observe that the tangent part of the track is in the safe zone (no-crack zone), but there is a shift to the crack (positive) zone when the curve radius is decreased, especially for the higher friction values. The topmost curves represent a friction coefficient of 0.5 with a Kalker's reduction factor of 60%. It is also affirmed with the shakedown diagram that a higher friction coefficient leads to a higher probability of crack generation, which is also seen in Figure 6(a) and (b). The friction coefficients with the highest values give the highest FI values, since at higher friction the shear stresses are higher.

The second graph from the top has a lower FI value, as it has a lower friction coefficient value of

0.4 and a reduction factor of 45%. It can be seen that, by lowering the utilised friction from $\mu = 0.5$ to $\mu = 0.4$, the probability of crack generation is decreased by $25 \pm 5\%$ on both the high and the low rail. Here, a friction coefficient of 0.4 with a reduction factor of 45% is considered as reduced friction, but it is quite often the case that the friction between the rail and wheel is near this value even without friction control. This can happen due to various deposits on the rails from trains and the ambient atmosphere (e.g. moisture).

The next step is to study the friction at $\mu = 0.3$ with a reduction factor of 30%, which is the third curve from the top in Figure 6(a) and (b). The probability of crack generation is reduced by $55 \pm 5\%$ in both the high and the low rail. With this friction coefficient and reduction factor, the FI value has been reduced considerably. However, there will still be cracks on the

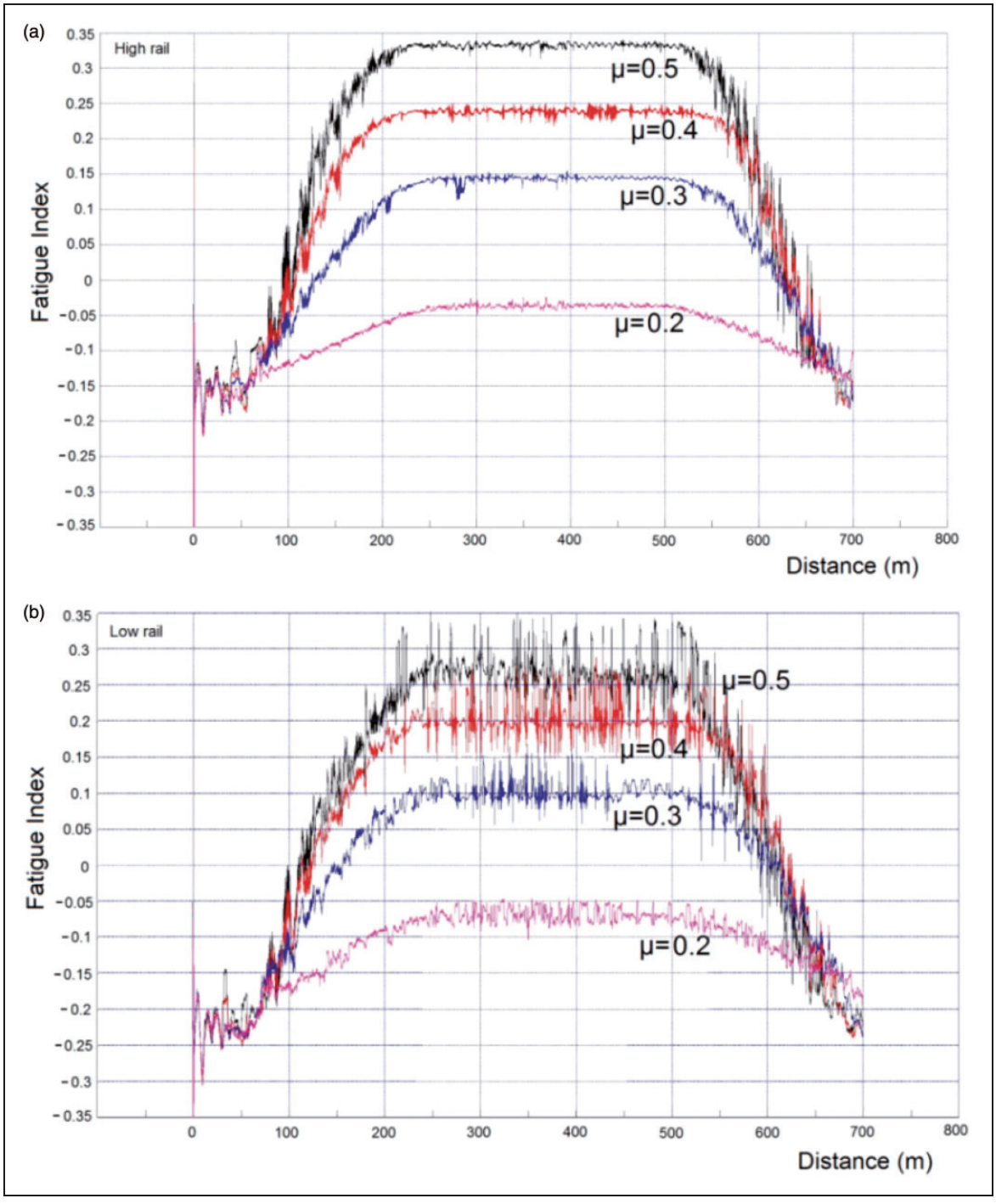

Figure 6. Fatigue index for a 200 m curve radius at different friction values with respect to the distance in the curve: (a) high rail and (b) low rail.

rail surface, because the traction force reduction is not sufficient to prevent the generation of cracks. Generally, the friction modifier manufacturers claim that, at this value, crack formation can be avoided, but this has not been observed in the simulations. By reducing the Kalker's reduction factor to a lower value, crack generation can probably be avoided. It should be noted that this study has used old profiles with irregularities, which also increase the risk of crack generation.

The lowest graph represents friction control with $\mu = 0.2$ and a reduction factor of 15%. At this level of friction control, the FI value for both the high and the low rail is in the safe zone. According to the railway safety regulations, such a low friction ($\mu = 0.2$) is not recommended on the top of the rail. However, many researchers have shown that the friction coefficient can decrease down to 0.2, or even lower, with the presence of water or excess friction modifier[18] and to even lower values in the case of crushed leaves.[25] Such a low friction can increase the risk of a long braking distance and the possibility of wheel slippage.

On comparing Figures 6(a) and (b), it can be noted that there are large disturbances in the circular curve on the lower rail. These disturbances depend on how well the rail and wheel fits each other and/or presence of track irregularites. By reducing the friction to lower values, the traction force decreases, which in turn also supresses the small disturbances due to worn profiles and track irregularities.

It can also be noted that the FI values for the high rail, for the respective friction control values, are somewhat higher, and the reason for this may be flange hitting. The wheelset wants to travel straight, but the gauge on the high rail presses against the flange of the wheelset, which forces the wheelset to shift (creep) in the lateral direction, causing more creep forces. This flange hitting could be higher on sharp curves because of cant deficiency. Cant deficiency is the difference between the actual field cant and the theoretical cant required at a particular speed to compensate for the centrifugal forces. The cant values used in this study are the actual cant values present in the field, but the field cant values are generally lower than the theoretical value; here a compromise was made due to the occurrence of different traffic and speeds. The cant deficiency can be calculated using the following formula

$$h_d = \frac{2b_o}{g} \cdot \frac{v^2}{R} - h_t \tag{3}$$

where h_d is the cant deficiency (m), $2b_o$ is the track gauge (m), v is the velocity of train (m/s), R is the curve radius (m), h_t is the actual cant (m) and g is the gravitational acceleration.

For a 200 m curve, the cant deficiency is equal to 0.062 m.

Fatigue index value for various axle loads

It is always desirable to increase the axle load from a load capacity point of view, but in doing so the maintenance cost increases. By controlling the friction there is a possibility that the axle load can be increased without reducing the lifetime of the rails due to surface-initiated cracks. However, the actual economic efficiency and reduction in maintenance costs to be achieved through friction control are still unknown. In order to study the effect of friction control for a range of axle loads, simulations were performed for axle loads of 30 to 40 tonnes. It is not convenient to represent all the curves using different loads and different friction coefficients, and therefore the 95th percentile of all the FI values in the circular curve was used to represent the whole curve. In order to avoid RCF, the FI value should always be lower than zero. If the FI value becomes greater than zero due to irregularities or any other disturbances, a crack will occur. However, selecting the highest FI value as a representative value is not correct because that may result in $FI > 0$ for all cases. The maximum value depends on the length of the simulation and the longer a simulation is, the bigger is the risk that the wheel will pass a larger track irregularity. Therefore, the 95th percentile value was chosen instead of the maximum value, because the former is a stable value and independent of the length of the simulation. The 95th percentile means that 95% of the time, the FI value is at or below the 95th percentile value. Conversely, 5% of the FI values may exceed this value, but this 5% is ignored.

Figure 7(a) to (e) shows the 95th percentile for curve radii from 200 m to 3000 m and include all the friction coefficients with different Kalker's reduction factors shown in Figure 1 in the 'Friction values' section. Also included in Figure 7(a) to (e) are the individual values for both the high and the low rails. In each successive figure from Figure 7(a) to (e), the axle load is gradually increased by 2.5 tonnes up to 40 tonnes.

In Figure 7(a) to (e), it can be clearly seen that, on increasing the curve radius, the FI values decrease. This is because, when the curve radius is increased and the other parameters are kept constant, the traction forces decrease. From the load point of view, it can be seen that an axle load increment from 30 to 40 tonnes has a negligible effect on the FI value. The FI value depends on the contact pressure, which is the load divided by the contact area. The contact area between the rail and wheel increases with an increasing axle load. Therefore, the FI values are not linearly related to the axle load. This can also be confirmed by calculating the contact pressure according to the Hertz theory at different axle loads. It has been calculated that, on increasing the axle load by 33% (i.e. from 30 to 40 tonnes), the maximum contact pressure increases only by 9%. If we focus on the

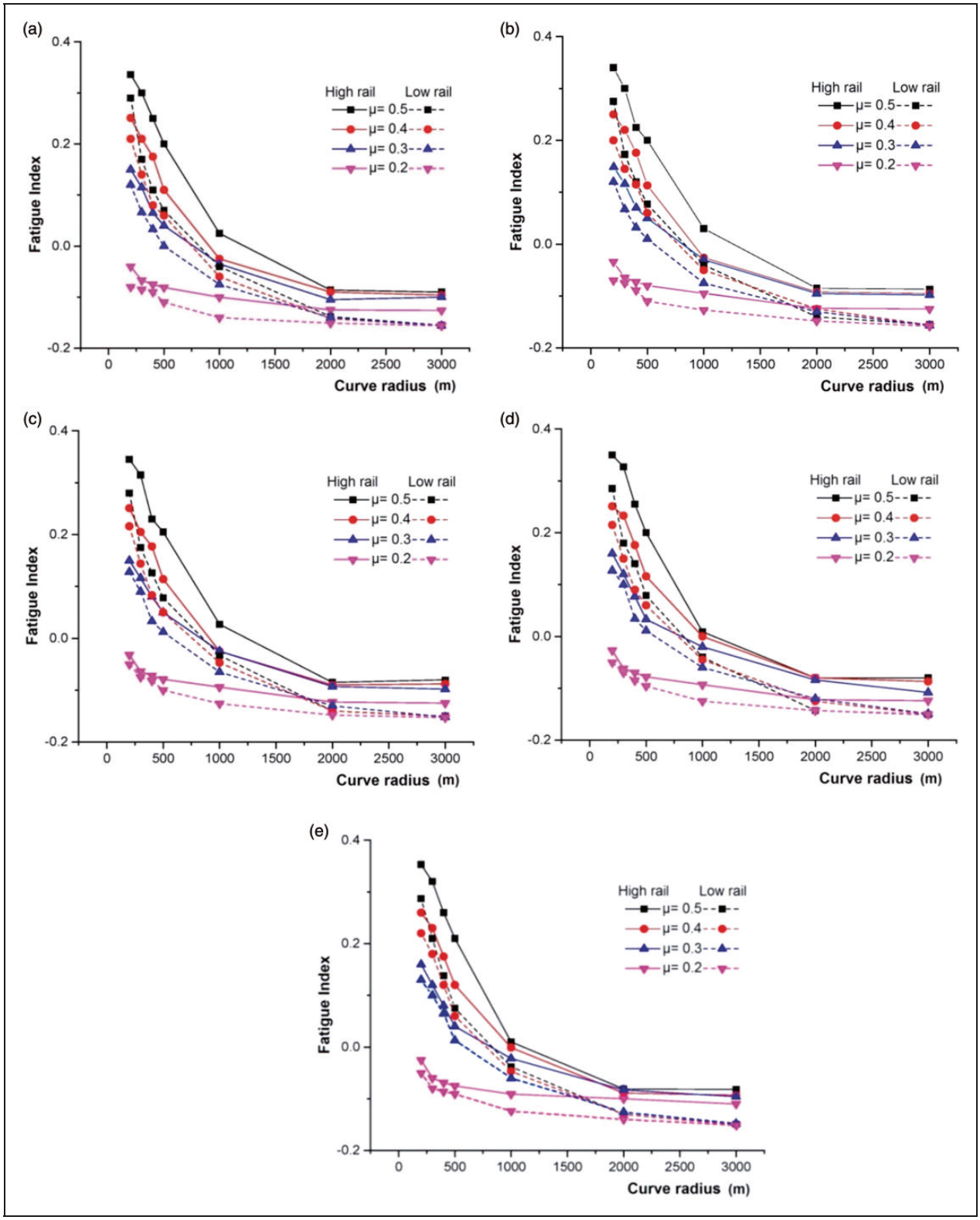

Figure 7. Fatigue index values (95th percentile) of all the curves from 200 m to 3000 m at various friction control levels, both for high and low rails: (a) 30 tonne axle load, (b) 32.5 tonne axle load, (c) 35 tonne axle load, (d) 37.5 tonne axle load, and (e) 40 tonne axle load.

FI values, the increments in the FI values due to load increments are quite small and it is quite difficult to see the difference in the various FI charts at different loads in Figure 7(a) to (e). The shape of the rail and wheel profile plays an important role concerning the FI sensitivity to a load change. If the rail and wheel fit each other well, the area of the contact point easily grows, as in this case, and the FI values are not sensitive to the axle load. However, there could be other cases where the rail and wheel do not fit each other so

well and the FI values could be more sensitive to the axle load. The effects of profile changes on the FI values are not covered in this paper.

Another aspect which can be observed is that, with an increasing curve radius, the difference in the FI values between the different friction control values decreases. The reason for this is that, with larger curve radii, the traction forces are generally lower and hence the reduction in the FI due to friction control is not significant. The difference in the FI values is small for curve radii $\geqslant 1000$ m. For curve radii of 2000 m and higher, the FI value almost stabilised and all the values are within the safe zone. Therefore, from an RCF point of view, friction control does not play any major role for curves with a radius larger than 1000 m. Friction control probably still plays an important role in reducing corrugation, hunting and squeal noise due to the stick-slip condition, but these areas of research are not within the scope of this study.

Conclusions

Based on the use of the FI method in this study to predict the effect of friction control on top-of-rail cracks, the following conclusions can be drawn.

1. By controlling the utilised friction, reducing the friction coefficient to 0.4 and using a reduction factor of 45%, for curve radii smaller than 1000 m, the probability of crack formation is decreased by at least 25%.
2. In the case of sharp curves ($R < 500$ m), by using a friction coefficient of 0.30 and a Kalker's reduction of 30%, the probability of crack generation is reduced by at least 50%, but there is still a probability of crack generation. Curves with a radius larger than 500 m are mostly in the safe zone for this friction control level.
3. The friction coefficient should be at most 0.2 to avoid crack generation in curves smaller than 500 m (and even in curves with a larger radius in some cases involving the high rail). However, this friction control level will probably result in too long a braking distance.
4. For higher curve radii (>1000 m), friction control does not have any major effect on crack formation but may still result in other benefits, such as a reduction in the fuel/power consumption, corrugation and hunting.
5. On increasing the axle load, no major changes in the FI value are observed. The FI value depends on the pressure and, on increasing the axle load, the contact pressure does not increase at the same rate. This implies that the curve radius has much more impact on the crack generation than the axle load. However, an increased load may have other negative effects on the maintenance cost.
6. It is possible that, on reducing the Kalker's reduction factor at $\mu = 0.3$, the working point may shift to the no-crack zone. This implies that the simulation results are highly dependent on the Kalker's reduction factor.

Acknowledgements

The authors would like to acknowledge gratefully the support rendered by Thomas Nordmark, Matthias Asplund and Matti Rantatalo at the Division of Operation and Maintenance of Luleå University of Technology for their assistance and expertise.

Declaration of Conflicting Interests

The author(s) declared no potential conflicts of interest with respect to the research, authorship, and/or publication of this article.

Funding

The author(s) disclosed receipt of the following financial support for the research, authorship, and/or publication of this article: This research was supported and funded by Luleå Railway Research Centre (JVTC) and Trafikverket (the infrastructure manager in Sweden).

References

1. European Commission. *White paper: Roadmap to a Single European Transport Area–Towards a competitive and resource efficient transport system*. Epubl ahead of print 2011. DOI: 10.2832/30955.
2. Stenstrom C, Parida A, Galar D, et al. Link and effect model for performance improvement of railway infrastructure. *Proc IMechE, Part F: J Rail Rapid Transit* 2013; 227: 392–402.
3. Andersson E, Berg M and Stichel S. *Rail vehicle dynamics course book*. Stockholm: KTH, 2014.
4. Bower AF and Johnson KL. Plastic flow and shakedown of the rail surface in repeated wheel-rail contact. *Wear* 1991; 144: 1–18.
5. Eadie DT, Vidler B, Hooper NE, et al. Top of rail friction control: Lateral force and rail wear reduction in a freight application. In: *Proceedings of international heavy haul association conference*, Dallas, TX, USA, 5–9 May 2003, pp.573–581, 7–35.
6. Eadie DT, Oldknow K, Maglalang L, et al. Implementation of wayside top of rail friction control on north american heavy haul freight railways. In: *Proceedings of the seventh world congress on railway research*, Montreal, Canada, 2006, pp.2–11.
7. Lu X, Makowsky TW, Eadie DT, et al. Friction management on a Chinese heavy haul coal line. *Proc IMechE, Part F: J Rail Rapid Transit* 2012; 226: 630–640.
8. Spiryagin M, Sajjad M, Nielsen D, et al. Research methodology for evaluation of top of rail friction management in Australian heavy haul networks. *Proc IMechE, Part F: J Rail Rapid Transit* 2014; 228: 631–641.
9. Hardwick C and Lewis R. The effects of alternative top of rail friction materials on pre existing rolling contact fatigue. In: *Proceedings of the second international*

conference on railway technology: Research, development and maintenance. Scotland: Civil-Comp Press, 2014.
10. Eadie DT, Elvidge D, Oldknow K, et al. The effects of top of rail friction modifier on wear and rolling contact fatigue: Full-scale rail-wheel test rig evaluation, analysis and modelling. *Wear* 2008; 265: 1222–1230.
11. Ekberg A, Kabo E and Andersson H. An engineering model for prediction of rolling contact fatigue of railway wheels. *Fatigue Fract Eng Mater Struct* 2002; 25: 899–909.
12. Dirks B and Enblom R. Prediction model for wheel profile wear and rolling contact fatigue. *Wear* 2011; 271: 210–217.
13. Olofsson U and Telliskivi T. Wear, plastic deformation and friction of two rail steels - A full-scale test and a laboratory study. *Wear* 2003; 254: 80–93.
14. VanderMarel J, Eadie DT, Oldknow KD, et al. A predictive model of energy savings from top of rail friction control. *Wear* 2013; 314: 155–161.
15. Gensyshttp://www.gensys.se (accessed 1 April 2016).
16. Kalker JJ. A fast algorithm for the simplified theory of rolling-contact. *Veh Syst Dyn* 1982; 11: 1–13.
17. Lu X, Cotter J and Eadie DT. Laboratory study of the tribological properties of friction modifier thin films for friction control at the wheel/rail interface. *Wear* 2005; 259: 1262–1269.
18. Lundberg J, Rantatalo M, Wanhainen C, et al. Measurements of friction coefficients between rails lubricated with a friction modifier and the wheels of an IORE locomotive during real working conditions. *Wear* 2014; 324–325: 109–117.
19. Johnson KL. *Contact mechanics*. Cambridge: Cambridge Press, 2003.
20. Suda Y, Iwasa T, Komine H, et al. Development of onboard friction control. *Wear* 2005; 258: 1109–1114.
21. Nia SH. *An investigation of the iron-ore wheel damages using vehicle dynamics simulation*. Sweden: KTH, 2014.
22. Voestelpine. Heat treated high performance rail 350 LHT, https://www.voestalpine.com/schienen/static/sites/c011/downloads/downloads/Guetenfolder_350LHT_HSHx_en.pdf (accessed 11 April 2016).
23. Dirks B. *Simulation and measurement of wheel on rail fatigue and wear*. Sweden: KTH, 2015.
24. Oldknow K, Eadie DT and Stock R. The influence of precipitation and friction control agents on forces at the wheel/rail interface in heavy haul railways. *Proc IMechE, Part F: J Rail Rapid Transit* 2012; 227: 86–93.
25. Gallardo-Hernandez EA and Lewis R. Twin disc assessment of wheel/rail adhesion. *Wear* 2008; 265: 1309–1316.

Paper 2: Prediction of top-of-rail friction control effects on rail RCF suppressed by wear

Khan, S. A., Persson, I., Lundberg, J. and Stenström, C. (2017) 'Prediction of top-of-rail friction control effects on rail RCF suppressed by wear', Wear, 380–381, pp. 106–114.

Wear 380-381 (2017) 106–114

Contents lists available at ScienceDirect

Wear

journal homepage: www.elsevier.com/locate/wear

Prediction of top-of-rail friction control effects on rail RCF suppressed by wear

Saad Ahmed Khan [a,*], Ingemar Persson [b], Jan Lundberg [a], Christer Stenström [a]

[a] Division of Operation and Maintenance, Luleå University of Technology, Sweden
[b] AB DEsolver, Östersund, Sweden

ARTICLE INFO

Article history:
Received 31 October 2016
Received in revised form
11 March 2017
Accepted 12 March 2017
Available online 14 March 2017

Keywords:
Multi-body simulation
Wear
Rolling contact fatigue
RCF
Energy dissipation
Rail Cracks

ABSTRACT

Rolling contact fatigue (RCF) and wear, two major deterioration processes, limit the lifetime of rails. These deterioration processes are even more severe on the curves of tracks used by heavy haul trains. Because wear is a material removing process, it can suppress the formation of RCF (also known as surface initiated cracks). In railways, cracks have a higher risk of instigating a catastrophic failure than wear; hence, it is comparatively better to have wear than to have cracks. By controlling the top-of-rail friction, both of these deteriorating processes can be reduced to enhance the lifetime of rails. In order to achieve these possible advantages, the infrastructure manager of the Swedish railway is planning to implement a top-of-rail friction control technology on the iron ore line in northern Sweden wherein RCF is a major problem on the curves. The present study uses a damage index model in a multi-body simulation software and predicts the probability of RCF formation with suppressing effect of wear for different friction control values. The effect of friction control is simulated on curve radii ranging from 200 to 3000 m and axle loads ranging from 30 to 40 t at a constant train speed of 60 km/h. Findings show that on a very sharp circular curve, radius < 300 m, RCF can be eliminated without friction control due to the high wear rate. On moderate curves, 300 < radius < 1000 m, a friction coefficient (μ) of, at most, 0.3 with a Kalker's coefficient of, at most, 30% is required to avoid RCF.

1. Introduction

Until 1987, rolling contact fatigue (RCF) was not perceived as a major problem in the railway sector [1]; however, today, it is universally acknowledged as critical, particularly for heavy axle load trains [1]. RCF decreases the lifetime of the rail, and to ignore RCF is to invite catastrophe. Once a crack is generated, little energy is required to propagate it; if the depth of the crack exceeds a particular limit, the rail must be changed. A high rate of wear can remove the surface that is about to crack and even eliminate newly generated micro-cracks, but excessive wear reduces track life, making it necessary to reduce both wear and RCF.

As a form of preventive maintenance, grinding (also known as artificial wear) is conducted at regular time intervals to remove cracks. It also assists in retaining a proper cross sectional rail shape and promoting better wheel–rail contact. When the loss of rail material, due to natural or artificial wear, reaches a particular limit, the rail has to be replaced. However, both grinding and rail replacement are expensive, not only in terms of maintenance cost, but also in terms of track access time and delays affecting timetables.

Blame for higher RCF may be attributed to high speed passenger and heavy haul railways [1]. However, the pressure and creep forces between the rails and wheels cause the actual damage [2]. These creep forces depend on several variables related to track geometry, third body between rail and wheel, train dynamics, wheel–rail profiles, etc., leading to wide variations in contact area size and position.

Properly the matched wheel profile curving ability (conicity) and curving requirement can considerably reduce creep forces [3]. Moreover, the degree of utilised friction significantly affects the creep forces and, hence, wear and RCF. To control the degree of utilised friction and reduce traction forces at a particular range, a product known as a friction modifier (FM) was developed and published in 2003 [4]. FM manufacturers claim that their products provide a fixed range of friction coefficient (μ) and Kalker's coefficient on top of the rail (running surface). Kalker's coefficient takes care of the basic tendency of creepage between the rail and wheel as a function of traction forces at lower creepage levels. For the detail of creepage, refer to reference [5] and for the implication of kalker's coefficient, refer to reference [6]. Field works [6–8] and lab tests [9,10] in the USA, Canada and China have determined the

* Corresponding author.
E-mail address: saad.ahmed.khan@ltu.se (S.A. Khan).

http://dx.doi.org/10.1016/j.wear.2017.03.010
0043-1648/

benefits of using friction-control products, including the reduction of RCF, wear, corrugation, noise and fuel consumption. In contrast, Lundberg et al. [11] found that such products give unacceptably low friction and can cause long braking distance and slippage if used in large amount.

Implementation of the top-of-rail friction control (TOR-FC) technology on the Swedish part of the iron ore line (IOL) is being considered by the Swedish Transport Administration (Trafikverket). The IOL is also known as Malmbanan, a Swedish translation of IOL. It was implemented in 1903 to transport mineral ores (mainly iron ores) from Kiruna and Malmberget to sea ports in Luleå (Sweden) and Narvik (Norway). The total track length from Narvik to Luleå is 473 km. The railway line is a single track, electrified line mainly utilised by the ore freight trains operated by LKAB. Freight trains from LKAB have an axle load of 30 t, which is the heaviest in Europe. At present LKAB is attempting to increase the axle load of the trains which transport ores and trains with 32.5 t axle load are under test [13]. This railway line is the northernmost railway in Sweden and it is experiencing the problem of RCF on its curves.

Directly implementing a TOR-FC system could be expensive, because reliability of such a system is never accessed for the conditions of IOL. Simulation is a smart alternative to expensive field tests to determine the effect of friction control. This study evaluates the utility of implementing the technology using computer based simulations. More specifically, the effects of using friction control on RCF of the IOL are studied by performing dynamic multi-body simulation (MBS). Such simulations are one of the possible tools to predict the effect of friction control on wheel–rail damage. They also have the ability to analyse the life cycle cost of the rail when a friction controller is used between the wheel–rail interfaces. The present study uses a method, which combines the wear and RCF prediction method, to predict the combine effects of RCF and wear. This method was developed and validated by Burstow [14,15]. These simulations are a part of an on-going four year project, which includes both field tests and simulations. In the project, these simulations are the initial theoretical studies that used already validated method and will be compared to the field tests in later stages.

2. Methods

The simulation software used in the present study is a MBS package from GENSYS [16]. It contains mass-spring-damper physical models and geometrical equations to represent different parts of a track and a train. The package used in the present study is updated with an IOL wagon model along with the measured IOL rail and wheel profiles. To generate outputs, the MBS models the wheel–rail contact mechanics based on the Hertzian theory, in combination with the simplified theory by Kalker called FASTSIM [17], as shown in Fig. 1. The outputs from the MBS, such as creep forces, creepage, and size of the contact area, etc., are used in the prediction model, as discussed in Section 2.1. The model used in the present study is based on a combined RCF and wear prediction method, which involves the trade-off between wear and RCF. The model only predicts the chance of RCF with the suppressing effect of wear in the form of an index.

The final index depends on pressure, creep force, and creepage, etc., which are sensitive to numerous factors, including wheel–rail profile, bogie suspension, track stiffness, stiffness and damping between ground, ballast bed and rails. Because the present work focuses on the effects of friction control on wear and RCF, all the parameters except friction control values and axle loads are kept constant for all simulations. To determine the effect of FM, variations in friction coefficient and Kalker's coefficient are sufficient.

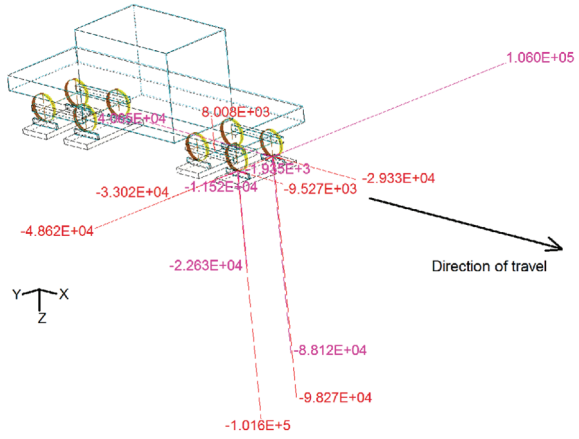

Fig. 1. Dynamic model of a wagon and a track section, showing the generated forces during a negotiation of a 200 m curve. Length of the bars represents the magnitude of the generated forces.

The influence of third body particles such as dust from the environment and different additive in the FM, e.g. anti-wear additive, is ignored. As discussed earlier, Trafikverket is planning to increase the axle load of the trains; therefore, the simulations are also performed using high axle loads. The speed of the train in the present simulations is fixed at 60 km/h, as loaded iron ore trains run at this speed and in the recent future there is no plan to change the train speed.

2.1. Damage index (DI) model

The theoretical basis of DI model is summarised as follows:

- Normal stresses and force are based on Hertzian contact theory.
- Shear stresses due to frictional forces are calculated by using Kalker's theory, Hertzian contact theory and disc-disc laboratory test.
- Wear calculations are based on energy dissipation and disc-disc laboratory tests.
- The probabilities of RCF generation are based on shakedown theory.

In general, it is well known that wear and RCF are two different processes. To obtain a realistic output, a combination of wear and RCF is required as excess wear can minimize or in some cases eliminate RCF. Burstow combines the shakedown and energy dissipation method to create a combined index method, as shown in Fig. 2. The shakedown limit, which is also sometimes known as a dynamic shakedown curve, represents the limit for generating RCF without considering the effect of wear. Energy dissipation, which is a product of creep force and creepage, is used to calculate

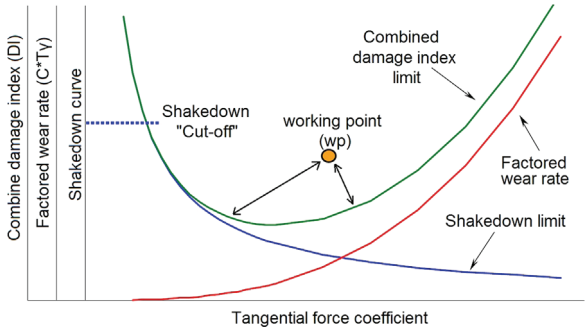

Fig. 2. Combined damage index limit based on Shakedown and factored wear rate. Adapted from [15].

the factored wear rate. Moreover, a combine damage index is the combination of the shakedown limit and factored wear rate.

As shown in Fig. 2, when the working point (WP) lies above the combine damage limit, RCF will exist, and the displacement of the WP from the border of the combined damage index limit defines the value of damage, which is called as damage index (DI) in the present work. The DI value can be calculated using the formula given in Eq. (1). The larger the value of DI, the higher is the probability of having a crack. If the WP lies below the combine DI limit, then the DI values will be negative and there will be no probability of RCF. In the case of no RCF, a low value of energy dissipation indicates that the pressure is not sufficient to generate any crack; however, a high value of energy generation indicates that wear dominated the formation of RCF [18].

$$DI = FI - C(T\gamma) \tag{1}$$

where FI represents the fatigue index method [20,21], which is based on shakedown theory [21] and $C(T\gamma)$ represent the factored wear rate based on the energy dissipation.

According to the FI method, the occurrence of RCF depends upon the contact pressure, the creep forces in the contact area and the material yield stress in shear. If the external stresses exceed the threshold value, which is known as the shakedown limit, the RCF will occur due to accumulated plastic strain. The FI index can be calculated as follows: [19]

$$FI = \frac{\sqrt{F_{nx}^2 + F_{ny}^2}}{F_n} - \frac{k}{p_o} \tag{2}$$

where P_o [N/m^2] is the contact pressure, K [N/m^2] is the shear strength of the material, F_{nx} and F_{ny} [N] are the longitudinal and lateral creep force tangential to the contact surface, respectively, and F_n [N] is the normal force at the contact point.

Wear rate is a function of energy dissipation $(T\gamma)$. Laboratory experiments and dynamic simulations have yielded relationships between wear rates and energy dissipation, which depends on the properties of the material. Energy dissipation is the sum of the individual products of local creep forces T and local creepage γ, which can be calculated by the given formula [22]

$$T\gamma = T_x\gamma_x + T_y\gamma_y \tag{3}$$

As wear rate is a function of energy dissipation, a factor C is required so that wear and RCF can be combined together. In the present study, this constant is calculated using the DI graph developed by Evans et al. [23], see Fig. 3. The material used by Evans is 350 grade steel, which has similar properties as the steel used in the IOL. In the present simulation, the value of C before $T\gamma = 135$ is considered as zero. As in this zone, the wear is mild to medium, which is not sufficient to suppress the probability of RCF generation, it can therefore be ignored. According to the Evans diagram (Fig. 3), after $T\gamma = 135$, wear starts reducing the RCF generation and the line has a constant slope. By using Fig. 3, the value of C can be calculated by keeping DI=0 at $T\gamma = 400$ in Eq. (1).

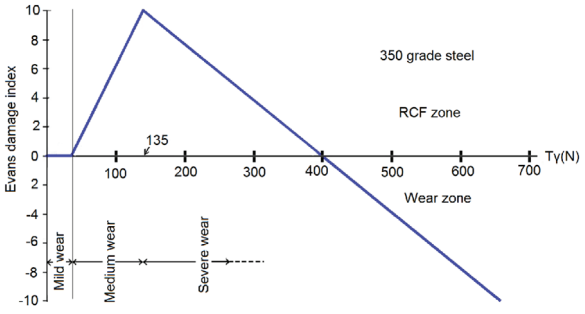

Fig. 3. Relationship of Evans DI to energy dissipation (Tγ) for 350 grade rail steel. Adapted from Evans et al. [23].

A limitation of this model is that it does not take spin creepage into account, which can be up to 6–7% [24] of the total creepage. As lateral and longitudinal creepages cover at least 93% of the total creepage, the spin creepage will not make any major difference in the final DI values. It should also be considered that the DI model has an empirical nature; it needs calibration for each material and third body interface [22]. Such indices are generated by performing a laboratory test or a dynamic simulation, which lack realistic environment and third body interfaces. Moreover, laboratory tests have a problem of scale.

2.2. Assumptions for FM

According to the manufacturers, an FM assists in controlling friction coefficients at 0.35 ± 0.05 between the wheel–rail interface [25]. However, Lundberg et al. [11] have shown that when a FM is used, the friction coefficient can be as low as 0.2. In contrast, Spiryagin et al. [26] have reported that some FM can have a friction coefficient of up to 0.4. It is obvious that friction control is highly dependent on FM composition, amount of application and ambient condition.

Another important factor to consider is Kalker's coefficient. The wheel–rail (steel–steel) friction coefficient can be as high as 0.65 [27]. However, practically, in dry conditions, the rail surfaces always have some deposits from the environment and trains (e.g. moisture, leaves and deposits from trains). These deposits act as a third body (lubricants) and decrease the shear forces between the rail and wheel and hence reduces the friction coefficient and the degree of utilised friction, i.e. degree of slip in rolling contact. To take care of this degree of reduction, a reduction coefficient is required. This reduction coefficient is known as Kalker's coefficient, which is generally derived by performing disc–disc lab tests. In case of a full slip, this coefficient is 100%; however, in practical, rail wheel contact is rarely full slip. In the case of non-lubricated rail conditions caused by surface deposits, a friction coefficient of 0.5 and Kalker's coefficient 60% is considered [2]. In the case of a FM, Kalker's coefficient is even lower. For the lowest friction coefficient used here, 0.2, a Kalker's coefficient of 15% is considered [28]. Kalker's coefficient for the intermediate friction coefficients of 0.4 and 0.3 are unknown. However, these values can be interpolated using the highest and lowest values. The present study assumes intermediate Kalker's coefficient values of 45% and 30% for friction coefficient of 0.4 and 0.3, respectively. These interpolated values cover the gap between the maximum and minimum values, so a proper trend can be studied. It should be noted that change in applied load can vary both friction and kalker's coefficients. The present study has used coefficients derived using laboratory tests under single load and the present study cover a range of loads. To cover the variation in coefficients due to change in loads, a range of coefficients is used, which covers the lowest and highest practical values.

When a train is negotiating a curve, most of the forces (especially lateral forces) are distributed on the top of the low rail and on the gauge corner and gauge face of the high rail. In the present study, it is assumed that FM also reaches on the gauge corner and gauge face. As experienced in the field, when an FM modifier is applied using wayside equipment on the top of the rail, it eventually reaches the gauge face due to gravity. Therefore, in the present simulation, friction is controlled both on the top of the rail and the gauge face and it is same all over the high and low rails.

2.3. Vehicle and track design

The wagon implemented in the simulation has four axles

Table 1
Weight distribution of different parts of the wagons.

Parts	Number of unit	Weight (kg)
Car body	1	12536
Bolster beam	2	1050
Side frame	4	400
Axle	4	1341

divided into two individual three-piece bogies, which has become very popular because they are cheap and have a simple design. These bogies have a primary suspension between an axle and a side frame and a secondary suspension between side frames and a bolster beam. The primary suspension is relatively soft to promote good radial self-steering capabilities on curves; this causes a small angle of attack and thus, creates smaller creep forces. Such an arrangement maintains good running performance on curves, but limits the highest possible speed on tangent tracks because of hunting oscillation [29]. The weight distribution of the individual part considered as rigid bodies is given in Table 1.

In the present simulation, the variations in the track stiffness level due to seasonal change are not considered. For further details on the vehicle and track model used here, refer to Nia et al. [29].

2.4. Wheel–rail profiles

Wheel–rail profiles are very important to regulate both wear and RCF, since the adjustment between the rail and wheel profiles affects the contact area, which in turn affects creep forces. The profiles used in the present study are worn profiles from the Swedish part of the IOL. Profiles remain new for a short period of time compared to the entire lifetime of the rail and wheel; hence, worn profiles are more realistic. The base wheel profile for both high and low wheels is WP4, which is constant throughout the simulation, and the base rail profile is UIC 60E1. After the first grinding, the high rail profile changes to MB1; however, the low rail profile remains 60E1. Rail profiles were subjected to grinding 8 months before measurement. The profiles were measured using a laser based Calipiri device from NEXTSENSE GmbH. The measured profiles, as shown in Fig. 4, are used as input for the simulation.

As reflected in Fig. 4, both the high and low rail profiles have an inclination of 1/30, a standard inclination in Sweden. These wheel–rail profiles are special profiles, with generally two or more contact points between the rail and wheel. These contact points depend on the facets generated by the grinding of rail and wheel. The standard steel grade used for the IOL is 350LHT rail steel.

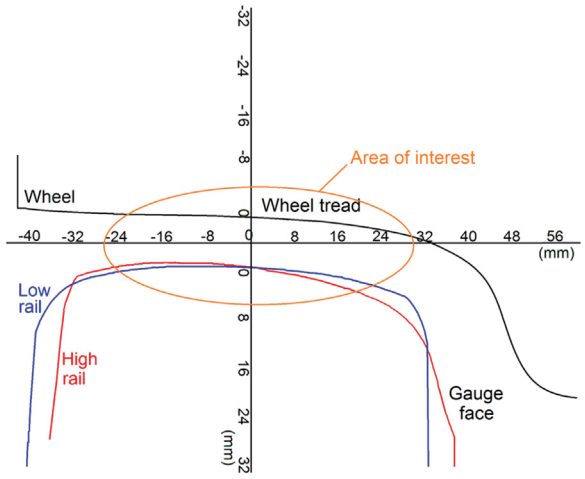

Fig. 4. Worn profiles of wheels and rail (both high and low) used in the simulations [20].

Table 2
Cant values used in the simulation for the respective curve radii.

Curve radius (m)	Cant (m)
200	0.15
300	0.15
400	0.10
500	0.10
1000	0.05
2000	0.00
3000	0.00

2.5. Curve details

The curve radius in the simulation varies from 200 to 3000 m and the cant (super elevation) values are from 15 to 0 cm, which represent the sharpest to the largest curve, respectively. The cant values used in the simulations are the intermediate cant for heavy haul and passenger railway traffic; for exact cant values, see Table 2. The speed of the train is fixed at 60 km/h, which is the speed of IOL trains. At a speed of 60 km/h, the traction force on a 3000 m curve and a tangent track are equivalent; thus, 3000 m curve radius is considered as a tangent track in this study.

As shown in Fig. 5, all the curves used in the simulation turn towards the right when facing in the direction of travel and the total length of the track is 750 m. The left rail represents a high rail and the right rail represents a low rail. The length of the track is decided by taking an average length of the curves present in the field. It is not possible to directly combine a tangent track and a circular curve with cant; therefore, a transition curve is added to give a smooth transition between the tangent track and the circular curve. These transition curves can be parabolic or linear. In the present simulation, only linear transition curves are used, as in practice, the advantages of parabolic curves are very small [2].

3. Results and discussion

Creep forces are often higher at the leading axle of the leading bogie than at the trailing axle; thus, the leading axle is more prone to damage [30]. Therefore, the results discussed are from the leading axle only.

Initially, all the simulations were executed using track irregularities. A raw example of low and high rail at a 200 m curve radius and non TOR-FC condition is shown in Fig. 6. The figure shows disturbances due to irregularities, which can make the figure unreadable when curves of various friction coefficients are presented together. Therefore, results in the following sections are presented after removing disturbances. To remove these disturbances, all the simulations were rerun after removing irregularities, i.e. by using ideal track without irregularities.

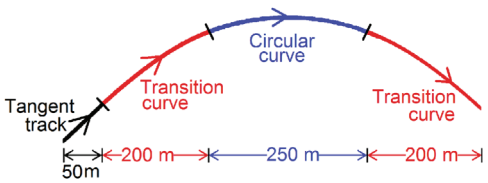

Fig. 5. Length of the various zones of the curve used in simulation.

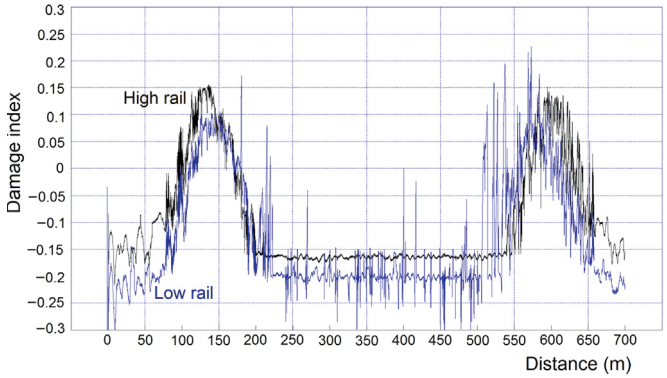

Fig. 6. A raw example, with disturbances, of a high and low rail at a friction coefficient of 0.5 and Kalker's curve coefficient of 60%.

3.1. DI chart for a 200 m curve

Initially, simulation is conducted for the sharpest curve of a 200 m radius and an axle load of 30 t. Fig. 6(a) and (b) represent the high and low rail, respectively. The y-axis represents the DI values, and the x-axis represents the position of the wheel starting from zero distance. The DI model includes the suppressing effect of wear on RCF, as reflected in the middle part of the curve, i.e. the circular curve.

From 0 to 50 m, the tangent part of the track is in the negative zone, indicating only little wear and no RCF, since in this part of the track, forces are very low. After 50 m, as the transition curve starts, the DI values start to increase, whereas the curve radius decreases gradually. With a decrease in curve radius, the creep forces increase and hence increases the DI. Initially, with the increase in the distance on the track, the probability of RCF increases, as wear rate is in this region is negligible to supress RCF. However, after the middle of the transition curve, the DI values start to decrease. After passing DI=0, the effect of wear due to high energy dissipation dominates over RCF. The excess rate of wear eliminates the probability of cracks generation, i.e. the material that is about to crack is worn-off.

On reaching the circular curve, the DI values stabilise, as the forces are quasi-static. As can be noted from Fig. 7(a) and (b), the DI values for all the friction values in the circular curve are in the safe zone, i.e. no RCF zone. This indicates that energy dissipation in the circular curve is higher than 400 N, and excessive wear eliminates the RCF formation, as shown in Fig. 3.

If we compare the DI values at the circular curves, i.e. middle of the track, the difference between the highest and the lowest friction control is not large; however, there is a significant difference in the transition curves wherein the DI values reach the positive zone, i.e. RCF zone, because wear rate is not sufficient.

According to Fig. 7(a) and (b), for the entire curve to be in the safe zone, the friction control should be at most $\mu=0.3$, with Kalker's coefficient of at most 30%, for both the high and low rails.

3.2. DI value for various axle loads and curve radii

This section presents the DI values for different curve radii and for axle loads ranging from 30 to 40 t. The high and low rails are presented in the same graph by continuous and dashed lines, respectively (see Figs. 8 and 9). As seen in Fig. 7(a) and (b), there is a difference in the DI values of the circular and transition curve; therefore, the DI graphs showing the different curve radii are divided into circular and transition curves. It is not convenient to show a DI graph for a complete circular or tangential curve at different load levels and curve radii. Therefore, a 95th percentile is used to represent the complete circular or tangential curve. 95th

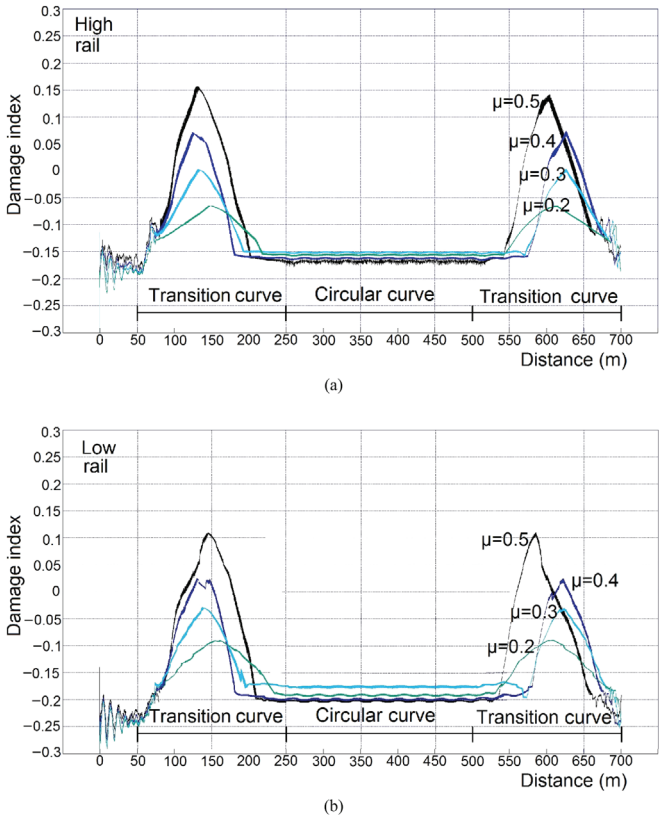

Fig. 7. DI for 200 m curve radius, 30 t axle load at different friction values with respect to distance on the curve: (a) high rail; (b) low rail. * Note: increasing the friction does not mean that the wear is reduced. It only means that the probability of crack generation will increase more than the increase of wear.

percentile of the DI value means, 95% of the time, the DI value is at or below the 95th percentile value. Conversely, 5% of the DI values may exceed this value, but are ignored.

To sum up, firstly, the 95th percentile value of the complete circular or tangential curve is calculated as a representative value. Then, the representative DI values of either an entire circular curve (Section 3.2.1) or a transition curve (Section 3.2.2) are plotted on the y-axis as a data point with respect to different curve radii on the x-axis. One plot contains all the friction values and curve radii for both high and low rail. The procedure is then repeated for all axle loads ranging from 30 to 40 t.

3.2.1. DI value for circular curves

Fig. 8(a) to (e) represent the DI values in circular curves with different curve radii, axle loads and friction control values. Herein, the y-axis represents the 95th percentile of the DI value of the circular curve and the x-axis represents the curve radius. For the sharpest curve of a 200 m radius, the DI value is negative for all friction coefficients. The DI values initially increases with the increase in curve radius. As the wear rate in sharps curves is high, the probability of RCF is eliminated. The wear rate gradually decreases with increase in curve radius. When the curve radius reaches 400 m, the wear rate is already insufficient to supress the formation of RCF. With increasing curve radius, the creep forces decrease, which decreases the energy dissipation and hence both wear and the probability of RCF. However, for curves from 300 to 1000 m radius, creep force (and hence the wear) is insufficient to supress RCF formation. From all the DI figures showing the various loads, it can be concluded that the curves with radius from 300 to 1000 m, which can be classified as a moderate curve, are more prone to RCF when there is no friction control. As seen in Fig. 8, for

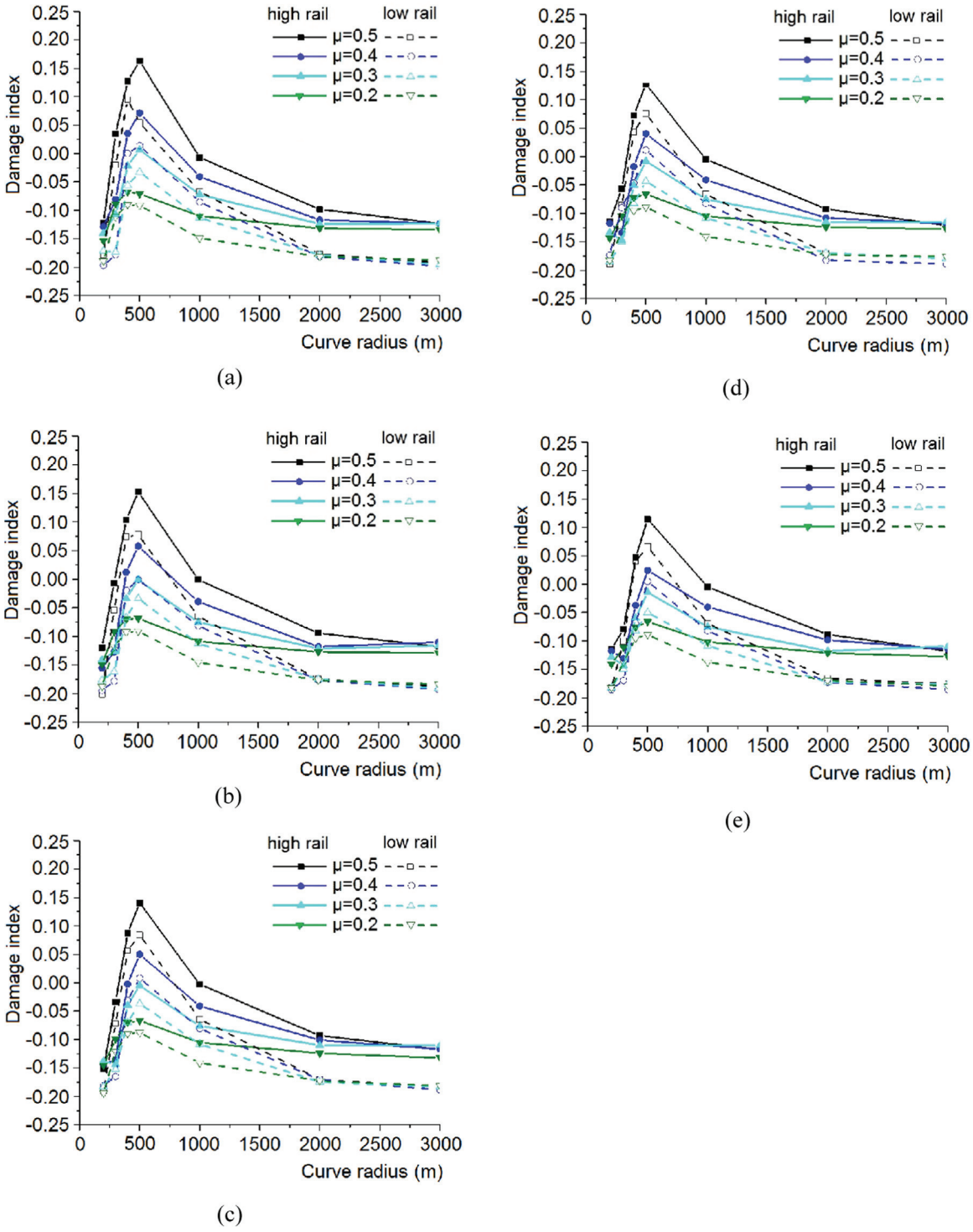

Fig. 8. DI values (95th percentile) of circular curve from 200 to 3000 m at various levels of friction control for both high and low rails: (a) 30 t axle load; (b) 32.5 t axle load; (c) 35 t axle load; (d) 37.5 t axle load; (e) 40 t axle load.

moderate curves, on controlling the friction at $\mu=0.4$ with corresponding Kalker's coefficient of 45%, the probability of RCF is decreased, but inadequate to eliminate RCF formation. At the given friction values, the DI values approach zero, i.e. the energy dissipation is reduced, but it is not low enough to avoid RCF. At the friction control value of $\mu=0.3$ or lower and a Kalker's coefficient of 30% or lower, the DI values are in the no RCF zone for both high and low rails for all the curve radii. According to the diagram, it can be said that the friction value of 0.3 or lower with Kalker's coefficient of 30% or lower is required to avoid RCF on circular curves with a radius ranging from 300 to 1000 m.

On comparing the different axle loads, the graphs show that when the axle load is increased from 30 to 40 t, there is no significant change in the DI values. Since, according to used Hertzian contact theory with the increase in the axle load, the contact area between the rail and wheel also increases; therefore, the DI is not directly proportional to the load increment.

On close observation, it can be noted that the DI values slightly decrease in the case of curves with radius less than 1000 m when the axle load is increased. With an increase in the axle load, the

energy dissipation increases, which results in increased wear rate; however, the probability of RCF does not increase with the same rate. All the graphs from 7(a) to (e) follow the same trend, with a slight shift towards the wear zone because of increased energy dissipation.

It should be noted that the DI method only tells about the competition between the wear and RCF and both of them are deteriorating processes. Negative DI values indicate no RCF, but it can have a very high wear rate, which limits the lifetime of the rail. However, this natural wear can delay, or may be eliminate in some cases, the expensive and time consuming grinding process.

3.2.2. *DI value for transition zone*

As shown in Fig. 9(a) to (e), the DI values of the transition curve

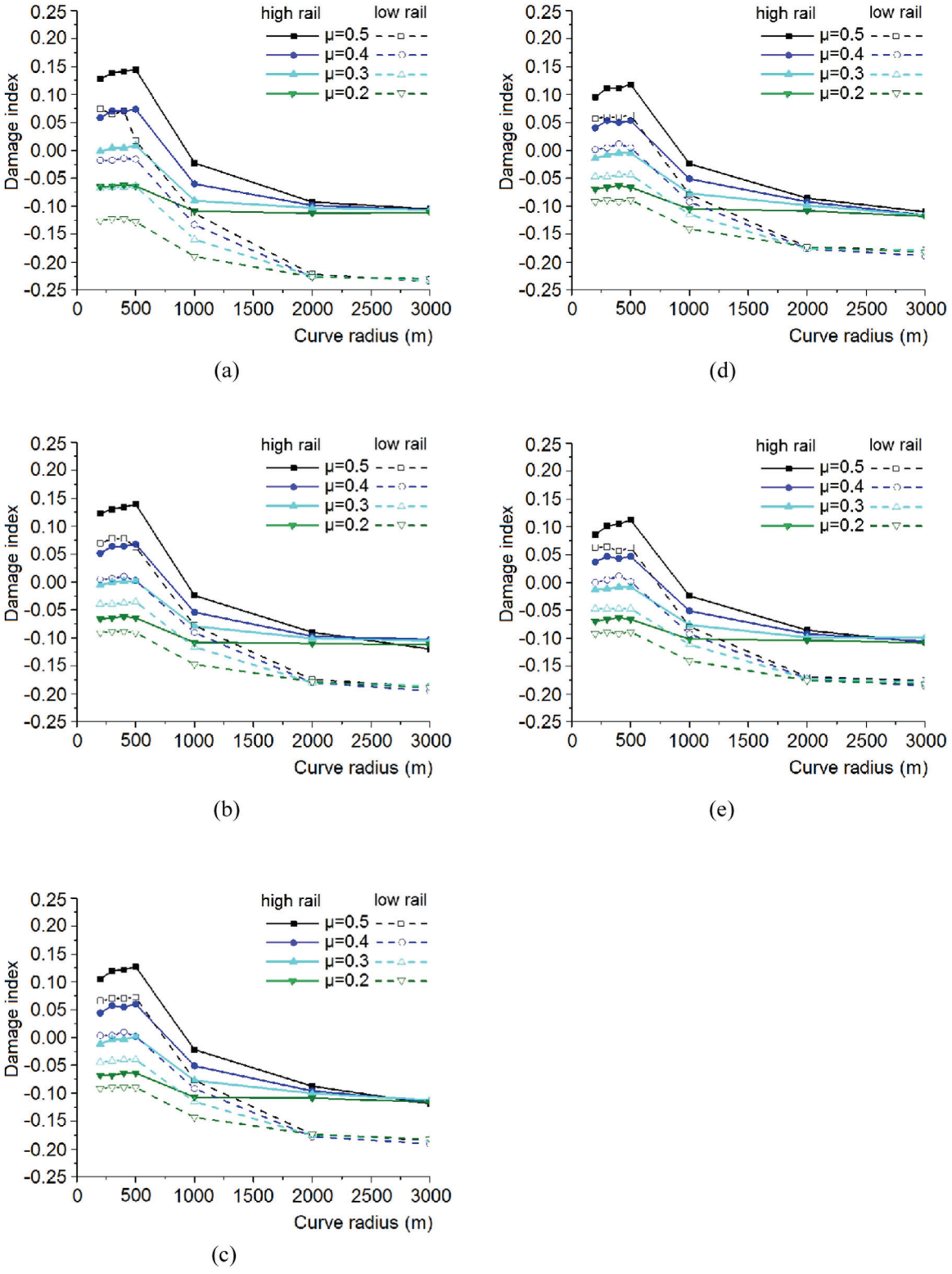

Fig. 9. DI values (95th percentile) of transition curve from 200 to 3000 m at various levels of friction control, for both high and low rails: (a) 30 t axle load; (b) 32.5 t axle load; (c) 35 t axle load; (d) 37.5 t axle load; (e) 40 t axle load.

Table 3
Chance of getting RCF (in a yes or no) for different curve radii and friction values. The values are similar for all axle loads ranging from 30 to 40 t.

	Zones	μ	Wear	RCF
Very sharp curves R < 300 m	**Circular**	0.5	Severe	No
		0.4	Severe	No
		≤0.3	Severe	No
	Transition	0.5	Mild to severe	Yes
		0.4	Mild to severe	Yes
		≤0.3	Mild	No
Medium curves 300 < R < 1000 m	**Circular**	0.5	Mild to severe	Yes
		0.4	Mild to severe	Yes
		≤0.3	Mild	No
	Transition	0.5	Mild to severe	Yes
		0.4	Mild	Yes
		≤0.3	Mild	No
Large curves R > 1000 m	**Circular**	0.5	Mild	No
		0.4	Mild	No
		≤0.3	Mild	No
	Transition	0.5	Mild	No
		0.4	Mild	No
		≤0.3	Mild	No

are discussed separately in this section. Herein, the y-axis represents the 95th percentile of the DI values of the transition curve and the x-axis represents the respective curve radius. As discussed earlier, a transition curve connects a tangent and a circular track and its radius changes linearly from a tangent track to its respective circular curve radius. The average tangential force coefficient in the case of a transition curve is lower than that of a circular curve. As in a transition curve, the radius starts from infinite and decreases linearly to reach the value of circular radius.

For the sharpest curve with a 200 m radius, the DI values in the transition curve are higher than those in the circular curve. Due to the larger radius compared to the circular curve, herein, the wear rate is not sufficient to eliminate RCF on a complete transition curve. Therefore, for a very sharp curve, there will be RCF only on the transition curve. As in the circular sharp curve, wear rate is high enough to eliminate RCF. Such a trend of having more RCF on a transition curve is also seen by the IOL track specialist at Trafikverket on some sharp curves in the field. From Fig. 9(a) and (e), it can be observed that for curves sharper than 1000 m curve radius, a friction coefficient of at most 0.3 and a Kalker's coefficient of at most 30% is required.

In addition, when the axle load is increased on sharp and moderate curves, DI values shift downwards and DI values in graphs approach the no RCF. In other words, with the increase in axle load, the probability of RCF decreases due to increase in wear rate. However, for larger curves wherein DI values are negative, when the axle load is increased, the DI values shift towards zero, i.e. RCF zone. For a larger curve, the creepage, hence the wear, is negligible and an increase in axle load has more impact on the RCF.

For a curve radius of 1000 m and above, friction control does not play a major role in controlling the formation of RCF. It may have a positive effect on problems such as corrugation, noise and fuel consumption, but these issues are not covered in the present study.

Table 3 gives an overview of the results for all friction and curve radii.

4. Conclusion

The findings of the DI method using a MBS and considering the IOL at a train speed of 60 km/h are as follows:

1. For very sharp curve radii, i.e. 300 m or less, there will be no RCF (30 t is exception) in the circular curve even without friction control as wear dominates RCF. But the transition curve will have RCF, if no FM is applied.
2. Moderately sharp curves, i.e. 300 to 1000 m, will have RCF along the circular and transition curves if there is no friction control.
3. Large curves, i.e. 1000 m or higher, do not experience RCF and friction control has no major role from RCF point of view.
4. For curve less than 1000 m, at the friction coefficient of 0.4 and Kalker's coefficient of 45%, the probability of RCF is reduced considerably, but does not reach zero.
5. For curves less than 1000 m, a friction coefficient of $\mu = 0.3$ or lower with a Kalker's coefficient of 30% or lower is required to avoid RCF on a complete curve.
6. The DI values are not sensitive to the axle load, i.e. increase in axle load will not have any significant effect on the RCF.

5. Future work

More research is required to determine the exact characteristics of friction control in a realistic environment such as snow, rain, dirt, and lubricant from trains. Other issues requiring investigation include the exact friction value and Kalker's coefficient for a top-of-rail friction modifier. Moreover, the effect of different axle load on ballast and clips should be considered.

Acknowledgement

This research was supported and funded by the Luleå Railway Research Centre (JVTC) and the Trafikverket (Swedish Transport Administration). The authors gratefully acknowledge the support of Thomas Nordmark, Matthias Asplund and Matti Rantatalo at the Division of Operation and Maintenance of Luleå University of Technology.

References

[1] D.F. Cannon, H. Pradier, Rail rolling contact fatigue research by the European Rail Research Institute, Wear 191 (1996) 1–13, http://dx.doi.org/10.1016/0043-1648(95)06650-0.
[2] E. Andersson, M. Berg, S. Stichel, Rail Vehicle Dynamics Course book, KTH, Stockholm, 2014.
[3] E.E. Magel, Rolling Contact Fatigue: A Comprehensive Review, Washington DC, USA. 2011 http://www.fra.dot.gov/Page/P0001.
[4] D.T. Eadie, B. Vidler, N.E. Hooper, P. Eng, T.W. Makowsky, Top of rail friction control: lateral force and rail wear reduction in a freight application, Proc. Int. Heavy Haul Assoc. (2003) 7–35.
[5] J.J. Kalker, Survey of wheel rail rolling contact theory, Veh. Syst. Dyn. 8 (1979) 317–358, http://dx.doi.org/10.1080/00423117908968610.
[6] J. VanderMarel, D.T. Eadie, K.D. Oldknow, S. Iwnicki, A predictive model of energy savings from top of rail friction control, Wear 314 (2013) 155–161, http://dx.doi.org/10.1016/j.wear.2013.11.037.
[7] D.T. Eadie, M. Santoro, K. Oldknow, Y. Oka, Field studies of the effect of friction modifiers on short pitch corrugation generation in curves, Wear 265 (2008) 1212–1221, http://dx.doi.org/10.1016/j.wear.2008.02.028.
[8] X. Lu, T.W. Makowsky, D.T. Eadie, K. Oldknow, J. Xue, J. Jia, G. Li, X. Meng, Y. Xu,

Y. Zhou, Friction management on a Chinese heavy haul coal line, Proc. Inst. Mech. Eng. Part F J. Rail Rapid Transit 226 (2012) 630–640, http://dx.doi.org/10.1177/0954409712447170.
[9] D.T. Eadie, D. Elvidge, K. Oldknow, R. Stock, P. Pointner, J. Kalousek, P. Klauser, The effects of top of rail friction modifier on wear and rolling contact fatigue: full-scale rail-wheel test rig evaluation, analysis and modelling, Wear 265 (2008) 1222–1230, http://dx.doi.org/10.1016/j.wear.2008.02.029.
[10] C. Hardwick, R. Lewis, The effects of Alternative Top of Rail friction materials on Pre existing Rolling contact fatigue-paper181.pdf, in: Proceedings of the Second International Conference Railw. Technol. Res. Dev. Maint., Civil-Comp Press, Scotland, 2014.
[11] J. Lundberg, M. Rantatalo, C. Wanhainen, J. Casselgren, Measurements of friction coefficients between rails lubricated with a friction modifier and the wheels of an IORE locomotive during real working conditions, Wear 324–325 (2014) 109–117, http://dx.doi.org/10.1016/j.wear.2014.12.002.
[13] Heavier Ore Trains for Increased Capacity, (n.d.). ⟨http://www.lkab.com/sv/Press/Koncernnyheter/?Ni=8252⟩ (Accessed 28 October 2016).
[14] M.C. Burstow, Whole Life Model Application and Development for RSSB – Continued Development of an RCF Damage Parameter, Derby, UK, 2004.
[15] M.C. Burstow, Whole Life Rail Model Application and Development: Development of a Rolling Contact Fatigue Damage Parameter, 2003, pp. 2–3.
[16] Gensys, (n.d.). ⟨http://www.gensys.se⟩ (Accessed 1 October 2016).
[17] J.J. Kalker, A. Fast, Algorithm for the simplified theory of rolling-contact, Veh. Syst. Dyn. 11 (1982) 1–13, http://dx.doi.org/10.1080/00423118208968684.
[18] A.E. Beagles, M. Beagles, M.C. Burstow, J.R. Evans, A. Kapoor, A.S. Watson, Whole Life Rail Model: Six Month Report, T115 Repor, 2003. ⟨http://www.rssb.co.uk/SiteCollectionDocuments/pdf/reports/Research/T115_rpt2_final.pdf⟩.
[19] A. Ekberg, E. Kabo, H. Andersson, An engineering model for prediction of rolling contact fatigue of railway wheels, Fatigue Fract. Eng. Mater. Struct. 25 (2002) 899–909, http://dx.doi.org/10.1046/j.1460-2695.2002.00535.x.
[20] S.A. Khan, I. Persson, J. Lundberg, C. Stenstro m, Prediction of the effects of friction control on top-of-rail cracks, in: Proceedings Inst. Mech. Eng. Part F J. Rail Rapid Transit, vol. 0, 2016, pp. 01–11. doi: ⟨http://doi.org/10.1177/0954409716674984⟩.
[21] A.F. Bower, K.L. Johnson, Plastic flow and shakedown of the rail surface in repeated wheel-rail contact, Wear 144 (1991) 1–18, http://dx.doi.org/10.1016/0043-1648(91)90003-D.
[22] B. Dirks, Simulation and Measurement of Wheel on Rail Fatigue and Wear, KTH, Sweden, 2015.
[23] J.R. Evans, T.K.Y. Lee, C.C. Hon, Optimising the wheel/rail interface on a modern urban rail system, Veh. Syst. Dyn. 46 (2008) 119–127, http://dx.doi.org/10.1080/00423110701882355.
[24] G.I. Alarcón, N. Burgelman, J.M. Meza, A. Toro, Z. Li, The Influence of Rail Lubrication on Energy Dissipation in the Wheel/rail Contact: A Comparison of Simulation Results with Field Measurements, 2015, pp. 1–16. doi: ⟨http://doi.org/10.1016/j.wear.2015.01.008⟩.
[25] LB Foster Rail Technologies, (n.d.). ⟨http://www.lbfoster-railtechnologies.com/Friction_Modifiers.asp⟩ (Accessed 1 October 2016).
[26] M. Spiryagin, M. Sajjad, D. Nielsen, Y.Q. Sun, D. Raman, G. Chattopadhyay, Research methodology for evaluation of top-of-rail friction management in Australian heavy haul networks, J. Rail Rapid Transit. 228 (2013) 631–641, http://dx.doi.org/10.1177/0954409714539943.
[27] U. Olofsson, K. Sundvall, Influence of Leaf, Humidity and Applied Lubrication on Friction in the Wheel – Rail Contact : Pin-on-disc Experiments, vol. 218, 2016, pp. 235–242.
[28] Y. Suda, T. Iwasa, H. Komine, M. Tomeoka, H. Nakazawa, K. Matsumoto, T. Nakai, M. Tanimoto, Y. Kishimoto, Development of onboard friction control, Wear 258 (2005) 1109–1114, http://dx.doi.org/10.1016/j.wear.2004.03.059.
[29] S.H. Nia, P.A. Jonsson, S. Stichel, Wheel damage on the Swedish iron ore line investigated via multibody simulation, in: Proceedings Inst. Mech. Eng. Part F J. Rail Rapid Transit, vol. 228, 2014, pp. 652–662. doi: ⟨http://doi.org/10.1177/0954409714523264⟩.
[30] M. Ishida, T. Moto, M. Takikawa, The effect of lateral creepage force on rail corrugation on low rail at sharp curves, Wear 253 (2002) 172–177, http://dx.doi.org/10.1016/S0043-1648(02)00096-0.

Paper 3: Carry distance of top-of-rail friction modifiers

Khan, S. A., Lundberg, J. and Stenström, C. (2018) 'Carry distance of top-of-rail friction modifiers', Proceedings of the Institution of Mechanical Engineers, Part F: Journal of Rail and Rapid Transit, 232(10), pp. 2418–2430.

Original Article

Institution of MECHANICAL ENGINEERS

Journal of RAIL AND RAPID TRANSIT

Proc IMechE Part F:
J Rail and Rapid Transit
2018, Vol. 232(10) 2418–2430

DOI: 10.1177/0954409718772981
journals.sagepub.com/home/pif

SAGE

Carry distance of top-of-rail friction modifiers

Saad Ahmed Khan, Jan Lundberg and Christer Stenström

Abstract

Rail issues such as corrugation, rolling contact fatigue, noise and wear have been increasing with the increase in railway traffic. The application of top-of-rail friction modifiers (TOR-FMs) is claimed by their manufacturers in the railway industry to be a well-established technique for resolving the above-mentioned issues. There are various methods for applying friction modifiers at the wheel–rail interface, among which stationary wayside systems are recommended by TOR-FM manufacturers when a distance of a few kilometres is to be covered. TOR-FM manufacturers also claim that by using wayside equipment, the TOR-FM can be spread over a minimum distance of 3 km, over which it maintains a coefficient of friction of $\mu = 0.35 \pm 0.05$. To determine the carry distance of TOR-FMs, some researchers use tribometers to measure the coefficients of friction. However, moisture and deposits from the environment and trains can alter the top-of-rail friction and give a misleading indication of the presence of a friction modifier. Therefore, the coefficient of friction itself is not a clear indicator of the presence of TOR-FMs. In the present study, cotton swabs dipped in a mixture of alcohol and ester were used to collect surface deposits (a third body) from both the wheel and rail at various distances from the point of application. Subsequently, the third body collected on the cotton swab was analysed using an energy dispersive X-ray analysis. The results have shown that the maximum carry distance of TOR-FMs on the top of the rail is limited to 70 m when using a TOR-FM from one manufacturer and to 450 m when using a TOR-FM from another manufacturer. The carry distance on the contact band of the wheel is limited to 100 m and 340 m. The friction modifier on the edges of the contact band was detected over a distance of up to 3 km; however, this will not minimise the damage or friction at the wheel–rail interface.

Keywords

Friction modifier, carry distance, top-of-rail, wayside equipment, top-of-rail friction modifier

Date received: 1 July 2017; accepted: 24 March 2018

Introduction

With the current demand for high efficiency in railway systems, the train speed is being increased in the case of passenger trains and the axle load in the case of heavy haul trains. Such increments cause the traction forces at the wheel–rail interface to increase and the lifetime of both the wheels and rails to decrease.[1] To withstand the high forces, a high-strength material is a generic recommendation. A proper combination of wheel and rail profiles with the biggest possible contact area is also desired, as this decreases the pressure.[2] From a tribological point of view, introducing a third body (generally a lubricant) is recommended to reduce the shear forces between the rubbing surfaces, as well as to take advantage of anti-wear additives. The use of an added third body at the wheel–rail interface started long ago; in Sweden, this practice was widely introduced during the 1970s.[3] However, initially, it was only applied on the gauge face.[4,5] The introduction of an additional third body known as the top-of-rail friction modifier (TOR-FM), between the top of the rail and the running surface of the wheel, was first studied in 2003.[6]

This study is limited to water-based TOR-FMs. Presently, only these TOR-FMs have been approved as compliant with the environmental regulations by Sweden's infrastructure manager, the Swedish Transport Administration (Trafikverket), which handles most of the tracks in Sweden. These TOR-FMs basically consist of soft particles suspended in a solvent (mainly water). However, some manufacturers use

Division of Operation and Maintenance Engineering, Luleå University of Technology, Lulea, Norrbotten, Sweden
Porsön Luleå, Sweden
Luleå University of Technology, Luleå, Sweden

Corresponding author:
Saad Ahmed Khan, Division of Operation and Maintenance Engineering, Luleå University of Technology, Luleå SE–97187, Sweden.
Email: saad.ahmed.khan@ltu.se

additional chemicals along with water as the base solvent. The exact content and composition of the different TOR-FMs are unknown as these details are not revealed by the manufacturers, but the benefits claimed for the different FMs (reduction in wear, rolling contact fatigue (RCF), etc.) are similar. At present, TOR-FM manufacturers claim that their products provide a coefficient of friction ranging (μ) from 0.3 to 0.4 and are used by many railway operators across the world. By studying the websites of the suppliers, it was found that at a consumption of 250–300 ml of TOR-FMs for 1000 axle passages, a minimum carry distance of 3 km can be achieved.

TOR-FM manufacturers claim various benefits, such as a reduction in noise,[7] wear,[6,8] energy consumption,[8] RCF[9–11] and short pitch corrugation.[12] In contrast, Lundberg et al.[13] showed in a study of one TOR-FM that it gave unacceptably low friction and thus could cause a long braking distance and slippage if used in large amounts. Moreover, Lemma et al.[14] claimed that friction values measured with a handheld tribometer were more dependent on the weather conditions, for example the temperature and humidity, than on the presence of an FM. Lemma et al.[14] also stated that they had obtained the coefficients of friction ranging from 0.5 to 0.6 even though there had been two sets of TOR-FM equipment installed in the vicinity. It should be noted that a coefficient of friction is not a clear indication of the presence of an FM, as moisture and other contamination from the environment can alter the coefficient of friction. Trafikverket is considering the implementation of a top-of-rail friction control technology using wayside equipment on the Swedish part of Malmbanan, the Swedish Iron Ore Line (IOL). The IOL was opened in 1903 to transport mineral ores (mainly iron ores) from Kiruna and Malmberget to the sea ports of Luleå in Sweden and Narvik in Norway. The total length of the track from Narvik to Luleå is 473 km. The line is a single-track electrified line and is mainly utilised by ore freight trains operated by LKAB, the Swedish mining company. The freight trains of LKAB have an axle load of 30 tonnes, which represents the heaviest axle load in Europe at present.[15] LKAB is considering a further increase in the axle load of their trains and is currently testing a train with a 32.5 tonne axle load.[15] According to information from LKAB and Trafikverket, RCF is presently the foremost problem on the IOL; it shortens the life of both the wheels and rails and is the primary reason for rail and wheel replacements. Preliminary results[16] from tests of the train with a 32.5 tonne axle load show a 14% increase in the RCF of wheels. LKAB has informed us that, with the present conditions for the IOL, the wheel removal cost for LKAB is 15 million Swedish kronor/annum and the rail removal cost for Trafikverket is 20 million Swedish kronor/annum (1 Swedish krona = 0.1 Euros), and an increase in the axle load will entail an additional cost.[16] TOR-FM suppliers claim that their products decrease the traction forces and hence decrease the RCF and increase the lifetime of the rails and wheels. However, the reliability and economic efficiency of a wayside TOR-FM system in Nordic conditions are unknown.

Table 1. Summary of all the experiments, including the application method at both locations and the respective positions on both the rail and wheel where the samples were collected.

Phase	Location	Method	Object	Position
1	Gullträsk	Wayside equipment	Rail	Running surface
2	Kiruna	Manually	Rail	Running surface
			Wheel	Running surface
			Wheel	Contact band

Initial simulations using inputs from the IOL in a multi-body simulation program have shown that by controlling the coefficient of friction, the traction forces and hence the RCF can be controlled.[17,18] In an on-going project run by the Luleå University of Technology in cooperation with LKAB and Trafikverket, simulations in combination with pilot field tests are being performed to observe the utility of a TOR-FM system. As part of that project, the present study has evaluated the carry distance of two different FMs using swabs dipped in a mixture of alcohol and ester-based solvent and subsequently analysed for elements using an energy dispersive X-ray (EDX) analyser equipped with a scanning electron microscope.

Method

In the present study, experiments were performed in two phases, denoted as phase 1 and phase 2. In both the phases, as presented in Table 1, FMs from two different suppliers were used.

The wheel–rail system

On the main track of the IOL, there are four main rail profiles, namely the 60E1, MB1, MB4 and MB5; MB stands for Malmbanan (i.e. IOL) profile[19]. In phase 1, the wayside equipment was installed before a narrow curve with a radius of 395 m; on such a narrow curve, the MB1 profile is used for the high rail and the 60E1 for the low rail. This curve experiences mixed traffic consisting of freight, passenger and maintenance trains. In phase 2, the track was a tangent track; the MB4 rail profile is the standard profile for the tangent track on the IOL. The locomotive used in phase 2 had a recently developed wheel profile, namely the WPL5V2.[19] At the time of the experiments, the rail and wheels were in good shape and free of recurring surface defects.

Description of the TOR-FMs

A friction modifier consists of polar molecules that are added to lubricants to minimise the surface contacts during a sliding and rolling motion. As long as the frictional contact is moderate, these molecules provide a protective layer which minimises the wear of rubbing surfaces. If the contact pressure is high enough, then the molecules are sheared off, eliminating any potential benefits of the additives.[20] In railway applications, a friction modifier performs a similar task. It is generally a thick liquid which consists of soft particles suspended in a solvent and which is applied between the top of the rail and the running surface of the wheel. A friction modifier reduces abrasive contact with asperities at the wheel–rail interface and, specifically, reduces the coefficient of friction from high levels (0.5–0.8) under dry and FM-free conditions to an intermediate coefficient of friction (0.3–0.4).[21]

The FM from supplier A was designated as FM-A; it is a smoke-grey-coloured thick liquid similar to a latex paint and is designed to dry rapidly at the wheel–rail interface. The manufacturer claims that it contains no oil. The FM from supplier B was designated as FM-B; it is a black-coloured thick liquid that resembles black particles suspended in water and behaves like a conventional very soft grease that does not dry rapidly. Stock et al.[5] classified the TOR-FM as a pure water-based material which has no trace of oil and dries rapidly. However, FM-B contains some slow-drying solvent along with water. Since the manufacturer states that FM-B is a TOR-FM, it is classified as a TOR-FM in the present study. The descriptions given above are based on the physical appearance of the FMs, as no declaration of ingredients was provided by the suppliers. In order to determine the elements present in the FMs, both of them were analysed using EDX, and the results were compared with those for an FM-free rail surface selected for a reference sample. The elements' weight percentages (wt%) detected using EDX are presented in Table 2. The FM samples were collected from the pool of FM at the distributing bars, as shown in Figure 2(b) and (c), whereas the reference sample was collected 35 km away from the installed wayside equipment. As indicated in Table 2 with 'ticks', two elements not found in the reference sample were observed in FM-A: magnesium (Mg) and molybdenum (Mo). In FM-B, in addition to Mg and Mo, barium (Ba) was also observed. These elements are denoted as FM elements in the present study, since one can conclude from their presence that an FM is present. Other elements that could represent ingredients of FMs were either present in the reference sample or in FM-A and FM-B in negligible quantities, and hence were ignored.

Figure 1(a) to (c) illustrates a wheel–rail interface without an FM, a wheel–rail interface with FM particles with carrier solvent and a wheel–rail interface with dried FM particles, respectively. Figure 1(a) shows a wheel–rail interface where there is no FM and the third body consists mainly of brittle materials such as wear debris, oxides, sand, residue from trains, etc. On application of an FM, the already present third

Table 2. Elements' wt% of both the FMs and the reference, i.e. the FM-free sample.

	Elements' wt%			FM elements	
	FM-A	FM-B	FM-free	FM-A	FM-B
C	35.8 ± 16.5	30.1 ± 12.3	30.9 ± 7.4		
O	17.9 ± 4.6	29.1 ± 9.1	30.8 ± 7.2		
Mg	3.6 ± 1.4	7.2 ± 3.4	0.1 ± 0.1	✓	✓
Si	6.4 ± 3.1	7.7 ± 3.9	3.1 ± 1.9		
S	12.1 ± 7.6	8.2 ± 5.5	1.9 ± 0.9		
Fe	0.8 ± 0.1	0.6 ± 0.1	36.9 ± 11.8		
Zn	1.3 ± 0.3	0.0 ± 0.0	0.0 ± 0.0		
Mo	16.1 ± 12.8	15.3 ± 10.7	0.0 ± 0.0	✓	✓
Ba	0.14 ± 0.03	8.7 ± 3.7	0.0 ± 0.0		✓
W	1.0 ± 0.2	0.0 ± 0.0	0.0 ± 0.0		

Note: The elements representing the presence of FMs are ticked. The results are an average of five measurement points with a standard deviation.

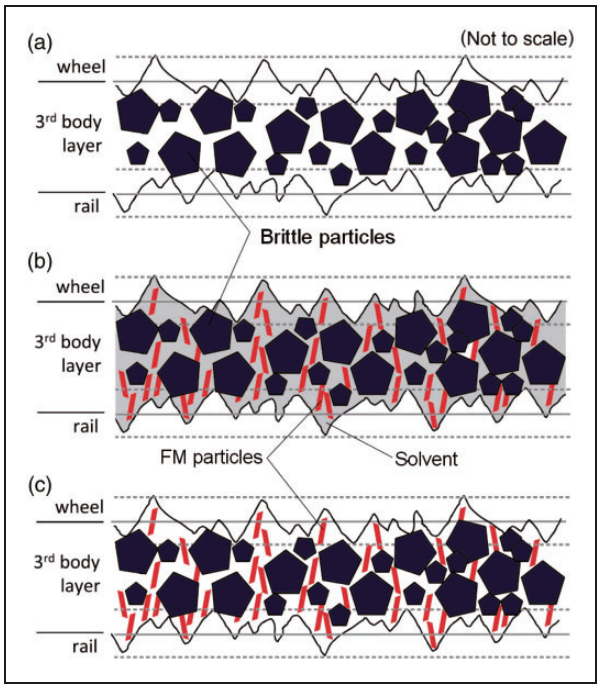

Figure 1. (a) Dry wheel–rail interface with a third body layer; a mixture of different third body materials, including wear debris, oxides, sand, etc. (b) FM particles with a carrier solvent at the wheel–rail interface providing boundary or mixed lubrication conditions. (c) Dried FM particles adjust the shear properties of the third body layer, thereby adjusting to the desired friction level.
Source: Adapted from Stock et al.[5]

body is mixed with the soft FM particles and carrier solvent, as shown in Figure 1(b). The carrier solvent helps in distributing the FM particles. Figure 1(c) shows a wheel–rail interface in a dry state where the FM particles stick to the rubbing surface and optimise the friction conditions through a shear displacement compensation mechanism in the third body layer. It should be noted that, since FM-B is expected to be a slow-drying FM, stage c (Figure 1(c)) is slowly or never reached with this FM, because the solvent is partially or not at all evaporated. The choice of solvent is critical, as the carry distance of the FM particles depends on the properties of the carrier solvent.[5] Moreover, the solvent can further provide a reduction of friction through a mixed lubrication mechanism according to the Stribeck curve.[22]

Application of TOR-FMs

In phase 1, stationary equipment (shown in Figure 2(a)) was installed before a sharp curve with a radius of 395 m on the IOL at Gullträsk in Sweden. The installed equipment is powered by a 12 V battery, which is recharged by an attached solar panel and wind turbine, since no electricity is available at this place. A wheel detecting sensor (Figure 2(d)) is attached to the rail, which sends a signal to the equipment for every wheel pass. The equipment is set to discharge a specific amount of FMs on the rail when it detects a wheel. The FM is pumped from the tank to the distributing bars through hoses. The FM is carried forward on the rail when a wheel passes over the pool of FM created by the distributing bars, as shown in Figure 2(b) and (c). Distributing bars of types recommended by the respective manufacturers were installed on a side of both the high and low rail. The same main unit was used for the tests of the two TOR-FMs, as it has the capability to function with both types of distributing bars and FMs. In the installed equipment, the pumping time and hence the quantity of FM can be controlled. In the present study, the pump was set at the maximum level of 1 litre/1000 axles, which is approximately four times the amount recommended by the suppliers. This excessive amount of FM was used so that the real carry distance would not be underestimated. Initially, the tank was filled with FM-A for 10 months, after which the tank was cleaned and filled with FM-B. To avoid any mixing of the two FMs, sample collections for FM-B were performed two months after changing the FM.

The carry distance of the two FMs observed in phase 1, especially that of FM-A, was very short in comparison with the carry distance claimed by the manufacturer. Supplier A offered an explanation which can be supported by a research performed by Stock et al.[5] and which asserts that a water-based FM is carried forward with the help of the wheels and is partially transferred to the rail as long as the FM is wet. As soon as the carrier solvent evaporates, i.e. becomes dry, the FM particles will adhere to the wheel and limit further inter-surface material transfer between the rail and the wheel. However, this may not be true in the case of FM-B, whose solvent contains an additive together with water.

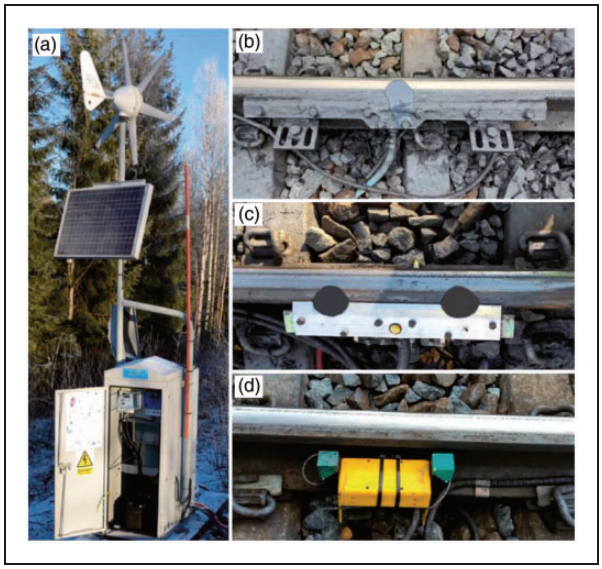

Figure 2. The wayside TOR equipment installed at Gullträsk in Sweden: (a) main unit, (b) distributing bars used for FM-A, (c) distributing bars used for FM-B and (d) wheel detecting sensor.

It was not possible to stop the trains near the installed wayside equipment to obtain samples from the wheels. Therefore, the study was extended to comprise a second phase, which was performed at the LKAB station in Kiruna, Sweden. Here tests were performed using an IORE locomotive, which has an axle load of 30 tonnes and is currently operational on the IOL. In the second phase, 15 ml of FMs were applied manually with a brush on 7.4 m of rail. The length of rail on which the FM was applied was double the circumference of the locomotive wheel, so that the wheel would have a theoretical chance multiplied by two to pick up the FM. The amount of FM applied was four times the amount recommended by the suppliers, as in the case of the stationary equipment used in phase 1 of the study. As shown in Figure 3, FM-A was applied to the left rail and FM-B to the right rail. It should be noted that during all the experiments, the weather was sunny and the temperature was between 5° and 12 °C.

Sample collection and analyses

Cotton swabs dipped in a mixture of alcohol and ester-based solvent were used to obtain the third body samples from different locations on the top of the rail and the running surface of the wheel. The samples were collected using a plastic slot measuring 4×60 mm^2, and the swab was rubbed inside the entire slot to collect as much as possible of the third bodies available within the slot. Afterwards, the third bodies on the swabs were analysed using an EDX analyser,

which provides elemental identification and quantitative compositional information. The fundamental principle of the analyser is that each element has a unique atomic structure which gives a unique set of peaks on its electromagnetic emission spectrum;[23] It should be noted that the height of a peak may not be proportional to the element's wt%. For each sample, EDX analysis for element detection was performed at five different locations on the cotton swab. Figure 4 shows the image of a sample from FM-A subjected to EDX and the output from the EDX analyser showing the peaks for different elements of this TOR-FM.

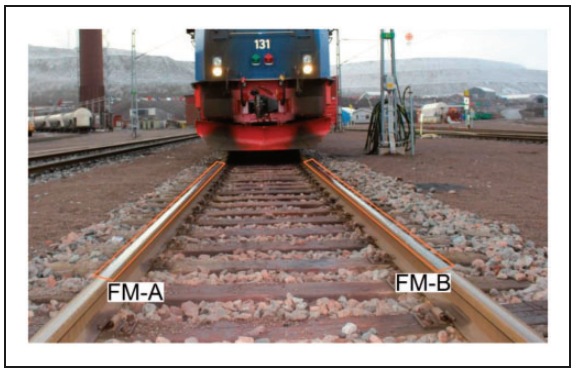

Figure 3. Phase 2: IORE locomotive standing before a section of rail on which FM was applied manually; FM-A was applied to the left rail and FM-B to the right rail.

In phase 1, the samples were collected from the in-service rail, as described above, at the locations where the stationary TOR-FM equipment was installed. In phase 2, the samples were collected from both the rail and the wheel on a track section where the TOR-FM had been applied manually. The samples from the rail were obtained from the complete running surface in both phases. However, in the case of the wheels, which were included in phase 2, the samples were collected following two different approaches. In the first approach, the samples were collected from the

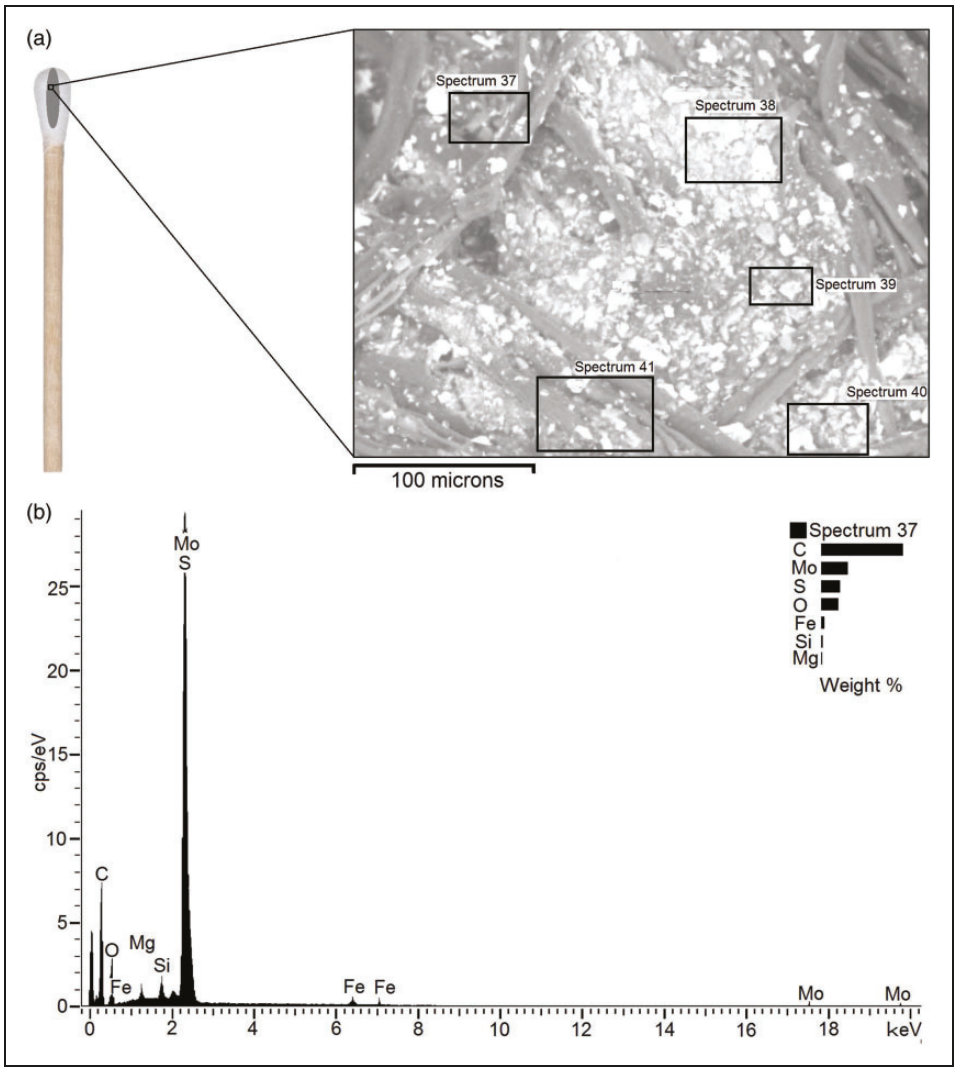

Figure 4. Example of an EDX result for FM-A: (a) image of a sample subjected to EDX analysis showing the five locations focused on and (b) output of the analyser for one of the five locations focused on.

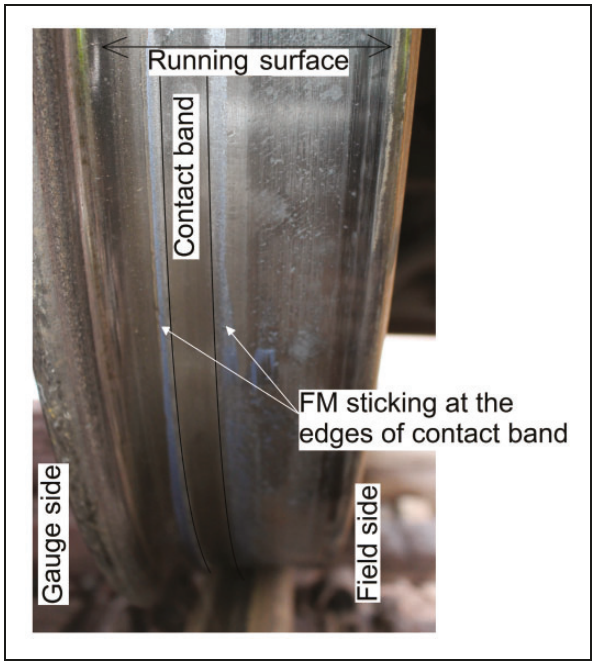

Figure 5. Image showing the various zones of the wheel, along with the FM sticking on the edges of the contact band.

complete running surface of the wheel, whereas in the second approach, they were collected only from the middle of the contact band, as shown in Figure 5. The reason for applying the second approach was that there is a small contact area at the wheel–rail interface which experiences all the traction forces and FM is required in this particular area. However, due to the pressure at the wheel–rail interface, the FM can easily be pressed out to the edges of the contact area (see Figure 5) or some grooves and stay there for a long distance without coming in the wheel–rail contact.

EDX results with respect to different FM thicknesses

In this section, a correlation is made between the film thickness and the element's wt% resulting from the EDX analysis. The following amounts of FMs were applied to a defined area of 300×60 mm^2: 5, 3, 2, 1 and 0.25 ml. The FM film thickness was calculated by dividing the volume of FM applied by the given area. Finally, the film was cleaned off the area of application with an alcohol-based cleaner; i.e. a theoretical zero film thickness was created. However, the pores and micro-cracks still held some FMs. The samples (one at each location) were collected as described above from all six layers and were analysed using EDX. Figure 6 shows the elements' wt% with respect to the different film thicknesses. Curve fitting was performed using equation (1), which is based on the asymptotic regression model:

$$Y = a - bc^x \quad (1)$$

where variable Y is an average of the element wt% of a given film thickness, presented by variable x, and a, b and c are constants which are shown in Figure 6. The samples taken using swabs, as described in the Sample collection and analyses section, were non-homogeneous, and therefore, the EDX analysis was carried out on a number of spots on the samples, which gave a variation in the element wt% for the same film thickness axis. For the final results, equation (1) was reversed to calculate the film thickness for each element wt%. It should be noted that equation (1) is used to convert the element wt% into the FM film thickness, but the fitting equation used for the final results is different.

The actual film thickness on the top of the rail is unknown. However, if we assume the carrying distances of the TOR-FMs claimed by the manufacturers to be correct, then an estimated film thickness can be calculated for those carry distances. To calculate the FM film thickness, the consumption mentioned on the companies' websites can be taken, i.e. 300 ml for 1000 axle passages, which means that 300 ml of TOR-FM will be sufficient to make an FM film which is adequate for the parameter of 1000 wheels. The diameter of the wheel was taken to be 1 m and the width of the contact band to be 10 mm; these values are generic values. The expected film thickness can then be calculated as follows:

$$\begin{aligned}
&\text{Volume of recommended FM} \\
&= 300\,\text{ml for 1000 axle passages} \\
&\quad \Leftrightarrow 150\,\text{ml for 1000 wheel passages} \\
&\text{The total circumference of 1000 wheels} \\
&= \pi \times \text{diameter of wheel} \times 1000 \\
&= 3.14 \times 1000 \times 1000\,\text{mm} = 3.14 \times 10^6\,\text{mm} \\
&\text{Total contact area} \\
&= 10 \times 3.14 \times 10^6\text{mm}^2 = 3.14 \times 10^7\text{mm}^2 \\
&\text{FM film thickness} \\
&= \frac{\text{volume of the FM used}}{\text{total area of contact band for 1000 wheels}} \\
&= \frac{15 \times 10^4}{3.14 \times 10^7} \times 1000 = 4.8\,\mu\text{m}
\end{aligned}$$

Based on the calculations, it can be stated that a film thickness of approximately 5 µm is required on the top of the rail to minimise the traction forces. Therefore, according to the claim of the TOR-FM suppliers, a film thickness of approximately 5 µm should be observed for up to 3 km from the place of application in order to achieve sufficient damage protection and friction control. Since the film thickness required to minimise the traction forces in practice is not known, in the present study, the longest distance up to which any FM element can be detected is considered as the carry distance of the FM in question.

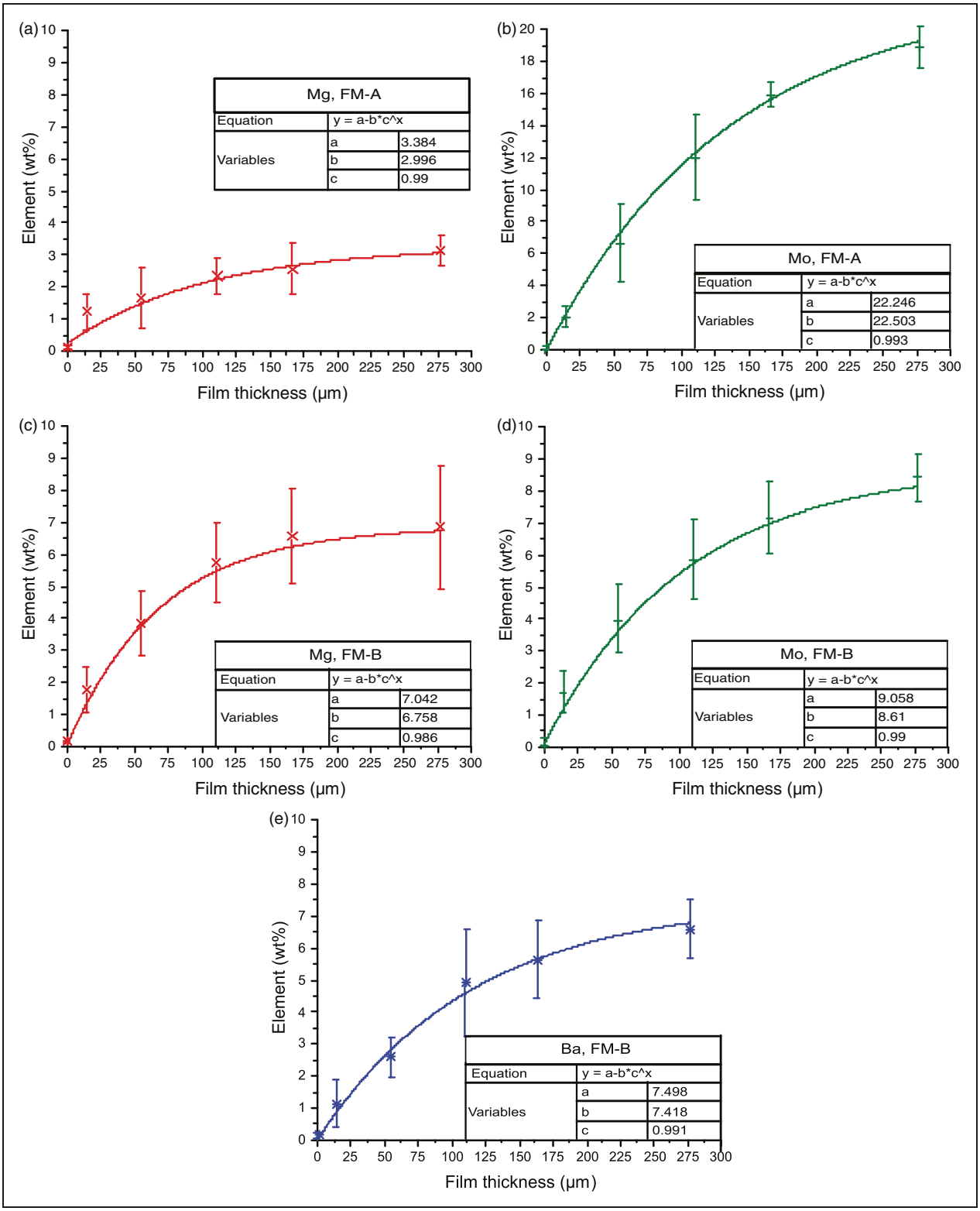

Figure 6. Element wt% of the FM elements detected by EDX for different film thicknesses: (a) Mg, FM-A, (b) Mo, FM-A, (c) Mg, FM-B, (d) Mo, FM-B and (e) Ba, FM-B.

Results and discussion

Since the carry distances in most of the cases were limited to less than 1 km, all the graphs are limited to a distance of 1000 m. In order to make the graphs more readable, the film thicknesses are limited to 50 μm in the case of phase 1 and 30 μm in the case of phase 2.

Phase 1: Carry distance results obtained with the stationary equipment

The carry distance results for phase 1 were obtained with an application rate of 1 litre/1000 axles, which is four times the rate recommended by the manufacturer. In Figure 7(a) and (b), which presents the

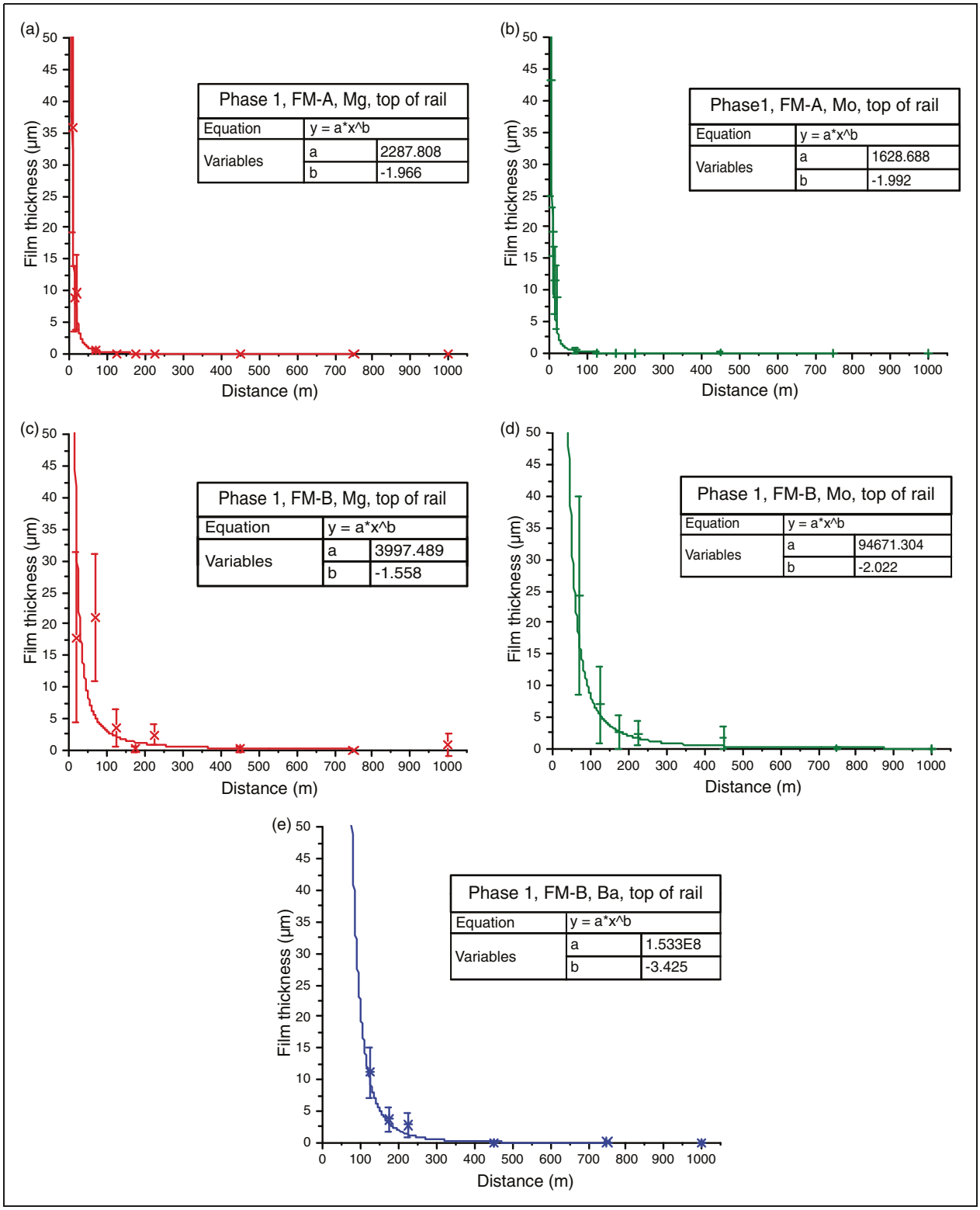

Figure 7. FM film thicknesses based on the element wt% at various distances from the TOR-FM equipment – phase 1 results: (a) Mg, FM-A, (b) Mo, FM-A, (c) Mg, FM-B, (d) Mo, FM-B and (e) Ba, FM-B.

results for FM-A, which was claimed by the manufacturer to have no oil content, a poor carry distance of 70 m is observed; i.e. the FM film thickness is zero after 70 m. This carry distance is extremely small compared with the claims of the manufacturer asserting a carry distance of more than 3 km. The results for FM-B, which is believed to contain a slow-drying additive, are presented in Figure 7(c) to (e), which shows that this FM has a carry distance of up to 450 m, which is approximately six times longer than that of FM-A, but still notably shorter than the distance claimed by the manufacturer. Table 3 summarises the carry distances corresponding to each element.

Table 3. Carry distance corresponding to each FM element – phase 1 results.

	Carry distance (m)	
Element	FM-A	FM-B
Mg	60	360
Mo	70	450
Ba	–	325

Table 4. Carry distance corresponding to each FM element – phase 2 results for the top of the rail.

	Carry distance (m)	
Element	FM-A	FM-B
Mg	50	160
Mg	65	320
Ba	–	290

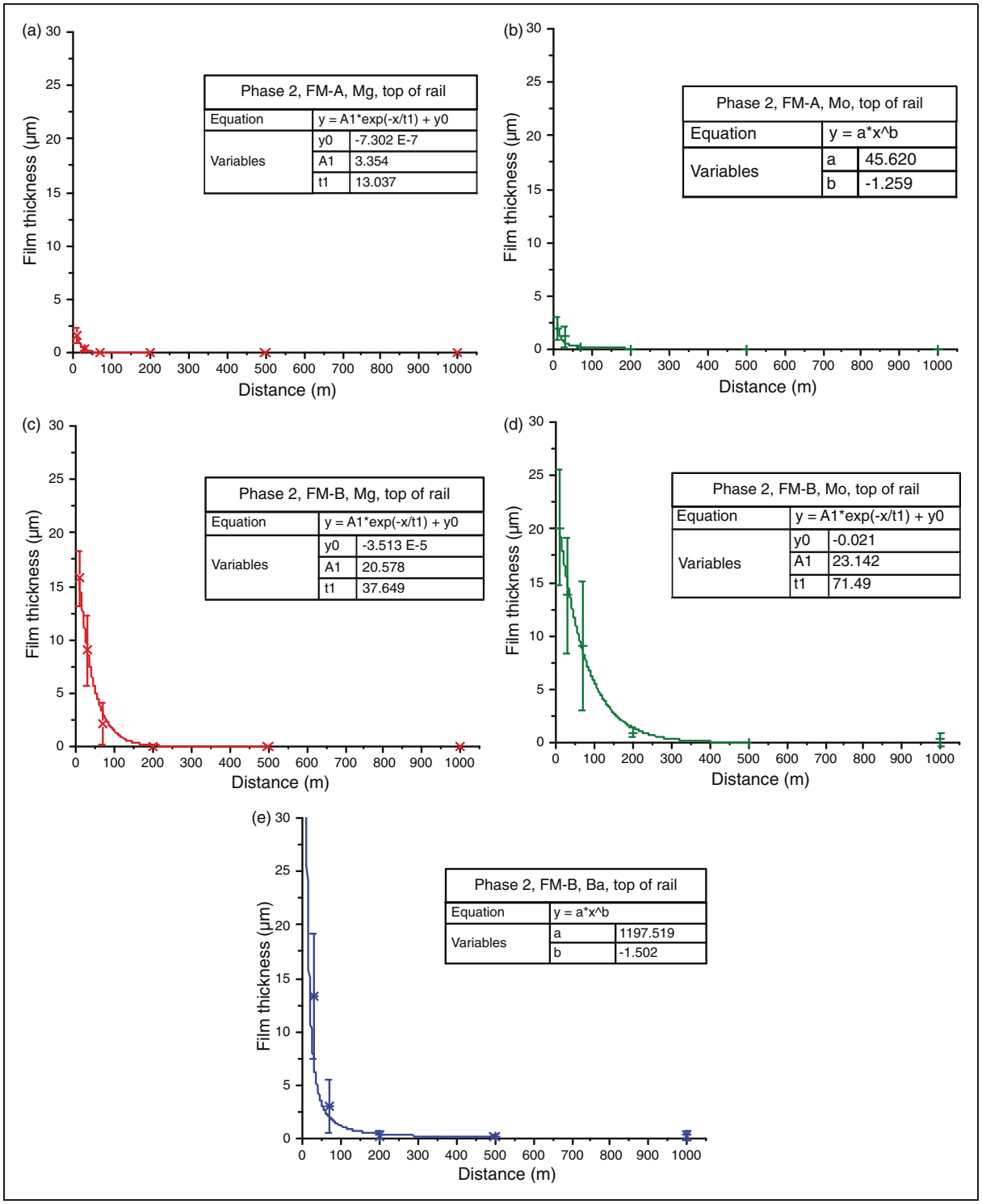

Figure 8. FM film thicknesses based on the element wt% at various distances from the location of application – phase 2 results for the top of the rail: (a) Mg, FM-A, (b) Mo, FM-A, (c) Mg, FM-B, (d) Mo, FM-B and (e) Ba, FM-B.

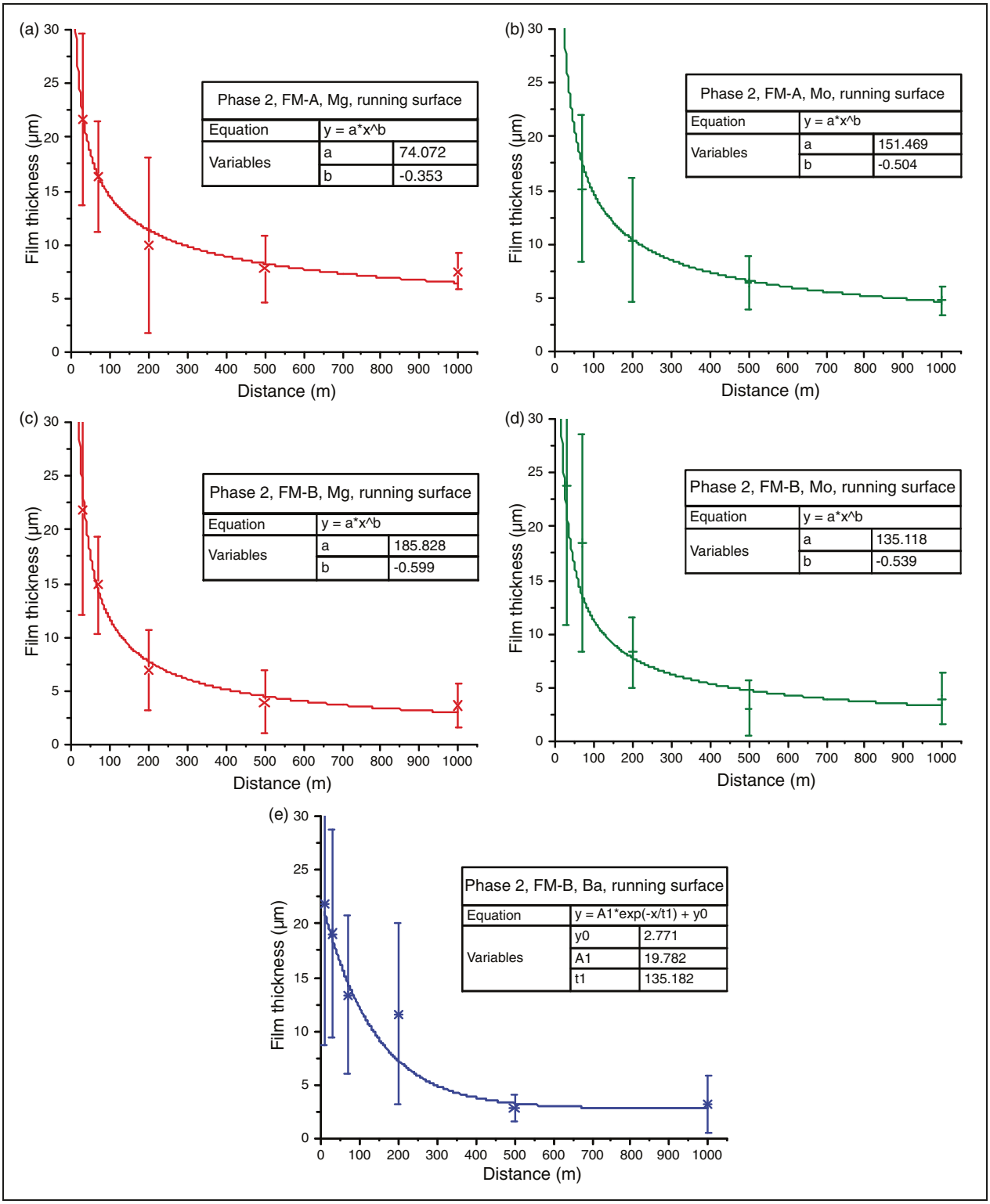

Figure 9. FM film thicknesses based on the element wt% at various distances from the location of application – phase 2 results for the complete running surface: (a) Mg, FM-A, (b) Mo, FM-A, (c) Mg, FM-B, (d) Mo, FM-B and (e) Ba, FM-B.

Phase 2: Carry distance on a wheel and rail when a limited amount of FM is applied manually

Samples collected from the top of the rails. Figure 8(a) and (b) presents the carry distance for FM-A and shows that this FM is barely carried forward to 65 m from the point of application. Figure 8(c) to (e) presents the results for FM-B and shows that the FM elements of this FM can be observed over a distance of up to 320 m. It appears that FM-A dried fast and could not be transferred to the rail over a distance longer than 65 m, whereas FM-B dried slowly and was transferred over a longer distance (Table 4).

Table 5. Carry distance corresponding to each FM element – phase 2 results for the complete running surface.

	Carry distance (m)	
Element	FM-A	FM-B
Mg	>3000	>3000
Mg	>3000	>3000
Ba	–	>3000

Note: Results are shown up to 1000 m for consistency in all the graphs.

Samples collected from a cross-section of the complete running surfaces of the wheels. Figure 9(a) and (b) presents the results for FM-A and Figure 9(c) to (e) presents those for FM-B. For both the FMs, a carry distance of more than 3 km was observed (Table 5), but the graphs in Figure 9 present the results over a distance of 1000 m to achieve consistency in all the graphs. The results for the samples from the complete cross-section of the wheels do not, however, provide information as to whether or not the FMs stick to the corner of the wheel–rail contact bands and stay there

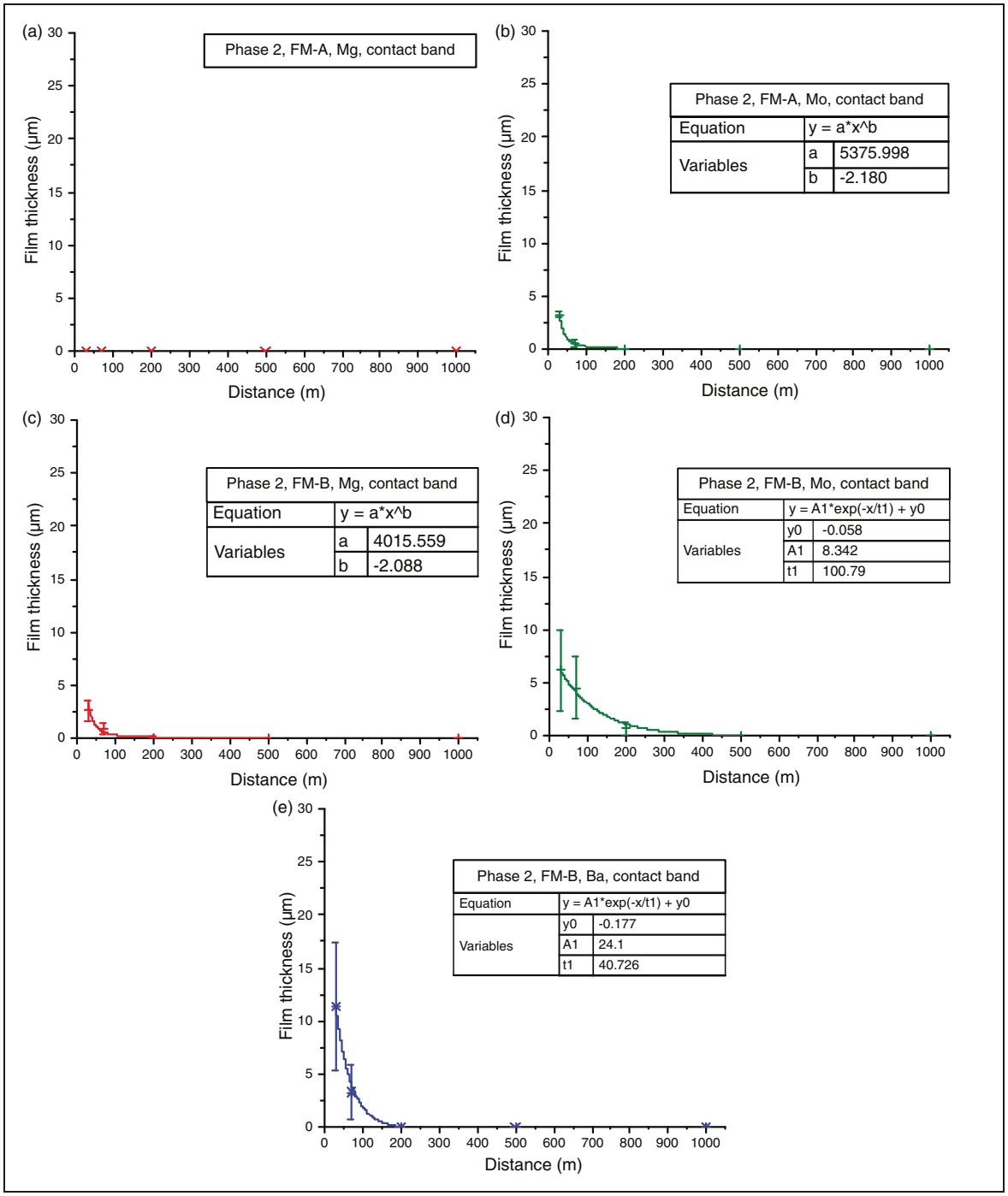

Figure 10. FM film thicknesses based on the element wt% at various distances from the location of application – phase 2 results for the middle of the contact band: (a) Mg, FM-A, (b) Mo, FM-A, (c) Mg, FM-B, (d) Mo, FM-B and (e) Ba, FM-B.

without entering the contact bands over a distance of more than 3 km. During a visual inspection of the wheels after the test, it was observed that the FM had stuck mainly to the edges of the contact band or to a cavity in the wheel (see Figure 5). Therefore, samples from the middle of the contact band were collected and the results are discussed in the next section.

Samples collected from the wheel–rail contact band. As discussed earlier, when a wheel passes over a pool of FM, as in the case of the stationary equipment, due to pressure and splashing, the FM is pressed out from the contact band, sticks to the non-contact running surface of the wheel and stays there for a long distance. However, the FM is actually needed on the contact band. Therefore, samples were also collected from the middle of the contact band and the results of their analysis are presented in this section.

Figure 10(a) and (b) presents the results for FM-A and Figure 10(c) to (e) presents the results for FM-B. At the start of the experiments in phase 2, the contact band and the complete running surface were not treated separately. However, after discovering that the FM was mainly sticking to the edges of the contact band, samples from the middle of the contact band were also collected. Therefore, in this set of experiments, the samples were collected from positions 30 m and forward from the place of application. In contrast to the results for the complete running surface, the results for the contact band for FM-A show that one FM element was detected over a distance of up to 100 m, whereas the corresponding results for FM-B show that all the FM elements were detected over a distance of up to 340 m (Table 6).

For the purpose of providing an overview of all the experiments, Table 7 summarises all the carry distance results for both FMs.

It should be noted that all the figures show the approximate film thickness at various distances from the point of application using curve fitting. Theoretically, a minimum film thickness of approximately 5 μm is required and a film thickness lower than 5 μm may not provide sufficient damage protection according to the manufacturers. However, the film thickness required to achieve damage protection in practice is not known.

Conclusions

- When an FM is supplied continuously at the rate of 1 litre/1000 axles passages, the maximum carry distances of 70 m for FM-A and 450 m for FM-B were observed on the running surfaces of rails. For both the FMs, the carry distance was much shorter than that claimed by the manufacturers.
- The FM cannot withstand the high pressures at the wheel–rail contact band for any long distance and shears off at a distance of approximately 100 m for FM-A and 340 m for FM-B. The reason for the slightly longer carry distance can be expected for FM-B due to its slow-drying property.
- The FM can stay for a distance longer than 3 km on the non-contact running surface of a wheel, but, after being pressed out to the edges of the wheel–rail contact band, does not re-enter the contact band.

Table 6. Carry distance corresponding to each FM element – phase 2 results for the middle of the contact band.

	Carry distance (m)	
Element	FM-A	FM-B
Mg	0	105
Mo	100	340
Ba	–	155

Acknowledgements

The authors gratefully acknowledge the support of Lars Strand and Lennart Elenius at LKAB for their assistance in providing an IORE locomotive and the support of Per Gustafsson from LKAB in providing technical help in the initial stage of the study. The authors would also like to thank colleagues at Luleå University of Technology: Johnny Grahn at the Division of Materials Science for helping with the scanning electron microscopy and Thomas Nordmark and Matti Rantatalo at the Division of

Table 7. Summary of carrying distance for FM-A and FM-B.

Source	Position of sample collection	Carry distance (m)	
		FM-A	FM-B
Manufacturer's claim		3200–6400	5000
When supplied continuously by the stationary equipment	Top of rail	70	450
When applied once manually	Top of rail	65	320
	Wheel's running surface	>3000	>3000
	Wheel's contact band	100	340

Operation and Maintenance Engineering for providing technical assistance.

Declaration of Conflicting Interests

The author(s) declared no potential conflicts of interest with respect to the research, authorship, and/or publication of this article.

Funding

The author(s) disclosed receipt of the following financial support for the research, authorship, and/or publication of this article: This research was funded by Luleå Railway Research Center (JVTC) and Trafikverket.

References

1. Dirks B and Enblom R. Prediction model for wheel profile wear and rolling contact fatigue. *Wear* 2011; 271: 210–217.
2. Asplund M, Famurewa SM and Schoech W. A Nordic heavy haul experience and best practices. *Proc IMechE, Part F: J Rail and Rapid Transit* 2017; 0: 1–11.
3. Waara P. Lubricant influence on flange wear in sharp railroad curves. *Ind Lubr Tribol* 2001; 53: 161–168.
4. Eadie DT, Oldknow K, Santoro M, et al. Wayside gauge face lubrication: how much do we really understand? *Proc IMechE, Part F: J Rail and Rapid Transit* 2012; 227: 245–253.
5. Stock R, Stanlake L, Hardwick C, et al. Material concepts for top of rail friction management: classification, characterization and application. *Wear* 2016; 366–367: 225–232.
6. Eadie DT, Vidler B, Hooper NE, et al. Top of rail friction control: lateral force and rail wear reduction in a freight application. *In: Proceedings of the IHHA, Dallas*, TX, USA, 2003, pp.7–35.
7. Eadie DT and Santoro M. Top-of-rail friction control for curve noise mitigation and corrugation rate reduction. *J Sound Vib* 2006; 293: 747–757.
8. VanderMarel J, Eadie DT, Oldknow KD, et al. A predictive model of energy savings from top of rail friction control. *Wear* 2013; 314: 155–161.
9. Lu X, Makowsky TW, Eadie DT, et al. Friction management on a Chinese heavy haul coal line. *Proc IMechE, Part F: J Rail and Rapid Transit* 2012; 226: 630–640.
10. Eadie DT, Elvidge D, Oldknow K, et al. The effects of top of rail friction modifier on wear and rolling contact fatigue: full-scale rail-wheel test rig evaluation, analysis and modelling. *Wear* 2008; 265: 1222–1230.
11. Stock R, Eadie DT, Elvidge D, et al. Influencing rolling contact fatigue through top of rail friction modifier application – a full scale wheel-rail test rig study. *Wear* 2011; 271: 134–142.
12. Eadie DT, Santoro M, Oldknow K, et al. Field studies of the effect of friction modifiers on short pitch corrugation generation in curves. *Wear* 2008; 265: 1212–1221.
13. Lundberg J, Rantatalo M, Wanhainen C, et al. Measurements of friction coefficients between rails lubricated with a friction modifier and the wheels of an IORE locomotive during real working conditions. *Wear* 2014; 324–325: 109–117.
14. Lemma Y, Asplund M, Rantatalo M, et al. Top-of-rail friction measurements of the Swedish iron ore line. In: *Proceedings of the 3rd International Workshop and Congress on eMaintenance*, Luleå, Sweden, 2014.
15. Nordmark T. *Increased axle load to 32.5 tonnes: what operational and maintenance effects will it have for the rolling stock?* Report, Luleå University of Technology, Luleå, 2016..
16. Nordmark T. *Vagnsrapport - Provtåg 32,5 Tons Axellast: November 2016*. Report, LKAB, Kiruna, 2016.
17. Khan SA, Persson I, Lundberg J, et al. Prediction of the effects of friction control on top-of-rail cracks. *Proc IMechE, Part F: J Rail and Rapid Transit* 2016; 0: 1–11.
18. Khan SA, Persson I, Lundberg J, et al. Prediction of top-of-rail friction control effects on rail RCF suppressed by wear. *Wear* 2017; 380–381: 106–114.
19. Asplund M, Khan SA and Nordmark T. Improved wheel-rail system of Sweden's iron ore line. In: *Proceedings of the IHHA*, Cape Town, South Africa, 2017.
20. Sunqing Q, Junxiu D and Guoxu C. A review of ultrafine particles as antiwear additives and friction modifiers in lubricating oils. *Lubr Sci* 1999; 11: 217–226.
21. Hardwick C, Lewis S, Lewis R, et al. The effect of friction modifiers on wheel/rail isolation at low axle load. *Wear* 2011; 271: 71–77.
22. Spikes HA. Mixed lubrication – an overview. *Lubr Sci* 1997; 9: 221–253.
23. Goldstein JI, Newbury DE, Echlin P, et al. *Scanning electron microscopy and X-ray microanalysis*. Boston: Springer, 2011.

Related paper: Improved wheel-rail system of Sweden's Iron Ore Line.

Asplund, M., Khan, S. A. and Nordmark, T. (2017). Improved wheel-rail system of Sweden's Iron Ore Line, Proceeding of the 11th International Heavy Haul Conference (IHHA 2017), Cape Town.

Improved wheel-rail system of Sweden's iron ore line

M. Asplund
Swedish Transport Administration, Trafikverket, Luleå, Sweden
S.A. Khan & T. Nordmark
Luleå University of Technology, Luleå, Sweden

ABSTRACT: The Swedish Iron Ore Line (IOL) is the only heavy haul line in Europe. The northern part of the line is located above the Arctic Circle, a very harsh climate. Because of the introduction of new vehicles with a 30-tonnes axle load, the track were gradually replaced between 2006 and 2009 with heavier rails, mostly with a steel grade of R350LHT. Just after the first replacement of track in 2006, the project presented herein was established with the primary goal of improving the life length of the rail, and monitoring activities started. This project now has a unique database of rail degradation data. So far, the information has been used to improve the performance of the wheel-rail system and thus extend the life length of the rail, as well as to improve our knowledge of heavy haul operations in a cold climate. The paper discusses the project progress in general and gives some examples of improvements that have been successfully implemented, such as new rail profiles and a higher grinding frequency. Finally, it discusses the challenges of future capacity improvements, such as an increase in the axle load, and how these can be addressed.

1 INTRODUCTION

This paper deals with the Nordic iron ore line (IOL), Malmbanan in Swedish, and the heavy haul traffic operating on it. In operation since 1903, the IOL is a 473 km single standard gauge track section located in northern Sweden and northern Norway. The line is above the Arctic Circle, a harsh and cold climate. The axle load for heavy haul trains is 30 tonnes. Trains are 750 m long and consist of 68 wagons with one pulling units – two IORE locomotives. Their gross weight is about 8500 tonnes. The trains operate loaded at 60 km/h. In the rolling stock fleet of 17 trains, there are more than 1100 wagons, with about 80 approved for a 32.5-tonnes axle load.

The information and data in the paper come from 2007 to 2015 and were collected mainly by the project members.

The wheel and rail are interacting systems and, thus, should not be treated separately. In fact, the wheel-rail interface plays a significant role in the performance of the entire railway system. To reach a high quality of service, especially with the demanding conditions imposed by high axle loads, the wheel-rail interface needs to be managed particularly well. This paper deals with this important system and shows how it has been improved during the last ten years.

2 THE NORDIC IRON ORE LINE AND THE MONITORED SECTIONS

The IOL is the only heavy haul line in Europe. This investigation looks at the northern-most part. The IOL and the monitored areas, sections 4-6, are shown in Figure 1. The middle of the figure shows Northern Sweden; there is a harbour in the south (Luleå) and another in the north (Narvk). Situated between the harbours are two mines, one in Kiruna and the other in Malmberget. The IOL links the mines with the harbours.

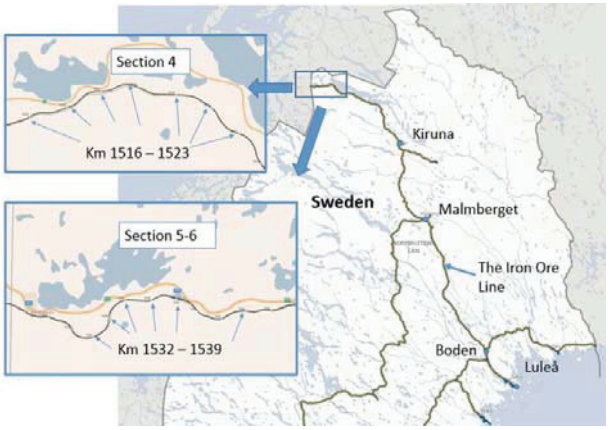

Figure 1. Northern Sweden with the geographic situation of the IOL and monitored sections 4-6

Material from the northern mine (Kiruna) generally flows to the northern harbour, and material from the southern mine (Malmberget) goes to the southern harbour. These are called the northern and the southern loop, respectively.

The accumulated yearly tonnage on the northern loop is about 34 MGT and on the southern loop about 20 MGT. The traffic between the mines is about 6 MGT. For the northern loop, the increase in tonnage

from 2008, when the project started and a new track was in operation, to 2016 is about 43%.

The climate is characterized by dry periods in summer and extremely cold winters (under –40C°), interrupted by wet weather conditions in spring and autumn.

The track is electrified and contains mixed traffic, but the main traffic is heavy haul trains, with about 12 loaded trains per day on the northern loop and four loaded trains on the southern loop; a further two trains are test trains with heavier axle load of 32.5 tonnes.

From 2006 to 2009, a new track was laid from Kiruna to Riksgränsen (the border between Sweden and Norway). It was equipped with 60E1 head-hardened rails of grade R350LHT (CEN, 2011), concrete sleepers, and elastic fastenings.

The IOL has about 20 wayside monitoring systems of different types and applications. The wheel profile is monitored by a wayside wheel profile measurement system (WPMS) located on the southern loop close to Luleå. The WPMS has been in operation since 2011 and delivers information on wheel profiles to the rolling stock owner (Asplund et al., 2014), were two methods have been suggested to improve the data quality (Asplund & Lin 2016; Asplund et. al., 2016). The WPMS has also been used to develop a new rail profile adapted for actual worn wheels in service; this rail profile is called MB5 (Malmbanan profile 5).

In the northern loop, track sections have been carefully monitored by manual profile measurements since the renewal of the track in 2006. The monitoring sections (3-6) are divided into curve segments, (A to E) and tangent track (T). There are 43 curves and sections of tangent track, as shown in Table 1. The total number of rail profile measurements for the sections is about 465.

Table 1. Description of the curve types.

Type	Layout	Radius (m)	Number of curves
A	Curve	<550	9
B	Curves	550-650	17
C	Curves	650-750	3
D	Curves	750-850	2
E	Curves	850-1500	6
T	Tangent		6

3 THE RAIL

As mentioned above, after the track change on the northern loop, the rail is now 60E1 head-hardened rail of grade R350LHT. It has been regularly ground since the track change in 2006. The actually status of the rail is generally good in tangent track and in the high rail of curved track. The low rail of curves has some problems with spalling, however, especially in narrow curves.

On a test section, it is performed trials with rail grades of R370CrHT and R400HT (CEN, 2011). The results were good for the R400HT rail because there was less wear and material flow compared to the R350 LHT. This trial will be discussed later in the article.

One significant failure mode on rails, especially on heavy haul lines, is crack propagation caused by rolling contact fatigue (RCF) on the rail head. Good knowledge of the crack behaviour is important to plan grinding. Crack propagation and wear compete with other, as grinding and milling, artificial wear actions, are done to remove cracks. The crack growth should not be much larger than the wear, but in natural conditions, the crack growth rate is greater than the wear rate. The crack growth rate also has a different speed in different phases.

Figure 2 shows the surface of an IOL rail. The grade of this rail is R260 (CEN, 2011); it was removed from service because of RCF. At the top of the rail, it can be seen a white layer (likely a martensite layer) with a thickness of about 50 μm. This white layer can be produced in hard steel by adhesive sliding wear without lubrication (Siposet. al., 2008) of the rails. The crack angle changes direction dramatically after passing the white layer, most likely influenced by both material properties and pressure distribution.

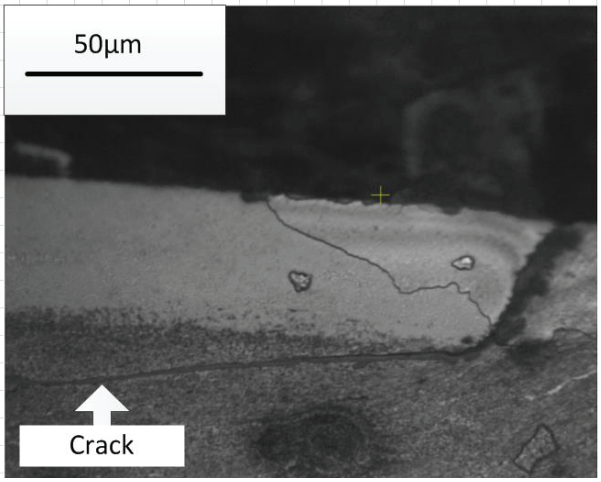

Figure 2. Crack propagation on the surface of an IOL rail.

The hardness of the rail varies; close to the surface, it is about 445 BHN. The hardness decreases as a function of the distance from the surface. At 0.5 mm from the surface, it is 339 BHN, and at 3 mm, it is about 300 BHN. The standard for R260 rail requires hardness between 260 to 300 BHN, and this is limit reached at 3 mm under the surface (CEN, 2011). Table 2 shows the hardness distribution for the rail head starting from the surface, in HV (Vickers) and BHN (Brinell).

Table 2. Hardness distribution as a function of distance from the surface.

From surface [mm]	HV	BHN
0.05	468	445
0.25	410	390
0.38	408	388
0.5	357	339
0.75	351	334
1	362	344
2	330	314
3	317	301
4	309	294
5	313	297
7.5	304	290
10	278	267
15	293	275

The crack is branching inside the rail during the load cycles of passing wheels, Figure 3 shows how a typical crack branches in a rail. This particular crack reaches almost 2 mm into the material at an angle of about 30º from the surface. In the end phase, the crack angle (bottom right of Figure 3) is about 70°.

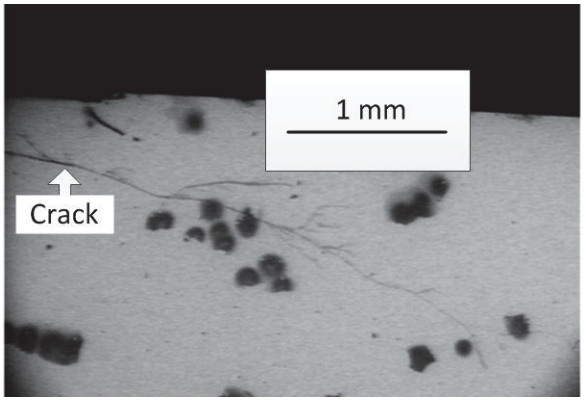

Figure 3. Crack branching inside the rail.

Another significant degradation mode is the wear of the rail. The natural wear in the wheel-rail interface is the loss of metal caused by sliding in the presence of an abrasive third body. Wear is directly related to the load, the type of stress and the configuration of the contact (Zarembski, 2005). The main wear mechanisms in wheel-rail sliding or rolling contacts are adhesive, abrasive, fatigue driven, thermal and oxidative wear processes (Lewis & Olofsson, 2009).

The average annual wear rate of the rail area monitored for 2009 to 2013 is shown in Table 3, separated out by curved and tangent track. Recall that curve types A-E are described in Table 1. An interesting observation is that after the introduction of larger axle loads of 30 tonnes in 2011, the natural wear of the rail increased but stabilised again after a couple of years.

Table 3. Natural wear in mm^2/MGT for different curve types during 2009 to 2013.

Year	A	B	C	D	E	Tangent
2009	0.36	0.26	0.11	0.03	0.05	0.09
2010	0.33	0.22	0.09	0.09	0.06	0.13
2011	0.58	0.39	0.27	0.20	0.17	0.10
2012	0.63	0.36	0.29	0.16	0.13	0.05
2013	0.05	0.29	0.29	0.28	0.06	0.09

Investigations of the IOL have shown that the natural wear rate is about two to five times higher in sharp curves than in mild curves or tangent track, and the natural wear rate is influenced by the annual tonnage on the track. Furthermore, more material is removed by grinding than by natural wear, and different track segments have different wear behaviour (Famurewa et al., 2015).

4 THE WHEEL

WPL9 became the wheel profile for IORE locomotives after 2009, but the recently developed locomotive wheel profile WPL5V2 was implemented in the fleet in 2016. This profile should extend the life length of the wheel by reducing rolling contact fatigue (RCF) on the wheel tread (Asplund et al., 2017).

Reliability investigations of locomotive wheels show that the wheel position in the bogie has an impact on the wear rate. Studies also indicate that the most frequent failure mode is RCF on the wheel tread (Lin et al., 2013; Lin et al., 2015). Figure 4 shows the fatigued surface of such a locomotive wheel.

Work is under way to fine-tune the wheel profiles and to find methods to reduce RCF. The wheel profile impacts on the rail, e.g. small contact patches and high stresses, while the track status impacts on the wheel, e.g. track gauge and unfavourable contact conditions. The contact area on the wheel can be divided into zones, each with its own RCF pattern (Deuce, 2007). One of the zones is more exposed to straight lines, one is exposed to the curves on the high rail, and one is exposed to the curves on the low rail. The different RCF zones (RCF 1 - 4) and the connections between the track and the zones are explained in Figure 4. In the figure, the RCF1 zone shows the connection to the low rail field side in curves; the RCF2 zone shows the connection to the gauge corner of the high rail; the RCF 3-4 zones are related to tangent track and mild curves. The circles indicate different RCF types (UIC, 2004). The RCF of locomotive wheels is well described in Ekberg et al. (2014).

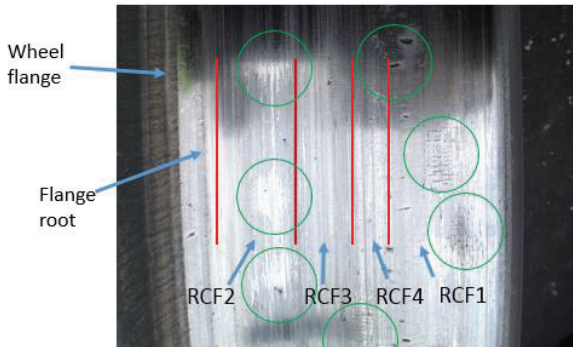

Figure 4. Surface fatigue on a locomotive wheel with locations of different patterns.

5 THE WHEEL-RAIL SYSTEM

There are four main rail profiles on the main track of the IOL: 60E1, MB1, MB4 and MB5. The MB4 rail profile is used for switches and crossings and is the standard profile for tangent track. Narrow curves have MB1 on the high rail and 60E1and MB5 on the low rail. Figure 6 shows profiles 60E1, MB1 and MB4. MB5 is a recent profile, developed for worn wheels in curves <650 m where gauge widening has taken place.

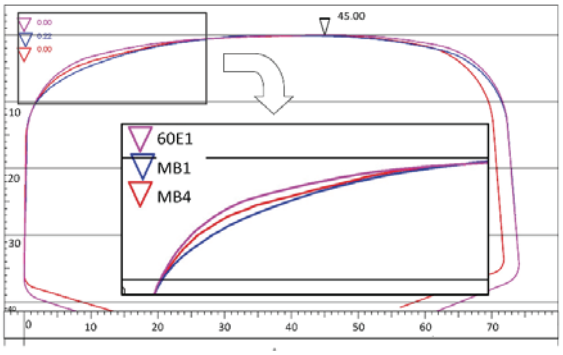

Figure 6. Three profiles used on the iron ore line.

The MB5 profile is close to the 60E1 profile, but is 0.4 mm higher on the field side and 0.1 mm higher on the gauge side. This gives a wider running surface to solve the emerging RCF problem on the low rail. Figure 7 shows the MB5 profile on the low rail; after one pass of the train with a 30-tonnes axle load, the contact band width is 30 mm.

The track gauge widening needs to be managed as well, as this parameter changes the wheel-rail contact conditions. Simply stated, it leads to an accelerated formation of RCF (Asplund et al., 2017). Investigation of the IOL in test sections A to E shows that the gauge widening is about 1.6 to 0.6 mm each year, depending on the radius of the curve. In general, a smaller radius leads to faster gauge widening, and the main cause of gauge widening is worn and broken fastenings.

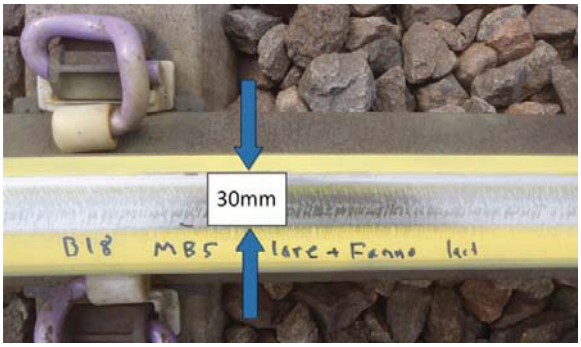

Figure 7. MB5 profile on the low rail where gauge widening take place.

It is discovered that a certain section had a large number of broken fastenings. This was surprising, as the curve in question does not have a specifically small radius; its radius is 765 m (D-curve; see Table 1). The accumulated tonnage for this curve is 240 MGT. The broken fastenings were investigated by the manufacturer who determined that fatigue cracking caused the failure. There were too many or too large force cycles in the vertical direction.

The manufacturer's recommendation was to use another type of fastening, change to a stiffer pad to reduce the deflection, and change the isolators to keep a better gauge in narrow curves. Figure 5 shows the typical failure mode and the fractured face of a fastening clip.

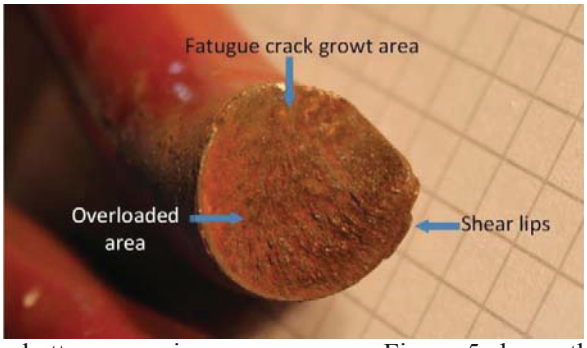

Figure 5. Fractured face of a fastening clip.

A new type of fastener with heavier clamping force was introduced in 2012, but the results so far are not revolutionary, Figure 7 shows the new type of fastening. With these fastenings, the degradation rate in curves < 550 m in radii went from 0.0603 mm/MGT to 0.0564 mm/MGT. For curves between 550 to 650 m the track gauge widening actually increased with the new fastenings; in addition, the standard deviation (STD) was larger for these curves. However, more traffic is needed before a final conclusion can be drawn. Table 4 shows the track gauge degradation rate mm/MGT for old and new fastenings.

Table 4. Track gauge degradation rate mm/MGT, new and old types of fastenings.

Curve size	Status	Mean*	STD
R<550 m	Old	0.0603	0.0174
R<550 m	New	0.0564	0.0161
550<R<650	Old	0.0304	0.0161
550<R<650	New	0.0750	0.1608

**** Mean degradation rate in mm/MGT***

6 FRICTION MANAGEMENT

6.1 *Lubrication in general*

To reduce shear forces between the rubbing surfaces, the introduction of a third body, generally lubricant, is recommended. For optimum rail operation, the friction between the gauge face and the wheel flange should be minimized as much as possible, but the friction between the top of the rail and the running surface of the wheel should be 0.3–0.4.

In railways, the application of an additive third body in the wheel–rail interference has been in practice for many years. It was initially limited to the gauge face (Stock et al., 2016). Gauge face lubrication in curves was widely introduced in Sweden during the 1970s (Waara, 2006). In the last two decades, an additive third body, known as top of rail (TOR) lubricants, has evolved to control the friction between the top of the rail and the wheel running surface. TOR lubricants can be applied separately or in combination with the gauge face lubricating system. Research across the globe has shown tremendous benefits of using TOR lubricants, including reductions in noise (Asplund et al., 2016, Eadie & Santoro, 2006), wear (Lu et al., 2012), energy consumption (VanderMarel, 2014), rolling contact fatigue (RCF) (Eadie et al., 2008, Khan, 2016, Stock et al., 2011) and short pitch corrugation (Eadie et al., 2008). TOR lubricants are generally classified according to their solvent and can be divided into three sub-classes:

- TOR oil (oil-based TOR fluid)
- TOR grease
- TOR–friction modifier, TOR−FM (water-based fluid)

6.2 *TOR FM tests on the IOL*

RCF is a major problem, especially on curves in the IOL, mostly because of the high haul trains. Therefore, Swedish Transport Administration (Trafikverket) is considering implementing the wayside TOR lubrication system on curves. An undergoing project is assessing the technical and economic efficiency of applying TOR–FM to the IOL's wayside equipment. In its initial phase, multi-body simulations (MBS) were performed after taking parameters of the IOL. The simulations focused on the effect of friction control on the generation of RCF. The MBS used basic theory such as shakedown and energy dissipation methods to predict the generation of RCF. A sample result from the MBS is a fatigue index (Ekberg & Kabo, 2005), based on shakedown theory, for a curve of 200 m radius. This is shown in Figure 8 and Figure 9. The fatigue index reports only the initiation of RCF. If the index is positive (>0), RCF will initiate; otherwise, there will be no RCF. The fatigue index value represents the proportion of the pressure which has overshot the limit for shakedown.

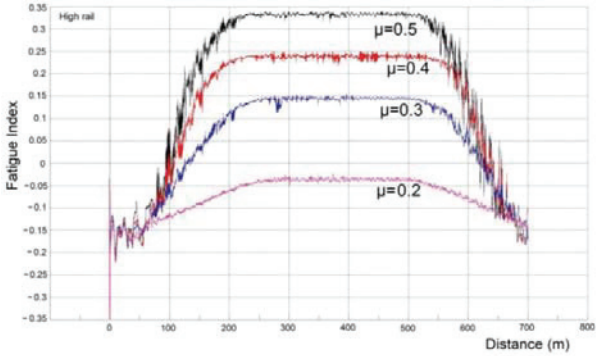

Figure 8. Fatigue index for a curve of 200 m radius and 700 m length at different friction values with respect to the distance in the curve of the high rail (Khan et al. 2016).

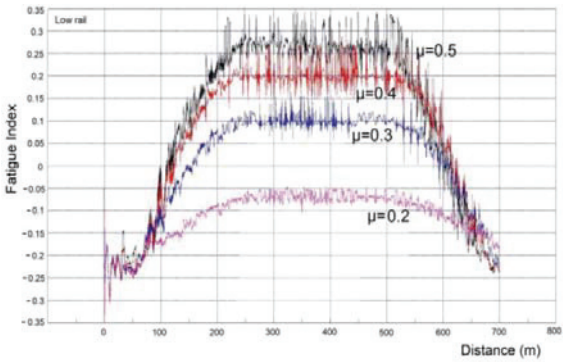

Figure 9. Fatigue index for a curve of 200 m radius and 700 m length at different friction values with respect to the distance in the curve of the low rail (Khan et al. 2016).

Despite the positive theoretical results, the presently installed wayside equipment (see Figure 10) does not seem a promising solution for the application of TOR–FM. The equipment is battery powered and is recharged using wind and solar energy; it is a challenge to keep the battery alive during winter, but installation of a direct power supply is costly and therefore is not possible in this project. In addition, to keep the equipment running, regular refill and maintenance are required. In an initial field test (Asplund & Nordmark, 2015) before the start of the current project, the similar wayside equipment is used, but observed no benefit. It was thought the benefits were negligible

because of good wheel and rail maintenance practices. However, more recent experiments show that the carry distance of TOR–FM when using wayside equipment is extremely short. With an application of 1 litre/1,000 axles, four times the recommended amount, it was observed a carry distance of 20 m when using the product from one supplier and 225 m when using the product from another. Possibly different solvents are used in the products, and this may explain the difference, but this is speculative, as the contents of the FMs are unknown. The carry distance of TOR–FM on wheels was also followed; it is observed a dried FM layer on the wheel surface for up to 1 km, but there was no FM in the contact band where it is actually needed.

The simulation results and various research results around the world suggest friction control is beneficial for both rail and wheels; however, wayside equipment does not seem to be a good candidate because of the short carry distance. An on-board system might overcome the issue. That being said, the reliability, maintenance cost and technical efficiency of on-board systems are not known in Nordic conditions. It is know how much on-board equipment is required per train in the case of freight trains from LKAB.

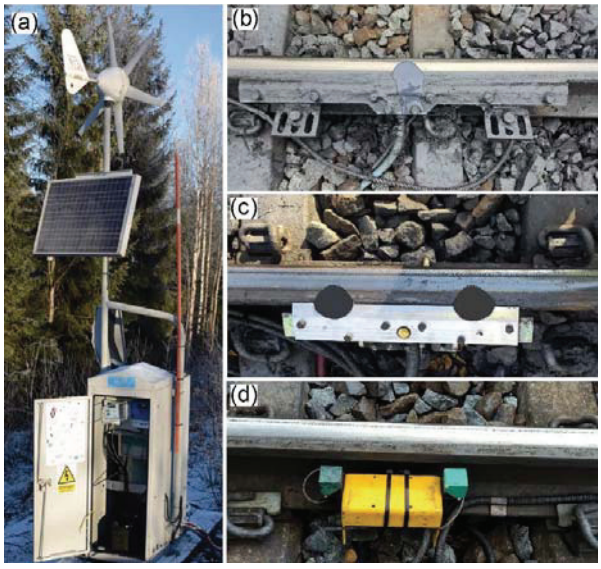

Figure 11. The wayside TOR equipment installed at Gullträsk, Sweden (a) Main unit (b) Distributing bars used for FM–A (c) Distributing bars used for FM–B (d) Wheel detecting sensor

7 MAINTENANCE

7.1 *Rail*

Machining is the main maintenance action for rails. Machining can be divided into milling and grinding. Milling is a cutting process, while grinding is an abrasive wear process to remove surface material. This paper only deals with grinding, as this is the practice used on the IOL.

Grinding is a "process of material removal from the top surface of the rail head through the use of abrasive girding materials, specially girding stones or wheels" (Zarembski, 2005). It is an established maintenance action to increase the life of rail and to improve its life cycle. For curves < 650 m radii, the IOL rail is ground every 15 MGT, and for other track, every 30-90 MGT. By introducing two grinding campaigns, the grinding depth of rails could be reduced from 0.7 mm to 0.4 mm each year.

Regular grinding has been implemented since 2006 with the installation of the new track. The use of a continuous grinding strategy has resulted in good rail condition. Although the rail in tangent tracks and on curves is good, the low rail on curves with a small radius needs more investigation. Figure 10 shows the low rail and its failure mode, line spalling.

Figure 10. Low rail with spalling on the running surface.

7.2 *Wheel*

The wheels on the heavy haul trains are regular re-profiled. The wagon wheels perform very well and are usually re-profiled after approximately 180,000 – 200,000 km. Their failure modes are 55% RCF and 45% wheel wear.

In contrast, the locomotive wheels are never reprofiled because of irregular profile or wear). Instead, the reason for turning locomotive wheels is surface damage like RCF (Ekberg et al., 2014). The wear rate differs between wheels, the natural wear rate is smaller than the artificial wear with a ratio of about two in avenged (Lin, Nordmark & Asplund, 2013). In general, the re-profiling intervals for locomotive wheels vary from 25,000 to 110,000 km. Therefore, in this project, the plan is to test wheel profile modifications and change in braking regimes, as well as wheel lubrication in different combinations, with selected locomotives.

8 ONGOING TRIALS

8.1 *The ReRail*

The ReRail is a totally new concept of how a rail is built up. The ReRail is a replaceable rail head made of hardened steel (martensitic micro structure) with a thickness of 10–12 mm. The concept of a replaceable rail head is shown in Figure 12.

Figure 12. ReRail is a replaceable rail head.

One advantage of ReRail is that there is less carbon emission in the rail production; another is that the material chosen can be harder than the regular rail.

A 6 m test rail is mounted as a high rail in a curve of 600 m radii on a section of the IOL. This has been in service since June 2016 and is loaded with about 10 MBT (until February 2017). This rail is carefully monitored in terms of wear, fatigue and conductivity. So far, the test shows positive results.

8.2 *R400HT*

The performance of new steel grades is also being tested. A curve (A6) has test rails with the steel grades R370CrHT and R400HT. While they show less wear than R350HT because of the greater hardness, the decreased RCF development is not sufficient to extend the grinding cycle from one year to two years. More investigation of the different steel grades will be done in the future; the findings will be the basis for changes to the steel grade.

8.3 *Trials with 32.5-tonnes axle loads*

In September 2015, LKAB and Trafikverket started a test in which they dispatched a dedicated test train with a 32.5-tonnes axle load once a day on the southern loop, from the Malmberget mine to the harbour in Luleå. The aim was to analyse the technical and economic effects on the railway system of upgrading the whole IOL to a 32.5-tonnes axle load.

In October 2016, the test was assessed and summarized. For Trafikverket's part, i.e., the infrastructure, including the rail system, and the subgrade, including bridges and culverts etc., the conclusion was that there was no sign of increased wear or downgrading of the infrastructure. For the train operator, LKAB, the result was also positive in the following aspects. The train load was increased by 8% but the punctuality was the same as for other trains. The negative aspect was that the energy consumption increased by 1% and the wagon wheels had 14% higher occurrence of RCF.

They decided to continue the test for another year, but with two trains per day.

9 CONCLUSIONS AND FUTURE WORK

First, for crack propagation, the crack angle seems to get larger as it goes deeper into the rail head. At about 2 mm under the surface, the crack angle is about 70°. This can give a different crack propagation behaviour after grinding if the cack is not totally removed. This new knowledge needs to be taken into account in the planning of grinding.

Second, the latest developed rail profile MB5 shows good results with a wide contact band. However, it should only be applied where the track gauge is under 1450 mm because wheels with hollow wear can destroy the rail.

Third, new fastenings that may show a lower degradation rate need to be investigated before their value can be summarised.

Fourth, with respect to TOR-FM, there are some problems in the carry distance capabilities of wayside equipment; depending on the product used, this varies from 20 to 225 m, but in all cases, the distance can be considered short. Luleå University of Technology and LKAB are discussing the installation of one or two on-board systems and calculating the life cycle cost of the on-board system.

Fifth, the ReRail findings are promising. ReRail has been used on track with about 10 MGT with no abnormalities; the trial will continue until 2019.

Sixth, trials with larger axle loads (32.5 tonnes) indicate this increase will have an impact on the formation of RCF on wheels.

Finally, work on improving the wheel-rail system is ongoing.

10 ACKNOWLEDGMENTS

The authors particularly acknowledge the work done by the other group members, in particular, Anders Frick, Malin Syk and Stefan Kallander from Trafikverket, Per Gustafsson and Robert Pallari from LKAB, Norbert Frank from voestalpine Schienen GmbH, Alexander Baltzewitsch and Wolfgang Schoech from Speno International, Björn Larsen from Jernbarneverket and Dr. Stephen Famurewa from Luleå University of Technology. They contributed greatly to the preparation of this paper.

REFERENCES

Asplund, A., & Nordmark T. (2015). Comparison of TOR lubrication systems on the iron ore line, International Heavy Haul Association: The 11th International Heavy Haul Association Conference held 21-24 June 2015 in Perth.

Asplund, M., Famurewa, S. M., & Shoech, W. (2017). A Nordic heavy haul experience and best practices [accepted for publication]. *Proceedings of the Institution of Mechanical Engineers, Part F: Journal of Rail and Rapid Transit,*

Asplund, M., Gustafsson, P., Nordmark, T., Rantatalo, M., Palo, M., Famurewa, S. M., & Wandt, K. (2014). Reliability and measurement accuracy of a condition monitoring system in an extreme climate: A case study of automatic laser scanning of wheel profiles. *Proceedings of the Institution of Mechanical Engineers, Part F: Journal of Rail and Rapid Transit, 228*(6), 695-704.

Asplund, M., Rantatalo, M., Johnsson, R., & Hiensch, M. (2016). Combating curve squeal noise. *World Congress of Railway Research: 29/05/2016-02/06/2016,*

Asplund, M., & Lin, J. (2016). Evaluating the measurement capability of a wheel profile measurement system by using GR&R. Journal of the International Measurement Confederation, 92, 19-27.

Asplund, M., Lin, J., & Rantatalo, M. (2016). Assessment of the data quality of wayside wheel profile measurements. International Journal of C O M A D E M, , 1-7.

CEN. (2011). *EN 13674-1:2011: Railway applications –Track - rail - part 1: Vignole railway rails 46 kg/m and above*. Brussels: European Committee for Standardization.

Deuce, R. (2007). *Wheel tread damages -an elementary guide line, 100115000* (Deuce, Roger; ed.). Netphen, Germany: Bombardier Transportation GmbH.

Eadie, D. T., Elvidge, D., Oldknow, K., Stock, R., Pointner, P., Kalousek, J., & Klauser, P. (2008). The effects of top of rail friction modifier on wear and rolling contact fatigue: Full-scale rail–wheel test rig evaluation, analysis and modelling. *Wear, 265*(9), 1222-1230.

Eadie, D. T., Santoro, M., Oldknow, K., & Oka, Y. (2008). Field studies of the effect of friction modifiers on short pitch corrugation generation in curves. *Wear, 265*(9), 1212-1221.

Eadie, D., & Santoro, M. (2006). Top-of-rail friction control for curve noise mitigation and corrugation rate reduction. *Journal of Sound and Vibration, 293*(3), 747-757.

Ekberg, A., & Kabo, E. (2005). Fatigue of railway wheels and rails under rolling contact and thermal loading—an overview. *Wear, 258*(7), 1288-1300.

Ekberg, A., Kabo, E., Karttunen, K., Lindqvist, B., Lunden, R., Nordmark, T., Olovsson, J., Salomonsson, O., Vernersson, T. (2014). Identifying the root causes of damage on the wheels of heavy haul locomotives and its mitigation. Proceedings of the Institution of Mechanical Engineers, Part F: Journal of Rail and Rapid Transit, 228(6), 663-672.

Famurewa, S. M., Asplund, M., & Kumar, U. (2015). Evaluation of rail wear characteristics on heavy haul track section using measurement data. *International Heavy Haul Association: The 11th International Heavy Haul Association Conference held 21-24 June 2015 in Perth.*

Khan, S. A., Persson, I., Lundberg, J., & Stenström, C. (2016). Prediction of the effects of friction control on top-of-rail cracks. *Proceedings of the Institution of Mechanical Engineers, Part F: Journal of Rail and Rapid Transit,* 0954409716674984.

Lewis, R., & Olofsson, U. (2009). *Wheel-rail interface handbook*. Cambridge: Elsevier.

Lin, J., Asplund, M., & Parida, A. (2013). Reliability analysis for degradation of locomotive wheels using parametric bayesian approach. *Quality and Reliability Engineering International,*

Lin, J., Pulido, J., & Asplund, M. (2015). Reliability analysis for preventive maintenance based on classical and bayesian semi-parametric degradation approaches using locomotive wheel-sets as a case study. *Reliability Engineering & System Safety, 134*, 143-156.

Lu, X., Makowsky, T. W., Eadie, D. T., Oldknow, K., Xue, J., Jia, J., Li, G., Meng, X., Xu, Y., Zhou, Y. (2012). Friction management on a chinese heavy haul coal line. *Proceedings of the Institution of Mechanical Engineers, Part F: Journal of Rail and Rapid Transit, 226*(6), 630-640.

Lin, J., Nordmark, T. & Asplund, M. (2013). Data Analysis of Wheel-sets' Running Surface Wear Based on Re-Profiling Measurement: A Case Study at Malmbanan. *International Heavy Haul Association: The 11th International Heavy Haul Association Conference held 21-24 June 2015 in Perth.*

Sipos, K., López, M., & Trucco, M. (2008). Surface martensite white layer produced by adhesive sliding wear friction in AISI 1065 steel. *Rev Latinoam Metal Mater, 28*(1), 46-50.

Stock, R., Eadie, D. T., Elvidge, D., & Oldknow, K. (2011). Influencing rolling contact fatigue through top of rail friction modifier application–A full scale wheel–rail test rig study. *Wear, 271*(1), 134-142.

Stock, R., Stanlake, L., Hardwick, C., Yu, M., Eadie, D., & Lewis, R. (2016). Material concepts for top of rail friction management–Classification, characterisation and application. *Wear, 366*, 225-232.

UIC. (2004). *Atlas of wheel and rail defects*. http://www.uic.org/etf/publication/publication-detail.php?code_pub=135: International Union of Railways.

VanderMarel, J., Eadie, D. T., Oldknow, K. D., & Iwnicki, S. (2014). A predictive model of energy savings from top of rail friction control. *Wear, 314*(1), 155-161.

Waara, P. (2006). Lubricants influence on wear in sharp rail curves. *[Doctoral Thesis], Luleå University of Technology,*

Zarembski, A. M. (2005). *The art and science of rail grinding* Simmons-Boardman Books.

Department of Civil, Environmental and Natural Resources Engineering
Division of Operation, Maintenance and Acoustics

ISSN 1402-1544
ISBN 978-91-7790-272-0 (print)
ISBN 978-91-7790-273-7 (pdf)

LULEÅ
UNIVERSITY
OF TECHNOLOGY